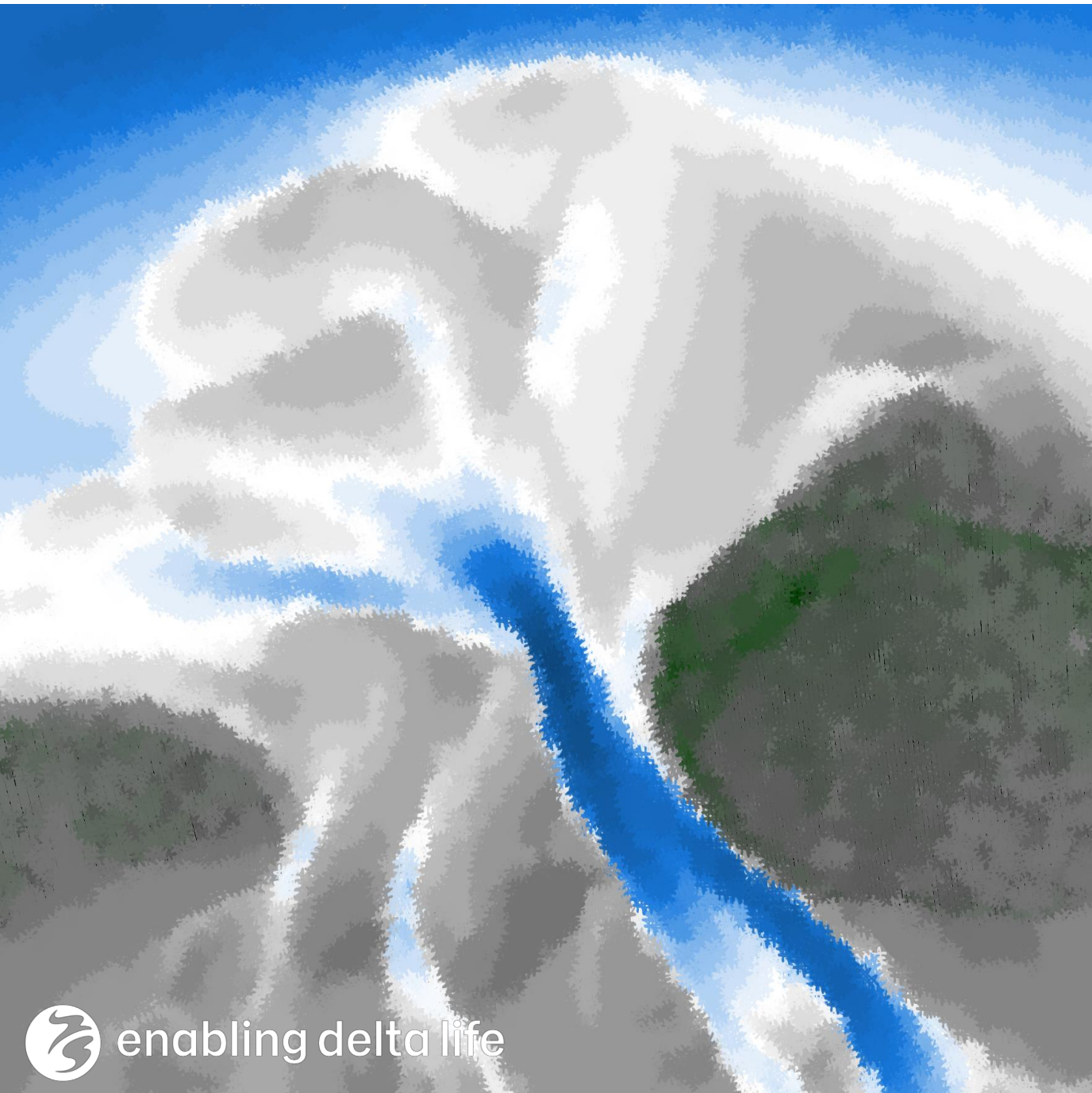


Morphodynamic Modelling of the Ameland Ebb-Tidal Delta

An Assessment of the 2018 – 2019 Pilot Nourishment



Morphodynamic Modelling of the Ameland Ebb-Tidal Delta

An assessment of the 2018 – 2019
pilot nourishment

by

D. Harlequin

In partial fulfilment of the requirements for the degree of

Master of Science

In Civil Engineering

At the Delft University of Technology (TU Delft)

To be defended publicly on Thursday November 25th, 2021 at 16.30 PM.

Student number:	4484207			
Chair committee:	Prof. dr. ir.	B.C. van Prooijen	Delft University of Technology & Deltares	chair
	Prof. dr. ir.	Z.B. Wang	Delft University of Technology & Deltares	
	dr. ir.	E.P.L. Elias	Deltares	
	ir.	S.G. Pearson	Delft University of Technology & Deltares	
	ir.	S. Pluis	Rijkswaterstaat WVL	

An electronic version of this thesis is available at <http://repository.tudelft.nl/>.

Morphodynamic Modelling of the Ameland Ebb-tidal delta
An assessment of the 2018-2019 pilot nourishment

Author(s)

Denzel Harlequin

Acknowledgements

This thesis concludes my study towards the degree of Master of Science in Hydraulic Engineering at the Delft University of Technology. This research was conducted at the research institute Deltares, Delft and it has been an honour for me to work on such an intricate project with the esteemed colleagues of Deltares. I am very grateful for the opportunity to work on my thesis in such a fostering and dynamic environment as Deltares.

This study would not have been possible without the endless support of my graduation committee. I would like to thank the committee members, Bram van Prooijen, Edwin Elias, Zheng Bing Wang, Stuart Pearson and Stefan Pluis for their time, effort and guidance throughout the research. My sincere gratitude goes to Edwin Elias and Stuart Pearson for giving me the opportunity to work on such a wonderful project and for their immeasurable support, motivation, and fruitful discussions during our meetings. I can't thank you enough; Without you this project would not have reached the latitude that it acquires today. I would also like to thank Bram, Zheng Bing and Stefan for their critical feedback, witted ideas to elevate this research and endless enthusiasm.

Furthermore, my utmost gratitude goes to my mother, Glenda: Thank you for your endless support, guidance, motivation and unconditional believe in me. This would not have been possible without you.

*Merci ma mère. Je chérir à jamais un souvenir
heureux du voyage que nous faisons pour le bon vieux du temps.*



Denzel Virgil Harlequin
Delft, October 2021

*Je n'ai fait celle-ci plus longue que parce
que je n'ai pas eu le loisir de la faire plus courte.*
– Blaise Pascal

Abstract

Ebb-tidal deltas play a key role in the morphology of barrier coastlines and tidal inlet systems as they serve as a natural source of sediment. They are typified by a dynamic morphology that interacts with the adjacent coastlines and sponsors a unique ecological habitat. Under increasing socio-economic, ecological and climate-induced constraints, it becomes imperative to obtain a better understanding of the evolution of ebb-tidal deltas in order to maintain and preserve these morphological features in the near-future time horizon. An increased interest has therefore been raised to understand, quantify and predict the development of ebb-tidal deltas.

In the context of developing a future-proof coastal management and maintenance strategy, the efficiency of ebb-tidal delta nourishments has been further investigated in research programmes such as Coastal Genesis 2.0. For the Ameland inlet, this entailed the construction of a 5 million m³ pilot nourishment over the course of March 2018 to February 2019 and subsequent monitoring in the years following. This research investigates the impact of this pilot nourishment to the natural behaviour of the Ameland ebb-tidal delta. The second goal is to build further knowledge on the modelling capabilities of present state-of-the-art models for the Ameland ebb-tidal delta.

To this end, a process-based Delft3D model is applied to hindcast the morphological development of the ebb-tidal delta with a particular interest in the evolution of ebb-shields and -chutes over the course of 2005 to 2020. It is identified that the representation of the wave-induced processes is key for capturing the development of ebb-shields and -chutes in the model predictions. Therefore, we applied and experimented with an updated nonlinear wave orbital velocity parameterisation and assessed its contribution to the modelling performance. This thesis demonstrates that the evolution of ebb-shields and chutes on the outer delta is contingent on its initial presence in the initial bathymetry. Hence, the initiation of ebb-shield development is not inherited in the model response. These insights have been integrated and synthesised to assess the application of the present state-of-the-art model as forecasting tool for the morphological development of ebb-tidal delta nourishments.

Ultimately, it is shown that a model using schematised boundary conditions and an efficient morphological updating scheme is able to predict the yearly-averaged development of the pilot nourishment on the ebb-tidal delta. It is demonstrated that the 2019 pilot nourishment only locally influences the behaviour of the Ameland ebb-tidal delta. Nourished sediment is likely to be redistributed along the ebb-shields, contributing on the long-term to the sediment exchange process with the downdrift coast of Ameland. The location of the ebb-tidal delta nourishment is thereby important for the sediment exchange process and the development of local features. Placing ebb-tidal delta nourishments to the south of the Westgat invokes a primary sediment exchange between the coast of Terschelling and surrounding morphological features. A secondary readjustment of the Westgat thereby influences the development of the ebb-shields and -chutes. Constructing an ebb-tidal delta nourishment north of the Westgat results in a sediment exchange between the local ebb-shields and the downdrift coast of Ameland. Our results also demonstrate that an increase in the pilot nourishment construction height enhances the redistribution of sediment along the ebb-shields.

Lastly, this study identifies further opportunities for improving medium-term morphodynamic models for the Ameland inlet by incorporating time-dependent boundary conditions including new transport formulations such as SANTOSS.

Contents

	Acknowledgements	5
	Abstract	7
1	Introduction	13
1.1	Background	13
1.2	Ameland Inlet	14
1.2.1	Ameland Inlet around 1600 CE	14
1.2.2	Regime Shift Ameland Inlet	15
1.2.3	Application of the cascade of scales	17
1.3	Previous Ameland model studies	18
1.4	Research Questions	18
1.4.1	Research Approach and Outline	18
2	Theoretical Background	22
2.1	Tidal Inlet Systems	22
2.1.1	Classification of tidal basins	22
2.1.2	Inlet classification	22
2.1.2.1	Barrier Islands in wave-dominated environments	23
2.1.2.2	Barrier Islands in mixed-energy environments	23
2.1.3	Morphology of a Tidal Inlet System	23
2.2	Relevant Physical Processes	25
2.2.1	Sediment Bypassing	26
2.2.2	Preferential Orientation of Main Inlet	27
2.2.3	Cyclicity Of Ameland Ebb-tidal delta – Previous Understanding	28
2.2.4	Cyclicity of Ameland Ebb-tidal delta – A Revised Understanding	30
3	The Study Area	34
3.1	General Setting	34
3.2	Present-day Morphology of the Ameland Inlet	35
3.3	Hydrodynamic Forcing	36
3.3.1	Water Level Variations	36
3.3.2	Wave Climate	37
3.4	Morphological development of characteristic periods	38
3.4.1	Behaviour 1926 - 2005	38
3.4.2	Recent Morphological Behaviour 2005 – 2020	39
3.4.3	Pilot Nourishment	42
4	Process-based Modelling	44
4.1	Grid and Bed Schematisation	44
4.2	Model Setup	47
4.2.1	Flow module	47

4.2.2	Wave Module	47
4.2.3	Morphodynamics	47
4.3	Model Improvements	48
4.4	Imposed Boundary Conditions	51
4.4.1	Flow Boundary Conditions – Morphological Tide Selection	51
4.4.2	Wave Boundary Conditions – Manual Selection of Wave Classes	52
4.5	Sediment-Transport Model	55
5	Morphological Model Validation	57
5.1	Model results Morphological Validation on Natural Behaviour	57
5.1.1	Description of model performance (2005 – 2010)	57
5.1.1.1	Annual runs	58
5.1.1.2	Two-year runs	59
5.1.1.3	Four year runs	60
5.1.2	Description of model performance (2010 – 2016)	61
5.1.2.1	Annual runs	62
5.1.2.2	Two-year runs	63
5.1.2.3	Four year runs	63
5.1.3	Description of model performance (2016 – 2020)	64
5.1.3.1	Annual runs	65
5.1.3.2	Two-year runs	66
5.1.3.3	Four year runs	67
5.1.4	Synthesis on morphological validation	67
5.2	Validation Pilot nourishment runs	68
5.3	Validation Run 2009 – 2021	69
5.3.1	Bornrif Platform	69
5.3.2	Growth ebb-chutes and -shields	69
5.3.3	Westgat	71
5.3.4	Zeehondenplaat and Coast of Terschelling	71
5.3.5	Synthesis of validation run	71
5.4	Nourishment Forecasting 2018 – 2028/2030 Runs	73
6	Morphological Impact Pilot Nourishment	75
6.1	Introduction	75
6.2	Analysis on T0 Behaviour	77
6.2.1	Flow patterns	77
6.2.2	Effect of wave climate on ebb-tidal delta morphology	80
6.2.3	Sediment Transport	84
6.2.4	Bed level changes	84
6.3	Description of T1 Behaviour	87
6.3.1	Impact on Morphological Wave Climate	87
6.3.2	Impact on water motion	89
6.3.3	Impact on sediment transport	90
6.3.4	Bed level changes	90
6.4	Description of alternative nourishment options	93
6.4.1	Nourishment considerations and elaboration on designs	93
6.4.1.1	Ebb-tidal delta Nourishment V1: Nourishment on third ebb-chute	94
6.4.1.2	Ebb-tidal delta Nourishment V2: Nourishment on Zeehondenplaat	94

6.4.1.3	Ebb-tidal delta Nourishment V3: Nourishment on second ebb-chute	94
6.4.1.4	Ebb-tidal delta Nourishment V4 & V5: Height variation of the 2019 pilot nourishment	94
6.5	Description of behaviour nourishment alternatives H1 & H2	95
6.5.1	Impact on Morphological Wave Climate	95
6.5.2	Impact on sediment transport	98
6.5.3	Impact on bed level changes	98
6.6	Description behaviour nourishment alternatives V1, V2 & V3	100
6.6.1	Impact on morphological wave climate	100
6.6.1.1	V1 Nourishment	100
6.6.1.2	V2 Nourishment	100
6.6.1.3	V3 Nourishment	101
6.6.2	Impact on sediment transport	102
6.6.2.1	V1 Nourishment	102
6.6.2.2	V2 Nourishment	102
6.6.2.3	V3 Nourishment	103
6.6.3	Influence on bed level changes	104
6.6.3.1	V1 Nourishment	104
6.6.3.2	V2 Nourishment	104
6.6.3.3	V3 Nourishment	105
7	Discussion	106
7.1	Modelling meso-scale evolution of the Ameland ebb-tidal delta	106
7.1.1	Implementation of nonlinear wave orbital velocity formulation	106
7.1.2	Ebb-chute and -shield development	106
7.1.3	Modelled response in tide- and wave-dominated areas	107
7.2	Impact of pilot nourishment on the Ameland ebb-tidal delta	108
7.2.1	Morphological behaviour of the pilot nourishment	108
7.2.2	Implication of nourishment height	110
7.2.3	Implication of nourishment location	110
8	Conclusions	112
8.1	Morphological capabilities of present-state-of-the-art Ameland models	112
8.2	Morphodynamic Impact of the pilot nourishment	112
9	Recommendations for future research	114
	Bibliography	116
	Appendices	119
A	Natural Behaviour of the Ameland Ebb-Tidal Delta – Production Runs	120
A.1	Figures of Annual Production Runs	120
A.2	Figures of Two-Year Production Runs	135
A.3	Figures of Four-Year Production Runs	145
B	Morphodynamic Impact of Pilot Nourishment 2018 – 2022 – Production Runs	151
C	Long-Term Behaviour of Ameland Ebb-Tidal Delta – Production Runs	158

1 Introduction

1.1 Background

The Dutch coastal system is a unique marine environment where many coastal management functions are integrated. The shorelines are a place where socio-economic drivers provide an ever-increasing convergence of local commercial and human activities. Meanwhile, coastal wetlands such as the Wadden Sea are one of world's largest pristine ecological habitats housing a wide variety of species and diverse flora and fauna (Blew et al., 2017; Ministerie van Landbouw Natuur en Voedselkwaliteit, 2017).

It is known that socio-economical constraints and climate-induced drivers are influencing the sediment demand of the Dutch coastal system (Luijendijk, 2019; Wong et al., 2014). Structurally, the coastal foundation acquires 12.4 million m³/year of sand to maintain its lower and upper shoreface under the present rate of relative sea level rise (Nolte et al., 2020). A portion of this structural demand is accounted for by the Wadden Sea. Annually, the basin acquires 4.5 million m³ of sand to balance its natural sediment demand – also referred to as the *sand hunger of the Wadden Sea*. The latter may be attributed to relative sea level rise and prior anthropogenic interventions (Rijkswaterstaat, 2021).

Ebb-tidal deltas play here an eminent role in the sediment balance of the Wadden Sea basins as they form a primary source of sediment for the inlet systems. With increasing tension from socio-economical and climate-induced drivers, it is expected that these coastal elements will face even larger sediment losses. Therefore, large efforts are needed on a structural basis to maintain these coastal elements. In this context, coastal maintenance strategies have been postulated in many national programmes such as the *national directive for Coastline Protection and Maintenance*¹. Moreover, in additional research programmes, viz. *Coastal Genesis 2.0*, *SEAWAD* and *KPP sea level rise*², the efficiency of ebb-tidal delta nourishments as innovative nourishment strategy has been further investigated.

This research builds further upon the pilot nourishment case study of the Ameland inlet (Figure 1-1). The aim of this case study is to build system knowledge on the intricate dynamics of tidal inlets and to further knowledge on the implications of pilot nourishments to the natural behaviour of the ebb-tidal delta. The choice for the Ameland inlet was founded on the perception that the Ameland basin is one of the most pristine basins of the Wadden Sea given its relative free reign wherein nature can develop and its little dependence to manmade interventions (Elias et al., 2019). This and the unprecedented wealth of available high-resolution data makes the Ameland inlet system an attractive case to assess its underlying physical processes.

In turn, this knowledge could be used to extend the current framework of dynamic coastal preservation and promote the application of ebb-tidal delta nourishment as coastal mitigation measure – also in consideration of future coastal management challenges.

¹ *dutch*, programma Kustlijnzorg en Beheer & Onderhoud Kust, B&O Kust.

² *KPP sea level rise* standing for Knowledge on Primary Processes regarding Management and Maintenance of the Dutch Coast – Thematic Programme sea level rise).



Figure 1-1: Satellite image of the Dutch Wadden Sea. An overview of the west Frisian barrier islands is presented wherein the Ameland inlet is demarcated with a yellow star. (Image Courtesy of USGS/ESA ©)

1.2 Ameland Inlet

The Ameland inlet is one of the tidal inlets located in the West Frisian Barrier Islands chain (Figure 1-1). The inlet is bordered by the coast of Ameland on the east and the coast of Terschelling on the west. As the inlet is a dynamic environment, the morphology of the Ameland inlet system has changed significantly over the past centuries.

1.2.1 Ameland Inlet around 1600 CE

The present-day position of the Ameland inlet was formed around 1600 CE after the reclamation of the *Middelzee* – a prior tidal basin in the medieval centuries of the Netherlands. First charts of the Wadden sea were published by Waghenaer (1584) and Haeyen (1585) (Figure 1-2). The Ameland inlet was around that time characterised by a two-channel inlet system with the Coggediep along the coast of Terschelling. And the Borndiep on the east of the inlet along the coast of Ameland (Van Der Spek, 1995). These inlets were separated by a large shoal – the Camperzandt in the inlet gorge. The Amelander gat was the main ebb-outflow on the ebb-tidal delta.

Periods of shoal formations at the outer delta were succeeded by cycles of channel migration, and outer channel breaching through the prior formed shoals. After 1800 AD, the Ameland inlet reached to a single-channel inlet system due to the siltation of the Coggediep and the attainment of the inlet shoals Camperzandt and 't Bosch to the Island of Terschelling. This single-inlet channel system is consistent with the present-day morphology of the Ameland inlet.

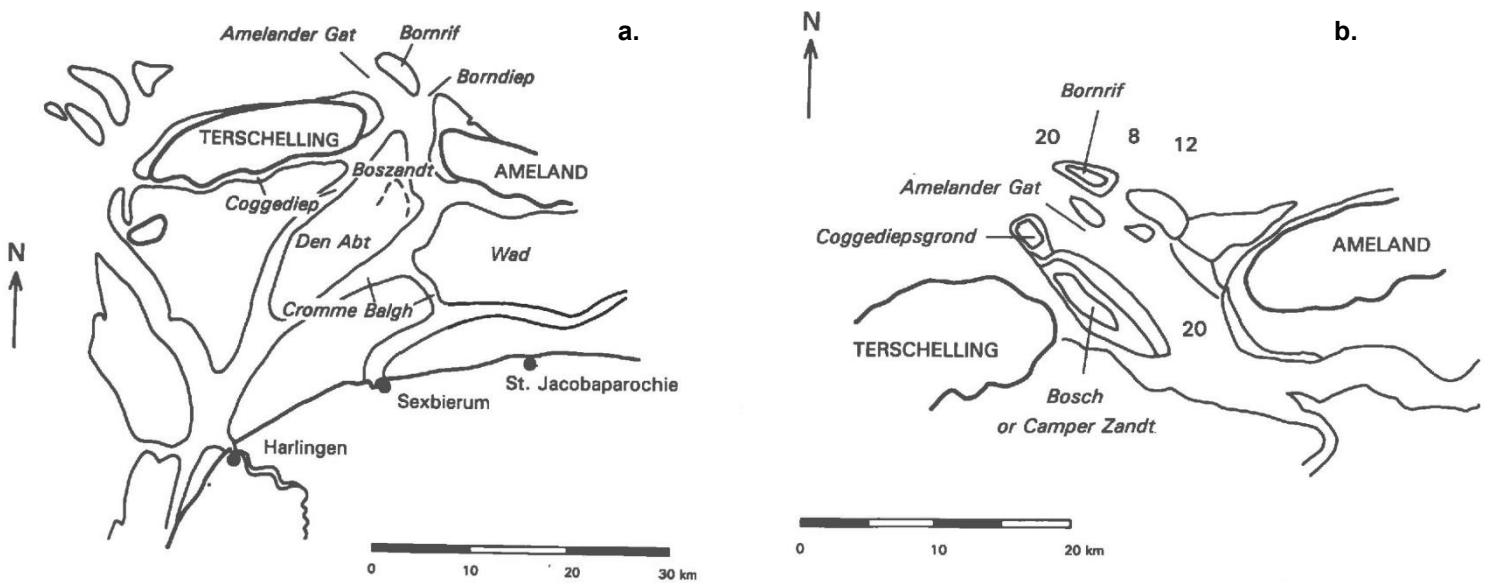


Figure 1-2: Simplified nautical charts of the Ameland gat around 1585 (a.) by Waghenaer (1584) and (b.) by Haeyen (1585) (from Van Der Spek, 1995).

1.2.2 Regime Shift Ameland Inlet

Several events of *outer delta breaching*, and *main-inlet relocation* had occurred over the centuries following. Recent analysis of the Ameland inlet by Elias et al., (2019) have illuminated a critical geomorphic transition in the morphodynamic behaviour of the Ameland inlet. A regime shift was evident in the 20th century from *outer delta breaching* to *main-ebb channel switching*.

In the more recent bathymetries around the beginning of the 20th century, the inlet was typified by a main-inlet *Borndiep*, a main-ebb outflow the *Akkepollegat*, and secondary marginal channels such as the *Westgat* (Figure 1-3). Gradually, the ones flood-dominated marginal channel *Westgat* superseded the role as main-ebb outflow from the *Akkepollegat*. Anthropogenic interventions to the *Middelzee* and continuous construction of coastal defence works had contributed towards the latter regime shift. Small instabilities thereafter instigated the formations of ebb-chutes and shields over the years after (approximately) 1926.

The underlying physical processes interacted in an entirely different manner resulting in a new driving mechanism for sediment bypassing. It may be seen that regime shifts of this sort are highly dependent on the history and geology of the tidal basin, and the apparent order wherein underlying physical processes prevail. These are stochastic processes that change depending on subtle nuisances in the morphology of the tidal basin within the time-window and state of the system (i.e. extrinsic conditions).

This research focusses on the evolution of ebb-chutes and -shields following from such subtle disturbances in the more recent morphology of the Ameland ebb-tidal delta after 2005.

1.2.3 Application of the cascade of scales

The significance of ebb-chutes and -shields development on the Ameland ebb-tidal delta can best be emphasised in the context of the cascade of scales (Figure 1-4). This concept highlights the chief principle that changes in the behaviour of a system transpire in the time- and spatial scale wherein they naturally occur.

Changes in the Wadden Sea system become apparent gradually $O(\text{centuries})$ while having a noticeable effect on the entire system $O(10 - 100\text{kms})$ – consider for instance the variations in the position of the tidal divides. These changes may drive in turn variations in the location of the main-ebb channel and the morphology of the individual basins $O(1 - 10\text{kms}$ and decades-centuries).

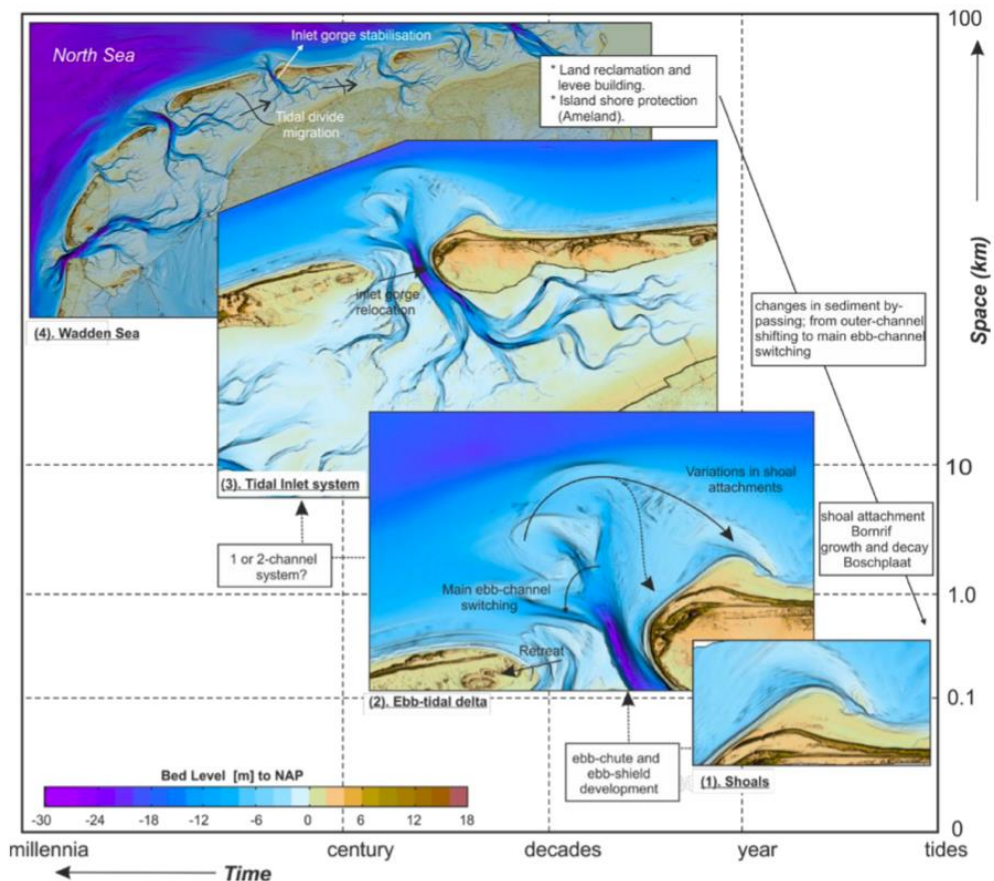


Figure 1-4: The cascade of scales highlighting the relevant spatial and temporal scales to describe the significant changes in the Ameland inlet system. Level 4 (Top tier) describes changes on the scale of the entire Wadden Sea system. Level 3 (Upper-Intermediate tier) describes the changes within the respective tidal basins of the Wadden Sea. Level 2 (intermediate tier) describes the relevant changes on the scale of the Ameland ETD. And lastly, Level 1 describes the changes of the individual shoals. It should be noted that the intermediate tier (Level 2) morphology is dependent on the interrelation between the level 1 (individual shoals) and level 3-4 morphology (After Elias & Tonnon, 2016).

In this research, the emphasis is placed on the morphological development which occurs on the time and spatial scale of the Ameland inlet – the *meso-scale medium-term morphology* of the Ameland Inlet. Changes at this scale may be driven by either long-term large-scale changes in the Wadden Sea system or by an interaction with morphological units up to the smallest scales of the individual shoals. The development of ebb-chutes and shields identify the significance of long-term large-scale morphology and short-term small-scale hydro- & morphodynamics to the decadal development of the Ameland ebb-tidal delta. Comprehension

of the interplay between larger and smaller scale interaction is hereby imperative for better morphological prediction of the meso-scale morphology. Hereto, the meso-scale morphology embodies the evolution of shoals and chutes on the Ameland ebb-tidal delta, under the effect of quasi-stationary extrinsic conditions.

1.3 Previous Ameland model studies

The analysis of high-resolution bathymetric data by Elias et al., (2019) have provided crucial insights into the dynamic interaction of physical processes and their effect on the (present-day) morphology of the Ameland inlet. Several modelling studies have been performed in the previous decades to capture the morphodynamic evolution of the Ameland inlet in numerical models (e.g. Steijn & Roelvink (1999), de Fockert (2008), Teske (2013), Jiao (2014), Elias et al. (2015), Elias (2018)).

These modelling studies showed that a model using schematised boundary conditions is an effective technique to reproduce the Ameland ebb-tidal delta morphology. A known challenge in the model predictions of the ebb-tidal delta is the reproduction of the prevalent erosion and deposition patterns along the main swash platform Bornrif. As the terminal lobe is a region dominated by wave-driven processes it is acknowledged that future research on the modelling capabilities of present-day Ameland models, should comprise an investigation into the representative morphological wave climate and the representation of wave-driven processes in process-based Delft3D models. (see for instance Elias & Tonnon, (2016)). Also, the interaction between the current-related and wave-driven processes should be further improved to promote a better alignment of accretion and erosion patterns and magnitude.

This research builds further upon the latter notions and aims to capture the evolution of ebb-chutes and shields over the timespan of 2005 – 2020. A modelling study which highlights these morphological patterns and trends in an accurate way remains thereby a wide and intricate field of interest.

1.4 Research Questions

The first goal of this thesis is to obtain a better understanding on the impact of the pilot nourishment on the natural behaviour of the Ameland ebb-tidal delta. Therefore, an analysis is undertaken into the natural dynamics of the Ameland ebb tidal delta.

Based on our established knowledge and modelling foundation on the natural behaviour of the inlet, we extend our research towards the case of the pilot nourishment which has been constructed on the Ameland ebb-tidal delta (ETD) in 2019.

The second goal is to improve the modelling capabilities of current state-of-the-art models for the Ameland ebb-tidal delta. A special interest is therewith raised in the model performance on the evolution of ebb-chutes and shields over the timespan of 2005 – 2020.

Hereto, this thesis aims to answer the following research question:

What is the morphological impact of the 2019 ebb-tidal delta nourishment on the morphodynamic behaviour of the Ameland ebb-tidal delta?

1.4.1 Research Approach and Outline

In order to achieve these goals, this research is divided in two parts. These parts aim to answer the following research objectives:

Determine the morphological capabilities of the present-state-of-the-art morphological models for the Ameland ebb-tidal delta in the context of ebb-chutes and -shield development. Therefore, the following question is answered:

- How well are present state-of-the-art morphodynamic models for the Ameland ebb-tidal delta capable of producing ebb-chutes and -shields on a short³-, medium⁴-, and long⁵-term scale?

Determine the morphodynamic impact of the pilot nourishment on the natural morphodynamic behaviour of the Ameland ebb-tidal delta. Therefore, we aim to answer to following questions:

- Is the model suitable as a forecasting tool for the prediction of ebb-tidal delta nourishment evolution on the Ameland ebb-tidal delta?
- What is the initial response⁶ of the Ameland ebb-tidal delta to the ebb-tidal delta nourishment?
- What is the long-term trend⁷ of the morphodynamic adjustment of the Ameland ebb-tidal delta to the ebb-tidal delta nourishment?
- How sensitive is the Ameland ebb-tidal delta to changes in the pilot nourishment location and volume?

The research method is presented schematically in Figure 1-5. In order to achieve the abovementioned research objectives, this research aims to identify the interrelation between the important physical processes, their dynamic interplay, and the time horizon wherein they are accurately reproduced. Therefore, a process-based modelling assessment is subsequently performed to aggregate medium-term datasets which reasonably represent the natural behaviour of the inlet system. We compare these model datasets with high-resolution observations of the present-day Ameland inlet and next extrapolate the results to assess the effect of ebb-tidal delta nourishments to the natural inlet behaviour of the ebb-tidal delta. Next, the simulation time horizon is further extended to 10 – 12 years timespans to investigate the onset of long-term morphological trends in the behaviour of the Ameland ebb-tidal delta. The associated implications for the fate of the ebb-tidal delta nourishment is thereby reflected through a volumetric trend analysis and assessment of near-yearly measured bathymetries of the Ameland ebb-tidal delta. Hence, this research is divided in three pillars:

- **Literature review**

This thesis starts with a literature review wherein the relevant theoretical background on tidal basins is reviewed (Ch.2) and a knowledge foundation is provided on the Ameland Inlet system. The theoretical background gives hereby further insights into the dominant physical processes and their important role in various mechanisms which drive changes in the evolution of tidal inlet systems. Subsequent parallels are also drawn between the theoretical background and the case study of the Ameland inlet to highlight its particular

³ Morphological simulations with a characteristic simulation horizon shorter than 4 years.

⁴ Morphological simulations with a characteristic simulation horizon of 4 – 10 years.

⁵ Morphological simulation with a characteristic simulation horizon of 10 – 12 years.

⁶ The initial response is here defined as the morphological adjustments that may be observed over a time span of 1 – 4 years post construction of the ebb-tidal delta nourishment.

⁷ Long-term trends are here defined as the persistency of prior observed morphological adjustments over a time span of 10 – 12 years post construction of the ebb-tidal delta nourishment.

evolution and the relevant mechanisms which have shaped the present-day morphology of the Ameland inlet system.

- **Data analysis (extended literature review)**

Furthermore, a data analysis has been performed by Elias et al., (2019) on the evolution of the Ameland ebb-tidal delta from the late 18th century on to the more recent years. Elias et al., (2019) exposed, hereby, a critical geomorphic transition in the morphodynamic behaviour of the Ameland inlet. Moreover, the role of the sediment-bypassing mechanism in the evolution of the present-day morphology of the Ameland ebb-tidal delta had been clearly identified. In this research, the hypotheses of Elias et al., (2019) are tested on the basis of several morphodynamic modelling assessments. The research findings of Elias et al., (2019) are therefore further outlined in the knowledge foundation on the Ameland Inlet system (Sec. 2.2 and Ch. 3).

- **Modelling Study**

Lastly, a modelling study is carried out to assess the evolution of the ebb-chutes and shields in the present-day Ameland inlet. To this end, a 2DH Delft3D morphodynamic model is developed to identify the modelling capabilities of the most recent state-of-the-art morphodynamic Ameland ebb-tidal delta model. Hence, the natural behaviour of the Ameland ebb-tidal delta is further assessed as well as the onset of ebb-shoals and chutes over the recent years from 2005 – 2020. Furthermore, modelling confidence is built by gradually expanding the simulation horizon to medium- (4 years) and long-term (10 – 12 years) temporal scales (Ch.5). Meanwhile, we highlight the role of an ebb-tidal delta nourishment in the morphodynamic response of the Ameland inlet pre- and post-deployment (Ch.6). The model setup is outlined in Ch. 4 and the results are described in the subsequent chapters Ch. 5 – 7.

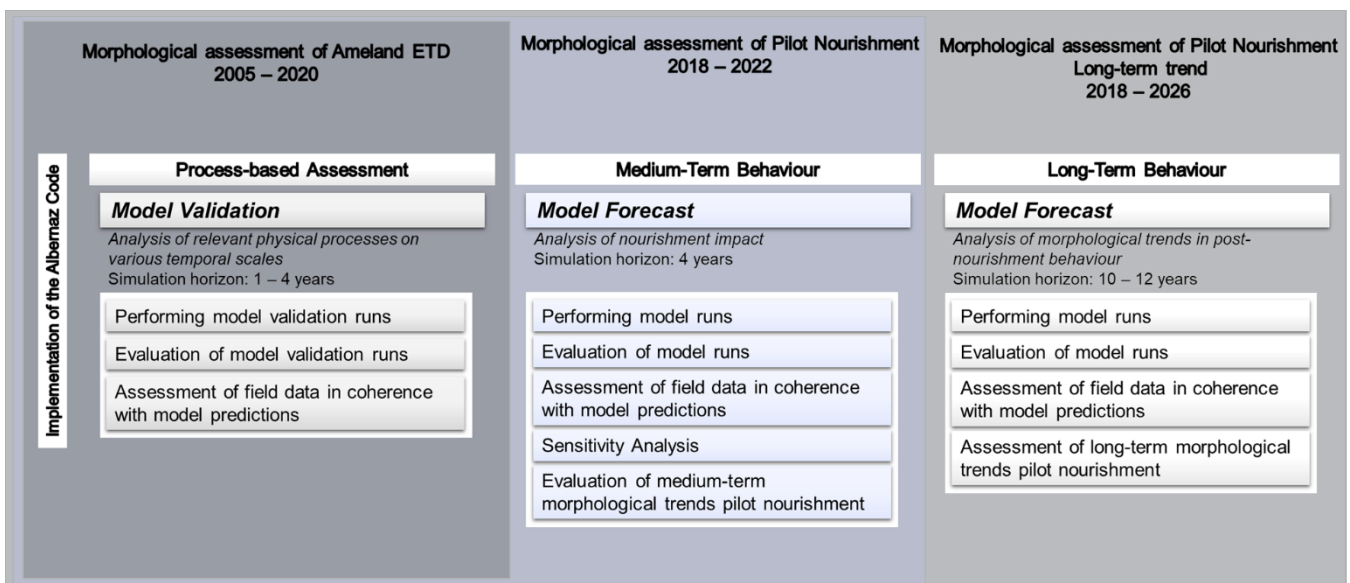


Figure 1-5: Schematic Overview of Research Method.

2 Theoretical Background

This chapter provides an overview of the relevant topics regarding the morphology of tidal inlet systems. The aim of this chapter is to propose a general theoretical foundation that gives insight into the dominant physical processes that shapes the morphology of tidal basins, and associated concepts. Therefore section 2.1 treats the morphology of tidal inlet systems, and section 2.2 discusses the relevant physical processes for the morphological assessment of tidal inlets.

2.1 Tidal Inlet Systems

2.1.1 Classification of tidal basins

Tidal inlets are passages through interrupted sections of barrier coasts. These openings form a connection between coastal shelf sea waters and partially enclosed water masses under the effect of the tidal current. Given the influence of the prevailing tide, *tidal inlets* may be seen as self-maintaining properties of the coast provided that the inlet is in equilibrium (Escoffier, 1940). Moreover, it is common to refer to these partially enclosed waters as *tidal basins*. Depending on the level of wave penetration, these tidal basins can be further classified (after Carter, (1988)):

Tidal lagoons are enclosed from the coastal shelf sea waters by barriers or spits. As a consequence, waves penetration in lagoons is often rather limited. In harmony with the flood and ebb motion of the prevailing tide, tidal lagoons experience tidal inflows and outflows through the tidal inlets between the barriers.

Tidal bays are relatively more open and better connected to the shelf sea and oceanic waters. These tidal basins are characterised by considerable wave penetration but to a smaller – even negligible – degree influenced by fresh water run-offs.

Estuaries may also be typified by their wide and open connection with the shelf sea and oceanic waters. The water motion in estuaries are however governed by the offshore tidal flow and upstream river discharges. In relation, estuaries receive significantly more fresh water inflows than the aforementioned basin types.

2.1.2 Inlet classification

12% of the world's coastlines is characterised by barriers (Bosboom & Stive, 2021). The majority of these coastlines is situated in coastal environments where the tidal motion is comparable or dominating over the apparent wave energy (Mulhern et al., 2017). These environments are also referred to as mixed energy and tide-dominated coastal environments respectively. The shape of distinct attributes of tidal inlet systems may be classified based on the coastal environment wherein they are formed (after Hayes, (1980)) (see Figure 2-1).

The relative influence of the offshore tidal current (expressed in terms of the tidal range) over the prevailing wave-induced flow (i.e. mean wave height) is here seen as a defining property for the morphology of the system:

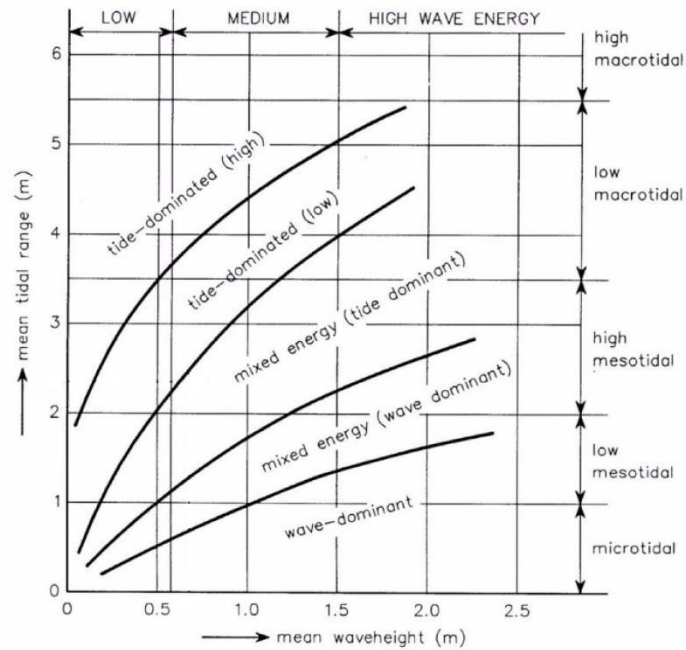


Figure 2-1: Hydrodynamic classification of tidal inlets after Hayes (1980).

2.1.2.1 Barrier Islands in wave-dominated environments

Barrier Islands in wave-dominated environments are characterised by their long-elongated shape and wide or narrow beaches. The island is formed by prior spit formations and the inlet area in between the barrier islands is relatively large. In wave-dominated environments, the ebb-tidal delta is usually small whereas the flood-tidal delta is often prominent.

2.1.2.2 Barrier Islands in mixed-energy environments

Barrier Islands in mixed-energy environments are often wide and short, with relatively small tidal inlets in between. In mixed-energy environment, the ebb-tidal delta is usually large in comparison with their flood-tidal delta. The barrier coast in a mixed-energy environment is often characterised by its drumstick-shaped barriers.

Mixed-energy environments can be further classified in mixed-energy (tide-dominated) and mixed-energy (wave-dominated) environments wherein the emphasis is placed on the characteristic formation of sedimentary features in the tidal basin.

Mixed energy (tide-dominated) barrier coastal settings, provide tidal inlet systems wherein the tidal basin is pronounced creating space for a wealth of secondary channels bordered by spacious intertidal flats. Conversely, for a mixed-energy (wave-dominated) barrier coast setting, the tidal inlet systems show a relatively modest back-barrier landscape wherein a distinct flood-tidal delta is formed (Hayes, 1980).

2.1.3 Morphology of a Tidal Inlet System

The main morphological elements of a tidal inlet system are: (1) an *ebb-tidal (outer) delta*, (2) a *flood-tidal delta*, and (3) an *inlet gorge* amidst of the barrier islands (Figure 2-2a). Strong tidal discharges through the inlet, enables sediment exchange between the shelf sea and the tidal basins (Bosboom & Stive, 2021). Local deposits of sediment could be found where sand has been entrained and displaced by the tide and/or waves. These deposits shape sedimentary features seaward and landward of the inlet gorge on the long-term – *the tidal deltas*. Meanwhile, the strong velocities through the inlet gorge ensures the self-maintaining tendency of the inlet (Escoffier, 1940).

A generalised schematisation of an inlet system is shown in Figure 2-2a with an overview of the primary sedimentary features. The geometry of the tidal inlet system depends strongly on the relative importance of the tidal in- and outflow through the inlet gorge and the wave-induced currents along the barrier coast. This is expressed in terms of a relative relation between the tidal prism P and the littoral drift M_{tot} (after Bruun & Gerritsen, (1959)):

$$r = \frac{P}{M_{tot}}$$

With:

P	The tidal prism	In m^3
M_{tot}	The littoral drift	In m^3/yr

Tidal basins in tide-dominated environments ($r > 300$) have pronounced ebb-tidal and flood-tidal deltas because of their large tidal ranges. The tidal power drives large flow velocities and discharges through the inlet driving the extended formation of the tidal deltas. Conversely, for wave-dominated environments, the wave energy tends to push sediment onshore and halts the offshore extension of the outer delta while promoting a distinct flood-tidal delta (Figure 2-2b).

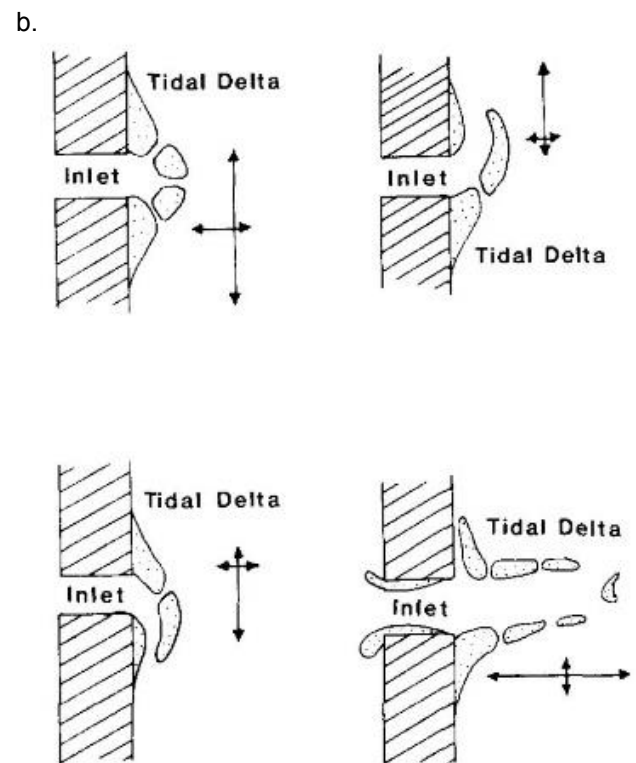
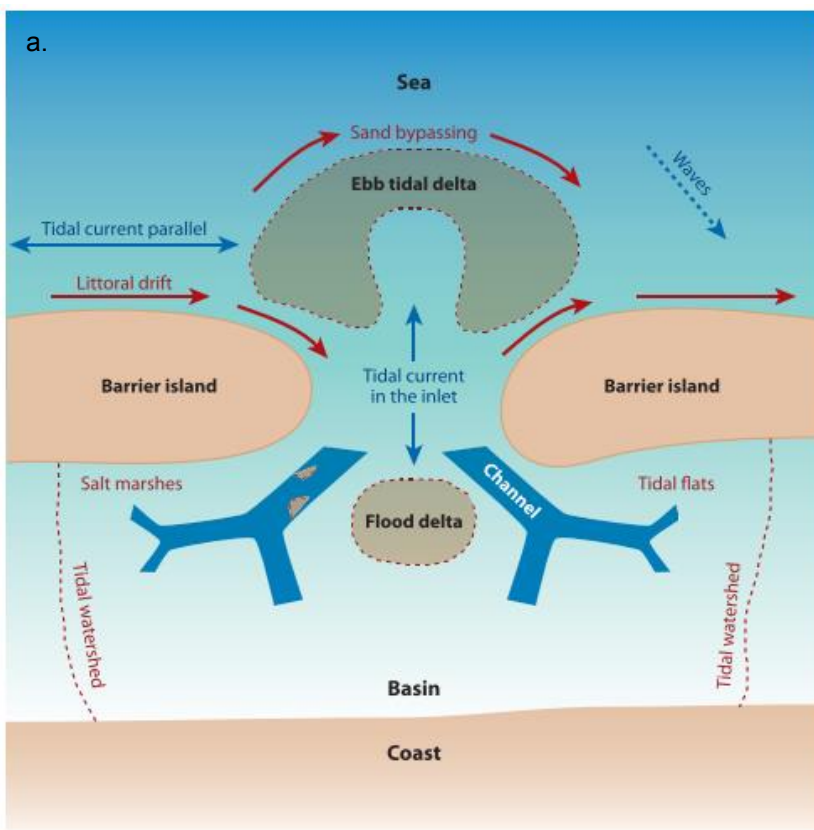


Figure 2-2 A): Schematisation of a tidal inlet system demarcated with the relevant sedimentary features and physical processes (after De Swart & Zimmerman, (2009)). And B): conceptual models illustrating the inlet classifications and associated morphology of ebb-tidal deltas (after Oertel, (1975)).

We can also make a further distinction in the morphological elements that make up the outer delta (Figure 2-3). Marginal channels are located parallel to the adjacent coastlines *along the margin of the main inlet*. The main inlet may also be referred to as the main-ebb channel since the main inlet promotes a central flow through the inlet during ebb. Conversely, during flood water tends to flank around the ebb-directed outflow. Along the *main-ebb channel* local accumulations of sediment may be observed as a consequence to the opposing ebb and flood currents which weld bars along the periphery of the channels. These are referred to as *channel margin linear bars*. Sediment accumulations are also found on the outer delta in the form of *swash platforms* and *swash bars*. These are built by the large accumulations of sand and the swashing of waves. Lastly, the seaward extend of the ebb-tidal delta is characterised by a steep sloping edge, *the terminal lobe*.

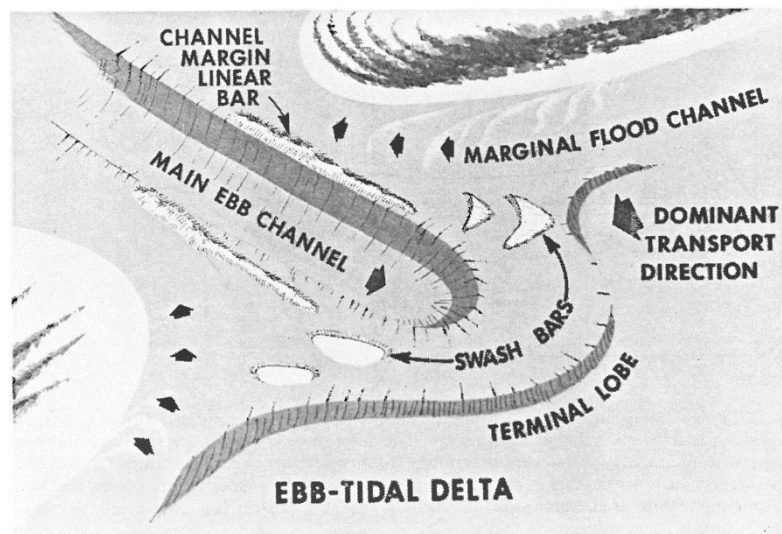


Figure 2-3: A schematised representation of the ebb-tidal delta morphology. Notice on the lower left-hand side of the plot the formation of the arcuate sedimentary deposits due to sediment bypassing processes (i.e. swash bar formation on swash platform). Also observe the formation of the linear bars along the main ebb-channel in the inlet gorge (Hayes, (1980)).

2.2 Relevant Physical Processes

Tidal inlets are commonly located in dynamic environments wherein their associated morphological features are constantly changing under the effects of (non)tidal currents, wave motion and wind. Morphological development may thereby be typified as the result of the interaction between wave motion, sediment transport and changes in the morphology (Wang et al., 2012). A series of phenomenological events which as a collection reflect a particular intrinsic behaviour of a system is also referred to as a physical process. This section gives insights into the relevant physical processes associated with the morphological development of tidal inlets.

2.2.1 Sediment Bypassing

A physical process relevant to the Ameland ebb-tidal delta is the *sediment-bypassing mechanism*. Sediment bypassing is the exchange of sediment over the outer delta (Bosboom & Stive, 2021). The combined effect of wave-induced currents, tidal throughflow and shore-parallel tidal currents promote hereby a particular sediment recirculation pattern on the outer delta. Depending on the relative importance of the tidal currents over the wave-induced current, different sediment bypassing mechanisms may become relevant for the inlet system (Oertel, 1972).

Bruun & Gerritsen, (1959) described in their study natural sediment bypassing mechanisms which they observed through aerial registrations of bar migrations along inlet systems. Here, they found that the sediment-bypassing is a function of the magnitude of the littoral drift and the magnitude of the tidal inlet current. For a ratio of littoral drift over the inlet current in the order of 10 – 30, the primary bypassing mechanism is flow-bypassing. For ratios in the order of 200-300 or larger, the primary bypassing mechanism is bar-bypassing over the periphery of the ebb-tidal delta.

More detailed concepts of sediment bypassing mechanisms were later derived by Bruun & Gerritsen, (1959), where it was further subdivided in three underlining processes (Herring & Winter, 2018):

- Flow bypassing and bar welding
- Sediment circulation
- and Ebb-tidal delta periphery bypassing

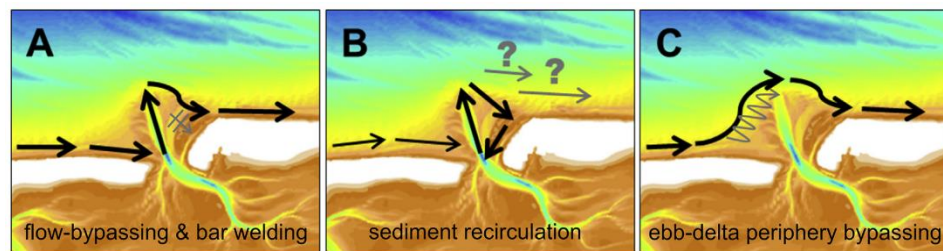


Figure 2-4: Three principal sediment bypassing mechanisms as described by Bruun & Gerritsen (1959) (source Herring & Winter, (2018)).

1. Flow bypassing and bar welding

This mechanism entails the transport of sediment as a consequence to the wave-induced littoral drift and tidal currents. Sediment at the updrift side of the inlet is transported by the inlet to the back-barrier basin where by means of strong ebb-dominated currents sediment is dispersed on the ebb-tidal delta (Figure 2-4a). On the ebb-tidal delta, waves stir the sediment deposits and in combination with the shore-parallel currents form arcuate⁸ bars which move along the periphery of the outer delta where they either:

- weld to the downdrift coast;
- create local accumulation on the swash platform;
- or migrate alongshore.

2. Sediment Recirculation

In the case of sediment recirculation, sediment advected by the littoral drift is also deposited on the ebb-tidal delta via main ebb-channel discharges. Also, here sediment is moved by means of wave-induced transport and shore-parallel currents along the outer delta margin in the form of arcuate swash bars. At the downdrift swash platform, these sedimentary accumulations are directed back to the inlet gorge where it is reintroduced to

⁸ *arcuate* refers here to the curved shape of the local sediment accumulations.

the main ebb-current and supports the maintenance of the downdrift ebb-tidal delta morphology (Figure 2-4b).

3. Ebb-tidal delta Periphery Bypassing

The periphery bypassing mechanism describes the transport of sediment by means of wave-induced processes (Figure 2-4c). Sediment from the updrift side of the inlet is transported in the form of bar formations along the ebb-tidal margin towards the downdrift coast.

2.2.2 Preferential Orientation of Main Inlet

Interaction between the currents induced by waves and tides are important for the manner wherein the ebb-tidal delta develops (Sha, 1989). That is, depending on the relative magnitude of the different processes, the main-ebb channel may become asymmetric in shape due to variations in the marginal⁹ flows.

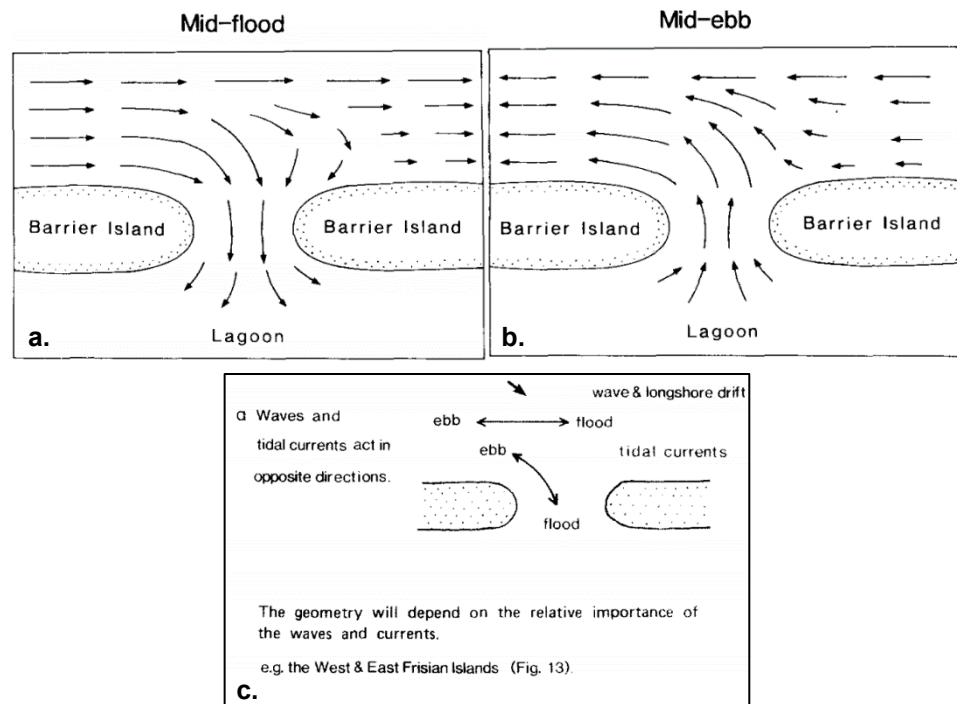


Figure 2-5: (a-b) Schematic representation of the interaction between the shore-parallel currents and the onshore- offshore tidal flow through the inlet. In this schematisation, the tidal wave propagation direction is in eastward direction (to the right). The littoral drift is in the same direction, such that updrift is west and downdrift is east of the inlet. (c) Conceptual model describing the effect of different processes on the development of the ebb-tidal delta (after Sha, 1989).

During flood tide, the combination of the shore-parallel flood currents and the flood-directed tidal inlet current creates an enhancement of the updrift marginal flood flows (Figure 2-5a). At the downdrift side the dominant inlet flow invokes a reversal on the prevailing flow patterns. During ebb, the shore-parallel currents are reversed, and the main-inlet current is ebb-directed. Also in this case, the updrift (i.e. west) side of the inlet shows an enhancement of the prevailing current. And, at the downdrift side the local currents are reduced due to a difference in direction between the inlet current and the shore-parallel currents (Figure 2-5b).

⁹ *Marginal* refers here to the flow flanking the main-ebb channel. (viz. directly updrift and downdrift from the inlet gorge).

As a result, over the tidal cycle, the confluence of the two tidal currents enables the emergence of a downdrift recirculation flow (Figure 2-5a/b).

If the tidal prism is large – indicative to the Ameland Inlet – the orientation of the ebb-tidal delta is dependent on the interaction between the tidal currents and the wave-induced longshore drift. For small phase differences between the shore-parallel tidal currents and the inlet current, an updrift flow enhancement is prevalent such that the main ebb-channel rotates in opposite direction of the littoral drift (Sha, 1989 - see also De Swart & Zimmerman, 2009). Hence, the ebb-tidal delta is ought to accumulate further seaward at the downdrift side than at the updrift side – and the ebb-tidal delta is said to be *updrift asymmetric in shape*. Consequently, the main-inlet will always try to align towards its preferential direction to the northwest.

The preferential updrift direction of the main-inlet does not reflect however the overall process of channel relocation on the outer delta. Wave-induced littoral drift and wave action enables the formation of shoals and swash bars on the downdrift side of the ebb-tidal delta. While these migrate along the periphery of the outer delta under the effect of sediment bypassing processes, they interact with the main-ebb channel and invoke a clockwise migration of the channel. Meanwhile, partial infilling of the main-ebb channel reduces its hydraulic efficiency and may result in the abandonment of the channel. At this point, the outer delta morphology is characterised by the formation of a new main-ebb channel. For this main ebb-channel its orientation aligns with the general perception of Sha,(1989) and is updrift oriented.

Conversely, if the tidal prism is small, the morphology of the ebb-tidal delta is dependent on the shore-parallel tidal currents, the littoral drift and the obliquely incident waves. Here, the orientation of the main ebb-channel is defined by the effects of sediment bypassing and the littoral drift which create accumulation of sediment at the updrift side of the tidal inlet. As a consequence, the ebb-tidal delta will build out further seawards at the updrift side of the inlet – the ebb-tidal delta is said to be downdrift asymmetric.

In case of a large phase differences ($\varphi \approx 90^\circ$), the interaction between the two tidal currents invokes small to nil enhancement of the prevailing currents. The tidal in- and outflow may be fairly symmetric (i.e. north-south flow) such that the ebb-tidal delta may develop almost symmetric around the tidal inlet (De Swart & Zimmerman, 2009).

2.2.3 Cyclicity Of Ameland Ebb-tidal delta – Previous Understanding

Under the effect of hydrodynamic and sediment bypassing processes the morphology of ebb-tidal delta is continuously changing in shape and amplitude. Sediment-bypassing enables the emergence of arcuate bar formations on the outer delta which interact in turn with the morphological features of the ebb-tidal delta. These bar formations may weld with larger morphological features which motivates the maintenance of larger features such as larger shoals and swash platforms. But these bars may also attach towards the coast by means of a variety of processes.

Up to the late 20th centuries, it was argued by coastal researchers that the *repetitive* emergence & attachment of bars and channel-bar interactions was seemingly cyclic in nature (see for example Israel & Dunsbergen, 1999). Conceptual models have been derived by amongst others FitzGerald (1988) to exemplify this cyclic behaviour of sediment bypassing and main-channel migration. Here, Fitzgerald described the cases of *ebb-tidal delta breaching*, *outer delta breaching* and *stable inlet processes* (after FitzGerald, 1988 – Figure 2-6):

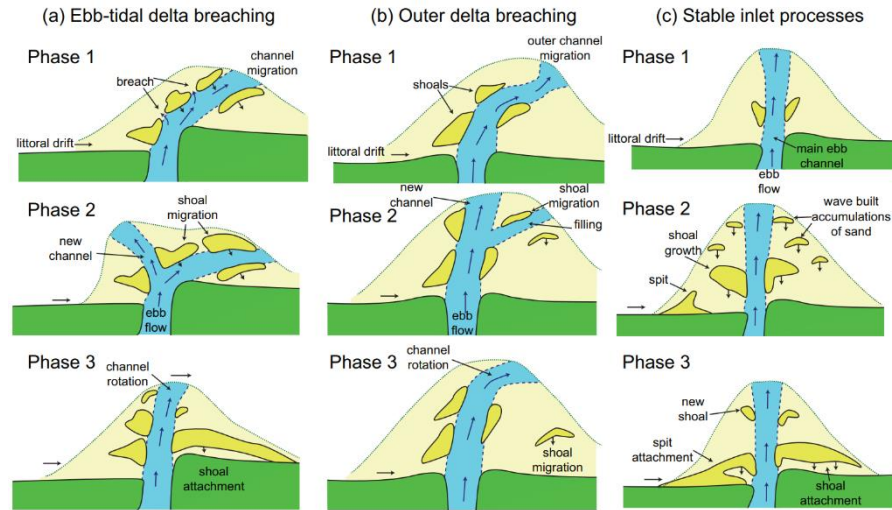


Figure 2-6: Conceptual models illustrating the previous understanding of ebb-tidal delta behaviour and the respective stages of cyclicality (after Fitzgerald, 1988).

Ebb-tidal delta breaching

In the case of ebb-tidal delta breaching, the littoral drift promotes the updrift accumulation of sediment on the western side of the inlet (Figure 2-6a). These accumulations shift the ebb-tidal asymmetry as the main ebb-channel – extending towards the delta margin – starts to rotate (Figure 2-6a, upper panel).

In the **second phase**, the formation and migration of bars and shoals forces the main ebb-channel to rotate even further. At a certain maximum rotation, the main ebb-channel tends to breach through the updrift bar formations, creating a new – more aligned – channel (Figure 2-6a, middle panel).

In the **third phase**, the growth of shoals and bars and the subsequent migration of these bars towards the downdrift coast, creates gradual infilling of the previous channel and the formation of bar welding. Finally, these bars travel towards the coast where they eventually merge (Figure 2-6a, lower panel). At the updrift side the sediment deposits cater again the formation and growth of new bars such that a cyclic behaviour prevails.

Outer delta breaching

Instead of ebb-tidal breaching, the main ebb-channel can also breach at the outer margin of the ebb-tidal delta – the so-called outer delta breaching. Here, the outer channel migrates and dissects further away from shore (Figure 2-6b).

Stable Inlet Processes

Lastly, in the case of a stable inlet (i.e. dominance of tidal inlet currents over littoral drift) the main ebb-channel attains its position throughout the phases of cyclic behaviour. Ebb-tidal deposits due to the sediment bypassing over the margin of the ebb-tidal delta enables the growth and formation of arcuate bars that migrate towards shore where they weld with the coastline (Figure 2-6c).

Subsequent conceptual models were further derived for several inlet systems of the West-Frisian Island coast. Israel & Dunsbergen (1999) provided a conceptual model for the Ameland Inlet based on a limited selection of bathymetric charts illuminating a seemingly 4-phase cyclic behaviour of the Ameland Inlet system (Figure 2-7).

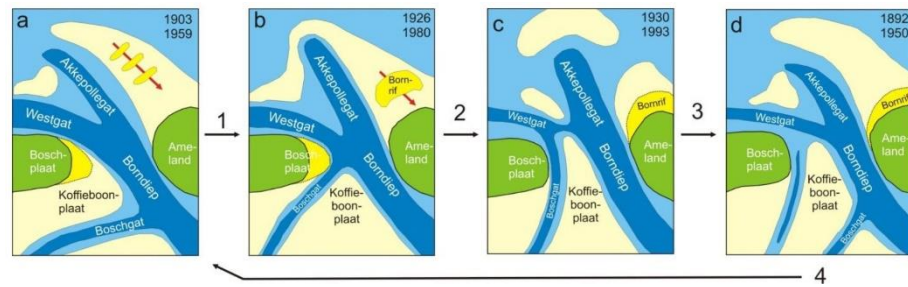


Figure 2-7: Conceptual model for the Ameland Inlet describing the different phases of its cyclic behaviour. The full cycle was claimed to have a typical recurrence of 50 - 60 years (after Israel & Dunsbergen, (1999)).

Phase 1: Channel Rotation and Shoal Migration (1-Channel System)

In the first phase, the ebb-channel rotates anticlockwise towards the coast of Terschelling under the effect of bar and shoal migration at the downdrift swash platform. Eventually the ebb-channel (i.e. the Westgat) breaches through the downdrift located deposits where a secondary channel emerges – the Akkepollegat (Figure 2-7a).

Phase 2: Development of Secondary Channel (Emergence of 2-Channel System)

The growth and landward migration of the shoals north from the Westgat, promote a partial infilling and landward migration of the Westgat. Subsequently, a further development of the Akkepollegat may be observed (Figure 2-7b). In the inlet, a second channel prevails along the margins of the Terschelling coast (i.e. Boschgat).

Phase 3: Secondary Channel Building and Rotation (2-Channel System)

In the third phase, the Boschgat becomes deeper and the Akkepollegat builds out further – a fully-developed channel prevails in the inlet. The Akkepollegat rotates at the outer delta margin whereas the Westgat observes continuous infilling from traverse bar formations that migrated seawards at the coast of Terschelling. Due to the formation of the Boschgat and the tidal currents, a channel margin linear bar is formed along the Westgat (Figure 2-7c).

Phase 4: From secondary channel to Main ebb-channel (transition from 2 to 1-Channel System)

The Akkepollegat becomes the main ebb-channel and migrates towards the coast of Ameland due to formations of a large shoal deposit at the updrift swash platform. At the same time the strong updrift asymmetrical shift of the morphology pushes the outer delta westward. Meanwhile, the Akkepollegat tends to create a new extension through the Westgat in an attempt to restore the preferable updrift direction of the ebb-channel (Figure 2-7d).

2.2.4 Cyclicity of Ameland Ebb-tidal delta – A Revised Understanding

Based on the up-till-now available data a 4-phase cyclic behaviour of the Ameland Inlet was deemed to be the most plausible synthesis on the prevailing events. The limitations of previous conceptual models for the Ameland inlet was however the availability of representative datasets for detailed analyses on the dynamics of the Ameland inlet. Recent studies based on high-resolution extended datasets has subsequently shed a different light on the cyclicity in the behaviour of the Ameland inlet (see Elias et al. (2019) for a further understanding of the dynamics of the Ameland inlet, and Herrling & Winter, (2018) for a discussion on sediment bypassing and cyclicity).

Elias et al (2019) illuminated the particularities of the sediment bypassing mechanism underlying the intricate dynamics of the Ameland Inlet. Up to the early 20th century, the Ameland inlet was characterised by a recurrent process of outer channel breaching along the margins of the ebb-tidal delta (see Sec. 1.2.2). Prior manmade interventions to the Ameland inlet system resulted in an eastward migration of the main-inlet and a subsequent confinement of the main-inlet to the Ameland coast. After a regime shift around 1926, the system changed from outer delta breaching to main-ebb channel switching. Under the new geomorphic regime, the role of main ebb-outflow has exchanged alternatively between the Westgat and the Akkepollegat. In between the switching of main-ebb channel instabilities may arise that grow out into ebb-chutes and shield formation on the ebb tidal delta. Once these formations are present, their development follows from a description of the underlying physical processes and is fully deterministic. However, the spatial and time-dependent criteria for the onset of ebb-chutes and shields following from a small-scale instability may not be so deterministic at all. More precisely, the trigger for ebb-shield development is rather stochastic and depends on the history of the morphology, and the apparent order wherein underlying physical processes prevail. These are stochastic processes that change depending on subtle nuances in the morphology of the inlet system.

In the more recent bathymetries – starting from 2005 – the first onset of an ebb-chute and shield formation has been observed in bathymetric data of the Ameland ebb-tidal delta. Elias et al., (2020) described this formation and the associated onset of a new sediment-bypassing cycle in a conceptual 2005 – 2019 model for the Ameland Inlet incorporating multiple stages of development (Figure 2-8).

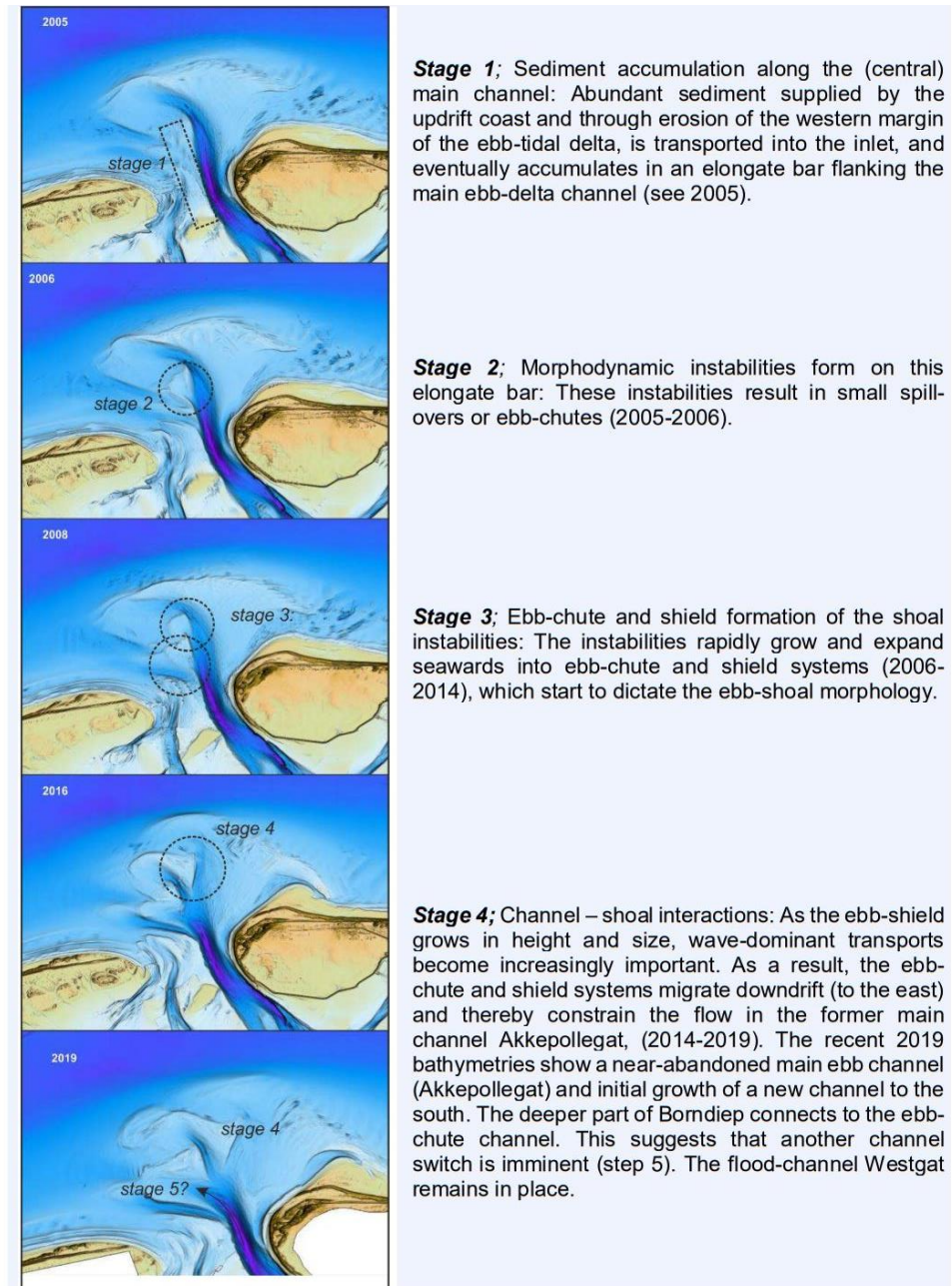


Figure 2-8: Multiple stages of development of a chute and shield system, and the initiation of a new sediment bypassing cycle (Elias et al., (2020)).

3 The Study Area

This chapter discusses the study area of this research, based on literature review and available datasets. In section 3.1. the study area is introduced. In section 3.2. an overview is provided of the hydrodynamic setting of the Ameland inlet, and Section 3.3. highlights the morphodynamic development of the Ameland inlet over the more recent years (2005 – 2020).

3.1 General Setting

The Wadden sea is connected to the North Sea and consists of a series of tidal inlets, from west to east: the Texel inlet, the Eierlandse gat, the Vlie inlet, the Ameland inlet and the Friesche Zeegat. The Ameland Inlet is the centrally located inlet in the West Frisian island chain, bordered by the Ameland Coast on the east and the Coast of Terschelling on the west (Figure 1-1).

The morphology of the Ameland inlet is governed by an interplay between tide-related and wave-driven processes (Elias et al., 2020). With typical tidal ranges up to 3 m and average significant wave heights around the 1.4 m, the Ameland Inlet may be classified as a mixed energy environment (Hayes, (1980) & Davis & Hayes, (1984)). Following the classification of Davis & Hayes, (1984), the relative importance of waves changes for the case of the Ameland inlet over the spring-neap cycle. During spring tide, the tidal range increases up to 3 m which places the Ameland inlet in the category of mixed energy – tide-dominated environments during spring tide. Conversely, during neap-tide the tidal range decreases to about 1.5 m which makes the Ameland inlet a mixed energy – tide-dominated environment during neap tide.

This could partially be observed by the appearance of a deep inlet and a large ebb-tidal delta (Elias, 2017). Also the presence of a large and stable inlet with short and drumstick-shaped coastlines is characteristic to mixed energy inlet systems such as the Ameland Inlet (Hayes, (1980) and see also Sec. 2.1.2).

Moreover, the inlet has a prominent ebb-tidal delta and a back-barrier basin with a length of 30 km and surface area of 270 km² (Elias, 2017). Further investigation on the Ameland ebb-tidal delta shows that the morphology of the outer delta is updrift asymmetric (Figure 2-12).

It should be noted that for the Frisian Islands the littoral drift is directed towards the east (i.e. from Texel to Schiermonnikoog); Estimates of the littoral drift at the coast of Terschelling and Ameland vary between the 0.5 – 0.6 Mm³/year (Tanczos et al., 2001).

3.2 Present-day Morphology of the Ameland Inlet

A concise overview is provided here of the relevant morphological features of the present-day Ameland ebb-tidal delta. To this end, the 2021 bathymetry of the Ameland inlet is taken as reference for the present-day morphology provided that the bathymetry is representative to the current layout of the Ameland inlet (Figure 3-1). The pilot nourishment may be seen on the periphery of the second ebb-shield [8] and is subsequently demarcated in the figure [22]. In the inlet gorge, the main ebb-channel (i.e. Borndiep) [1] can be observed at the east of Terschelling and close to the west of Ameland. On the outer delta, the Borndiep extends into the main-ebb outflow – the Akkepollegat [7]. The Akkepollegat is bordered by two ebb-chute and -shields – the second [9] and the new Akkepollegat [10]. These may be found on the updrift central part of the main swash platform and to the north of Westgat [6] – the Kofmansbult [11]. Right downdrift of these ebb-chute and shield another large swash platform may be allocated – the Bornrif platform [12].

In the 2021 bathymetry, the inlet is characterised by a 2-channel configuration showing the formation of a secondary inlet channel at the east side of the coast of Terschelling – the Boschgat [4]. The Borndiep [1] and the Boschgat [4] are separated by a large shoal platform in the inlet – the Zeehondenplaat [16]. Lastly, several shoal attainments may be allocated in the present-day Ameland morphology. At the coast of Terschelling a shoal attainment is present – the Boschplaat [18] – whereas at the coast of Ameland Bornrif strandhaak [14] and Bornrif bankje [13] may be found.

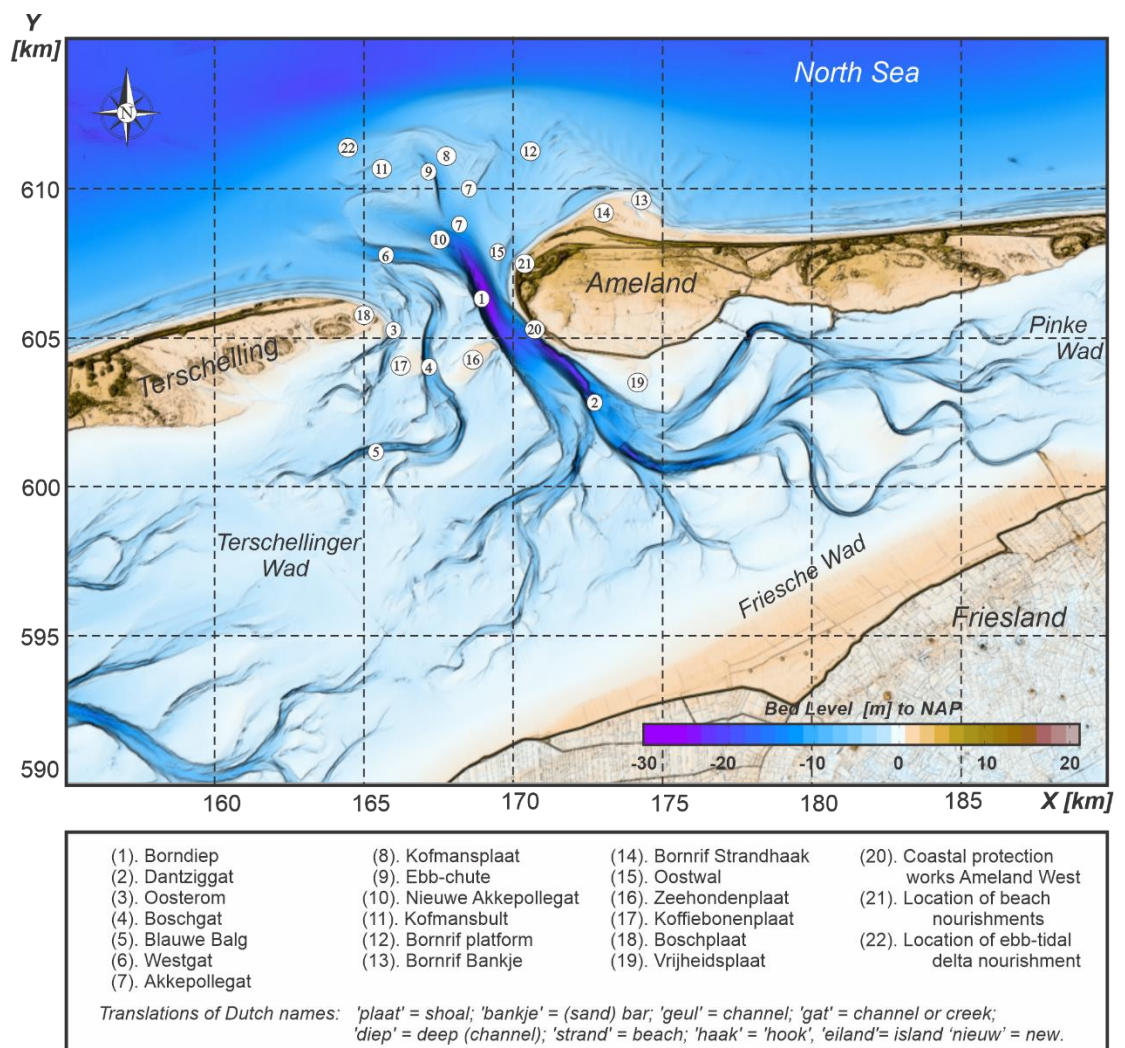


Figure 3-1: Overview of the morphological units, characteristic for the present-day morphology of the Ameland inlet (after Elias et al. (2021)).

3.3 Hydrodynamic Forcing

3.3.1 Water Level Variations

The tidal sea surface oscillation at the Ameland inlet is mainly generated by the North sea tide (Elias, 2017). As a coastally trapped Kelvin wave, the tidal wave is propagating along the Dutch coast from south to north. As the tidal wave approaches Den Helder, this wave interacts with a second eastward propagating tidal wave. The combination of these tidal oscillations provides an intricate tidal signal which travels along the Wadden sea inlets from the Texel inlet in the west to Friesche Zeegat in the east.

The resulting tidal signal is characterised by a mean tidal range of 1.4 m at Den Helder which increases in the direction of the Ameland inlet up to a tidal range of 2.15 m. The main constituents driving the tidal motion is the semi-diurnal lunar M2 tide (amplitude: 0.77 m) and the semi-diurnal solar S2 tide (amplitude: 0.2 m). Due to shoaling effects in the nearshore region where the tide propagates, the first overtide M4 provides a distinct asymmetry in the tidal signal with an amplitude of 0.05 m (Elias et al., 2019).

Tide-related water level variations are measured at three stations in the vicinity of the Ameland Inlet: the Terschelling North Sea station, the NES station and the Holwerd station. Figure 3-2 shows the tide-related water level variation for the month of January 2016. An overview of the main tidal constituents (Figure 3-3) is found based on the t-tide analysis (Pawlowicz et al., 2002) on the water level signal as shown in the previous figure.

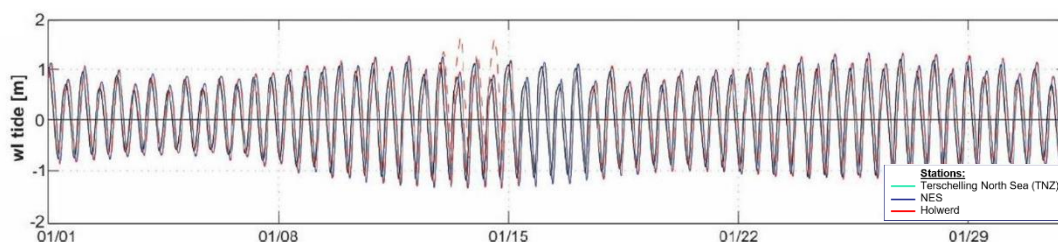


Figure 3-2: Tidal water level variations in the month of 2016 derived from station records of TNZ, NES and Holwerd stations (source: Elias, (2017)).

Constituent		Amplitude		Phase
Name	ϕ	[m]		[deg]
M2	28.98	0.86		234.07
S2	30.00	0.24		296.12
N2	28.44	0.15		211.71
O1	13.94	0.10		206.38
M4	57.97	0.08		330.04
K1	15.04	0.07		0.53
L2	29.53	0.07		237.37
K2	30.08	0.07		295.26
MU2	27.97	0.06		321.76
MS4	59.98	0.05		42.08
SSA	0.08	0.05		233.59
M6	86.95	0.05		60.42

Figure 3-3: Overview of the 12 significant tidal constituents making up for the North Sea tidal water level variation at the water level stations TNZ, NES and Holwerd in the month of January 2016 (source: Elias, (2017)).

These water levels are only derived from tide-related water level oscillations. The offshore water level at the Ameland inlet is also governed by wind-related and atmospherically-induced setup differences (Elias et al., 2020). These setup variations can become significant during storm events with additional water level variations up to 1.5 m.

3.3.2 Wave Climate

The Ameland ebb-tidal delta is a mixed-energy environment governed by wave and tide-related processes. The wave climate primarily consists of wind-generated surface gravity waves generated in the shallow North Sea basin (Elias, 2017). Relevant wave data for the Ameland inlet is hereby provided by long-term wave buoy measurements at the station Eierlandse Gat (ELD) and Schiermonnikoog (SON) since 1979. Moreover, two dedicated wave buoys were also stationed at the Ameland inlet from 2007 – 2017 to measure the local wave characteristics. Figure 3-4 shows the wave roses based on the aforementioned datasets. A comparison between the four wave roses highlights the close resemblance of the Schiermonnikoog dataset with the local observations of the AME station. Given the latter consistency, it is acknowledged by Elias et al., (2020) that the application of the extensive SON wave data would be beneficial as basis for the process of generating wave climate schematisations.

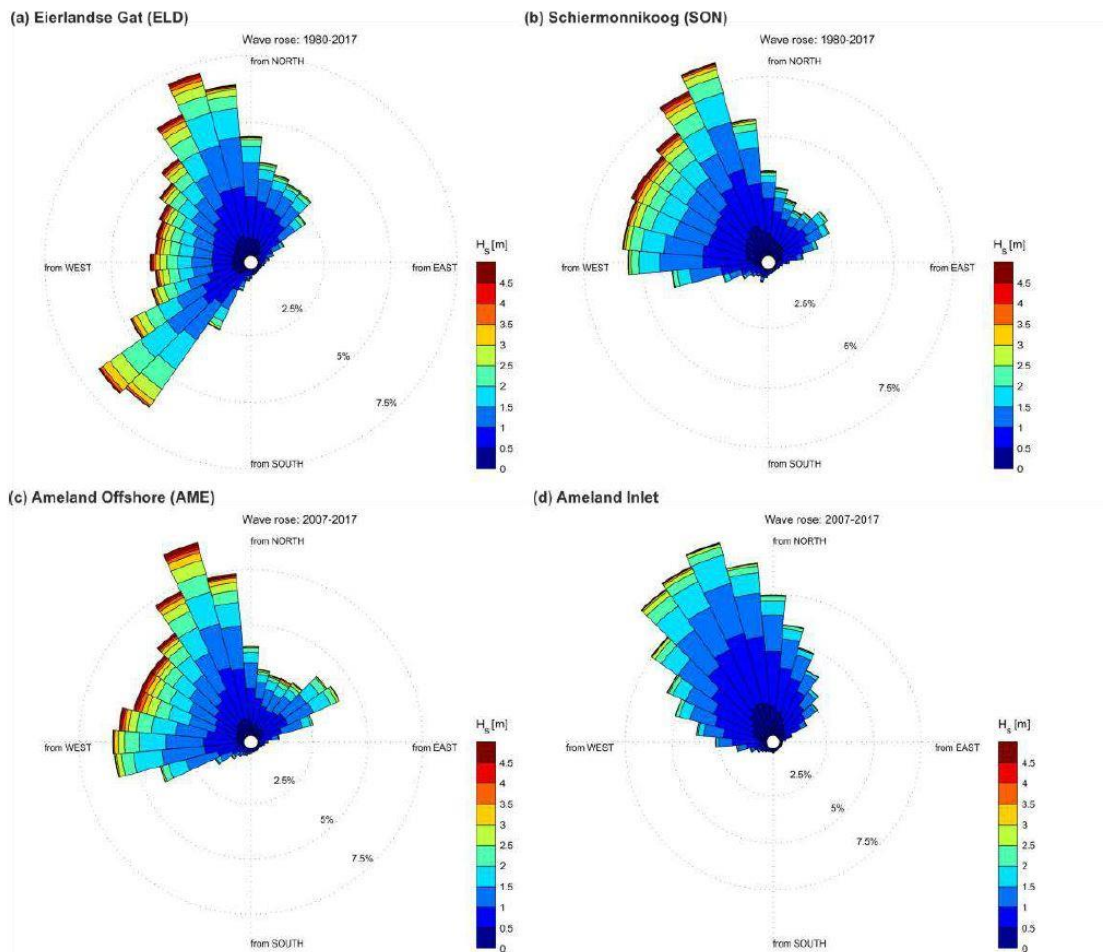


Figure 3-4: Wave roses for stations Eierlandse Gat (ELD), Schiermonnikoog (SON), and the dedicated measurement stations Ameland offshore (AME) and Ameland inlet (after Elias, (2020)).

3.4 Morphological development of characteristic periods

3.4.1 Behaviour 1926 - 2005

This section follows the data analysis of Elias et al., (2019) on the Ameland ebb-tidal delta morphology. Moreover, an overview is provided on the morphological development of the Ameland inlet between 1989 – 2020 and a particular interest is raised on the formation of ebb-chutes and -shields over this period. Therefore, the behaviour before and after the regime shift is separately discussed in the following paragraphs.

Ameland ebb-tidal delta between 1926 – 1989

The regime shift around 1926 instigated a transition in the geomorphic behaviour of the Ameland ebb-tidal delta from outer-channel shifting to main ebb-channel switching (Figure 1-3 and Figure 3-5). As a result of prior anthropogenic interventions to the tidal basin, the tidal divides migrated eastwards leading to the eastward relocation of the main-inlet. Defence works on the coast of Ameland thereby contributed to the attainment of the main-inlet to the Ameland over the successive years (e.g. years 1926 – 1940 (Figure 1-3), and 1950 – 1985 (Figure 3-5). Meanwhile, the Ameland inlet was characterised by a main-inlet [1] (i.e. Borndiep), a main ebb-channel [7] (i.e. Akkepollegat) and a marginal flood channel [6] (i.e. Westgat). It may be argued that the Westgat in these years must have been flood-dominant provided that in the bathymetries of late 20th century Ameland Inlet, no prominent ebb-shield was formed. The formation of a submerged bar along the connection between the Westgat and the Akkepollegat may also have been an indicator for the flood-dominant character of the Westgat.

Furthermore, may be seen from the bathymetric charts from 1892-1940 that the location of the Westgat and the Akkepollegat were rather consistent over the years following 1926. The Westgat maintained is west-northwest orientation and the Akkepollegat was northwest oriented while extending towards the outer delta margin. A clear updrift asymmetric shape was thereby apparent in the morphology of the outer delta.

From 1958 onwards to 1985, Westgat increased further in size and depth (Elias et al., 2019). Akkepollegat became partially filled in with sediment around the periphery of the main-ebb outflow and the updrift and downdrift shoal platforms connected creating a large unified outer delta front. A long, elongated bar aligned thereby the Westgat, which temporarily sheltered the coast of Terschelling from storm wave events. This enabled the strong growth of the Boschplaat that protruded well into inlet (Figure 2-11). Due to the siltation of the Akkepollegat, the Westgat became in that time the main-ebb outflow of the Borndiep.

Ameland ebb-tidal delta between 1989 – 2005

Although Westgat retained its size in depth over the years following, from 1989 onwards Westgat started to lose its connection with the Borndiep (Figure 3-6). Moreover, a large shoal was situated in the inlet in that time and extended well northward. As a consequence, the connection between the Westgat and Borndiep further reduced. Temporarily, the Westgat was able to connect directly to the Boschgat (i.e. 1993/1996). Due to the constriction of the Akkepollegat, the channel had ample space to increase in size and depth such that the Akkepollegat reinstated its function as main-ebb outflow of the Borndiep. Westgat switched again over the course of 1989 – 2009 from ebb-dominant to flood-dominant channel. Due to the reduced connection between Borndiep and Westgat in the intermediate time and the increase in size of the Akkepollegat, shoals started to develop north of Westgat (i.e. 1999 – 2005).

3.4.2 Recent Morphological Behaviour 2005 – 2020

A linear bar formation developed along the periphery of the main-ebb outflow Akkepollegat north of the Koffiebonenplaat [17]. Due to strong flow bypassing to the outer delta margin, the downdrift swash platform Bornrif platform [12] increased in size and – in combination with the preferential direction of the inlet – shifted the outer margins of the Akkepollegat westward (Figure 3-6). The presence of the channel margin linear bar prevented an updrift oriented rotation of the Akkepollegat to accommodate the growth of the Bornrif platform. Consequently, small instabilities were issued along the channel margin linear bar. Under the continuous pressure of the prevailing tidal throughflow multiple series of instabilities enabled the growth of ebb-chutes and -shields (i.e. 2006, 2008, 2014). The first ebb-chute and -shield [8] chute after the occurrence of the regime shift was observed on recent bathymetric maps of 2006. 2008 was the demarcation point for the onset of the second ebb-chute and -shield formation [9]. Due to its size, it largely absorbed the formation of the first ebb-chute and -shield making it the distinct feature of the central ebb-delta platform in recent bathymetries (i.e. 2008 – 2011). Around 2014, a third ebb-chute and -shield [10] formed in between the second ebb-chute and the Westgat. This shoal expanded rapidly in the northwest direction and rotated clockwise which gave rise to a large northward extension of its ebb-shield. The latter further confining the flow through the Akkepollegat. Around 2014 – 2016, the clockwise migration of the second ebb-chute and the new Akkepollegat [10] imposed a likewise rotation of the Akkepollegat associated with a partial infilling. The latter displacements enabled the migration and attachment of a part of the Bornrif platform to the Ameland coast – the Bornrif Bankje. Over the course of 2014 – present the third ebb-chute is observed to be steadily increasing in size. As the Akkepollegat is directed to the north-northeast in the present morphology – away from its preferential direction – and reduced its hydraulic efficiency by partial infilling from the adjacent shoals it may be argued if the Akkepollegat will remain the main ebb-channel in the present-day morphology of the Ameland inlet. Based on past channel relocations and given the rapid deepening and growth of the third ebb-chute after its emergence in 2014 it might be argued that the third ebb-chute may take over the role as main ebb-channel from the Akkepollegat over the coming years. This ebb-chute may ultimately merge with or connect to the Westgat (Elias et al., 2020).

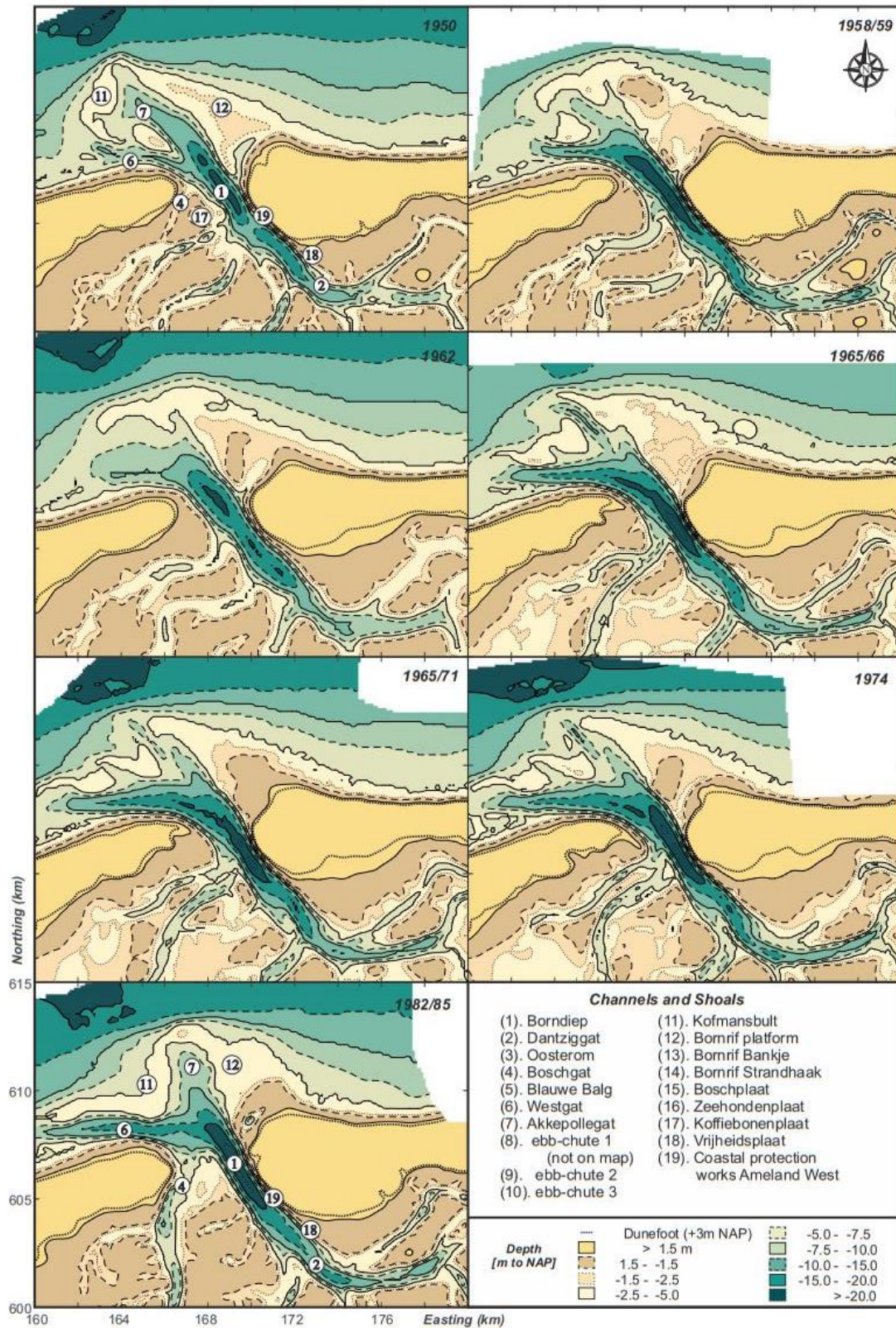


Figure 3-5: Bathymetric charts of the Ameland Inlet for the period between 1950 and 1985 (after Elias et al. 2019).

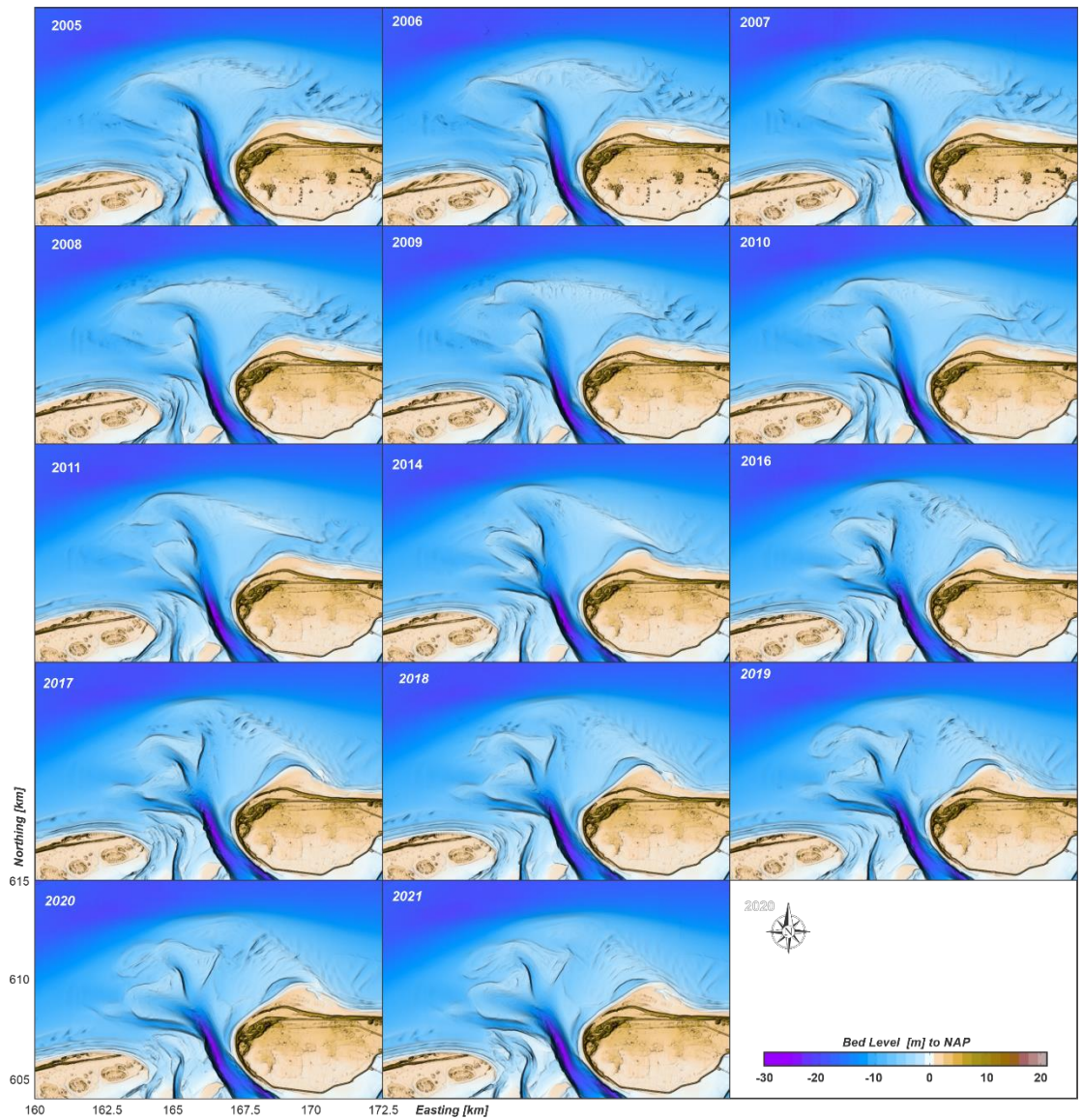


Figure 3-6: Overview of digital elevation maps for the Ameland ebb-tidal delta over the time span from 2005 - 2021 (after Elias et al. (2021)).

3.4.3 Pilot Nourishment

The Dutch Ministry of Infrastructure and Water Management started in 2015 with the knowledge and research programme Coastal Genesis 2.0 (KustGenese 2.0). The objective of this programme was to stimulate the knowledge development on the Dutch Coastal system in the context of future flood safety of the Dutch coast against increasing hydrological stressors. In order to establish a future-proof coastal management and maintenance strategy for the near-future time horizon after 2020, the efficacy of current-applied maintenance strategies was further investigated. In 2020, the research programme was finalised, and the conclusions were synthesised in a new coastal management policy. In the context of the Ameland inlet system, this involved the construction and assessment of the impact of a pilot nourishment to the Ameland ebb-tidal delta.

Starting from 2018, frequent bathymetric measurements has been taken (e.g. Rijkswaterstaat Vaklodingen) to monitor the volumetric changes during the construction of the pilot nourishment (Figure 6 3). Over the course of 2018 to 2019 (i.e. Stage A to B) the nourishment volume increased on average with 0.4 million m³/month leading towards the final volume of 4.9 million m³ of sand in the nourishment polygon. Stage B demarcates hereby the completion of the construction phase. From 2019 onwards, gradual erosion of the pilot nourishment was observed (i.e. from Stage B to C). In the first months right after the construction, a persistent erosive trend was apparent in the order of 0.1 million m³/month. This trend further intensified over the winter period between 22-11-2019 and 27-03-2020 (i.e. Stage C) where storm waves induced large erosion on the nourishment volume in the amount of 0.8 million m³. Over Stage C, the mild climate erosion trend reinstated with a general amount of 0.2 million m³ erosion/quarter.

The onset of the pilot nourishment in the polygon can also be observed on the basis of a bathymetric analysis. Lambregts (2021) has shown that the pilot nourishment morphology is initially driven by the shore-parallel currents. These currents promote the formation of local sedimentation along the periphery of the second ebb-shield. The secondary response of the pilot nourishment is characterised by the migration of bars around the outer margin of the second ebb-shield. Wave-induced processes instigated thereby the formation and landward migration of these sand bars whereas the shore-parallel tidal currents reinforce an eastward displacement of the sand bars in to the second ebb-chute. Figure 6 4 shows the timely response of the pilot nourishment after construction and its associated bathymetric changes over stages A to D.

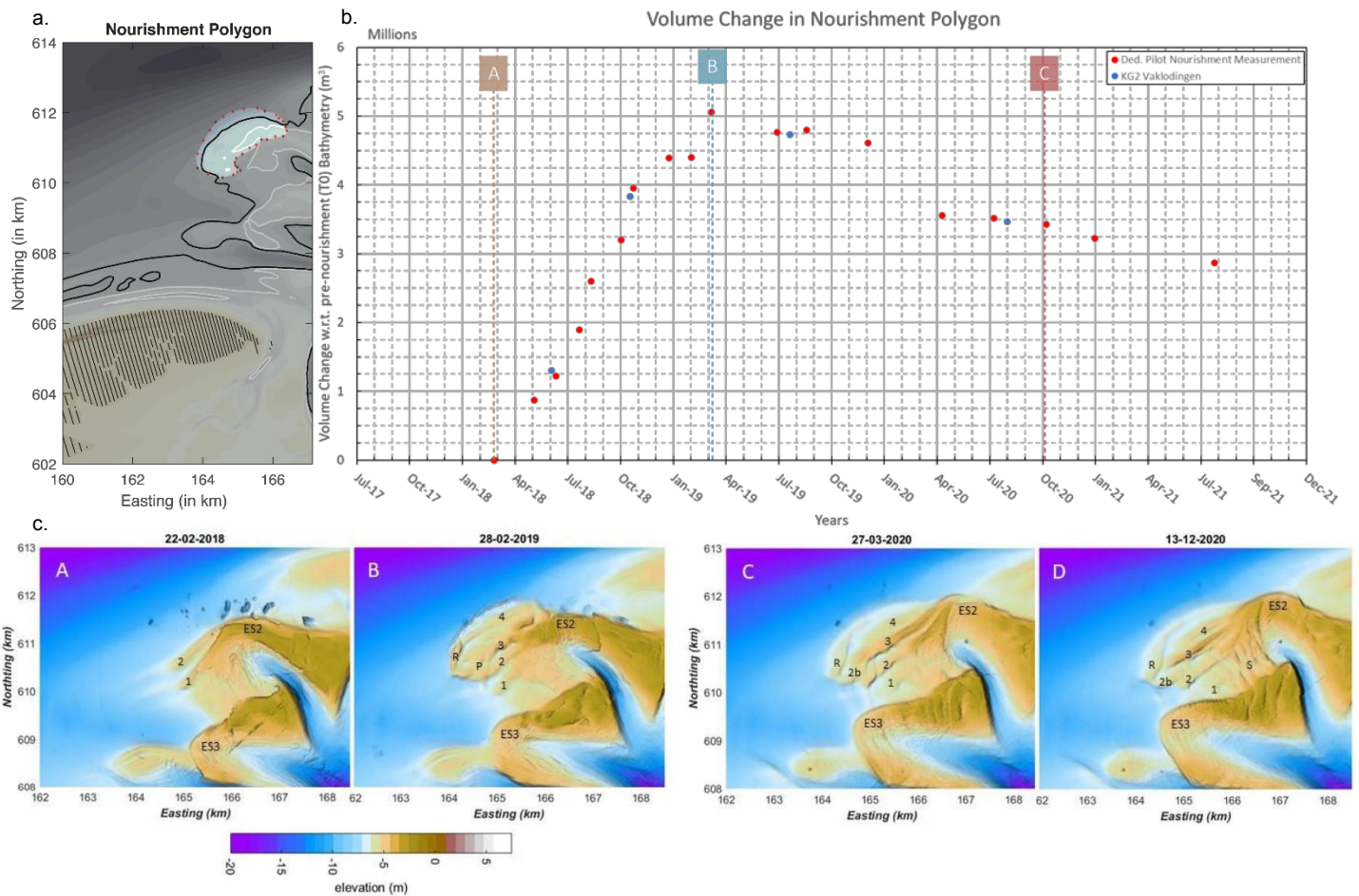


Figure 3-7: The development of the pilot nourishment in the nourishment polygon. (a.) shows the location of the nourishment site (nourishment polygon). (b.) illustrates the volume changes over time during and after construction of the pilot nourishment. Nourishment volumes are shown in order of million m^3 of sand. The banners A, B demarcate the start and completion of the construction respectively. Banner C highlights the storm impact on the pilot nourishment and the associated larger erosion in the polygon. (c.) shows the bathymetry chart of the second ebb-chute and -shield before and after construction of the pilot nourishment (stage A and B respectively), and the onset of the pilot nourishment after construction (stage C and D). sand bars are demarcated with numbers from 1-4 based on chronological order of occurrence and S demarcates the bar migration towards the outflow of the second ebb-chute driven by combined wave and current processes. (c. – source Lambregts (2021)).

4 Process-based Modelling

This chapter describes the model setup and application of the Ameland Inlet model in the Delft3D modelling suite. The model domain, grid schematisation and model settings are treated in Section 3.1. The Flow module and the wave module are described in Section 3.2. Subsequent model improvements are addressed in Section 3.3. Furthermore, the choice and derivation of the imposed model boundary conditions has been addressed in previous research (i.e. de Fockert (2008), Jiao (2014)) and further updated. An overview is provided in Section 3.4.

In this research, the coupled Delft3D online morphodynamic model produced by de Fockert (2008) and further adopted by Jiao (2014) has been taken as starting point for the modelling assessment of the shoal and chute formation at the Ameland ETD. The computational domain and the boundary conditions are inherited from the prior models, and the MorMerge approach (Figure 4-7) is activated to allow for efficient medium-term computations of the sediment transport.

The next sections elaborate further on the application of the Delft3D modelling suite in this research. Background information on the Delft3D modelling suite, the discretisation method, the formulation of the underlying processes, and possible morphological acceleration procedures is provided in Harlequin, (2020).

4.1 Grid and Bed Schematisation

The flow grid applied for the numerical computation of the hydrodynamics and sediment transport is characterised by a structured curvilinear grid which extends into the North Sea covering largely the adjacent coasts of Terschelling (on the West) and Ameland (on the East), and consists of the Ameland Inlet together with its back-barrier basin (Figure 4-1a).

The 101,875-cell flow grid has a variable grid resolution (30x40m to 300x350 m), providing grid cells of maximum 0.127 km² in the offshore domain and a minimum grid cell area of 0.0012 km² in the inlet domain. From previous research of Elias et al., (2019), it is known that baroclinic instabilities are negligible for the Ameland Inlet system. Therefore, only depth-averaged (2DH) computations are considered in this research (i.e. 1 lateral layer). Zero background salinity and temperature are prescribed and a water density of 1023 kg/m³ prevails in the computational domain. Necessary 3D processes are hereby captured by means of 3D-parameterisations of the relevant processes.

On the offshore North Sea boundary, the water levels are forced using astronomic constituents from a morphological tide selection procedure as proposed by Jiao (2014) (see Sec. 4.4.1 for the derivation of the morphological tide procedure). On the east and west-located boundaries, the surface level slope is being forced (i.e. Neumann boundary condition). A dike is located at the southern margin of the Island of Ameland and is represented as a thin dam in the model (Figure 4-1).

The initial model bathymetry varies throughout this study and is based on an extensive dataset of the Ameland Inlet morphology following from a variety of measuring campaigns (Rijkswaterstaat Vaklodgingen dataset offering bathymetries from 1989 to 2010, measurements collected from the SBW-Waddenzee project providing annual data from 2007 to 2010, and bathymetric surveys following from KustGenese 2 project Elias et al., (2019) for

an overview and analysis of the available datasets). By application of the calibrated model, the model predictions on the bathymetric changes are compared with the measured bed level changes observed over the timespan from 2005 to 2020.

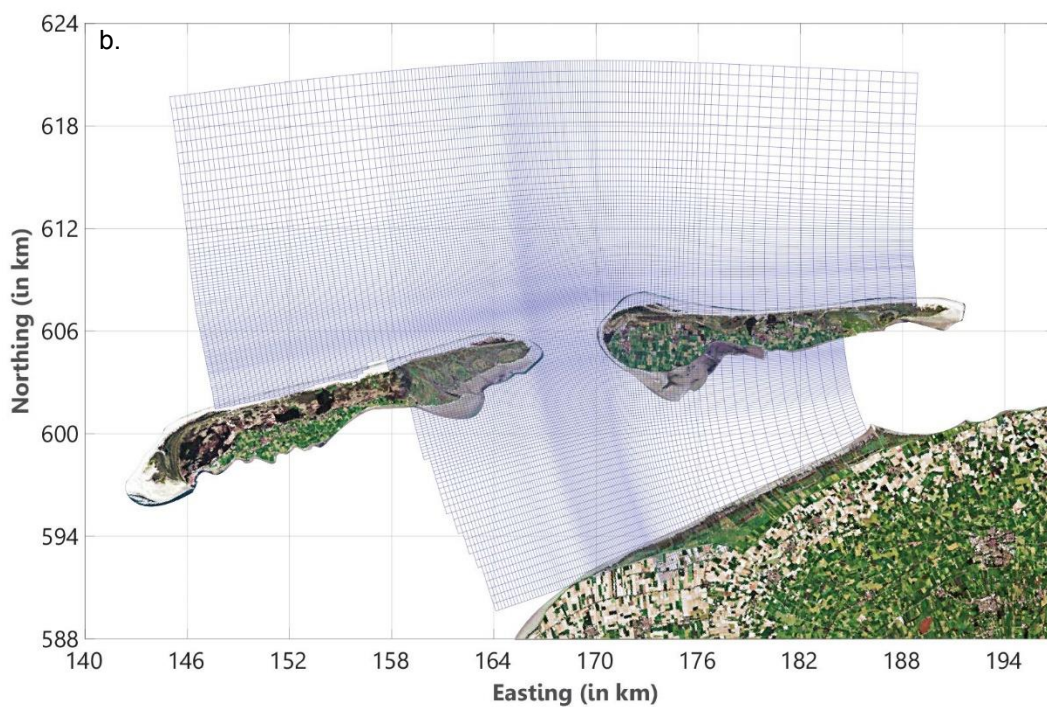
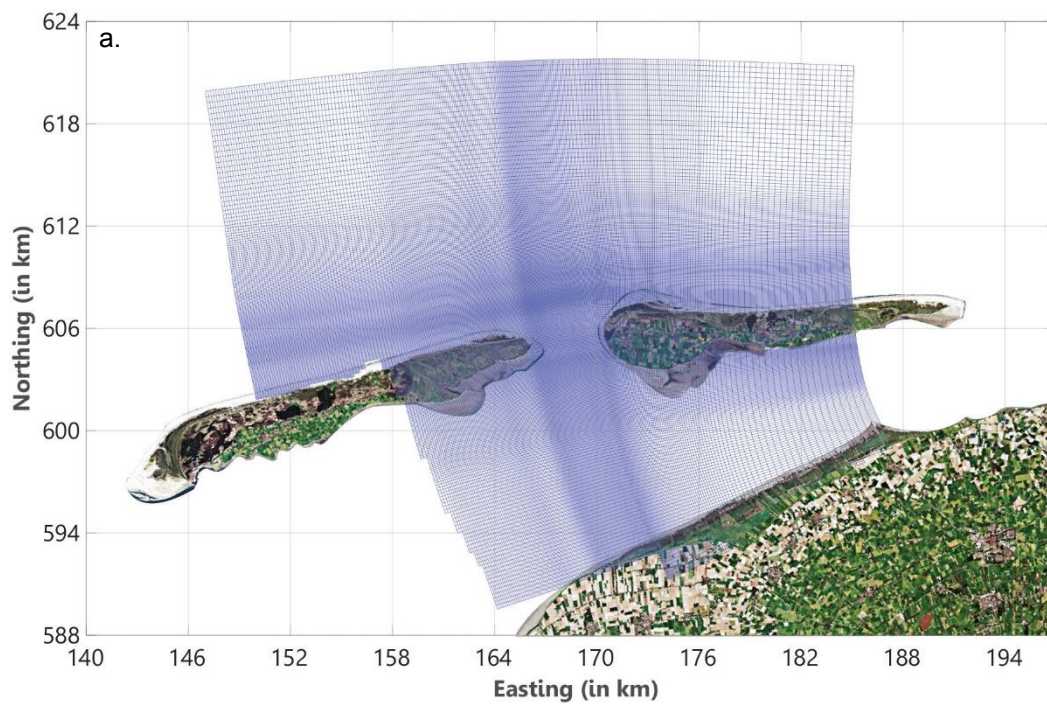


Figure 4-1: Delft3D model grid for the Ameland Ebb-Tidal delta. a.) shows the flow grid on which the hydrodynamic computations are performed and b.) illustrates the (coarser) wave grid for the SWAN computation. On the left in the image the Island of Terschelling is depicted whereas on the right (east) the Island of Ameland is located.

4.2 Model Setup

In order to analyse the effects of the various physical processes that shape the morphology of the ebb-tidal delta, coastal scientists apply process-based models to investigate and reproduce the observed morphodynamic behaviour on various spatial and temporal scales. Delft 3D 4.0 – a process-based structured grid modelling suite – shall be applied in this thesis to compute morphodynamic changes on the ebb-tidal delta. The modelling suite is divided into a set of individual modules that account for a series of processes (Deltares, 2020).

4.2.1 Flow module

The flow module of the Delft 3D 4.0 modelling suite comprises a separate numerical solver that accounts for shallow water flows in coastal regions. The flow solver is a hydrostatic solver based on the Reynold's averaged Navier-Stokes equations and it is thereby capable of computing the transport of water and other waterborne constituents in various flows. Moreover, an non-hydrostatic numerical solver is coupled to the hydrostatic scheme to correct the local flow state if the deviations are large compared to the hydrostatic case (Deltares, 2020). The flow solver is defined by the following constitutive relationships:

- Horizontal (u,v) momentum equations
- Continuity Equation with depth averaged velocities in the horizontal direction
- An advection-diffusion equation to account for waterborne constituents that may create concentration structure over the vertical.
- A turbulence closure model to relate the turbulent small-scale velocity fluctuations to the main-flow properties.

4.2.2 Wave Module

The wave module houses a separate numerical solver that incorporates the effect of wave-induced forces and currents. In this thesis, the third-generation wave model SWAN is applied which is an iterative numeric solver that due to its stable scheme (i.e. numerical convergence) is able to compute wave transformation towards shallower waters accurately. The wave module accounts for the following wave-induced processes:

- Wave energy dissipation due to breaking.
- Wave-induced bed shear stresses.
- Residual Motion (Stoke's Drift).
- Wave-induced near-bed streaming.

4.2.3 Morphodynamics

The morphodynamics is the final step in the numerical computation cycle and relates the prevailing flow patterns – due to combined wave and current-induced processes – to the transport of sediment in the computational domain. In the *online sediment* version of Delft3D FLOW the sediment transport is simultaneously resolved in the hydrodynamic flow cycle. Hereby the model incorporates the following sediment transport components:

- Wave and current-induced Suspended transport
The suspended transport is derived based on the advection and diffusion equation for waterborne constituents in the Flow module. Here, the suspended sediment transport is calculated for each specified sediment-size fraction. Changes in the vertical concentration profile (above a certain threshold height) are continuously computed throughout the numerical procedure. In case of a 2DH-setting these concentration profiles are subsequently integrated over the depth to define depth-averaged suspended sediment transport vectors.
- Wave and current-induced Bedload transport
The bedload transport is derived based on the solution procedure proposed by van Rijn (2007). van Rijn (2007) describes the application of a skewness-based sediment transport parameterisation which resolves the transport of sediment below a certain threshold height above the bed – the bedload transport. The incipience of

motion is thereby defined by the local near-bed velocity magnitude and the mobility parameter for each respective grain-size fraction. It follows then that the bedload transport is well-defined

- Suspended sediment Correction

Since, the advection-diffusion formulation for suspended particles computes the transport of suspended sediment over the entire water column a suspended sediment correction is proceeded as well in the morphodynamics module.

4.3 Model Improvements

Implementation of nonlinear wave-induced processes in process-based Delft3D models

Wave propagation in the shallow coastal shelf seas is usually accompanied by wave transformation. Waves develop a steepened and pitch-forward shape under depth-limiting effects in the geographic space. This wave nonlinearity provides the nett onshore transport of mass and momentum in the surf zone region. phase-resolving models such as the wave action balance for wave propagation in shoaling regions evaluate the hydrodynamics on the wave group scale and are therefore equipped to incorporate wave skewness and wave asymmetry in short-term hydrodynamic computations. On longer time scales and incorporating morphodynamic computations, phase-averaging models are applied which often use schematisations to account for changes in the wave shape and nett effect on the sediment transport. These schematisations often only describe changes in the wave shape as a consequence to wave skewness (Isobe & Horikawa, 1982). From recent studies on the Ameland ebb-tidal delta morphology (Elias, 2018; Elias & Tonnon, 2016) and previous modelling studies (de Fockert, 2008; Jiao, 2014; Teske, 2013; van Soest, 2021) was acknowledged that present-day models – in relation with such wave nonlinearity schematisations – overestimate the onshore-driven transport of sediment in the nearshore region creating overly steepened shorelines and strong seaward advancements of the outer delta.

Preceding wave-driven orbital velocity formulations by (Isobe & Horikawa, 1982) introduced wave-skewness as defining-property for the nonlinearity in the near-bed orbital velocity profile omitting hereby the combined effect of wave *skewness* and *asymmetry* (Figure 4-2).

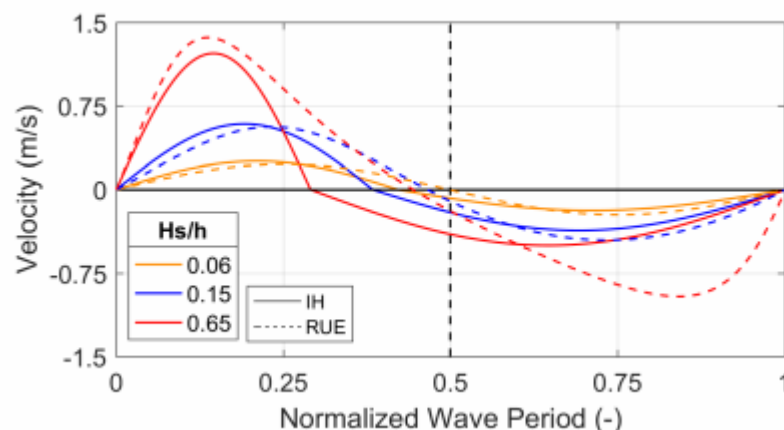


Figure 4-2: Illustration of velocity profile when only wave skewness (solid lines) is considered for increasing shallowing water depths. The dashed lines show the velocity profile for model simulations wherein wave asymmetry is also considered (from Boechet Albernaz et al. (2019))

Ruessink et al., (2012) found based on extensive datasets of wave measurements an empirical relation between the properties of the flow (i.e. wave orbital velocity) and intra-wave profiles (i.e. Asymmetry and Skewness) through the Ursell number (Wave nonlinearity parameter) (Figure 4-3). Using the constants of empirical curve fitting, the near-bed orbital velocity could be redefined to describe to the nonlinearity of the intra-wave shape (Table 4 2).

Near-bed orbital velocity formulation	
$u(t) = \begin{cases} u_{on} \sin\left(\frac{\pi t}{T_{for}}\right), & \forall t < T_{for} \\ -u_{off} \sin\left[\frac{\pi}{T_{back}}(t - T_{for})\right], & \forall t \geq T_{for} \end{cases}$	$u(t') = U_w f \frac{\sin(\omega t') + \frac{r \sin(\varphi)}{1+f}}{1 - r \cos(\omega t' + \varphi)}$
<p>With:</p> <ul style="list-style-type: none"> - onshore u_{on} and offshore u_{off} orbital velocity magnitudes - and flood (onshore) T_{for} and ebb (offshore) T_{back} durations of the wave orbital motion 	<p>With:</p> <ul style="list-style-type: none"> - orbital velocity magnitude U_w - nonlinearity wave shape parameters r and φ, - and $f = \sqrt{1 - r^2}$ for which $U_w f$ is the amplitude \hat{u} of the velocity
Isobe & Horikawa (1982) Wave Skewness	Ruessink et al. (2012) Wave Skewness and Asymmetry

Table 4-1: Description of wave-orbital velocity by Isobe & Horikawa (1982) and Ruessink et al. (2012).

Boechat Albernaz et al., (2019) conducted further research on the parameterisation of the near-bed orbital velocity under effect of waves and composed an updated Delft3D extension for the wave skewness & asymmetry formulation based on the work of Ruessink et al., (2012). This revised Delft3D model has been applied for a series of case studies for the coast of Katwijk, the Netherlands and the coast of Duck, USA with single wave conditions and full wave climates (Boechat Albernaz et al., 2019). In this study, it was shown that in uncalibrated state the revised coupled Delft3D model significantly reduced in maximum computed total

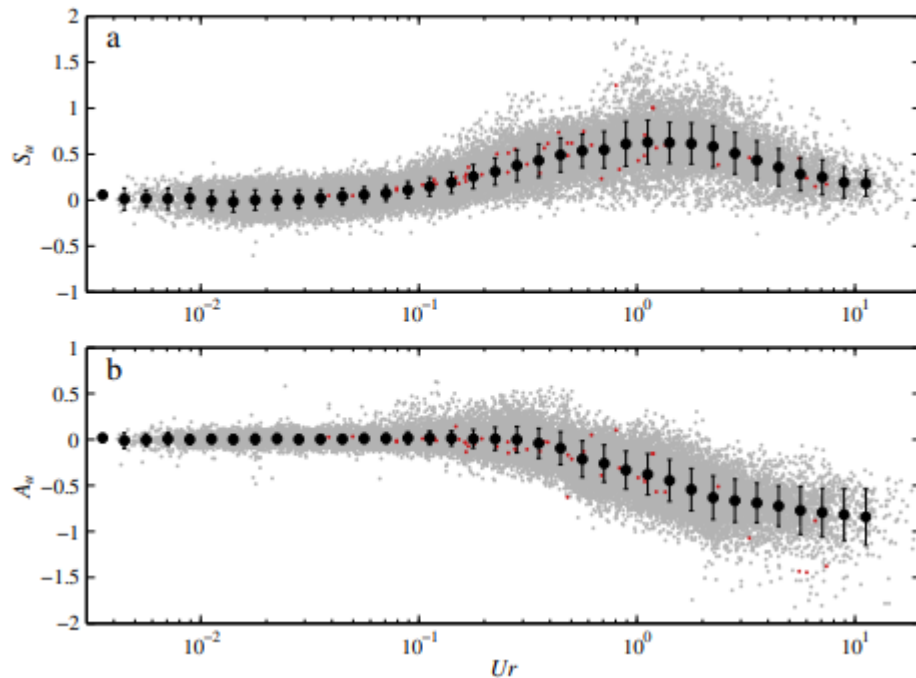


Figure 4-3: Empirical fitting of the scattered measurement to derive a relationship between the Ursell (U_r) number and the Wave Asymmetry parameter (A_s) and the Wave Skewness Parameter (S_k) respectively (From Ruessink et al. (2012)).

transport capacity in comparison with the standard Delft3D code on the basis of Isobe & Horikawa, (1982) (Figure 4-4).

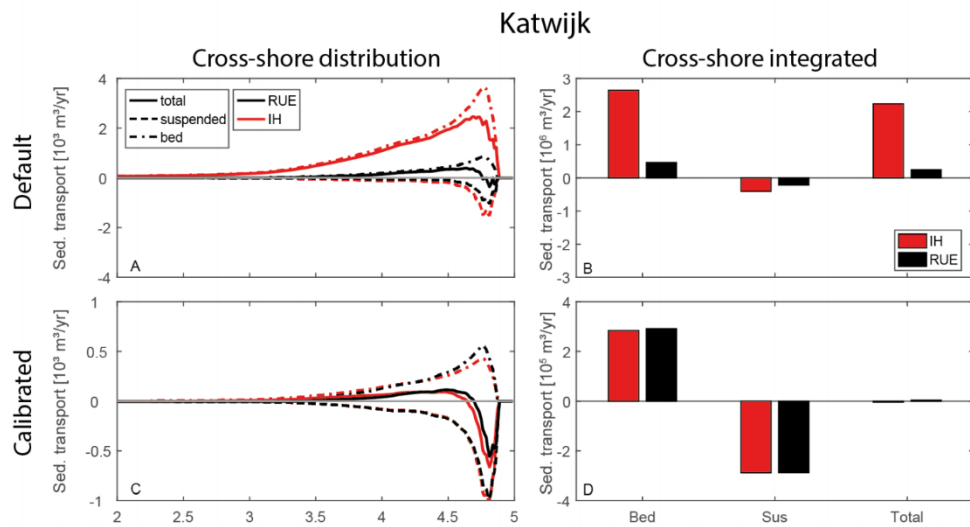


Figure 4-4: Computed total sediment transport for the coast of Katwijk using the wave skewness formulation (IH) (red lines) and the wave skewness and asymmetry formulation (RUE) (black lines). The cross-shore distribution of the sediment transport (upper left and right panel) shows that for RUE the order of magnitude of the suspended and bedload transport are comparable in the uncalibrated state. It should be stressed that net effect of the calibrated models is fairly the same (lower panels) – both models should produce the same sediment transport (from Boechet Albernaz et al. (2019)).

4.4 Imposed Boundary Conditions

4.4.1 Flow Boundary Conditions – Morphological Tide Selection

This section is a summary of the work of Jiao (2014) on the development of the morphological tide in the modified de Fockert model.

In this thesis, the water level boundary conditions are composed in line with the conditions as proposed by Jiao (2014). As such, a morphological tide is specified at the Northern boundary. This tide is found by selecting a representative tidal cycle that produces the same residual transport as for the astronomical spring-neap tidal cycle (Latteux, 1995). In the assessment of Jiao (2014) the main objective was to target the residual sediment transport through the inlet gorge (i.e. Borndiep). Hence, the selection of this representative tide proceeded with the following steps:

1. Run a preliminary tide-only simulation on the basis of the full spring-neap cycle to obtain information about the transport field in the inlet gorge (i.e. determination of transport magnitudes and directions). As a target measure, the average-residual transport \bar{s}_l through the inlet gorge is designated. Therefore, the averaged-residual transport \bar{s}_l through pre-defined transects in the inlet gorge should be established.
2. Next, a reference measure should be defined for the sediment transport through the inlet. Here, the minor sum is taken into account of the average-residual transport through the inlet transects corrected with the double tide-averaged period is taken into account, viz.:
 - a. Determine the double tide-averaged period $\bar{T}_l(t)$ which encompasses the daily inequality:

$$\bar{T}_l(t) = \frac{1}{T} \int_{t+0.5T}^{t-0.5T} (T_l(t)) dt$$

- b. Furthermore, Determine the reference transport $W(t)$ through the inlet by summation of the following ratio, viz.:

$$W(t) = \frac{1}{N} \sum_{i=1}^N \frac{\bar{s}_l}{\bar{T}_l(t)}$$

3. Lastly, the representative tide is selected by minimisation of the root mean squared error between the representative transport with the tide-averaged transport through the inlet:

$$E_{rms} = \sqrt{\frac{1}{N} \sum_{i=1}^N \frac{W(t) * \bar{T}_l(t) - \bar{s}_l}{\bar{s}_l}}$$

Hence, the tidal cycle that provides the smallest error in the residual transport compared to the reference transport is selected as boundary condition for the model. The final specification of the tidal components that are applied for the water level boundary condition may be found in Table 4-2 below.

Constituents	Frequency [°/hr]	Amplitude [m]	Phase [°N]
	0	0.1163	0
M1	14.497	0.122	183.45
M2	28.993	0.897	54.33
M3	43.49	0.01	100.44

M4	57.987	0.113	333.14
M5	72.483	0.008	79.19
M6	86.98	0.095	203.64
M7	101.477	0.007	224.60
M8	115.973	0.003	357.93

Table 4-2 Harmonic boundary conditions applied as excitation at the water level boundary of the computational domain.

4.4.2 Wave Boundary Conditions – Manual Selection of Wave Classes

Time series records at the Schiermonnikoog (SON) station are collected given its extensive set of long-term wave measurements (from 1980 – 2017, see Figure 4-5). Prior analysis of Elias et al., (2019) shows that the wave climate is mild with characteristic wave heights predominantly smaller than 2-2.5 m. The mean significant wave height is equal to 1.37 m. For a smaller 1% of the wave record wave heights of 4.5 m and higher are observed indicative to severe storm conditions. Most waves are obliquely incident to the Ameland inlet with wave directions ranging from the north-northwest to east. The dominant wave direction is hereby from the north-northwest (235° – 305°).

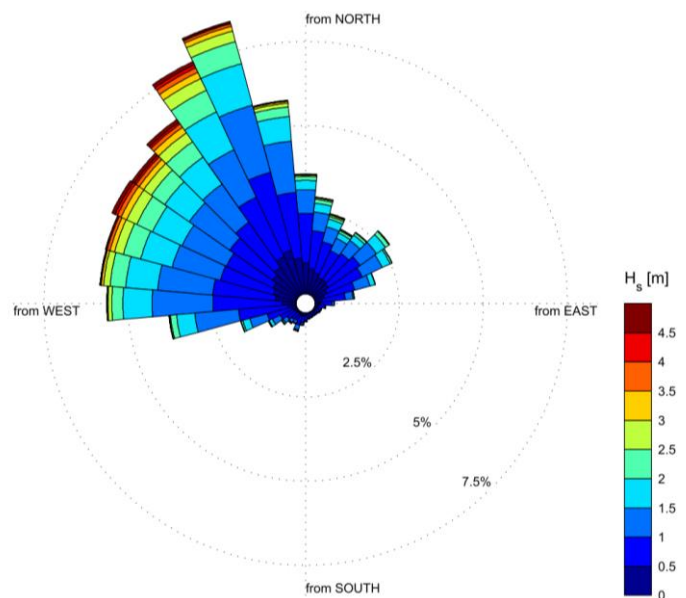


Figure 4-5: Wave rose of the Schiermonnikoog extended wave data set showing the wave climate from 1980 - 2017. (after Elias et al., (2019))

For this study, a new morphological wave climate has been derived mainly to trigger the wave-driven processes in the Delft3D coupled model that were to a limited degree accounted for in previous modelling studies (Elias, 2018).

This Research

A new morphological climate has been derived in this research using a manual selection procedure of wave classes. Initially a set of 8 wave conditions was considered allowing thereby for fast morphological assessment. Based on the extensive wave measurements from the Schiermonnikoog (SON) station, the wave height distribution is registered (Figure 4-6) and allocated in 4 directional bins (i.e. Northwest, North, North East, and the South) and 2 wave height bins (i.e. 0 – 1.2 m and >1.2m). Offshore wave directions are omitted in this analysis (i.e. 2 wave conditions between 90 °and 260 °), resulting in a set of 6 wave conditions to represent the morphological development of the full wave climate.

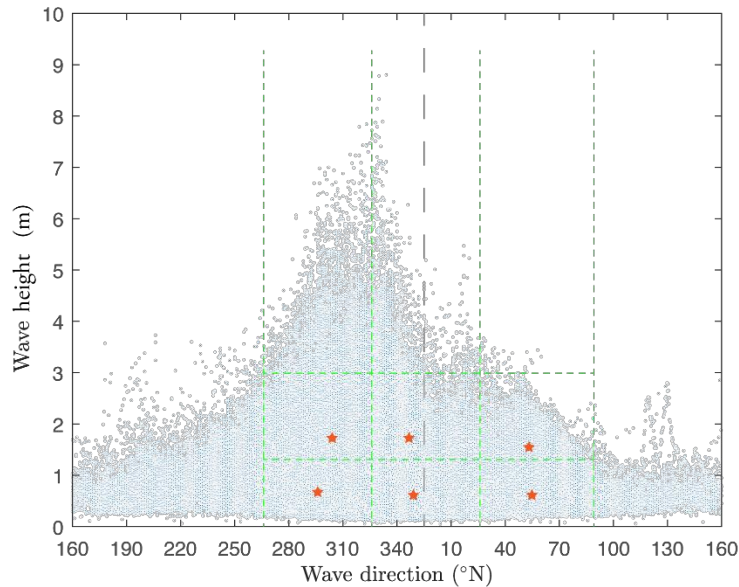


Figure 4-6: Resulting wave conditions for the manual selection procedure of wave classes using the equal wave binning approach. The dotted green lines demarcate the respective wave bins and the orange stars indicate the combinations of wave height and wave direction per wave bin.

Furthermore, the wind direction is aligned with the wave conditions to ensure optimal wave growth of the wind-generated waves as they propagate towards shore. The final wave conditions in this morphological climate are tabulated in Table 4-3 below.

Wave Condition	Wave Height (in m)	Wave Period (in sec)	Wave Direction (in deg°)	Probability of Occurrence (in %)	Wind Speed (in m/s)	Wind direction (in deg°)
1	0.80	4.27	293.10	27.41	6.71	293.10
2	0.75	4.70	352.56	23.97	6.57	352.56
3	0.75	3.79	56.32	11.93	6.57	56.32
4	1.87	5.29	298.08	21.34	9.77	298.08
5	1.83	5.49	346.96	11.83	9.66	346.96

6 1.66 4.72 51.86 3.52 9.17 51.86

Table 4-3 Final result of the manual selection procedure of wave classes based on the SON wave climate. Wave and Wind conditions used to model the Ameland Ebb-tidal delta.

A sensitivity analysis of the latter morphological wave climate is also performed in this research to investigate the morphological effect of more wave conditions and the effect of scenarios wherein storm waves are more apparent. The outcomes of this exercise provided that the model is insensitive to variations in the amount of wave conditions provided. Hence, the modelling assessment is continued with a morphological climate consisting of 16 wave conditions. (see Table 4-4 below).

Wave Condition	Wave Height (in m)	Wave Period (in sec)	Wave Direction (in deg°)	Probability of Occurrence (in %)	Wind Speed (in m/s)	Wind direction (in deg°)
1	0.83	3.96	276.59	13.06	6.80	276.59
2	0.77	4.62	312.20	13.57	6.63	312.20
3	0.75	4.70	352.56	23.29	6.57	352.56
4	0.75	3.79	56.32	11.59	6.57	56.32
5	1.55	4.62	278.04	7.31	8.86	278.04
6	1.57	5.16	312.01	7.46	8.91	312.01
7	1.55	5.19	348.83	8.55	8.86	348.83
8	1.52	4.50	54.07	2.90	8.77	54.07
9	2.38	5.34	281.34	2.44	11.23	281.34
10	2.43	5.81	312.57	3.53	11.37	312.57
11	2.40	5.78	345.15	2.95	11.29	345.15
12	2.27	5.18	47.30	0.51	10.92	47.30
13	3.53	6.26	285.70	0.49	14.52	285.70
14	3.63	6.80	312.29	1.57	14.81	312.29
15	3.54	6.79	341.88	0.76	14.55	341.88
16	3.21	5.88	41.34	0.01	13.60	41.34

Table 4-4: Morphological wave climate used for the modelling assessments performed in this research.

4.5 Sediment-Transport Model

The MorMerge Approach in combination with the coupled Delft3D model has been considered to compute the morphological changes in the computational domain within the hydrodynamic time step. The MorMerge Approach is hereby an efficient method to compute morphodynamic changes whilst considering multiple schematised input conditions (see for example Harlequin (2020) for an overview of commonly applied morphological acceleration techniques, and Roelvink (2006) as reference for the online morphology technique).

In the MorMerge Approach – a parallel online scheme – morphodynamic changes are computed parallelly for each set of input conditions and merged with the probability of occurrence in each hydrodynamic time step Δt . The merged bed level changes can also be aggregated with the factor of morfac (f_{morfac}), to speed up the morphological computations. Figure 4-7 shows the flow diagram of the MorMerge approach.

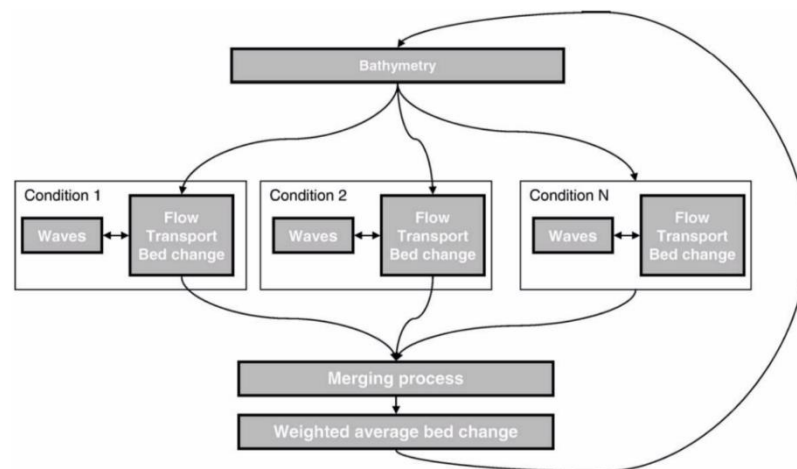


Figure 4-7 The flow diagram of the parallel online approach (MorMerge Approach) (after Roelvink 2006).

To obtain bed level changes, the coupled Delft3D model must be equipped with a sediment transport solver. Therefore, the TRANSPOR2004 (VR04) transport formulation has been included in the model. The VR04 computes the incipience of motion of non-cohesive sediment fractions and accounts for sediment transport through bedload transport and suspended transport mechanisms. Bedload transport is related to the entrainment and incipience of sediment particles near the bed and include the effect of wave orbital velocity asymmetry. The suspended sediment transport relates to the settling and suspension of sediment particles in the water column due to a balance between turbulent-induced lateral transport and the settling process of sediment fractions. This balance is described by the advection-diffusion equation for waterborne constituents in coastal regions. The VR04 formulation also allows for a separate treatment of wave-induced and current-induced sediment transport.

The sediment composition in the computational domain is represented by means of a single-size fraction composition. This is been characterised by the application of a median grain-size diameter (d_{50}) of 250 μm . The coupled Delft3D computations are proceeded with bed level updating such that the effect of the flow on the time-varying bed levels and the significance of time-varying sediment transport patterns could be included in the morphodynamic assessment of the chutes and shields at the Ameland ETD.

5 Morphological Model Validation

5.1 Model results Morphological Validation on Natural Behaviour

The first step in the morphological validation of the present-state-of-the-art Ameland model encompasses an analysis of the model performance. This analysis focusses on the model capability to reproduce the observed bed level changes over the 2005 – 2020 bathymetry of the Ameland ebb-tidal delta. The simulation time horizon is thereby subsequently increased to identify any correlation between the simulation time horizon and the model performance. The objective is overall to build model certainty on the medium-term temporal scale typified by a 4-year simulation timespan.

To this end, modelled bed level changes are compared with measured bed level changes to highlight anomalies with the natural response. Table 5-1 below provides an overview of the associated model simulations. The modelled results for the morphological simulations are shown in Appendices A – B.

Model validation runs				Processes			
Simulations	Qty.	Description	Tide	Waves	Wind	Morph	
Ameland ETD 2005 – 2020	13	Annual predictions from 2005 – 2020, (excl. 2012 – 2014 due to sparse data coverage)	Yes	Yes	Yes	Yes	
Ameland ETD 2005 – 2020	9	Biannual predictions from 2005 – 2020	Yes	Yes	Yes	Yes	
Ameland ETD 2005 – 2020	5	4-year predictions from 2005 – 2020	Yes	Yes	Yes	Yes	

Table 5-1: Overview of model simulation to assess the model performance on the natural behaviour of the Ameland ebb-tidal delta.

Based on the modelled results, three characteristic time intervals can be identified wherein the results over the various simulation time horizons are providing a similar response. These time-intervals are closely related to the time instances of ebb-chute and shield evolution. As such, the characteristics of the model performance are described on the time-intervals 2005 – 2010, 2010 – 2014 and 2016 – 2020 respectively.

5.1.1 Description of model performance (2005 – 2010)

The 2005 – 2010 Ameland ebb-tidal delta is characterised by the growth of two ebb-chutes: the first ebb-chute in 2006 (see Figure A 1) and the growth of a second ebb-chute around 2008 (see Figure A 3). An overview of the characteristic morphological features is provided in Figure 5-1 which shows the 2005 bathymetry of the Ameland ebb-tidal delta.

The Bornrif swash platform (Figure 5-1²) is connected with the updrift swash platform and is spanning along the entire seaward margin of the ebb-tidal delta. The main-ebb channel Akkepollegat (Figure 5-1³) is located north of the main-inlet Borndiep (Figure 5-1¹) and is extended well into the outer delta. The presence of a well-developed swash platform and the continuous growth of the main shoal (Figure 5-1⁴) on the central platform of the outer delta enforces an outer channel rotation of the Akkepollegat along the margin of the Bornrif swash platform.

This has also an effect on the growth of the Bornrif swash platform. Under influence of the continuous rotation of the Akkepollegat, the Bornrif swash platform steadily migrates

eastward towards the coast of Ameland in the years following. Thereby, considering the position of the well-defined Bornrif swash platform along the outer margin of the ebb-tidal delta, wave action also influences the morphological development of the platform in the consecutive years.

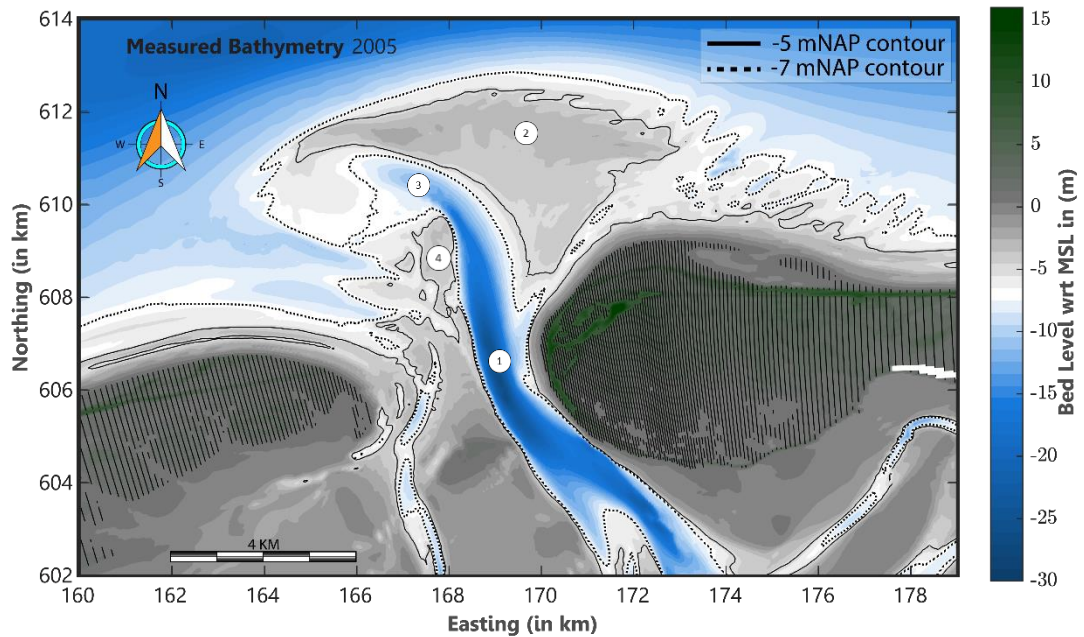


Figure 5-1: overview of the 2005 morphology of the Ameland ebb-tidal delta.

5.1.1.1 Annual runs

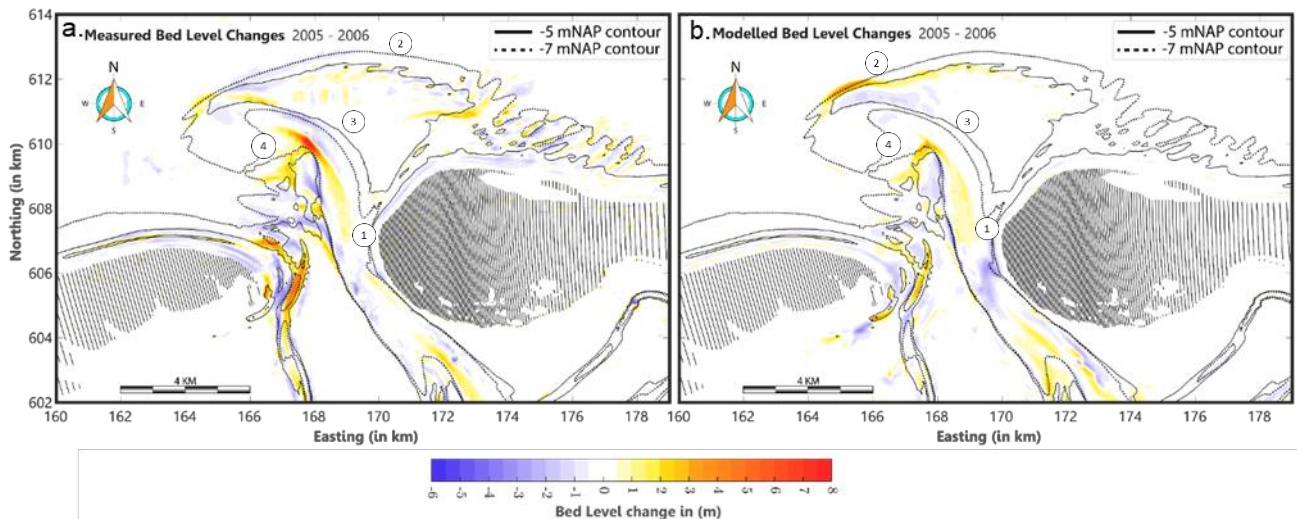


Figure 5-2: Model results of the 2005 – 2006 morphological computations for the Ameland ebb-tidal delta with the 2005 bathymetry as initial bathymetry.

For the annual morphological predictions of the Ameland ebb-tidal delta, the modelled and measured bed level changes are shown in Appendix A1 and highlighted in Figure 5-2.

The growth of the main shoal on the central platform of the outer delta can be clearly observed in the measured bed level changes. An elongated sedimentation pattern is therewith observed along the seaward margin of the main shoal and a local deepening is apparent along the eastward margin with the Akkepollegat (Figure 5-2a⁴).

Moreover, an erosion pattern is also present in the Akkepollegat north of the elongated deposition (Figure 5-2a³). This sedimentation and erosion pattern can be seen as an indication for the channel migration at the outer delta margin.

A comparison with the modelled annual bed level changes shows that the natural morphological development is reasonably well captured by the model. The model produces a local accretion along the main shoal and the Akkepollegat (Figure 5-2b⁴). Thereby the model results also depict an erosion along the eastern margin of the main shoal. However, the measured bed level changes show a larger magnitude of the erosion than is predicted by the model. This also holds for the accretion in the Akkepollegat which is smaller than is described by the measured bed level changes.

Furthermore, the morphological development on the terminal lobe is to a lesser degree captured by the model (Figure 5-2b²). From measured bed level changes, it follows that the terminal lobe is subjected to a substantial erosion whereas the modelled response shows a significant accretion along the terminal lobe.

On the main inlet Borndiep an erosion pattern can be observed in the measured bed level changes followed by a sedimentation pattern offshore and landward of the inlet (Figure 5-2b¹). This is reasonably well captured by the model. Small variations can therewith be observed between the modelled and measured amplitude of these local erosion patterns.

Lastly, it is apparent that the morphological development along the coastal sections of Ameland and Terschelling is not captured by the model (Figure 5-2b⁵ & ⁶). This entails the landward migration of local shoals on the Bornrif swash platform that are attaching to the Bornrif Strandhaak and the local formation of shore parallel bars along the coast of Terschelling.

5.1.1.2 Two-year runs

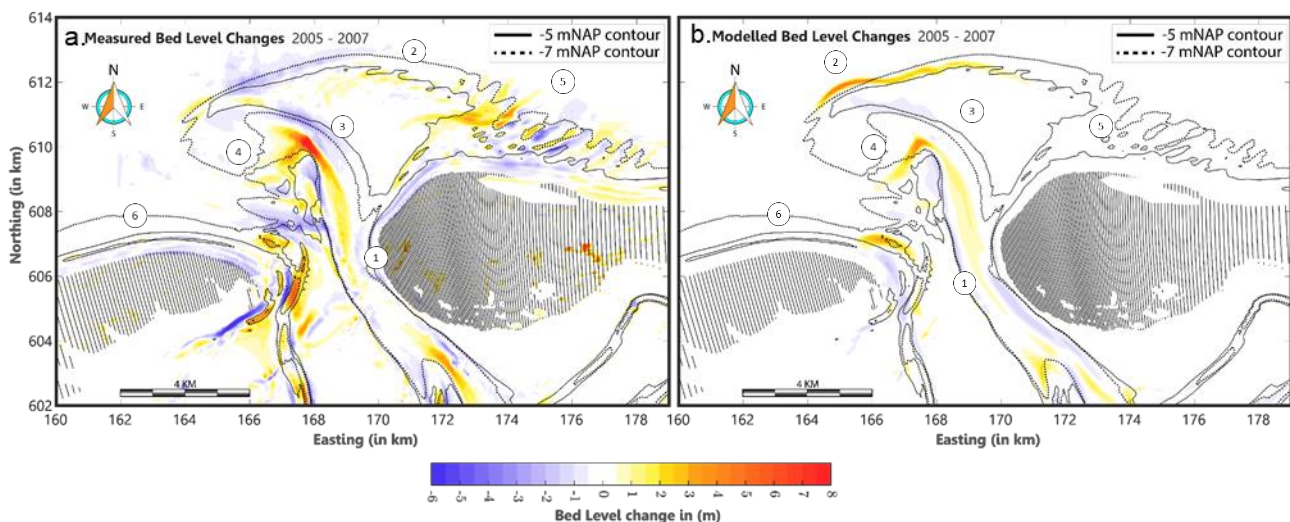


Figure 5-3: Model results of the 2005 – 2007 morphological computations for the Ameland ebb-tidal delta with the 2005 bathymetry as initial bathymetry.

For the two-year morphological predictions of the Ameland ebb-tidal delta, the modelled and measured bed level changes are shown in Figure 5-3. Based on a comparison between modelled and measured bed level changes over this simulation timespan, it can be concluded that similar patterns of modelled erosion and deposition are found as in the annual model predictions.

A similar accretion has been observed along the main shoal in the Akkepollegat in the annual run (Figure 5-3b⁴). As a consequence, the difference in morphological response with respect to the observed bed level changes along the main shoal appears to be larger in the two-year morphological simulation than in the annual model prediction.

Moreover, the modelled accretion along the terminal lobe illustrates a similar pattern along the ebb-tidal delta margin as in the prior morphological runs albeit that the magnitude of the local deposition pattern is slightly larger (Figure 5-3b²).

The channel migration of the Akkepollegat along the outer margin of the ebb-tidal delta is to a lesser degree captured in the two-year morphological run than in the annual runs. This can be clearly observed by the significant deviation in modelled response. Figure 5-3b³ depicts a local erosion in the order of 1 m whereas the measured bed level changes indicate variations in the order of 2 – 3 m.

The morphological response in the main inlet Borndiep shows in the modelled response a smoothing of the established erosion and deposition patterns in the annual run. Amplitude variations are apparent in the order of 0 – 1 m which is small compared to the measured changes over the 2-year timespan (Figure 5-3b¹). Thereby the erosive pattern in the Borndiep prevails an uninterrupted shape along the coast of Ameland which has not been observed in the natural response of the ebb-tidal delta.

Furthermore, the erosion and deposition along the coast of Ameland and Terschelling is not reproduced by the model. Only small variations can be observed close to the eastern margin of the coast of Terschelling.

5.1.1.3 Four year runs

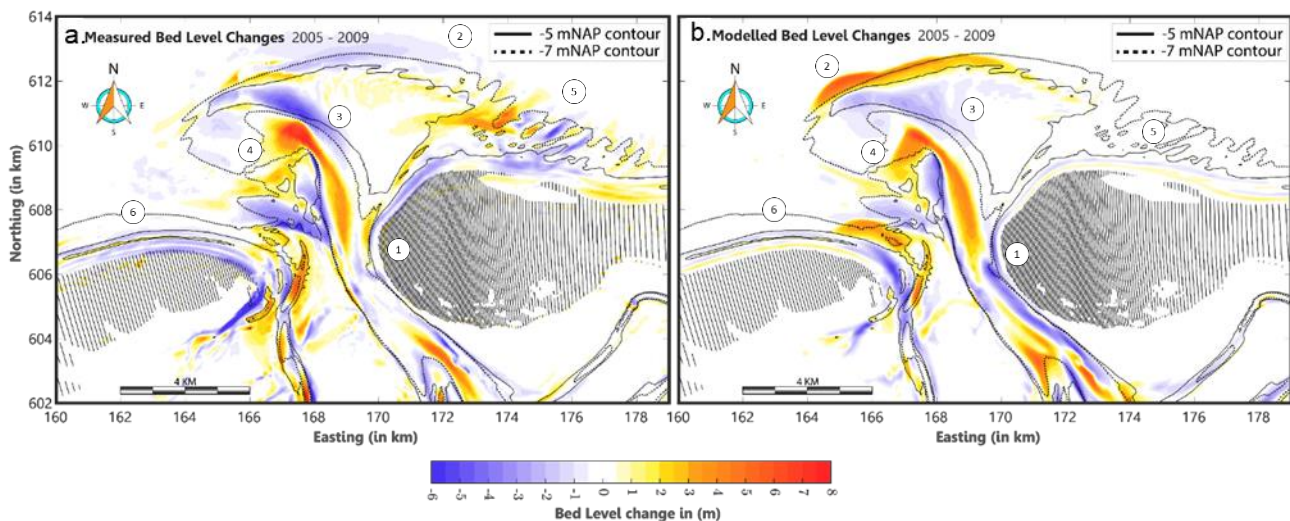


Figure 5-4: Model results of the 2005 – 2009 morphological computations for the Ameland ebb-tidal delta with the 2005 bathymetry as initial bathymetry.

Figure 5-4 shows the modelled response for the 4-year morphological simulation of the natural behaviour of the Ameland ebb-tidal delta. It can be seen that for the 2005 – 2010 timeframe the 4-year predictions provide the closest resemblance to the natural response than the shorter-term predictions. The morphological development in the Akkepollegat is thereby closely mimicked by the model (Figure 5-4b^④). The erosion patterns along the western margin of the Bornrif swash platform are also captured by the model (Figure 5-4b^③). Amplitude and shape variations prevail between the modelled and observed erosion, but the location of the erosion is consistent with the local measurements. Thereby, also the morphological development of the Westgat appears to be reasonably captured in the model albeit with average amplitude differences in the order of 2 – 3 m.

Conversely, the seaward advancement of the Bornrif swash platform remains a persistent feature in the modelled response (Figure 5-4b^②). Lastly, an important observation can be made for the morphological development along the coast of Terschelling and Ameland. On a 4-year simulation timespan the model appears to produce erosion and deposition patterns along the coastal sections with amplitude variations in the order of the observed morphological variations. Shore parallel bars are formed along the coast of Ameland with amplitudes in the order of 1 m. This is still smaller than the 2 m observed sedimentation along the coast of Ameland. The erosion in the Oostgat is close to the Borndiep reasonably well predicted. However away from the inlet, along the coast of Ameland, the modelled deepening is substantially smaller than the observed changes (Figure 5-4b^①).

5.1.2 Description of model performance (2010 – 2016)

In the 2010 – 2016 Ameland ebb-tidal delta, the growth of the second ebb-chute dominates the morphological development of the central platform of the outer delta (Figure 5-5). An increasing offshore directed growth of the second ebb-chute promotes a further channel migration of the Akkepollegat and the further development of the outer channel migration along the Bornrif swash platform. As a consequence to the eastward migration of the Akkepollegat, the Bornrif swash platform migrates towards the coast of Ameland. Thereby, the swash platform attaches to the Ameland coast at the Bornrif Strandhaak. The 2016 bathymetry (Figure 5-9) shows the attachment of the Bornrif swash platform to the coast of Ameland.

An overview of the characteristic morphological features over the 2010 – 2016 timespan is provided in Figure 5-5 which shows the 2010 bathymetry of the Ameland ebb-tidal delta.

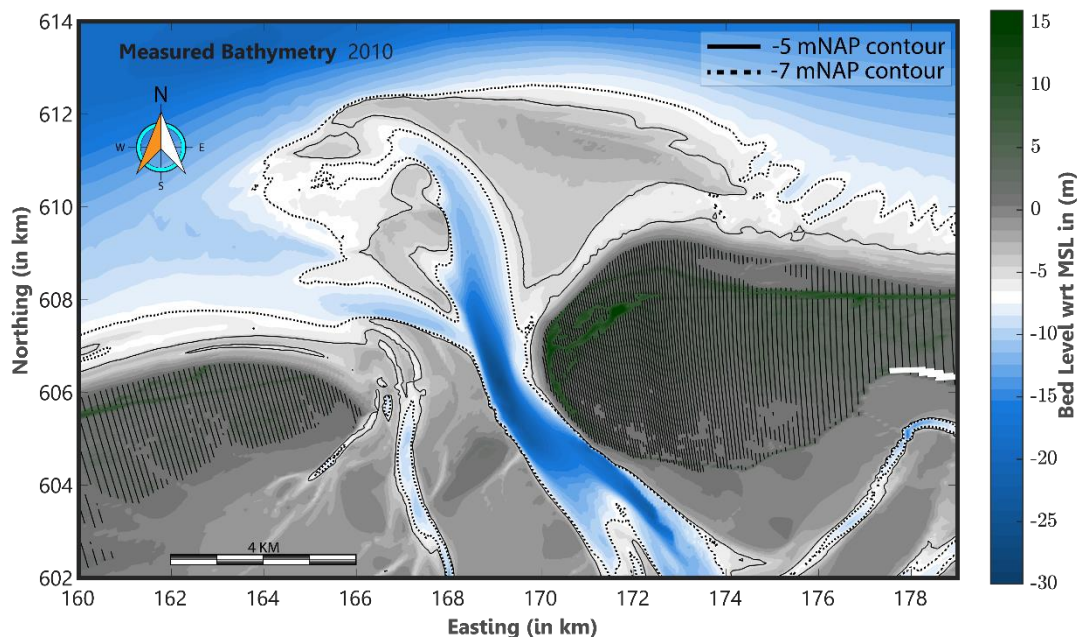


Figure 5-5: overview of the 2010 morphology of the Ameland ebb-tidal delta.

5.1.2.1 Annual runs

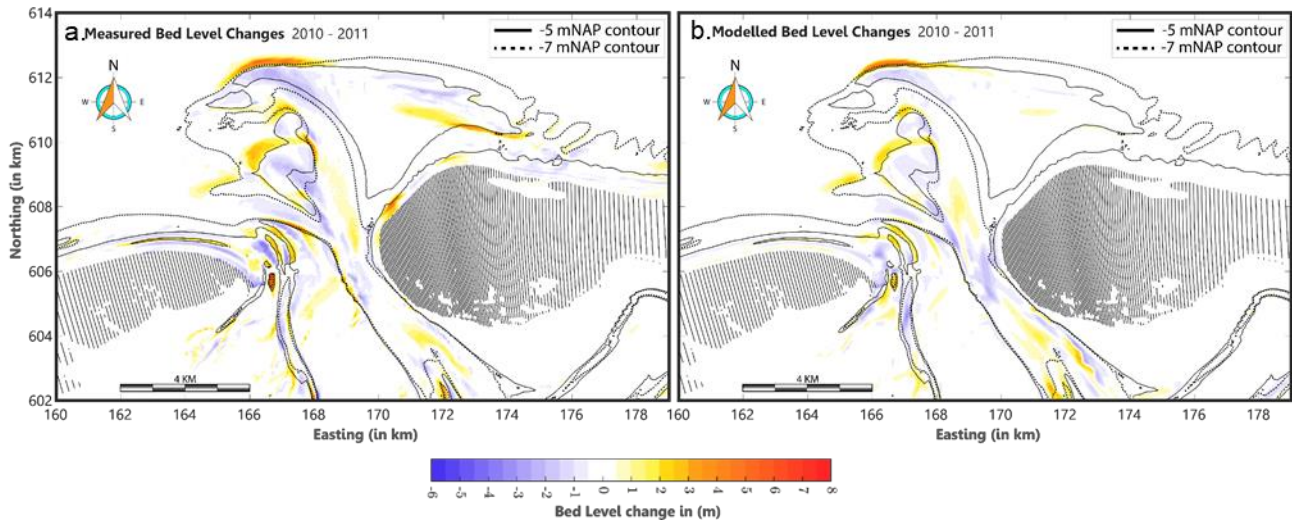


Figure 5-6: Model results of the 2010 – 2011 morphological computations for the Ameland ebb-tidal delta with the 2010 bathymetry as initial bathymetry.

In the annual validation runs for the Ameland ebb-tidal delta in the timeframe of 2010 – 2016, the modelled results show a better resemblance with the measured observations than in the timeframe from 2005 – 2010. Figure 5.6 shows the model results for the validation run performed over the period 2010 – 2011.

The sedimentation and erosion patterns over the margin of the Bornrif swash platform provide here a better representation of the measured morphological development. The amplitude and location of the patterns are consistent with the measured bed level changes with here and there small variations of the amplitude in the order of 0 – 1 m.

Furthermore, the growth of the second ebb-chute and -shield on the central platform of the outer delta is well reproduced by the model. The modelled seaward extension shows thereby to be slightly smaller than the observed bed level changes, yet the amplitude is comparable with the measured response. This can also be observed for the development of the Westgat and the sedimentation in the Akkepollegat.

The formation of a local bar on the Bornrif swash platform and its subsequent attachment to the Bornrif Strandhaak is however not captured by the model. Small accretion zones can be observed but are not representative for the natural changes that occur within this simulation timespan.

5.1.2.2 Two-year runs

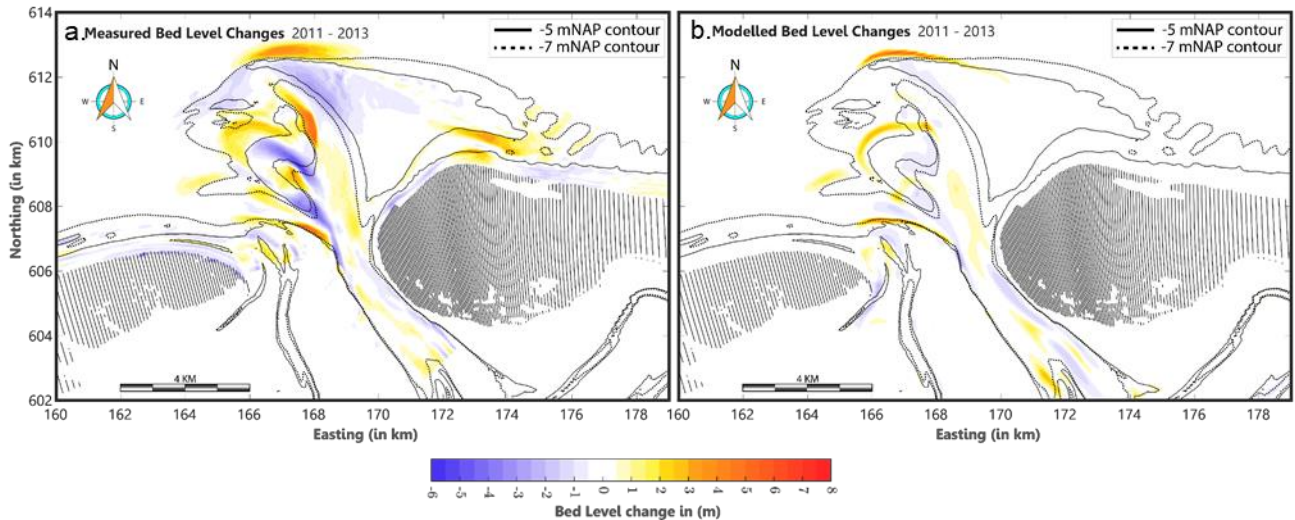


Figure 5-7: Model results of the 2011 – 2013 morphological computations for the Ameland ebb-tidal delta with the 2011 bathymetry as initial bathymetry.

The mere resemblance between modelled and measured behaviour that was identified for the annual model predictions seems not to be present over the two-years simulation runs over the 2010 – 2016 Ameland ebb-tidal delta. The locations of the sedimentation and erosion zones are consistent with the measured morphological changes; however, a significant amplitude anomaly prevails for the modelled response.

The accretion at the offshore margin of the Bornrif swash platform and the development of the Zeehondenplaat, west of the main-inlet Borndiep, shows thereby the most consistent morphological changes.

5.1.2.3 Four year runs

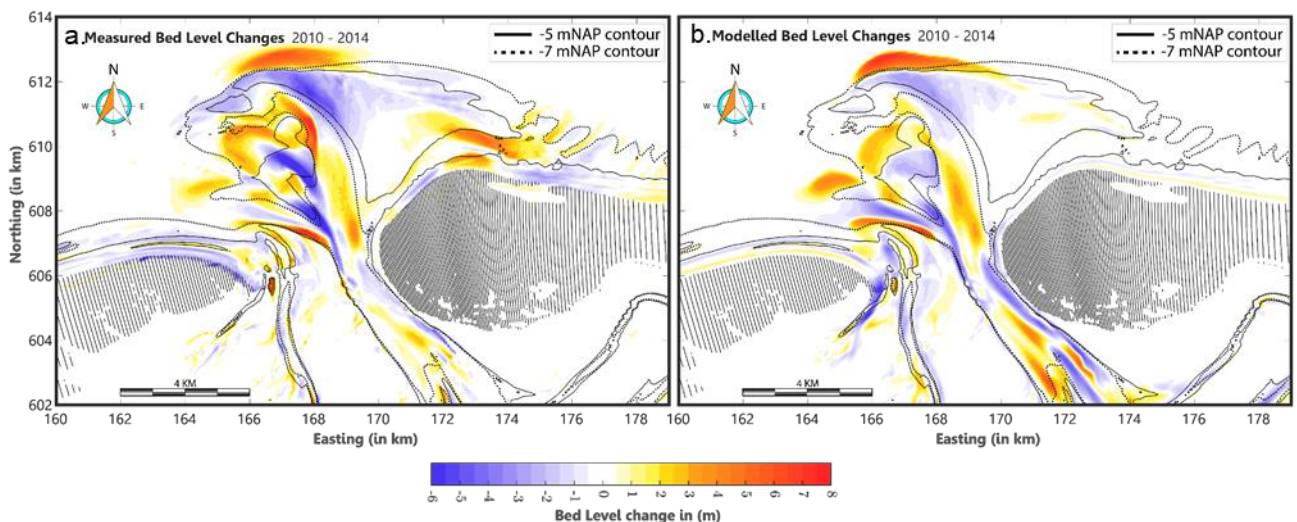


Figure 5-8: Model results of the 2010 – 2014 morphological computations for the Ameland ebb-tidal delta with the 2010 bathymetry as initial bathymetry.

Figure 5-8 shows the morphological results of the 2010 – 2014 validation run. Focussing on the spatial variation of sedimentation and erosion on the ebb-tidal delta, the four-year model prediction appears to capture the natural behaviour of the ebb-tidal delta reasonably well. The growth of the second ebb-chute and shield is well represented by the model. The magnitude of the seaward extension of the ebb-shield is comparable to the measured observations. However, the model predictions show a development of a wide and short ebb-chute whereas the measured bed level changes illustrate the formation of a narrow and long ebb-chute with a relatively small ebb-shield.

Furthermore, the offshore advancement of the Bornrif swash platform shows a comparable response in comparison with the measured bed level changes. The amplitude of the advancement is thereby consistent with the natural response of the ebb-tidal delta. A larger deviation prevails for the formation of the wide erosive plane on the central part of the Bornrif swash platform. The formation of this large-scale erosion of the swash platform can be attributed to the eastward migration of the Akkepollegat and the growth of the ebb-shield. The model shows an amplitude deviation in the order of 2 – 3 m between modelled and measured response. Nevertheless, the migration of the Akkepollegat and the formation of the second ebb-shield are reasonably well captured in the model.

5.1.3 Description of model performance (2016 – 2020)

Over the timespan from 2016 – 2020, the Ameland ebb-tidal delta is characterised by the formation and growth of the third ebb-chute. This ebb-chute is located in between the second ebb-chute and the Westgat on the central platform of the outer delta (Figure 5-9). Due to the subsequent attachment of the Bornrif swash platform to the coast of Ameland, it can be deduced that wave action is more relevant for the morphological development of the central platform of the outer delta. A set of morphological computations have been performed to assess the morphological development of the ebb-tidal delta over the 2016 – 2020 timespan.

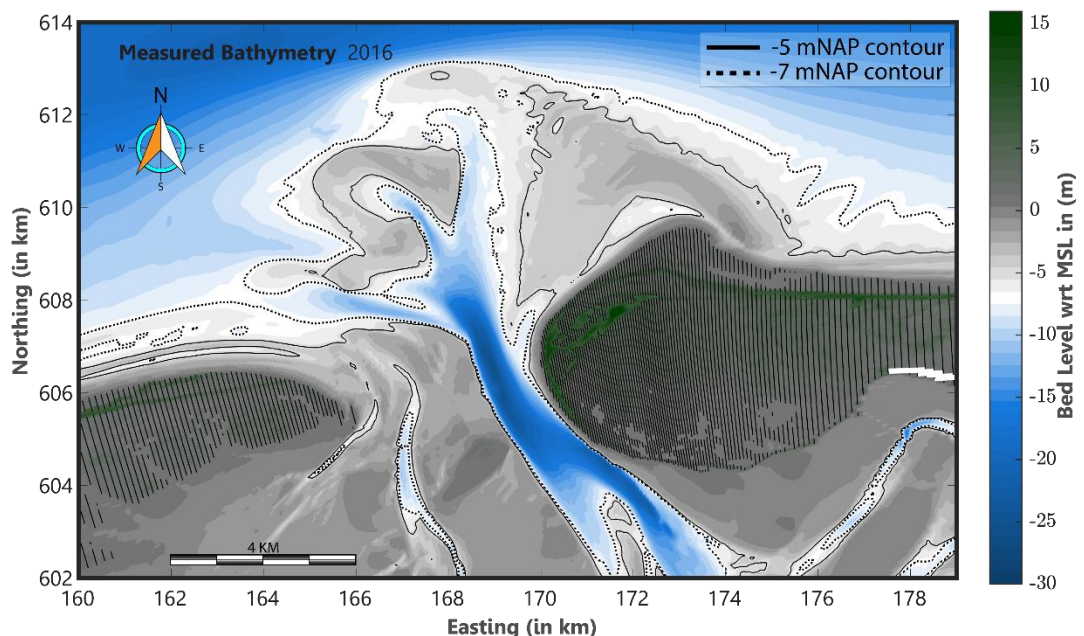


Figure 5-9: overview of the 2016 morphology of the Ameland ebb-tidal delta.

5.1.3.1 Annual runs

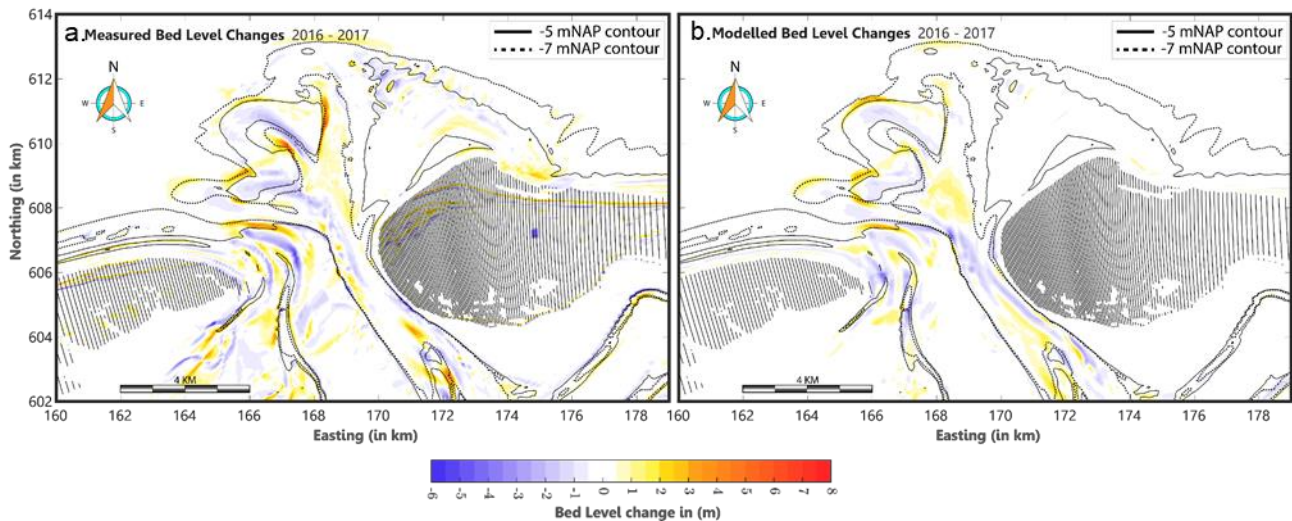


Figure 5-10: Model results of the 2016 – 2017 morphological computations for the Ameland ebb-tidal delta with the 2016 bathymetry as initial bathymetry.

Figure 5-10 shows the modelled response of the Ameland ebb-tidal delta over a period of 2016 – 2017. For this annual morphological computation, it can be seen that the model reproduces the morphological development of the ebb-tidal delta reasonably well. The location of erosion and deposition zones are thereby captured by the model; however, the magnitude show relevant anomalies in comparison with the natural response.

The development of the third ebb-shield is predicted by the model and the amplitude of the westward expansion is consistent with the measured bed level changes. The evolution of the second ebb-shield is however substantially underestimated; amplitude variations are observed in the order of 2 m along the inner margin of the second ebb-chute.

Furthermore, local sedimentation patterns in the Akkepollegat are reasonably well reproduced close to the Borndiep. Around the ebb-tidal delta margin the modelled morphological development is smaller than the observed changes. This follows also for the bar attachment on the Bornrif Strandhaak and for the advancement of the Zeehondenplaat.

At the terminal lobe the order of magnitude of the morphological changes is consistent with the observed response albeit that the seaward expansion is smaller than that the observations prevail.

5.1.3.2 Two-year runs

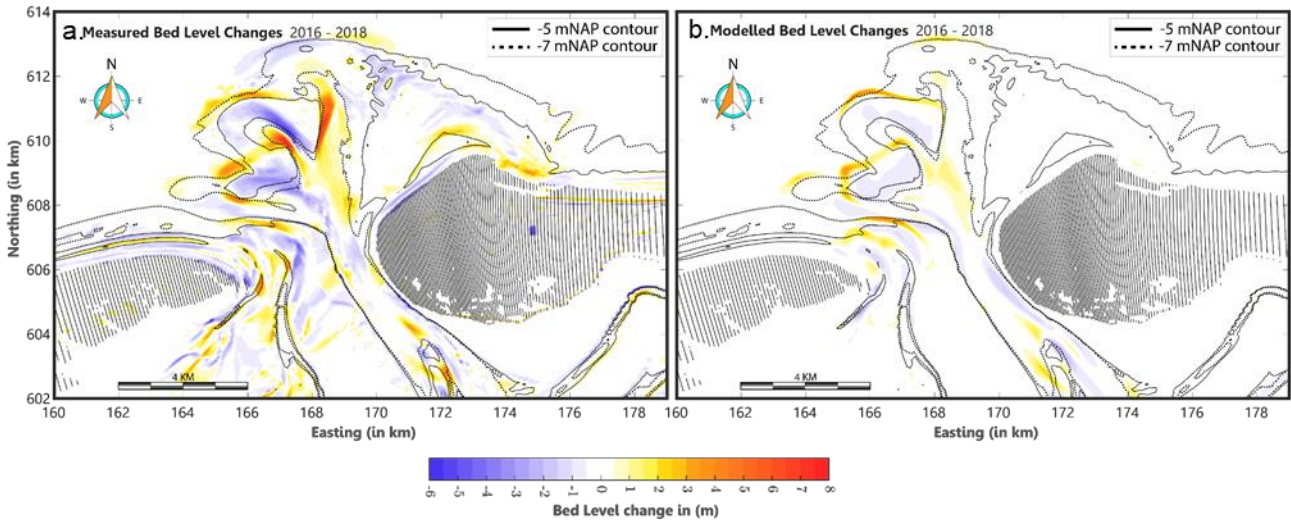


Figure 5-11: Model results of the 2016 – 2018 morphological computations for the Ameland ebb-tidal delta with the 2016 bathymetry as initial bathymetry.

For the 2-year morphological simulation for the Ameland ebb-tidal delta, the modelled response shows a limited coherence in morphological development. The evolution of the second and third ebb-shield is underestimated in comparison with the observations on the natural response. This can be seen from the relatively narrow region close to the ebb-shields where local sedimentation is observed. The results in a less pronounced seaward advancement in relation to what the measured bed level changes prevail.

The development of the Zeehondenplaat west of the Borndiep seems to provide a consistent accretion along the margin of the shoal. Moreover, the large infilling of the Akkepollegat is not captured by the model results. Also the erosion along the terminal lobe does not transpire in the modelled response. Lastly, the morphological development of the Borrif swash platform is not captured by the model. Solely, the seaward expansion of the terminal lobe can be observed in the model response.

5.1.3.3 Four year runs

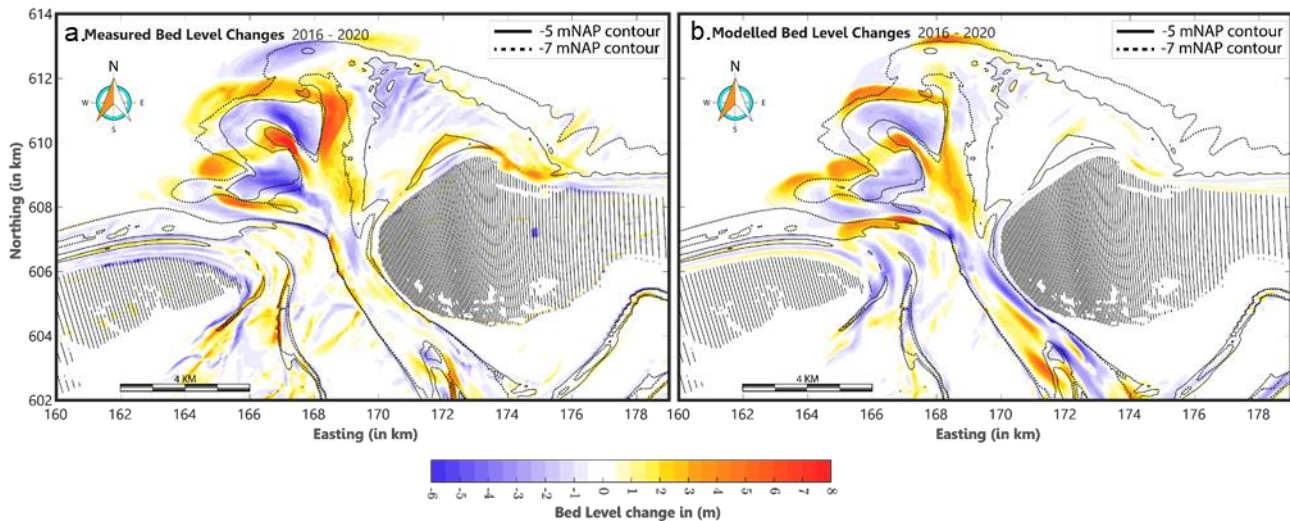


Figure 5-12: Model results of the 2016 – 2020 morphological computations for the Ameland ebb-tidal delta with the 2016 bathymetry as initial bathymetry.

The four-year morphological prediction of the Ameland ebb-tidal delta over a period from 2016 – 2020 is depicted in Figure 5-12, the morphological development shows thereby to reasonably well align with the observations on the natural response. Along the ebb-chutes and -shields the modelled response is consistent with the measured bed level changes. Small variations can thereby be identified in the shape of the accretion zone along second ebb-chute. Local erosion over the terminal lobe and the ebb-shields are reproduced by the model albeit with a smaller amplitude. This amplitude anomaly is estimated to be in the order of 2 – 3 m.

Furthermore, the morphological development of the Borrif swash platform is to a limited degree captured by the model. An erosion is predicted on the Borrif swash platform, yet the magnitude of the erosion is largely underestimated with respect to the measured bed level changes. This follows also for the sedimentation along the Borrif Strandhaak as a consequence to the migration of the Borrif swash platform.

5.1.4 Synthesis on morphological validation

Based on an assessment of the modelled bed level changes over the timespan from 2005 – 2020 the model's capability to reproduce the natural behaviour of the Ameland ebb-tidal delta has been further investigated. Model predictions have shown that the natural behaviour of the ebb-tidal delta can be reasonably well reproduced on a simulation time horizon of 4 years. Moreover, it has been observed that for the more recent timespans (i.e. 2010 – 2016, 2016 – 2020) the model produces a better morphological response than for the later timespans (i.e. 2005 – 2010). The best model predictions have overall been obtained for the 4-year morphological simulation of the 2016 – 2020 Ameland ebb-tidal delta where the model showed a consistent morphological response in the vicinity of the ebb-chutes and -shields.

5.2 Validation Pilot nourishment runs

In the preceding sections it is shown that in the vicinity of the ebb-chutes and -shields the model produces a consistent morphological response. This gives model certainty to assess the evolution of the 2019 pilot nourishment over the consecutive years after construction of the nourishment along the second ebb-shield.

From a timely volumetric analysis on the pilot nourishment, became clear that the initial response of the ebb-tidal delta is characterised by a large erosion. In the first months after construction of the pilot nourishment approximately 15% (roughly 0.7 million m³) of the initial 5 million m³ of sediment was lost in the nourishment polygon during the summer season (see Figure 3-7). Over the winter season, the pilot nourishment was subjected to even more erosion and lost another 19% (roughly 0.9 million m³) of its initial volume. Although in the months following the erosion of the nourishment reduced to approximately 0.1 million m³/month, an erosion in the nourishment polygon remained a persistent trend in volumetric analysis on till 2021 (Figure 5-13).

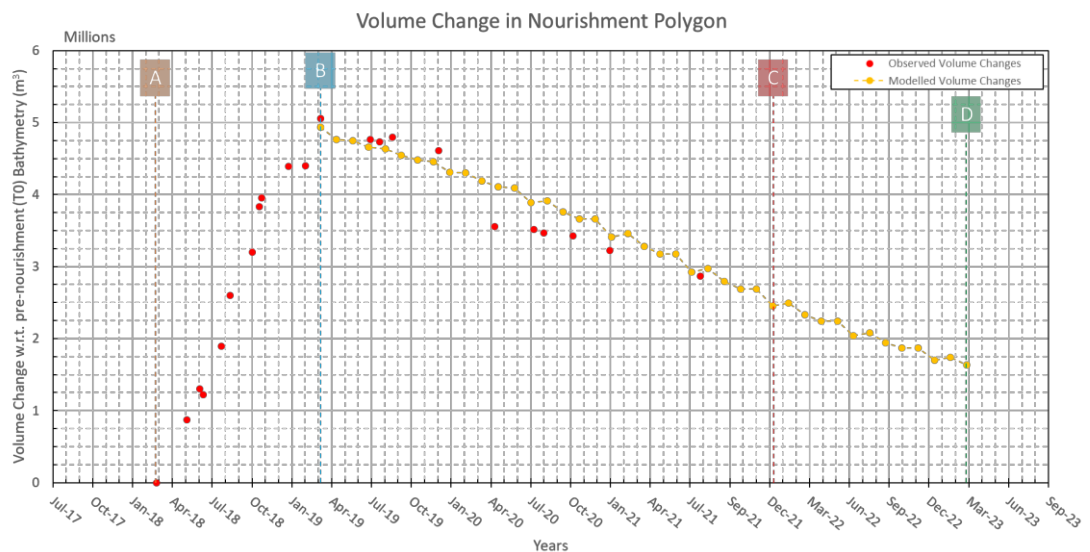


Figure 5-13: The development of the volumes in the construction polygon over the period after construction of the pilot nourishment. Stage A indicates the start of the pilot nourishment construction and stage B demarcates its completion. Stage C highlights the storm impact on the pilot nourishment and stage D indicates the end of the simulated morphological evolution of the pilot nourishment after stage B. It should be noted that stage B coincides also with the start of the model simulation.

To assess the model's capability to reproduce the morphological development of the pilot nourishment, a morphological simulation has been performed over a 4-year simulation time horizon. The model results are superposed on the natural volumetric trend in the nourishment polygon. A comparison between modelled volume trend and measured volume trend identifies that the model inherited the yearly-averaged morphological trend in the nourishment polygon. Hence, it can be concluded that by application of the present-state-of-the-art Ameland model an assessment can be performed on the impact of the pilot nourishment on the natural behaviour of the Ameland ebb-tidal delta.

5.3 Validation Run 2009 – 2021

To assess whether the erosion of the pilot nourishment remains a trend over a longer temporal scale, model simulations over an interval of 2018 – 2028/2030 respectively were performed with the post nourishment bathymetry as initial condition. Before these model results are further outlined, the validity of the model prediction is subsequently evaluated.

In light of the aforementioned, a validation run is composed to simulate the morphological development on a 12-year time interval from 2009 – 2021 (see Figure C 1 and Figure 5-16 below). Model results were subsequently compared with the measured bed level changes over the designated simulation period. What becomes clear from this comparison is that several morphological features are not well reproduced over a 12-year simulation time horizon. To get a better understanding on the long-term model performance, Figure 5-14 and Figure 5-15 illustrate the measured bathymetries of 2009 and 2021 respectively. The model predictions for the 2021 bathymetry are provided in Figure 5-16.

5.3.1 Bornrif Platform

In the 2009 bathymetry (Figure 5-14), the morphology of the Ameland ebb-tidal delta was typified by the evolution of the first [1] and second [2] ebb-chute system on the central platform of the outer delta, and the presence of the Akkepollegat [3] as the main ebb-outflow. The Westgat [4] was thereby the ebb-dominated marginal channel. Under the effect of the ebb-dominated tidal inlet current over the Akkepollegat, sediment bypassing processes enabled the seaward expansion of the Bornrif swash platform [5].

This was also observed in the model predictions for the natural behaviour of the outer delta using varying simulation time horizons (see also Sec. 5.1). Moreover, these results illustrated that the seaward advancement of the Bornrif swash platform [5] remained a persistent feature of the outer delta over the period of 2005 – 2016 (see Figure A 14 – Figure A 18 and Figure A 24). These findings are also coherent with the response observed for the prior performed validation run (Figure 5-16). The inherent tendency of the model to overpredict tide-driven transports however attributed to an overprediction of the Bornrif swash platform [5] expansion. And in combination with a longer simulation time horizon wherein the flow bypassing through the Akkepollegat [3] remained dominant, this only intensified in the validation run.

5.3.2 Growth ebb-chutes and -shields

This had further implications on the impact of wave-driven processes on the central platform of the outer delta. Consequently, the evolution of the second ebb-chute and -shield [2] was mainly governed by the tide-driven effect of the tidal inlet current. Over the period following, a large north-northwest growth of the ebb-shield [2] may therefore be observed.

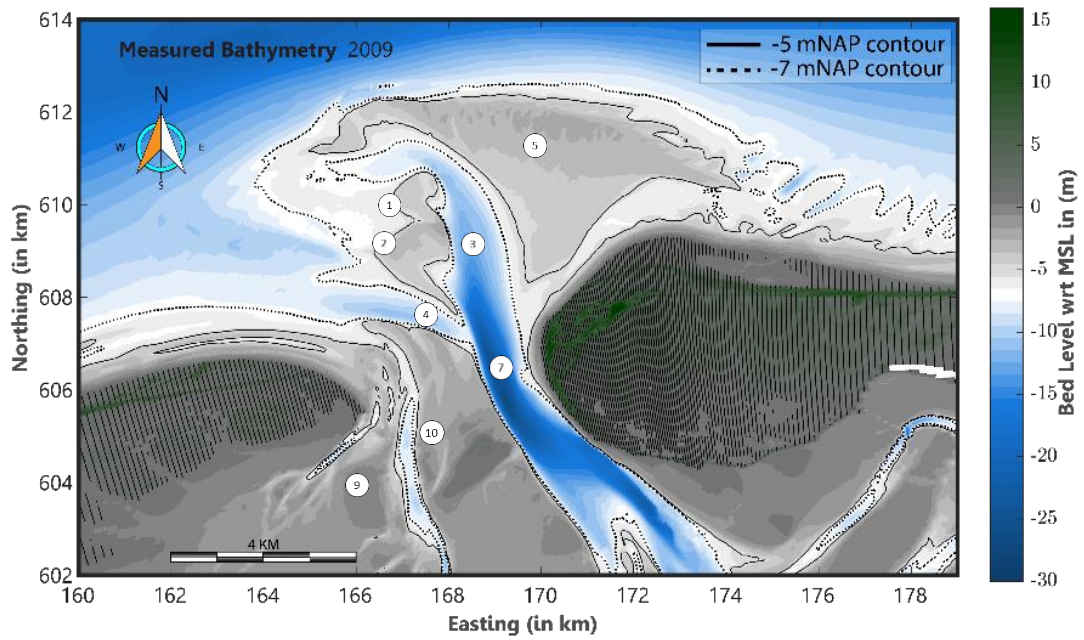


Figure 5-14: 2009 Measured Bathymetry of Ameland ebb-tidal delta.

Based on Figure 5-16, the model is able to capture the growth of the second ebb-shield on the central part of the outer delta albeit reasonably overpredicted. Thereby, a characteristic feature of the 2021 morphology of the Ameland ebb-tidal delta is the emergence of a third ebb-chute system [6] which developed in 2016. This has unfortunately not been reproduced by the model. It may be inferred from prior findings on the natural behaviour of the outer delta (see Sec.5.1) that the onset of ebb-chutes is directly related to the choice of initial bathymetry in the model simulation. Therefore, as the third ebb-chute system [6] is not present in the 2009 bathymetry, the onset of this feature in simulations beginning that year may not be guaranteed.

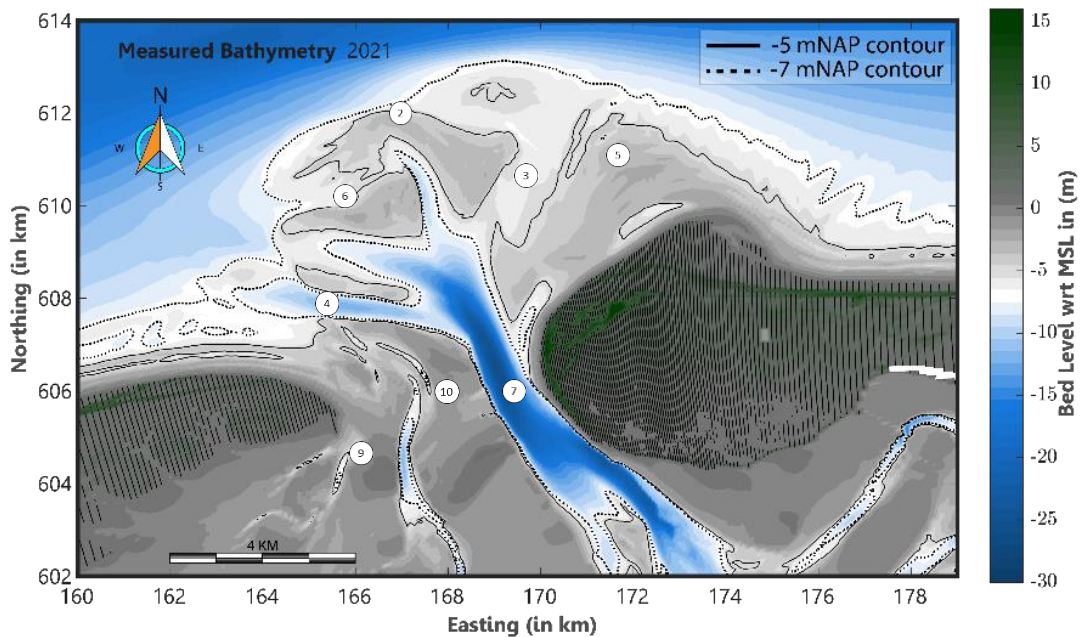


Figure 5-15: 2021 Measured Bathymetry of Ameland ebb-tidal delta.

5.3.3 Westgat

Furthermore, the model results appear to emphasize the dominance of the Westgat [4] as main-ebb outflow for the 2021 Ameland outer delta. In the modelled 2021 bathymetry (Figure 5-16a), it may be seen that the model anticipated on a further deepening and increase in size of the Westgat [4]. Moreover, in combination with the increasingly shallower predicted Akkepollegat [3], it seems that a main-ebb channel switch has been proceeded. The Westgat is hereby predicted to directly connect to the Borndiep [7] and serve as main ebb-channel. This is however a rather debatable outcome. From recent findings of Elias et al., (2019) it is questioned whether the Westgat [4] will take over as main-ebb outflow from the Akkepollegat [3]. Recent surveys of the outer delta (Figure 5-15) have shown that the Akkepollegat [3] is decaying whereas the third ebb-chute [6] is rapidly growing in depth and in size (Elias et al., 2019). The measured 2021 bathymetry (Figure 5-15) confirms this trend and suggests that the onset of a main-ebb channel switching is progressing. However it is hypothesised by Elias et al., (2019) that instead of a growth of the Westgat [4] the third ebb-chute [6] will further develop as the main-ebb channel in the forthcoming years. This is in contrast with model predictions for the year 2021 as followed by the 12-year morphological simulation (Figure 5-16). Clearly, the development of a main ebb-channel switch did not transpire in the model prediction provided that the model was not able to capture the initial development and growth of a third ebb-chute [6] at all.

5.3.4 Zeehondenplaat and Coast of Terschelling

The growth of the Westgat [4] in the model simulations had also further implications on the morphological features in the vicinity of the channel. It may be seen in Figure 5-16b that the widening of the flow through the Westgat [4] heralded an intensive growth of a shore-parallel channel margin linear bar [8] along the first ebb-chute [2]. This enabled also the wave sheltering of the Coast of Terschelling and the Borndiep [7] which promoted a coastline advancement and several deposition patterns are observed over the Zeehondenplaat. Also, a spit formation had emerged along the Zeehondenplaat [4] towards the Coast of Terschelling. From 2021 surveys of the Ameland ebb-tidal delta (Figure 5-15), it is known that instead of an elongated spit formation along the eastern tip of the coast of Terschelling the Zeehondenplaat increases in size and attaches to the adjacent coast of Terschelling. However, the tide-dominated character of the model prediction seems to enable an overestimation of the flow through the marginal channel Oosterom [9] and the Boschgat [10]. Consequently, local flow intensification contributes here to a significant deepening of the channels and the emergence of large coastal marginal outflow at the confluence of the two channels in the inlet gorge (Figure 5-16).

5.3.5 Synthesis of validation run

The validation run illuminated the model performance on temporal scales of 10-12 years. On these temporal scales, the model showed limited consistency with the observed morphological development on the ebb-tidal delta. This could be inferred from the modelled location of morphological features which misaligned with the measured bathymetry of the Ameland ETD and the appearance of significant dissimilarities in morphological variability over the time span of interest.

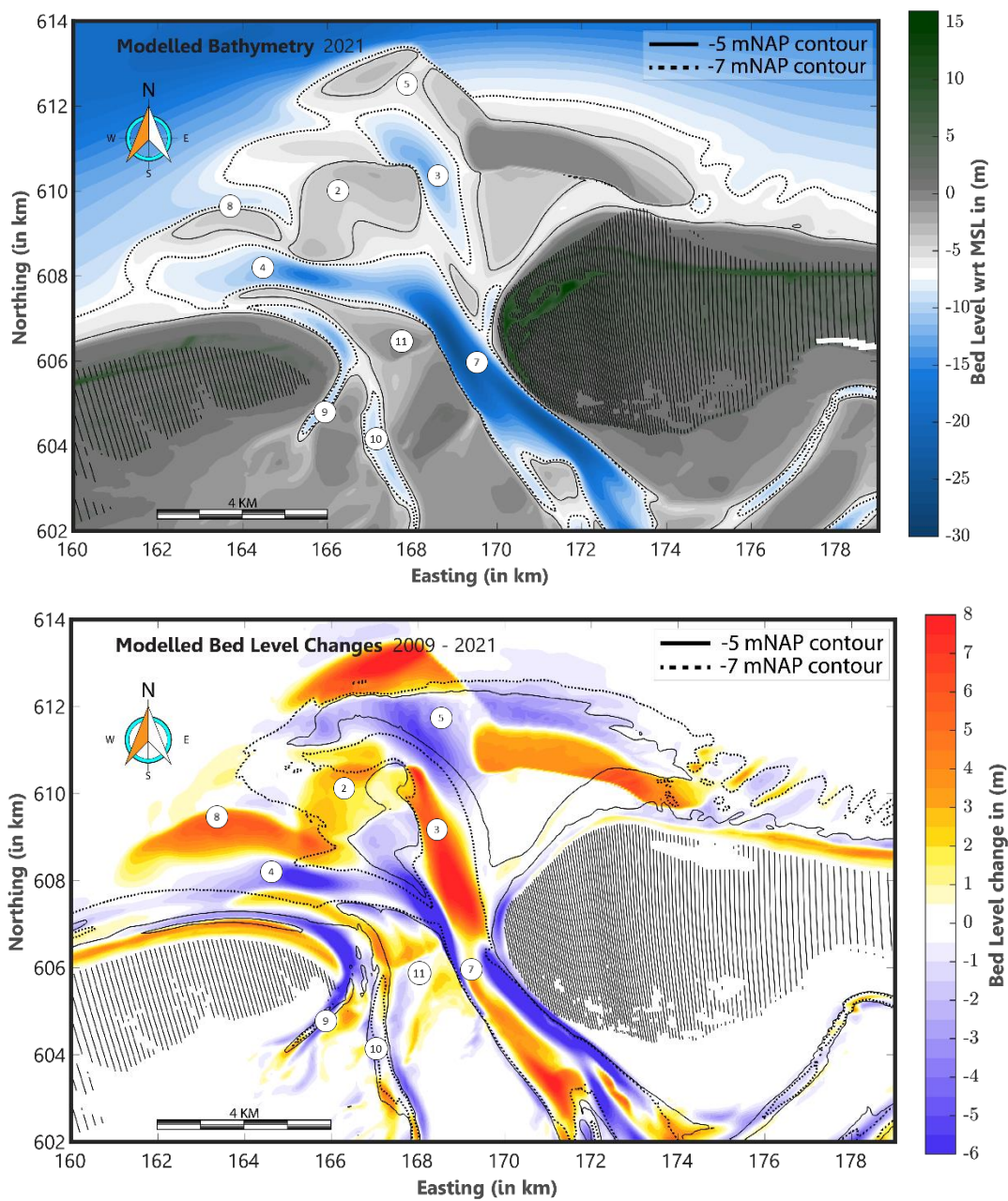


Figure 5-16: 12-year model prediction on the morphological development of the Ameland ebb-tidal delta. Results show (a) the modelled morphology of the outer delta in 2021, and (b) the modelled bed level changes over the simulation period from 2009 – 2021.

5.4 Nourishment Forecasting 2018 – 2028/2030 Runs

Therefore, the model was not fit to assess the morphological development of the ebb-chutes and -shields over longer temporal scales. This was also verified by the morphological computations of the impact of the pilot nourishment over the course of 2018 – 2028/2030 respectively (Figure C 2). The model results showed also here that the overpredicted deepening and widening of the Westgat severely influenced the evolution of the second [2] and third ebb-chute [6] system on the central platform of the outer delta (Figure 5-18). These formations had been pushed westward along the northern margin of the Westgat [4]. In combination with the overestimation of sediment accumulation on the central part of the outer delta platform (as known from the validation run) these ebb-chute systems are transformed into a main shoal.

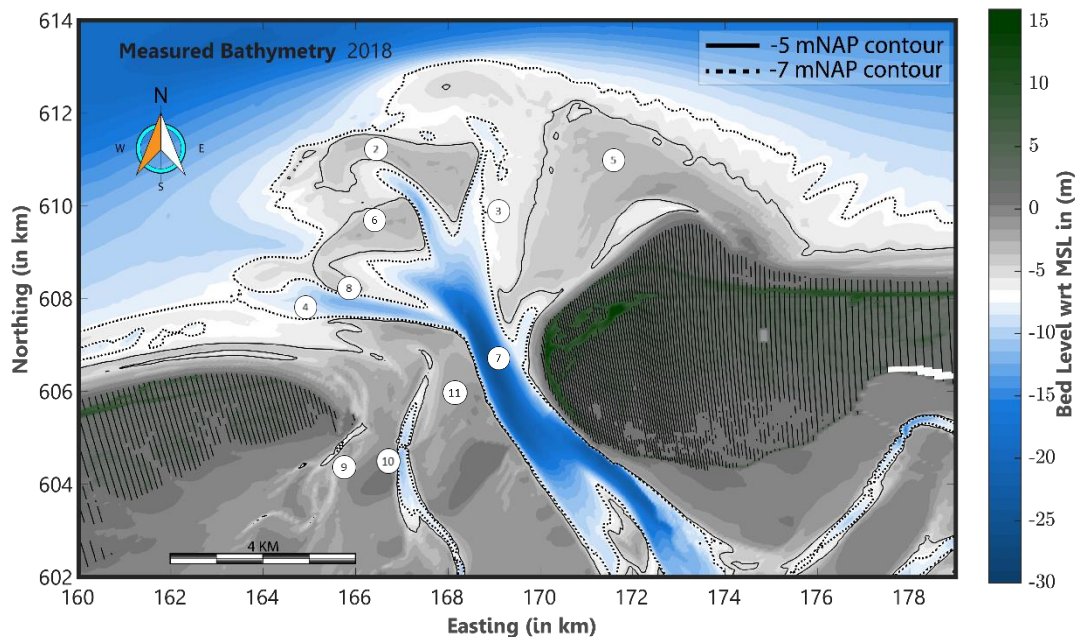


Figure 5-17: Measured 2018 bathymetry of the Ameland ebb-tidal delta.

Conversely, the appearance of the third ebb-chute in the initial 2018 bathymetry enabled its growth in the forthcoming years. In the computed 2021 bathymetry, the channel margin linear bar [8] – is evolved into a sill separating the flow through the Westgat [4] and the third ebb-chute [6]. Due to siltation of the Akkepollegat [3], these channels eventually form the main ebb-outflow in the post nourishment model results. As previously mentioned, it is questioned whether the Westgat [4] will increase in size and both channels will take over the function as main-ebb channel albeit that a further development of the third ebb-chute [6] is anticipated on based on recent data analysis (Elias et al., 2019). Therefore, it may be argued that this is correctly predicted by the model.

Lastly, it should be noted that the impact of the nourishment to the outer delta has not been properly captured by the model as expected. As on this temporal scale is acknowledged that the model predictability of the onset of the shoals and chutes on the central platform of the outer delta is limited, the impact of the nourishment have not been observed in the model results (Figure C 2 **Error! Reference source not found.**). More precisely, the nourishment seems to be completely dispersed over the entire offshore premises of the model domain (see Figure C 2g/h). Apparently, no distinct deviations had thereby been detected between

the pre- and post-nourishment bathymetry such that no clear conclusion could be drawn from these results on the evolution of the pilot nourishment.

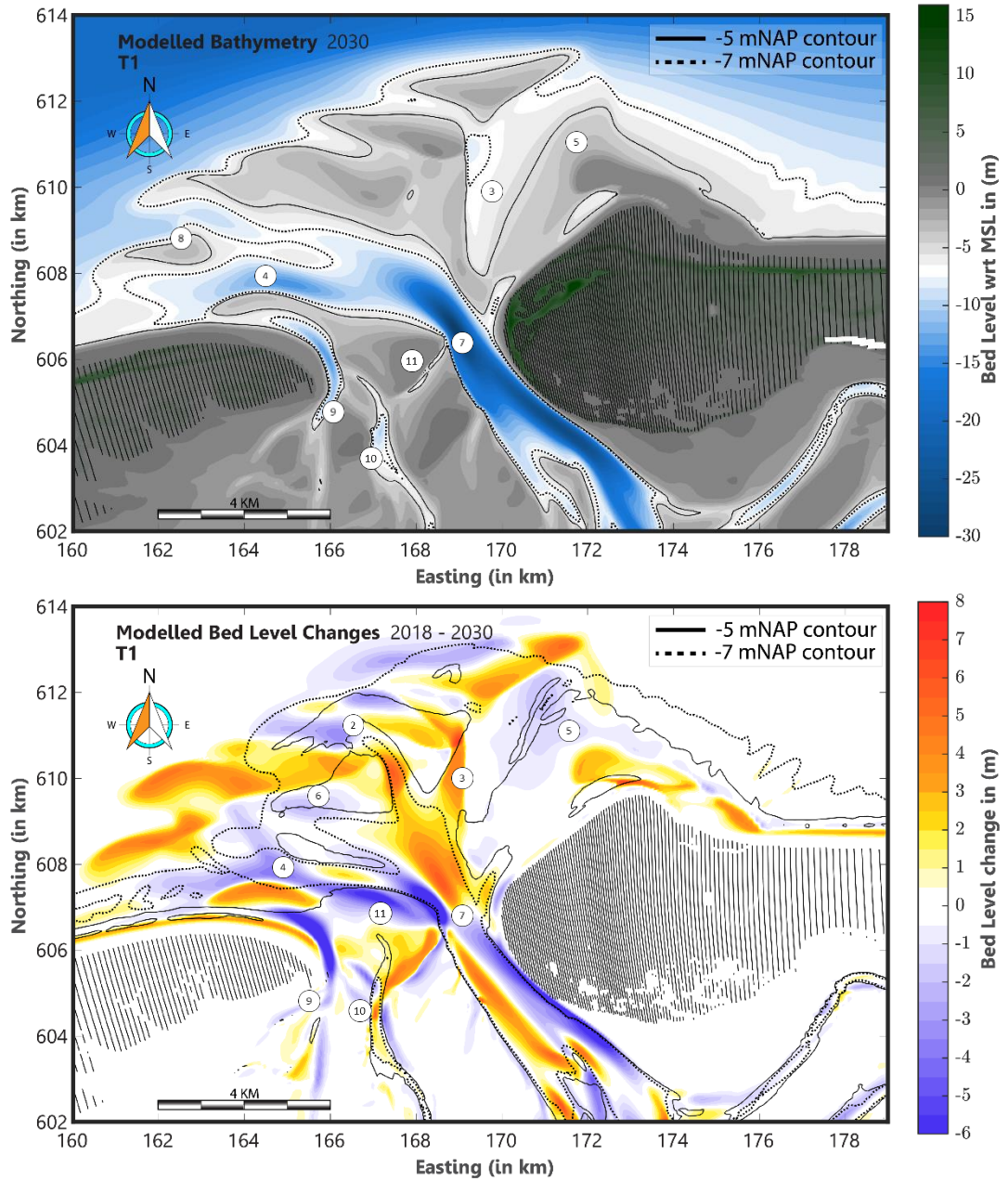


Figure 5-18: Model prediction of the Ameland ebb-tidal delta over the time span of 2018 – 2030. a) shows the computed bathymetry after 12 years of morphological climate and, b) shows the modelled bed level changes.

6 Morphological Impact Pilot Nourishment

6.1 Introduction

In this chapter, the effect of the 2019 pilot nourishment on the natural behaviour of the Ameland ebb-tidal delta is further investigated. Therefore, a morphological calculation is performed based on the 2018 pre-nourishment bathymetry of the Ameland ebb-tidal delta. An initial nourishment volume of 4.9 Mm³ is subsequently added to the latter bathymetry in the construction polygon to reflect the construction of the 2019 pilot nourishment (see Figure 6-1).

Based on a morphological assessment and comparison of the modelled response for the pre- and post-nourishment bathymetry, the impact of the pilot nourishment can be evaluated. For this morphological assessment, the present-state-of-the-art Ameland model is applied, using the simulation time horizon for which the model produces the best possible morphological prediction. As such a 4-year time horizon is considered for the assessment of the pilot nourishment (see Ch. 5).

Henceforth, Sec. 6.2. aims to build a further understanding of the natural response of the ebb-tidal delta by means of a bathymetric analysis, and an analysis of the water motion and sediment transport. Moreover, sec. 6.3. provides an investigation into the impact of the pilot nourishment by means of a comparative assessment on the pre- and post-nourishment changes in volume, bathymetry and sediment transport. To get further insights into the interaction of the pilot nourishment with the ebb-tidal delta morphology, several ebb-tidal delta nourishment alternatives are also addressed in this chapter. Sec. 6.4. – 6.6. elaborates on these nourishment alternatives (Figure 6-13) and their implications on the morphological response of the ebb-tidal delta. An overview of the morphological runs for this assessment is provided in Table 6-1 below.

Model Runs				
2019 Pilot Nourishment runs				
Simulations	Processes			
	Tide	Waves	Wind	Morph
Ameland ETD 2018 – 2022 (T0)	Yes	Yes	Yes	Yes
Ameland ETD 2018 – 2022 (T1)	Yes	Yes	Yes	Yes

Ebb-tidal delta Nourishment runs				
Simulations	Processes			
	Tide	Waves	Wind	Morph
Ebb-tidal delta nourishment (V1) Third ebb-chute	Yes	Yes	Yes	Yes
Ebb-tidal delta nourishment (V2) Zeehondenplaat	Yes	Yes	Yes	Yes
Ebb-tidal delta nourishment (V3) Second ebb-chute	Yes	Yes	Yes	Yes
Ebb-tidal delta nourishment T1 w/ -2.5mNAP height (H1)	Yes	Yes	Yes	Yes
Ebb-tidal delta nourishment T1 w/ -0mNAP height (H2)	Yes	Yes	Yes	Yes

Table 6-1: Overview of the morphological runs that are performed in the assessment of the morphological impact of the pilot nourishment.

6.2 Analysis on T0 Behaviour

6.2.1 Flow patterns

The Ameland ebb-tidal delta is situated in a dynamic environment where both tidal currents and wave action influence the morphological development of the outer delta features. The interaction between the tidal current through the inlet and the shore-parallel tidal current is therewith essential for the characteristic flow and transport patterns on the ebb-tidal delta. To get a better understanding on the hydrodynamic conditions, the water motion and flow patterns have been studied for different instances throughout the tidal cycle (see Figure 6-2). A double tidal cycle is chosen to ensure that daily inequality in the tidal oscillation is captured in this analysis. Snapshots of the flow patterns during the respective instances (*I – VII*) are presented in Figure 6-3.

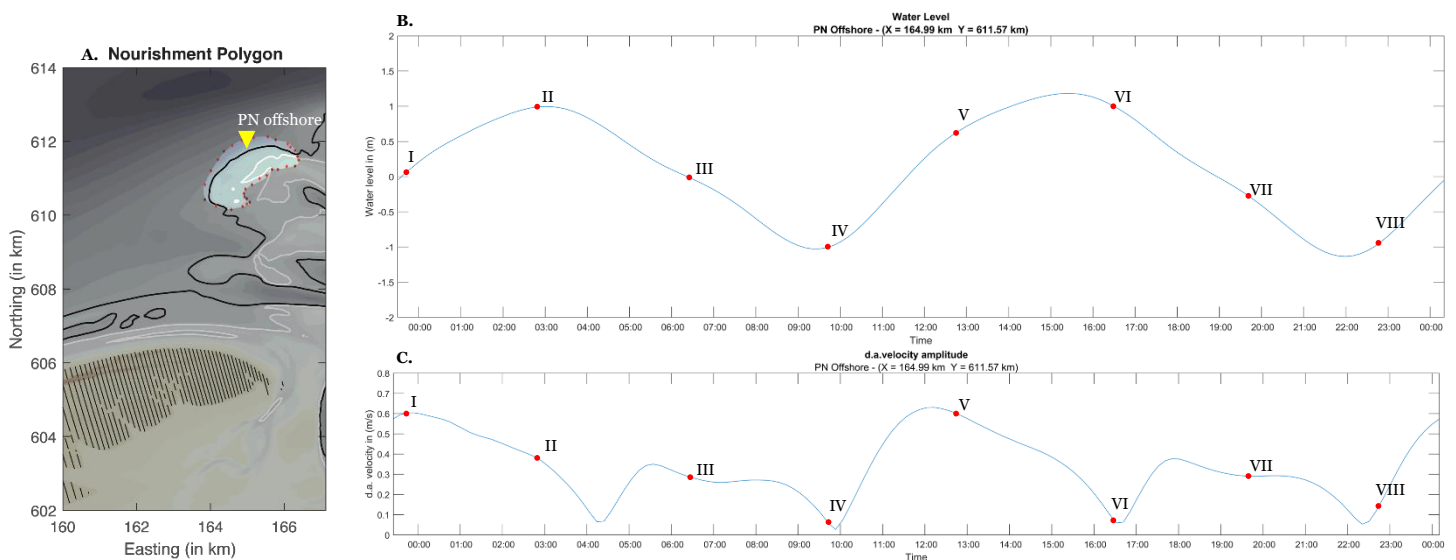


Figure 6-2: Time series of the tide-induced water level variation over a double-tidal period starting from 03-01-2018 to 04-01-2018. (a.) shows the location of the observation point (yellow triangle) on the ebb-tidal delta. (b.) shows the water level variation of time whereas (c.) illustrates the variations in depth-averaged velocity.

The North Sea tide propagates along the Ameland inlet as shore-parallel tidal current from west to east. Next, via the Westgat along the coast of Terschelling and over the ebb-chutes, the flood tide penetrates the main-inlet Borndiep from the west. The largest velocities can be therewith observed westward from Borndiep. During flood tide (Stage *I*), large velocity magnitudes of about 0.8 m/s can also be observed in the observation point PN just offshore from the pilot nourishment polygon (Figure 6-2C). During ebb tide (e.g. Stage *III* & *IV*), the flow velocities are significantly smaller; flow velocities of 0.2 – 0.4 m/s are commonly observed with local minima even dropping to 0.1 m/s.

The topography of the outer delta in conjunction with the tidal inlet current provides an extra complexity to the prevailing current patterns (Figure 6-3). The interaction between the shore-parallel tidal currents and the tidal inlet currents create flow patterns in the direction of the inlet gorge. The flow along the eastern section of the ebb-tidal delta – along the Borndiep swash platform – turns during flood towards the inlet gorge where the flow patterns converge (e.g. Stage *II*, *V* & *VI*). Since, all velocity vectors are directed to the Borndiep where they converge, relatively large velocity vectors can be found in the inlet, but also in the ebb-chutes.

During ebb-tide (e.g. Stage III, IV, VII & VIII), the low water levels and strong flow through the Borndiep enables an outflow through the Westgat, the ebb-chutes and the Akkepollegat. A spreading (i.e. divergence) of the flow patterns can therewith be clearly observed.

The onset of the flow patterns in between Stage VIII and Stage I (i.e. Stage VIII → I) highlights an instance wherein the flow through the Borndiep is still ebb-dominated and the shore-parallel current is changing from westward propagation (ebb tide) to eastward propagation (flood tide). The combination of an ebb-directed outflow through the Borndiep and a developing flood-directed shore-parallel tidal current enables the persistence of a relatively large outflow over the Bornrif swash platform and the second ebb-shield, whereas the offshore flow and the flow through the Westgat illustrate significantly smaller velocities.

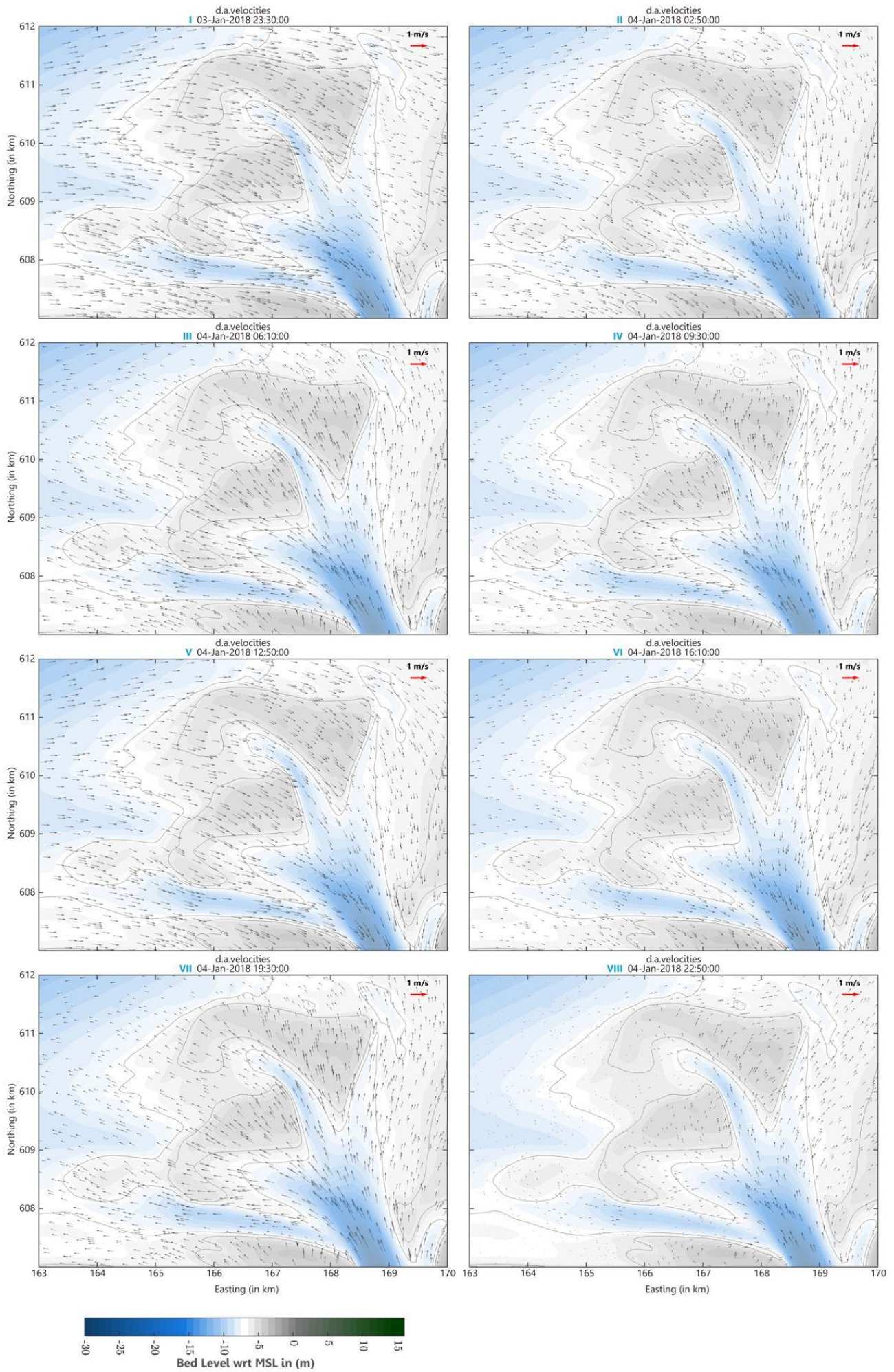


Figure 6-3: Snapshots of the depth averaged velocity on the ebb-tidal delta over the instances (I - VIII) in the tidal cycle.

6.2.2 Effect of wave climate on ebb-tidal delta morphology

Figure 6-4a gives a spatial overview of the yearly-averaged wave climate on the Ameland ebb-tidal delta. The yearly-averaged wave climate is obtained by summing the weighted contribution of the individual wave conditions in the morphological wave climate. The individual wave conditions in the yearly-averaged morphological wave climate is shown in Figure 6-5 and Figure 6-6.

The averaged wave climate for the pre-nourishment bathymetry shows a spatial variation of the wave height with a maximum of around the 0.7 m. These larger wave heights are found offshore of the ebb-tidal delta. Along the coast of Terschelling, waves can almost undisturbedly propagate towards shore. Therefore, the surf zone is relatively narrow and waves tend to break close to the shoreline. Wave height variations are thereby found close to shore with wave heights smaller than 0.25 m (Figure 6-4a). This can also be seen from the narrow bandwidth close to shore where wave energy dissipation is concentrated (Figure 6-4b). Along the coast of Ameland, east of Easting 177 km, a similar pattern can be observed.

On the shallower ebb-tidal delta platforms, waves are refracting towards the local depth contours and are breaking close to the margin of the shoaling platforms along the -5 m depth contour. This can be clearly observed for the larger waves (e.g. wave conditions 14, 15 and 16) which are breaking on the Bornrif swash platform (Figure 6-6). For low to moderate waves (e.g. wave conditions 1 – 8, see Figure 6-5), waves tend to break on the local shoal Bornrif Strandhaak. This can be seen from the increased wave attenuation (Figure 6-4a) and the increased energy dissipation (Figure 6-4b) around the Bornrif Strandhaak. The local breaking of waves is however not limited to the low - moderate waves as for large wave conditions the Bornrif Strandhaak as secondary breaker zone close to shore.

Moreover, the appearance of a shallower ebb-tidal delta platform allows for a significant wave attenuation offshore of the inlet Borndiep. This follows from the spatial variation of wave heights on the ebb-tidal delta. The wave heights are reduced from almost 1 m offshore to 0.5 m close to the inlet (Figure 6-4a). A small nuance can be identified close to the inlet; west of the Borndiep, relatively larger wave heights can be found as wave penetrate via the Westgat into the Borndiep.

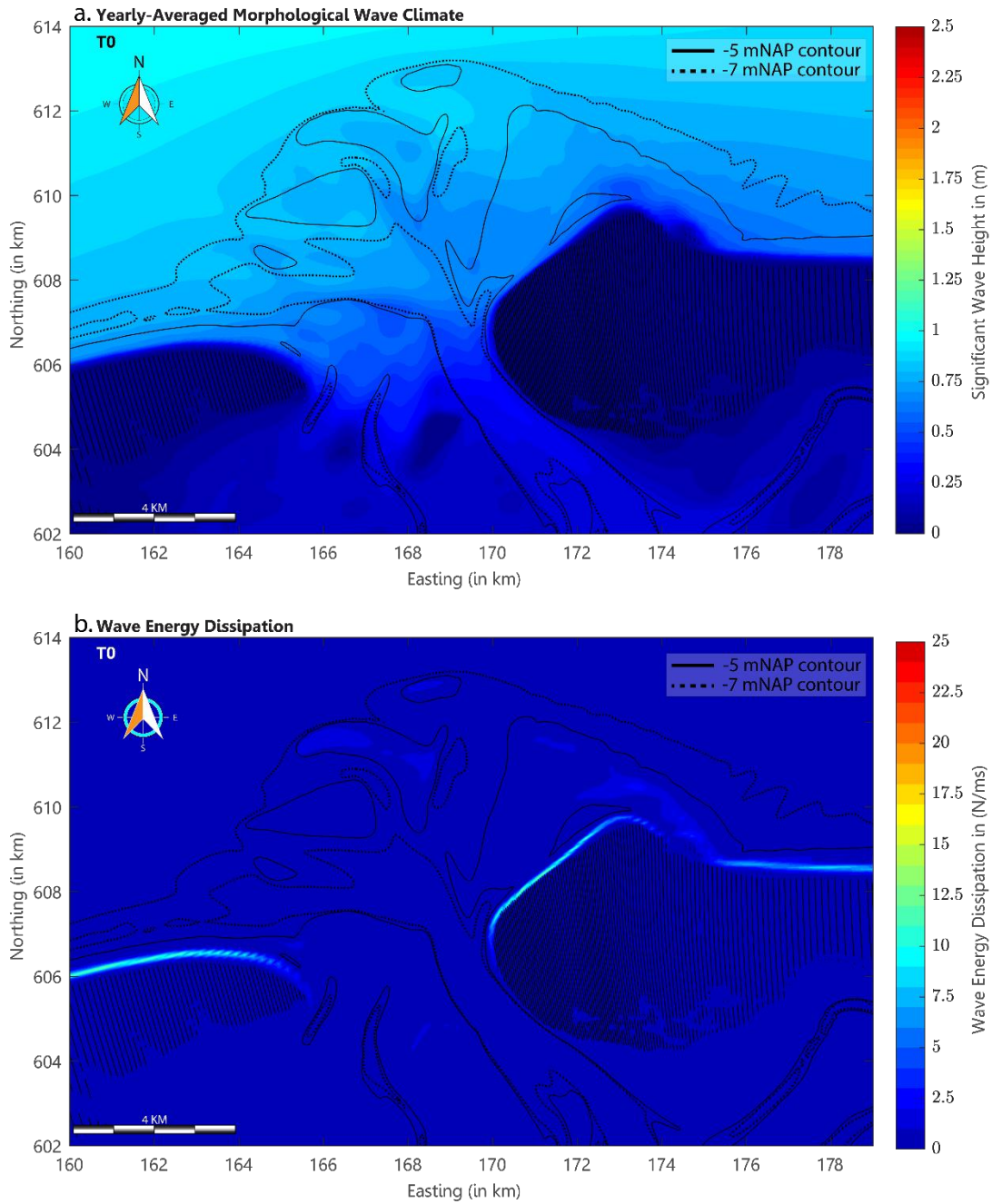


Figure 6-4: Overview of the yearly-averaged wave climate on the Ameland ebb-tidal delta before construction of the pilot nourishment. (a.) shows the yearly-averaged wave heights and (b.) shows the yearly-averaged wave energy dissipation over the ebb-tidal delta.

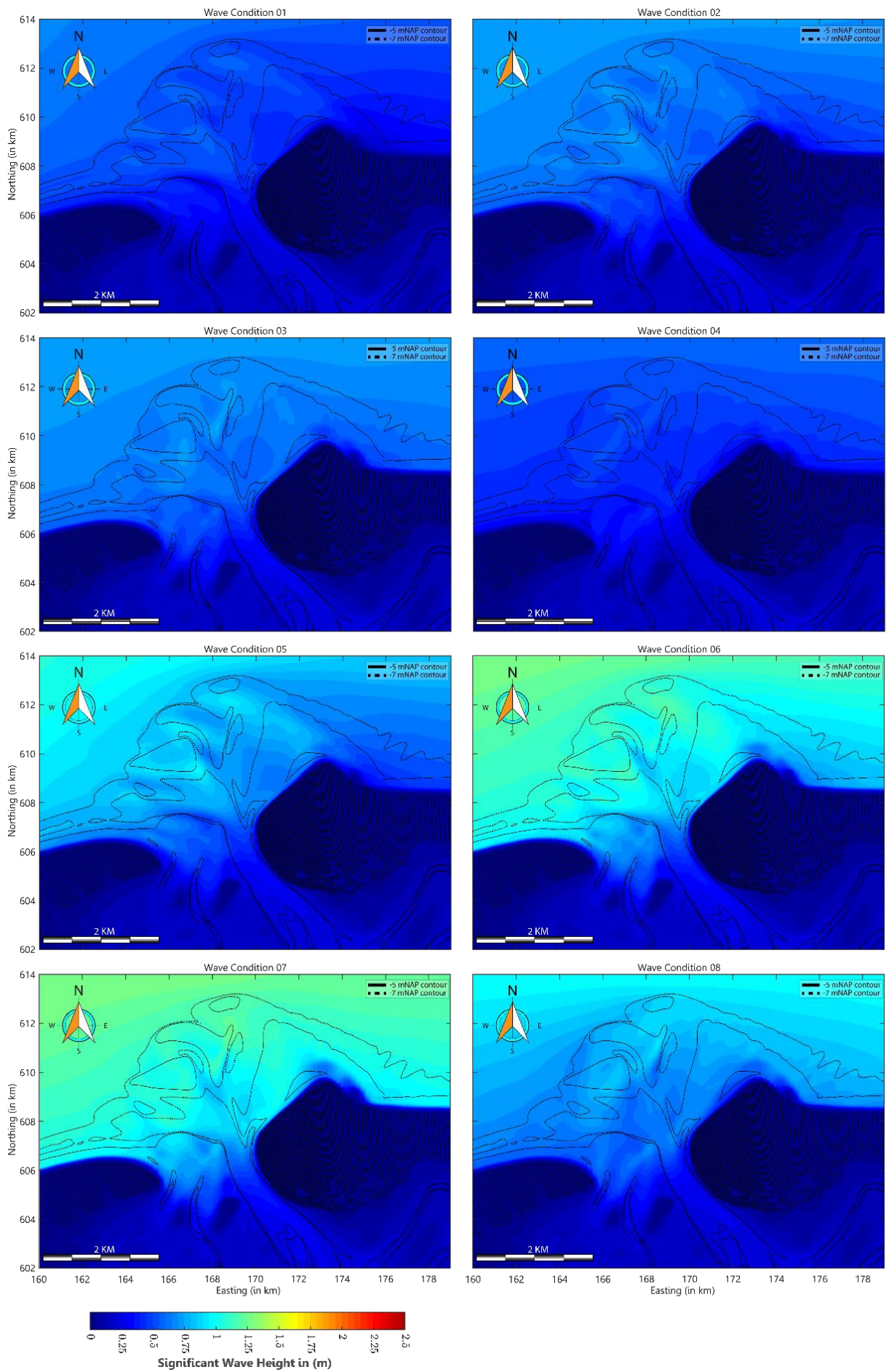


Figure 6-5: Overview of the individual wave conditions in the T0 morphological wave climate for the Ameland ebb-tidal delta. (1/2)

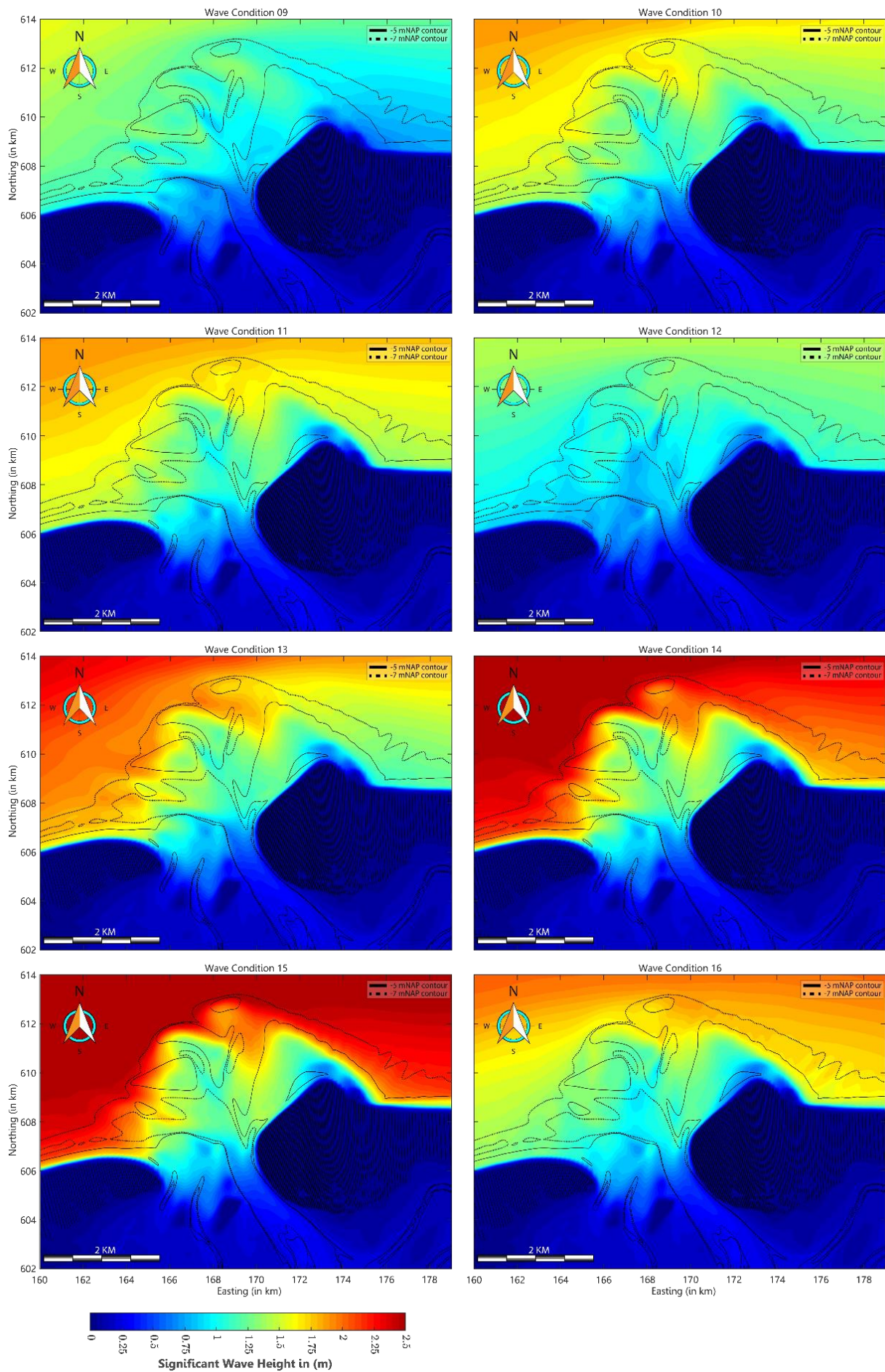


Figure 6-6: Overview of the individual wave conditions in the T0 morphological wave climate for the Ameland ebb-tidal delta. (2/2)

6.2.3 Sediment Transport

The instantaneous sediment transport patterns over a double tidal period are depicted in Figure 6-7. These sediment transport patterns follow from a morphological computation based on the pre-nourishment bathymetry wherein the effect of tides is taken into account. The sediment transport shows thereby consistent transport patterns with respect to the underlying water motion (Figure 6-3). This follows from the intrinsic relation between the prevailing depth average velocity and the sediment transport.

During ebb and flood tide, the largest sediment transport magnitudes are found close to the Borndiep, on the second ebb-shield and the Westgat. Thereby, a spatial variation can be observed over the ebb-chutes and -shields. During flood tide (e.g. Stage *I, II & IV*), the transport vectors converges over the ebb-shields in the direction of Borndiep, whereas during ebb tide (e.g. Stage *III, IV & VII*) a divergence of transport vectors is apparent.

A similar spatial variation can be shown for sediment transport interaction with the Borndiep. During flood tide (e.g. Stage *I, II & IV*), smaller sediment transport magnitudes are found in the Borndiep, and the transport vectors are concentrated along the Zeehondenplaat and in the Westgat. During ebb-tide (e.g. Stage *III, IV & VII*), conversely, larger sediment transport magnitudes can be found in the Borndiep and the transport vectors are widely distributed over the ebb-chutes and -shields.

Overall, it can be seen that over a tidal cycle the ebb-dominated transport over the central platform of the ebb-tidal delta is significantly larger than the flood-dominated transport. This also follows from an assessment of the residual sediment transport patterns. In addition, a morphological computation is performed to assess the effect of both tide- and wave-induced processes to the sediment transport. The resulting residual sediment transport patterns are depicted in Figure 6-8. Under these combined effects, the resulting sediment transport patterns prevail that the tide-induced transport patterns are sustained under the effect of waves. In fact, the effect of wave action is an increase of the sediment transport magnitudes. Hence, larger ebb-directed sediment transports magnitudes are found in the ebb-chutes and shields. A similar change has been observed for the sediment transport magnitudes in the Akkepollegat.

6.2.4 Bed level changes

The spatial variation in transport magnitude over the ebb-tidal delta has also an impact on the entrainment and deposition of sediment particles. In Figure 6-8, the resulting deposition and erosion patterns over one double tidal period has been illustrated alongside the residual transport patterns. In the context of the morphological computation, this tidal cycle aligns with a morphological development in the order of 3 months. Over this morphological period, it can be seen that the ebb-shields are characteristic regions governed by both sedimentation and erosion. Sedimentation zones are present on the seaward margin of the shield, and erosion zones can be observed in the ebb-chute along the inner margin of the ebb-shield. The central platform of the ebb-tidal delta is typified by sedimentation with a persistent erosion spot close to the inlet Borndiep. This can be linked with the flow convergence and divergence over the tidal cycle.

The pre-nourishment (T0) model prediction over a 4-year simulation timespan shows furthermore an aggregation of the results as illustrated in Figure 6-8. Figure 6-9 shows the accumulative sedimentation and erosion over the 4-year time horizon. Also, here distinct sedimentation and erosion zones can be observed along the ebb-shields and close to the Borndiep. In addition, it is also shown that the terminal lobe is characterised by sedimentation.

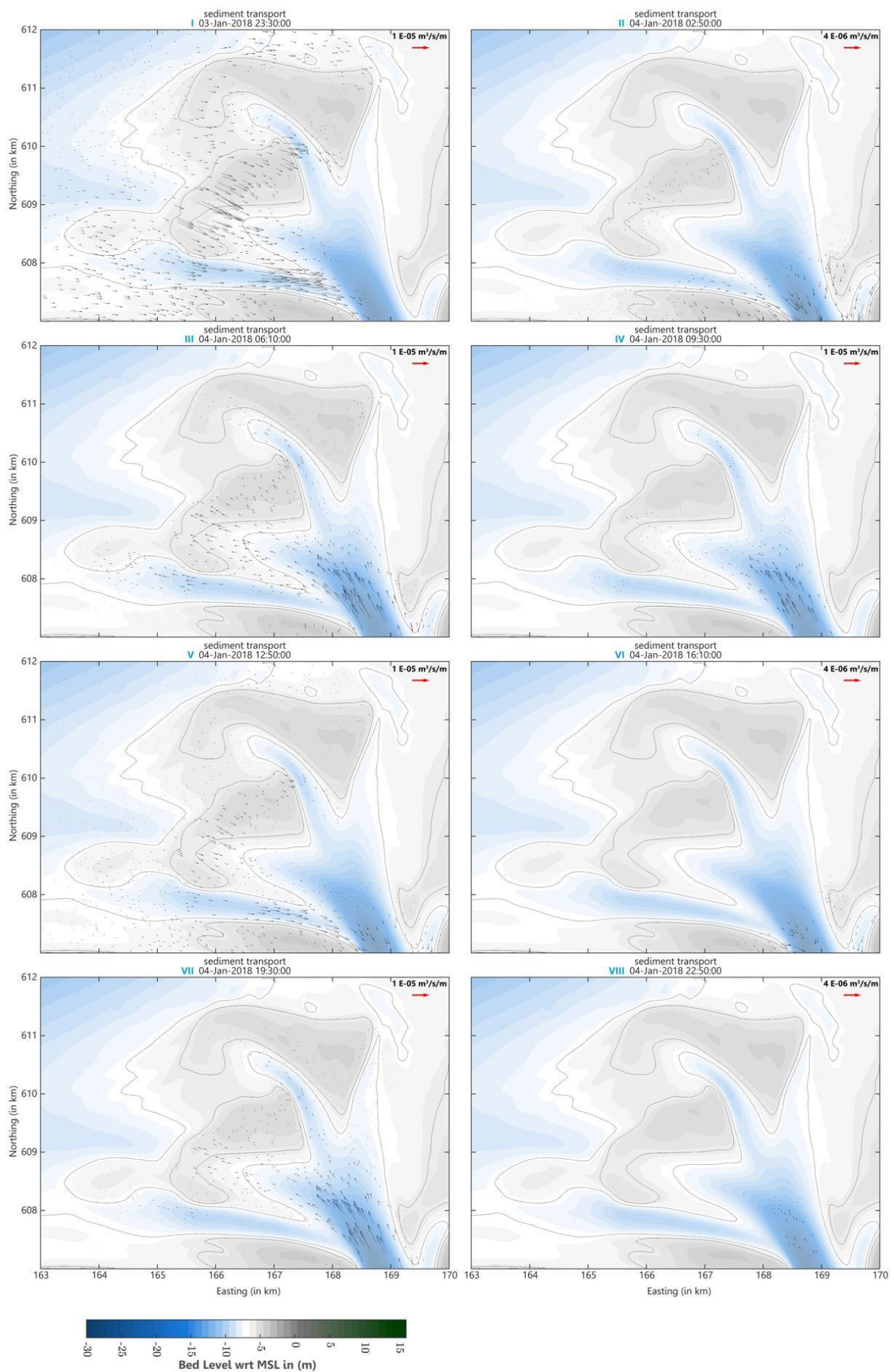


Figure 6-7: Snapshots of the tide-induced sediment transport on the ebb-tidal delta over the instances (I - VIII) in the tidal cycle.

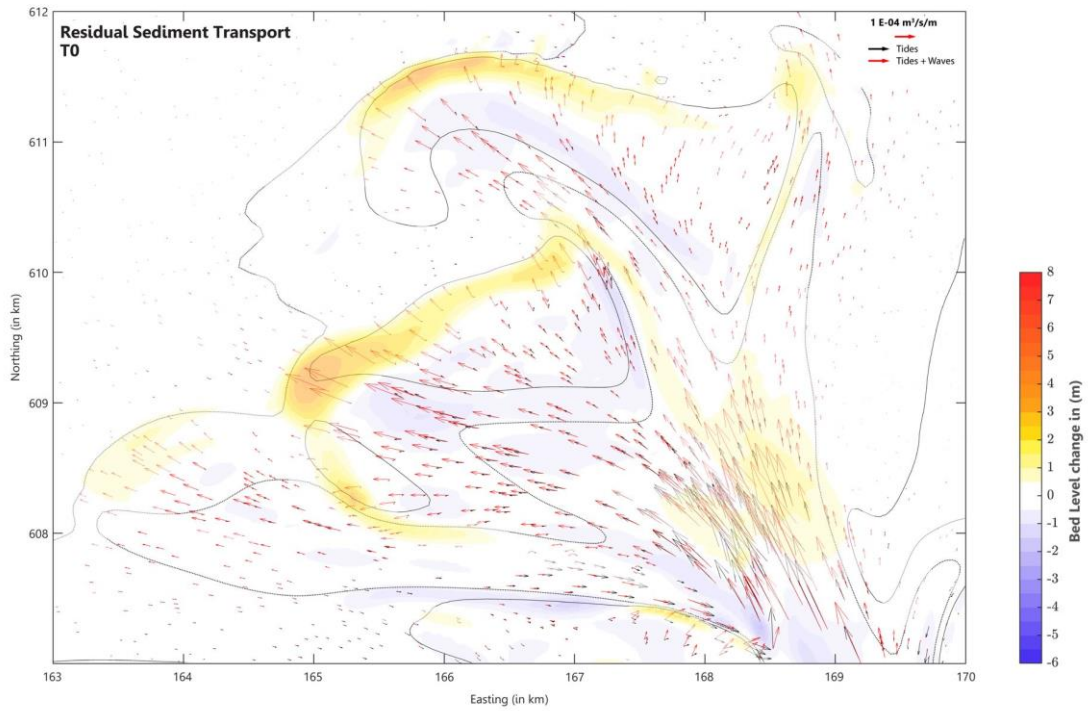


Figure 6-8: Residual sediment transport over a double tidal period. The black arrows highlight the sediment transport patterns under the effect of tides. The red arrows depict the sediment transport patterns under the combined effect of tides and waves. The transport patterns are superposed on the total bed level changes over a double tidal period. It should be noted that one double tidal period reflects a morphological timespan of 3 months.

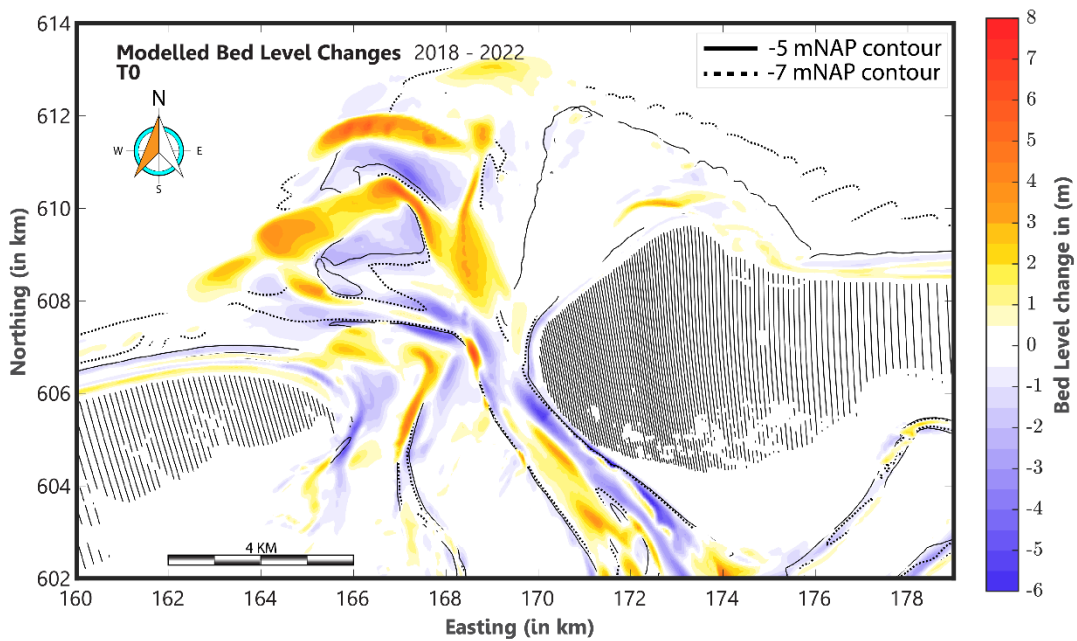


Figure 6-9: Model predictions of the 2022 morphology of the Ameland ebb-tidal delta with the pre-nourishment 2018 bathymetry as the initial bathymetry.

6.3 Description of T1 Behaviour

6.3.1 Impact on Morphological Wave Climate

Based on the results of the T0 behaviour, it can be stated the western section of the ebb-tidal delta is dominated by wave action. Along the margins of the ebb-shields significant wave attenuation can be observed for moderate – large waves in the morphological wave climate (Figure 6-5 and Figure 6-6). This can also be seen from the wave energy dissipation based on the T0 yearly-averaged morphological wave climate (Figure 6-4). Here, significant wave energy dissipation spots are observed on the terminal lobe and the second ebb-shield.

Consequently, it can be deduced that the placement of the pilot nourishment seaward along the second ebb-shield has an influence on the local wave energy dissipation. This follows also from a comparative assessment of the pilot nourishment. The results of the yearly-averaged morphological wave climate based on the post-nourishment bathymetry is shown in Figure 6-10a.

The averaged wave climate for the pilot nourishment case shows a similar spatial variation of the wave height as in the T0 behaviour. A spatial variation of wave heights is found from 0.7 m offshore to 0.3 m close to the Borndiep. As expected, along the coast of Terschelling and the coast of Ameland, the wave action seems to be unaltered. Overall, the morphological wave climate shows a resemblance to the pre-nourishment (T0) behaviour.

Moreover, Figure 6-10b shows the difference in wave energy dissipation with respect to the T0 behaviour. From these results can be deduced that noticeable differences are closely observed in the vicinity of the second ebb-shield – in the construction polygon of the pilot nourishment. Accordingly, local changes can be observed in the order of $2 \text{ Nm}^{-1}\text{s}^{-1}$ extra wave energy dissipation in the nourishment polygon – this amounts to approximately 20% of the yearly-averaged wave dissipation in the nourishment polygon. Hence, it follows that the appearance of the pilot nourishment has a positive effect on the local wave attenuation albeit to a minor degree at the scale of the ebb-tidal delta.

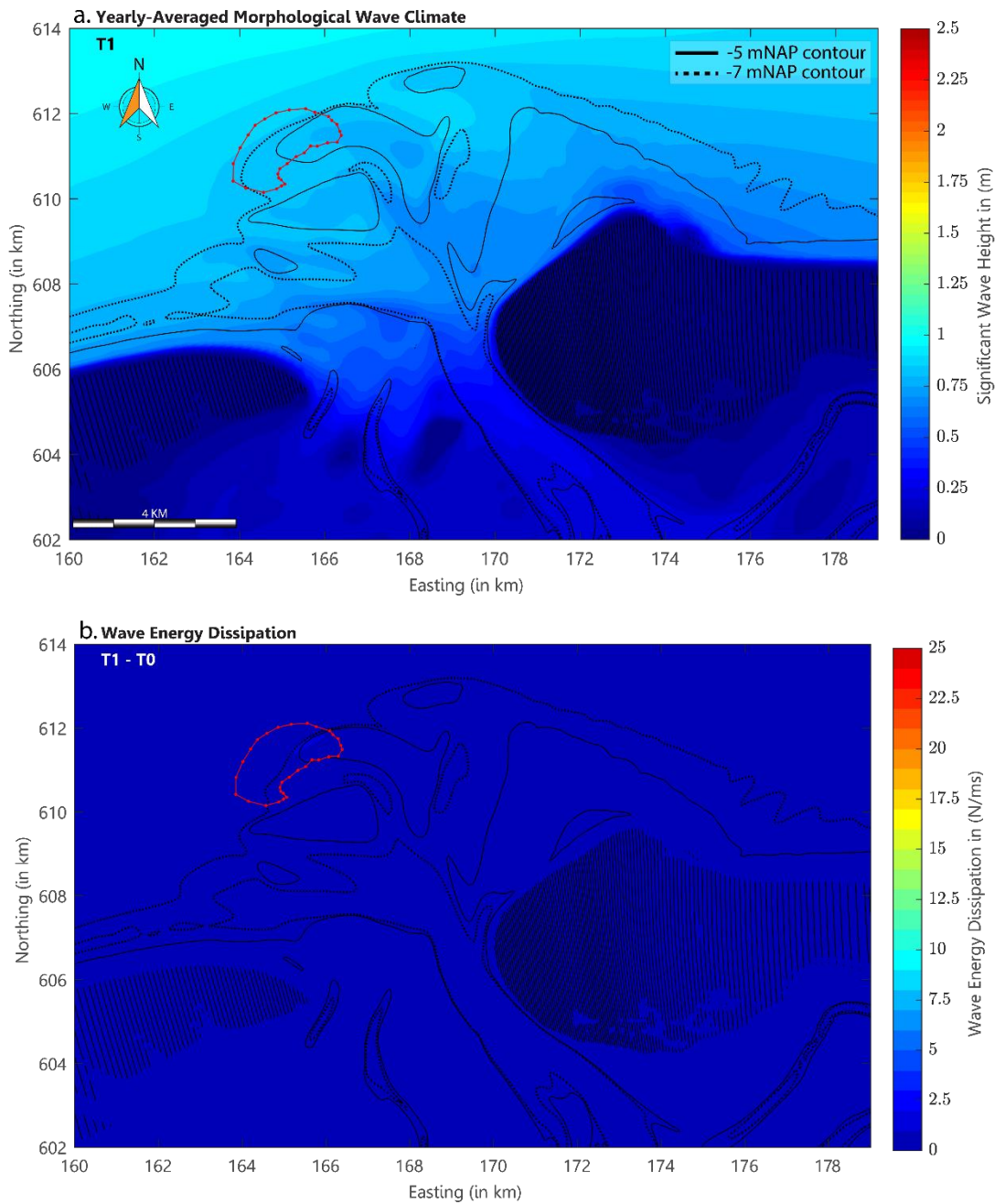


Figure 6-10: Overview of the yearly-averaged wave climate on the Ameland ebb-tidal delta after construction of the pilot nourishment. (a.) shows the yearly-averaged wave heights and (b.) shows the yearly-averaged wave energy dissipation over the ebb-tidal delta with respect to the T0 case. The red polygon indicates the location of the pilot nourishment.

6.3.2 Impact on water motion

An assessment of the impact of the morphological wave climate highlighted an increased wave energy dissipation on the second ebb-shield. This local increase of wave energy dissipation has also consequences for the water motion on the ebb-tidal delta. Figure 6-11 shows the difference in residual water motion between the pre- and post-nourishment behaviour. It follows that the enhancement of wave breaking in the pilot nourishment polygon induces an associated increase in the magnitude of the local velocity vectors. Consequently, the arrows indicate the location where larger velocities may be observed in the T1 response than in the T0 response.

Moreover, a noticeable adjustment in the velocity vectors can be observed in the pilot nourishment polygon directing the flow along the third ebb-shield (Figure 6-11 ①&②) and into the second ebb-chute (Figure 6-11 ③). At the seaward margin of the pilot nourishment, flow enhancement is apparent of the prevailing shore-parallel tidal current (Figure 6-11 ④).

The impact of the increased flow velocities along the third ebb-shield can also be observed in the third ebb-chute. Figure 6-11 ⑤ illustrates a recirculation flow over the third ebb-shield into the second ebb-chute. Furthermore, a convergence of velocity vectors prevails on the inner margin of the second ebb-shield which generate a resulting flow over the ebb-shield.

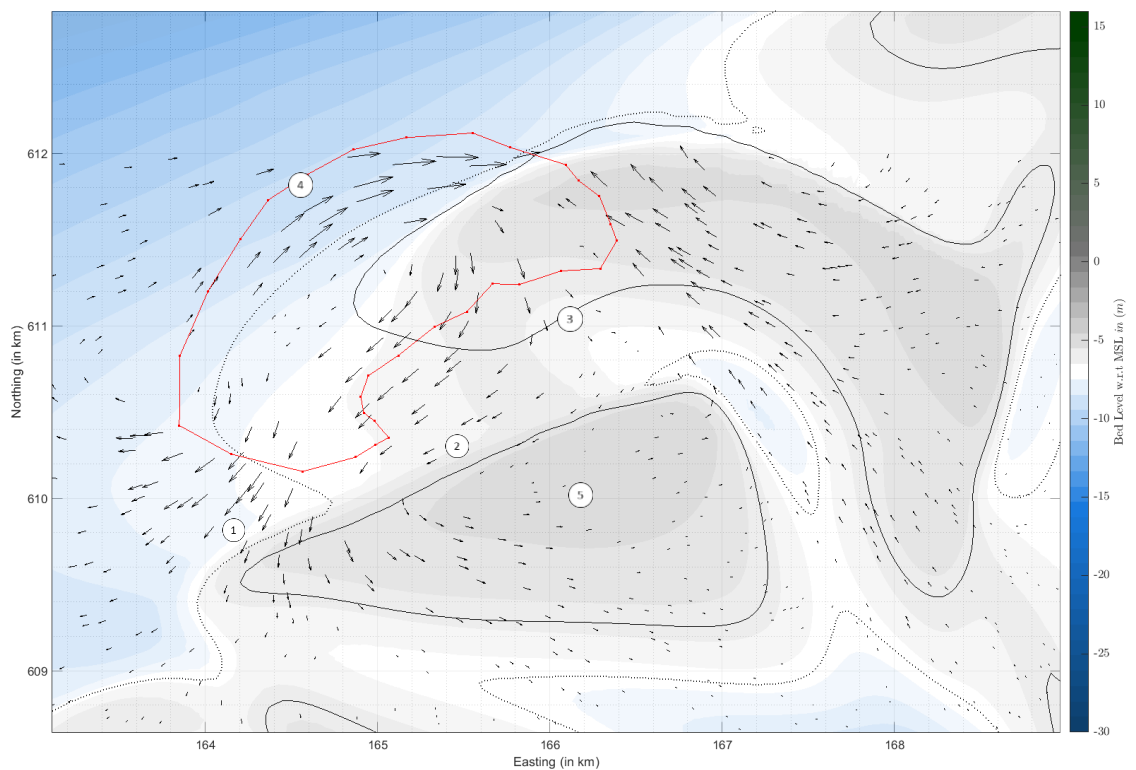


Figure 6-11: The relative differences in residual water motion on the ebb-shields based on a comparison between the water motion with and without the implementation of the pilot nourishment (i.e. T1 - T0).

6.3.3 Impact on sediment transport

To assess the impact of the pilot nourishment on the pre-nourishment (T0) morphological behaviour of the ebb-tidal delta, an analysis is performed on the sediment transport patterns. This analysis encompasses an evaluation of the relative impact on the residual sediment transport patterns after implementation of the pilot nourishment. Figure 6-12 illustrates the relative impact of the pilot nourishment on the predicted bed level changes (Figure 6-12a) and the relative impact on the resulting residual sediment transport patterns (Figure 6-12b). The impact on the residual transport is hereby defined as the difference between the post- and pre-nourishment residual sediment transport (i.e. $T1 - T0$). Hence, the arrows indicate the direction over which relatively more sediment is transported over the ebb-tidal delta after the construction of the pilot nourishment.

It can be seen from Figure 6-12b that the construction of the pilot nourishment impacts the local sediment transport patterns. Based on the previous assessment on the impact of the pilot nourishment on morphological wave climate, it is concluded that the pilot nourishment generates relatively larger wave energy dissipation on the second ebb-shield. The generation of local wave energy dissipation identifies the relevance of wave-induced processes in the morphological impact of the pilot nourishment. The assessment of residual water motion identified a similar pattern and showed locations of increased flow velocity with respect to the T0 response. Given the intrinsic relation between the sediment transport and the underlying water motion, similar patterns can be observed.

The diverging transport vectors over the pilot nourishment polygon (Figure 6-12b ①) can be directly linked to the local increase of the offshore velocities (Figure 6-11 ④). This creates a relative increase in sediment transport over the offshore margin of the T1 bathymetry in comparison with the T0 response.

Moreover, the readjustment of the flow velocity vectors at the inner margin of the second ebb-shield (Figure 6-11 ② & ③) show a decrease of the local velocities in the T1 response. These landward-directed velocity vectors can be attributed to the increased impact of wave breaking in the nourishment polygon. Hence, landward-directed residual sediment transport patterns can be observed which are directed to the third ebb-shield (Figure 6-12b ①).

The construction of the pilot nourishment on the second ebb-shield has also consequences on the residual transport patterns over the third ebb-shield (Figure 6-12b ②). This can be attributed to the increase in the local velocity along the third ebb-shield (Figure 6-11 ②).

Along the second ebb-shield a small increase in the local velocity vectors can be observed along with the local convergence of residual velocity vectors. This has also an implication on the local residual transport patterns. Consequently, larger transport vectors can be observed on the second ebb-shield (Figure 6-12b ③).

6.3.4 Bed level changes

The changes in sediment transport and water motion with respect to the T0 response, drive relative differences in the sedimentation and erosion on the T1 bathymetry. Figure 6-12a shows the relative impact of the pilot nourishment on the accumulative sedimentation and erosion patterns in the T1 response. It can be seen that significant bed level differences (i.e. difference larger than 1m) solely occur in the vicinity of the second and third ebb-chute and -shield (Figure 6-12a).

The increase of the offshore velocities and sediment transport induces a relatively larger erosion in the nourishment polygon (Figure 6-11⁴). This is compensated by a local accumulation of nourished sediment on the seaward margin of the second ebb-shield.

Moreover, the increase of the local transport vectors at the inner margin of the second ebb-shield generates a larger sediment transport in the direction of the second ebb-chute. This is accompanied by a significant erosion in the nourishment polygon and a subsequent accumulation in the second ebb-chute.

Lastly, the residual flow vectors (Figure 6-11² & ⁵) at the offshore margin of the third ebb-shield has also an implication on the local transport magnitudes. The residual transport vectors show a relative increase over the ebb-shield and the generation of local erosion. Consequently, an elongated erosion spot can be observed along the margin of the third ebb-shield.

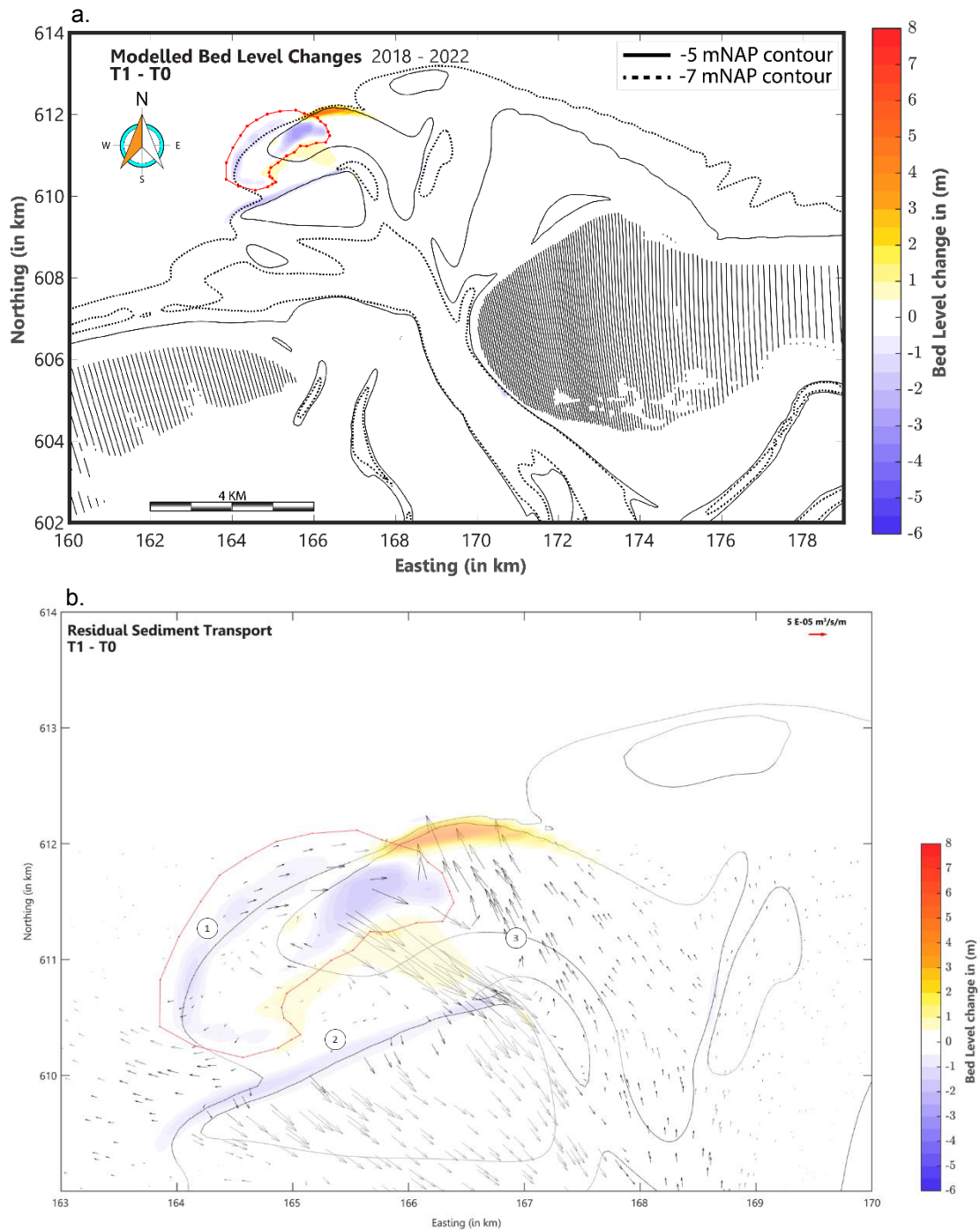


Figure 6-12: Results of morphological prediction of the Ameland ebb-tidal delta after a morphological timespan of 4 years and after construction of the pilot nourishment. (a.) illustrates the impact of the pilot nourishment to the accumulative bed level changes. (b.) shows the implication on the transport vectors superposed on the accumulative bed level changes and zoomed in on the area of influence.

6.4 Description of alternative nourishment options

6.4.1 Nourishment considerations and elaboration on designs

In the preceding section, the impact of the pilot nourishment on the natural T0 response of the Ameland ebb-tidal delta is investigated. Based on a comparative assessment on the water motion, sediment transport and bed level changes, the conclusion is made that the response of the ebb-tidal delta is limited to the morphological features in the close periphery of the pilot nourishment construction polygon. To assess whether this could be generalised for ebb-tidal delta nourishment construction on the Ameland ebb-tidal delta, several nourishment alternatives have been designed and investigated. Thereby, the second function of this analysis was to assess whether the construction of an ebb-tidal delta nourishment could structurally interfere the natural growth of the ebb-chutes and -shields on the ebb-tidal delta. Therefore, five nourishment alternatives are further investigated:

- Two alternative pilot nourishments with different nourishment construction height (i.e. Nourishment alternatives H1 and H2)
- An ebb-tidal delta nourishment on the third ebb chute (i.e. Nourishment alternative V1).
- An ebb tidal delta nourishment on the Zeehondenplaat (i.e. Nourishment alternative V2).
- And an ebb-tidal delta nourishment on the third ebb chute (i.e. Nourishment alternative V3).

Figure 6-13 below illustrates the respective nourishment locations on the ebb-tidal delta. The following subsections highlight the characteristic design of the ebb-tidal delta nourishment alternatives. These are subsequently summarised in Table 6-2 below.

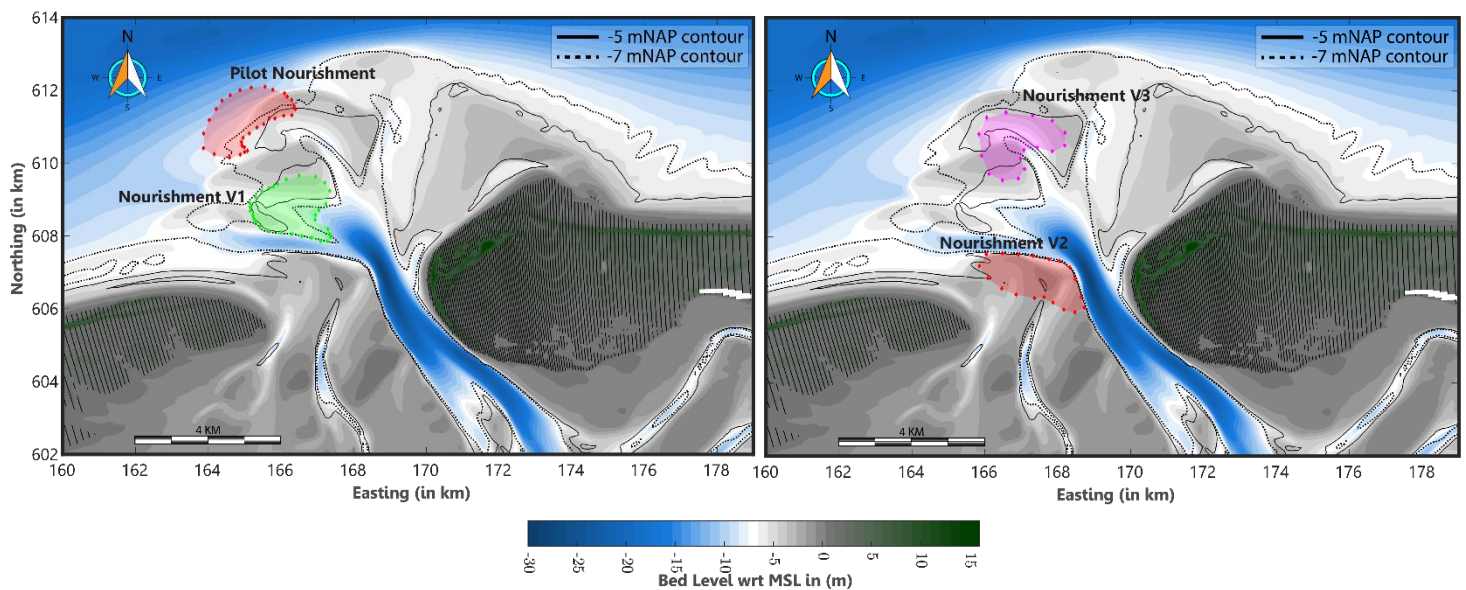


Figure 6-13: Overview of ebb-tidal delta nourishment designs superposed on the 2018 measured bathymetry of the Ameland ebb-tidal delta.

6.4.1.1 Ebb-tidal delta Nourishment V1: Nourishment on third ebb-chute

The first ebb-tidal nourishment encompasses the construction of a submerged nourishment on the third ebb-chute (Figure 6-13: Nourishment V1). The V1 nourishment covers a total surface area of 2.82 km² and add a volume of 5.37 Mm³ sand to the ebb-tidal delta. The V1 nourishment is designed as such that the total surface area and nourished volumes closely aligns with the original 2019 pilot nourishment. Small anomalies can be attributed to the tuning of the nourishment to the local topography of the third ebb-chute. This can also be seen in the construction height of the pilot nourishment. Given its location, this nourishment alternative has a nourishment height of -1.7 mNAP. The placement of the V1 nourishment results thereby in a local elevation of 1.3 m and 4 m of the third ebb-shield and ebb-chute respectively. After placement the length of the ebb-chute is effectively reduced.

6.4.1.2 Ebb-tidal delta Nourishment V2: Nourishment on Zeehondenplaat

The second ebb-tidal delta nourishment comprises the construction of a nourishment on the Zeehondenplaat, west of the main-inlet Borndiep (Figure 6-13: Nourishment V2). To align the nourishment volumes and area with the pilot nourishment, similar design considerations are applied for the design of the V2 nourishment. Consequently, this nourishment has a surface area of 2.78 km² and adds a volume of 5.72 Mm³ to the local shoal. The V2 nourishment has furthermore a construction height of 0.13 mNAP. The placement of the V2 nourishment results in an elevation of the Zeehondenplaat with 2 – 3 m.

6.4.1.3 Ebb-tidal delta Nourishment V3: Nourishment on second ebb-chute

The third ebb-tidal delta nourishment encompasses the construction of a nourishment on the second ebb-chute (Figure 6-13: Nourishment V3). This nourishment has a total surface area of 2.82 km² and adds a volume of 4.91 Mm³ to the second ebb-chutes. This nourishment has a height of -1.5 mNAP and increases subsequently the elevation of the ebb-chute and -shield with 2 m and 5 m respectively. Also in this nourishment design, the placement of the nourishment introduces a reduction of the length of the ebb-chute.

6.4.1.4 Ebb-tidal delta Nourishment V4 & V5: Height variation of the 2019 pilot nourishment

The last nourishment alternatives encompass the construction of the original 2019 pilot nourishment in the nourishment polygon (Figure 6-13: Pilot Nourishment) with different construction heights. The nourishment designs – nourishment H1 and H2 – shows thereby a pilot nourishment with a construction height of -2.5 mNAP and 0 mNAP respectively. The increase in construction height also alters the associated nourishment volume in the nourishment polygon. For the nourishment variants, the volume has increased from 4.94 Mm³ to an amount of 6.05 Mm³ (nourishment H1) and 6.53 Mm³ respectively.

Factsheet ebb-tidal delta nourishment alternatives				
	T1	V1	V2	V3
Surface Area (km ²)	2.77	2.82	2.78	2.82
Nourishment Height (mNAP)	-3.2	-1.7	0.13	-1.5
Nourishment Volume (Mm ³)	4.93	5.37	5.72	4.91

	T1	H1	H2
Surface Area (km ²)	2.77	2.77	2.77
Nourishment Height (mNAP)	-3.2	-2.5	0
Nourishment Volume (Mm ³)	4.93	6.05	6.53

Table 6-2: Summary of ebb-tidal delta nourishment alternatives with overview of construction volumes and heights, and total covered surface area.

6.5 Description of behaviour nourishment alternatives H1 & H2

Two morphological computations have been performed to assess the impact of nourishment height variations to the natural behaviour of the ebb-tidal delta nourishment – Nourishment alternatives H1 and H2. The location of the nourishment alternatives is thereby closely related to the location of the original 2019 pilot nourishment construction polygon. The following sections address the impact of the nourishment alternatives in unison given their mere resemblance in design.

6.5.1 Impact on Morphological Wave Climate

Figure 6-14a & Figure 6-15a give a spatial overview of the yearly-averaged morphological wave climate for the nourishment alternatives H1 and H2 respectively. These results show that the nourishment alternatives induce a relative increase in wave attenuation in the pilot nourishment polygon. This can be inferred from the strong reduction of the wave height over the pilot nourishment polygon from 1 – 1.2 m offshore to 0.25 – 0.5 m (H1) and 0.5 – 0.75 m (H2) respectively landward of the pilot nourishment polygon. Hence, it can be concluded that the effect of height variations on the morphological wave climate is an increase in local wave breaking. This can also be observed by means of an analysis on the wave energy dissipation with respect to the T0 response (see Figure 6-14b & Figure 6-15b). From the wave dissipation difference, it clearly follows that the height of the nourishment alternatives H1 and H2 influence the amount of wave attenuation in the nourishment polygon.

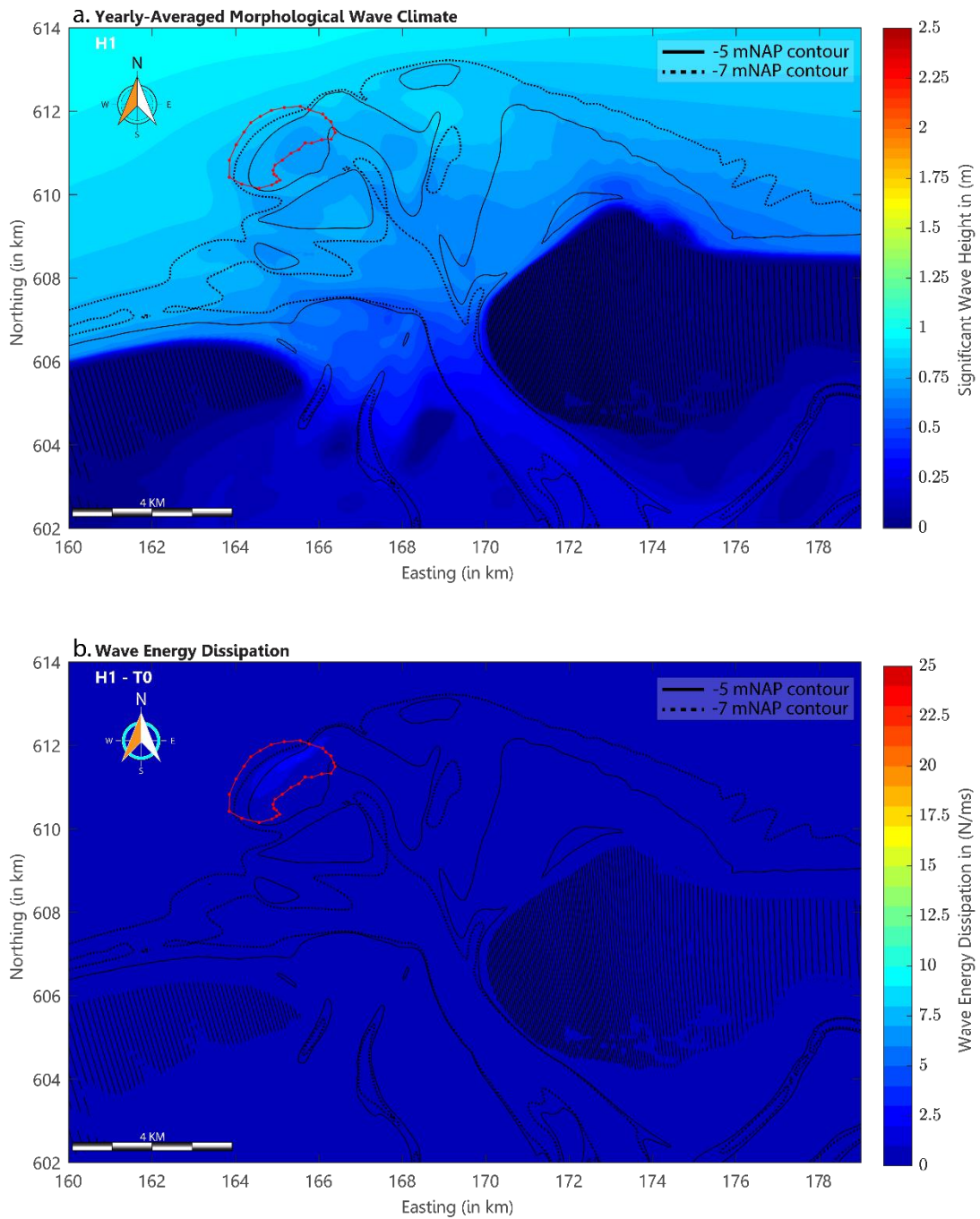


Figure 6-14: Overview of the yearly-averaged wave climate on the Ameland ebb-tidal delta after construction of the nourishment alternative H1. (a.) shows the yearly-averaged wave heights and (b.) shows the yearly-averaged wave energy dissipation over the ebb-tidal delta with respect to the T0 case. The red polygon indicates the nourishment construction polygon.

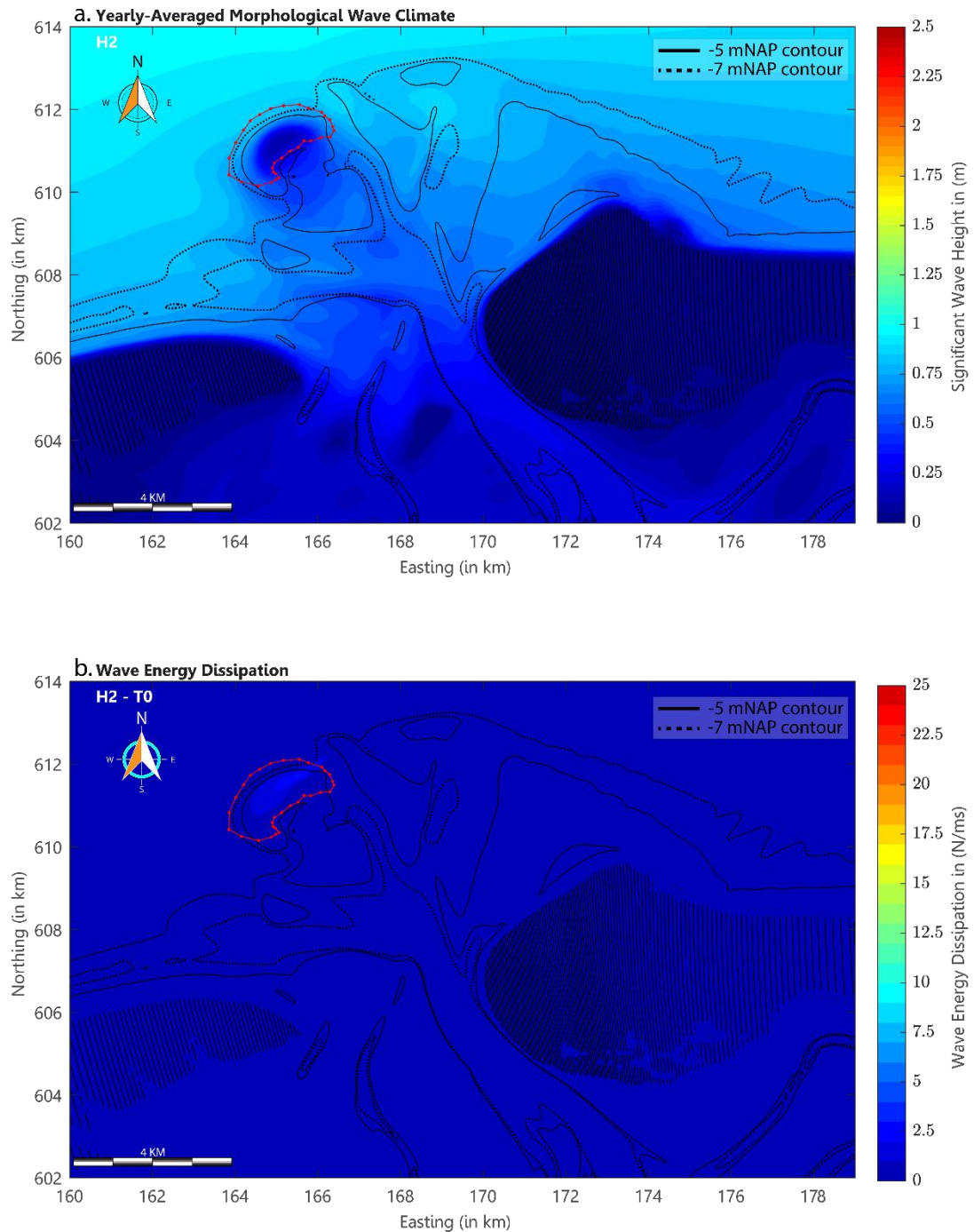


Figure 6-15: Overview of the yearly-averaged wave climate on the Ameland ebb-tidal delta after construction of the nourishment alternative H2. (a.) shows the yearly-averaged wave heights and (b.) shows the yearly-averaged wave energy dissipation over the ebb-tidal delta with respect to the T0 case. The red polygon indicates the nourishment construction polygon.

6.5.2 Impact on sediment transport

Based on the results of the morphological computations for the nourishment alternatives H1 and H2, an assessment can also be performed on the resulting sediment transport patterns. This assessment encompasses an evaluation of the relative impact of nourishment height variations on the residual sediment transport patterns after implementation of the nourishment alternatives. Figure 6-16 shows the relative impact of the nourishment alternatives on the resulting bed level changes and on the resulting sediment transport. The transport arrows show hereby the relative difference in magnitude and direction of the residual sediment transport in the pre- and post-construction response of the ebb-tidal delta (i.e. H2 – T0 and H1 – T0 respectively).

The residual transport differences for the height variation show a similar impact on the sediment transport as the original pilot nourishment (T1) run. For the T1 behaviour, it was concluded that the intensification of wave energy dissipation in the pilot nourishment polygon resulted in a local increase of the offshore transport vectors, a local increase in the landward directed transport over the pilot nourishment construction polygon, and an increase on the transport along the third ebb-shield.

This can also be observed for the height variations (H1 and H2) runs. The relatively larger wave energy dissipation in the nourishment polygon generates thereby larger sediment transport such that the aforementioned differences are becoming more pronounced with a subsequent elevation as shown for nourishment alternatives H1 and H2.

6.5.3 Impact on bed level changes

The impact of the nourishment height variation on the ebb-tidal delta is depicted in Figure 6-16. A comparison between the morphological impact of the pilot nourishment and the nourishment alternatives H1 and H2 identifies that the increase in elevation influences the magnitude of the cumulative sedimentation and erosion patterns. Hence, it follows that the locations of sedimentation and erosion are sustained under the subsequent elevation of the ebb-tidal delta nourishment.

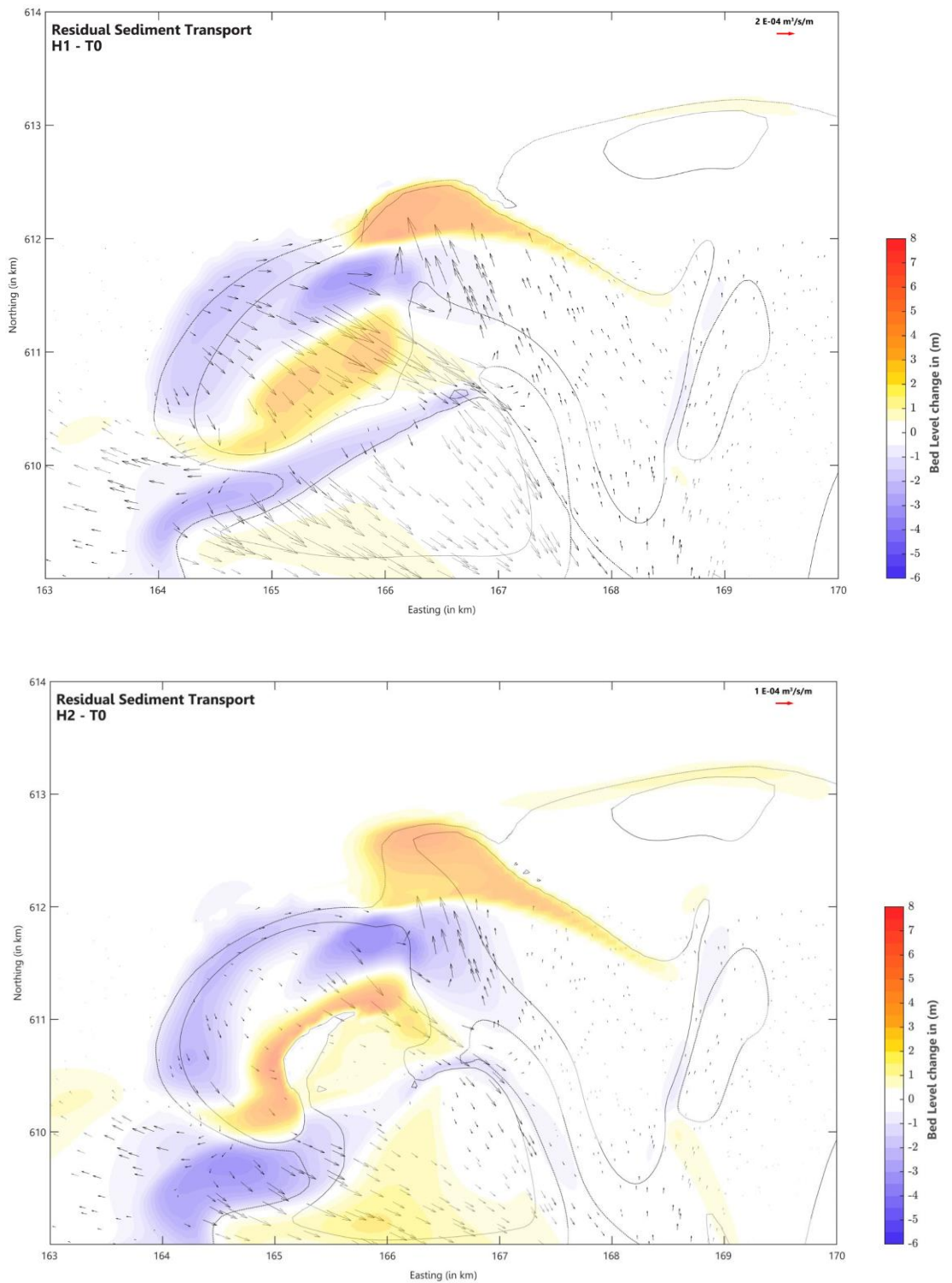


Figure 6-16: Results of morphological prediction of the Ameland ebb-tidal delta after a morphological timespan of 4 years and after construction of the height variation nourishments. (a.) shows the implication of the H1 nourishment on the transport vectors whereas (b.) illustrates the implication of the H2 nourishment on the transport vectors superposed on the accumulative bed level changes.

6.6 Description behaviour nourishment alternatives V1, V2 & V3

6.6.1 Impact on morphological wave climate

6.6.1.1 V1 Nourishment

The construction of the V1 nourishment on the third ebb-chute has a limited effect on the morphological wave climate but has a more pronounced effect on the wave energy dissipation. Figure 6-17 illustrates the spatial variation in wave energy dissipation after construction of the ebb-tidal nourishment. The figure shows that the construction of the V1 nourishment is associated with an enhancement of the local wave attenuation. This can also be observed for the eastward located shore-parallel bars.

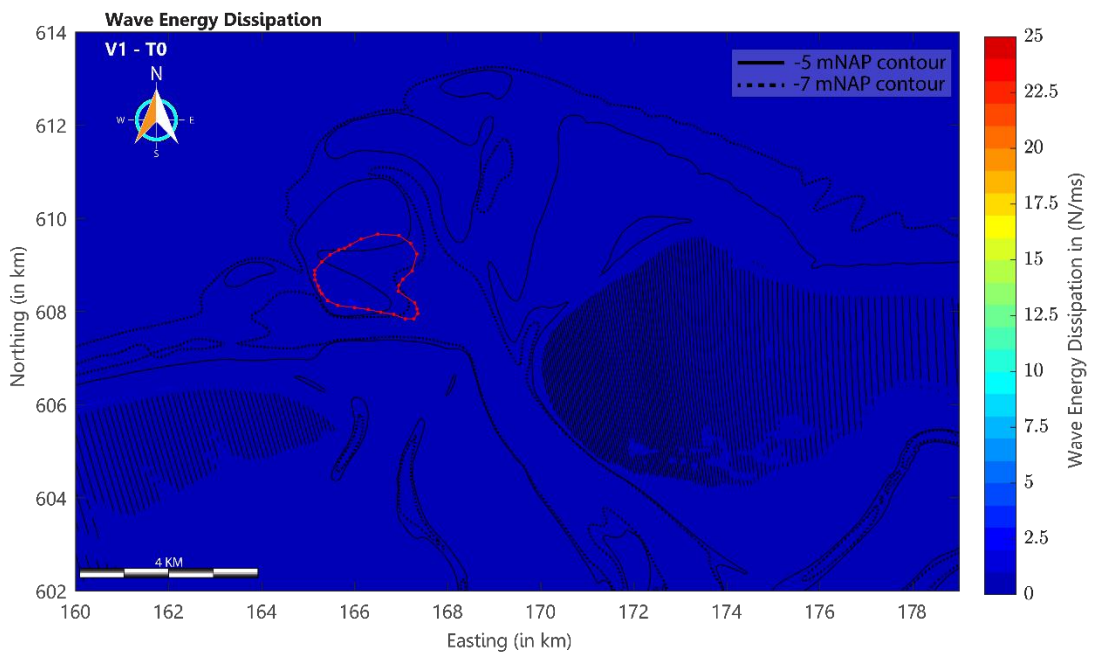


Figure 6-17: Yearly-averaged wave energy dissipation over the ebb-tidal delta with respect to the T0 case. The red polygon indicates the nourishment construction polygon.

6.6.1.2 V2 Nourishment

The increase in elevation of the Zeehondenplaat has a limited effect on the morphological wave climate. However, significant variations can be observed in the local wave energy dissipation close to the Borndiep and the eastern section of the coast of Terschelling.

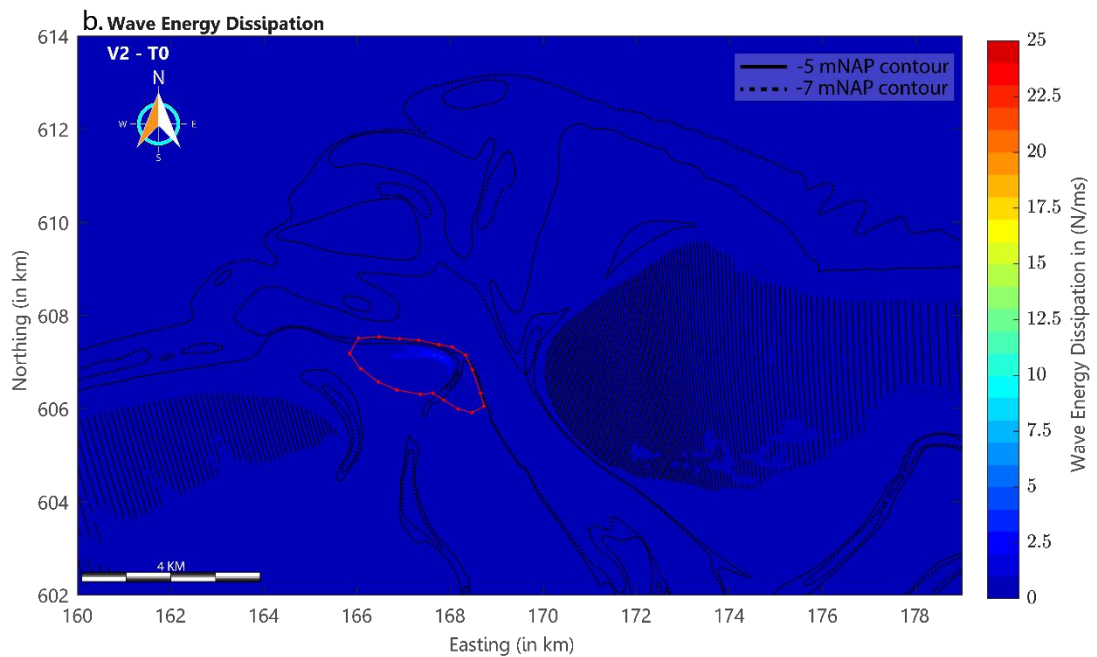


Figure 6-18: Yearly-averaged wave energy dissipation over the ebb-tidal delta of the V2 nourishment with respect to the T0 case. The red polygon indicates the nourishment construction polygon.

6.6.1.3 V3 Nourishment

The construction of this ebb-tidal nourishment alternative encompasses an increase in the local elevation of the second ebb-shield. As the second ebb-shield is located in a wave-dominated region, changes in the elevation may have considerable influence on the amount of local wave breaking. Figure 6-19 illustrates the wave energy dissipation along the second ebb-shield after construction of the V3 nourishment. It can be seen that the construction of the nourishment promotes the attenuation of local waves. This outcome is consistent with the results as found in the T1 analysis, but also in the height variation runs H1 and H2 respectively.

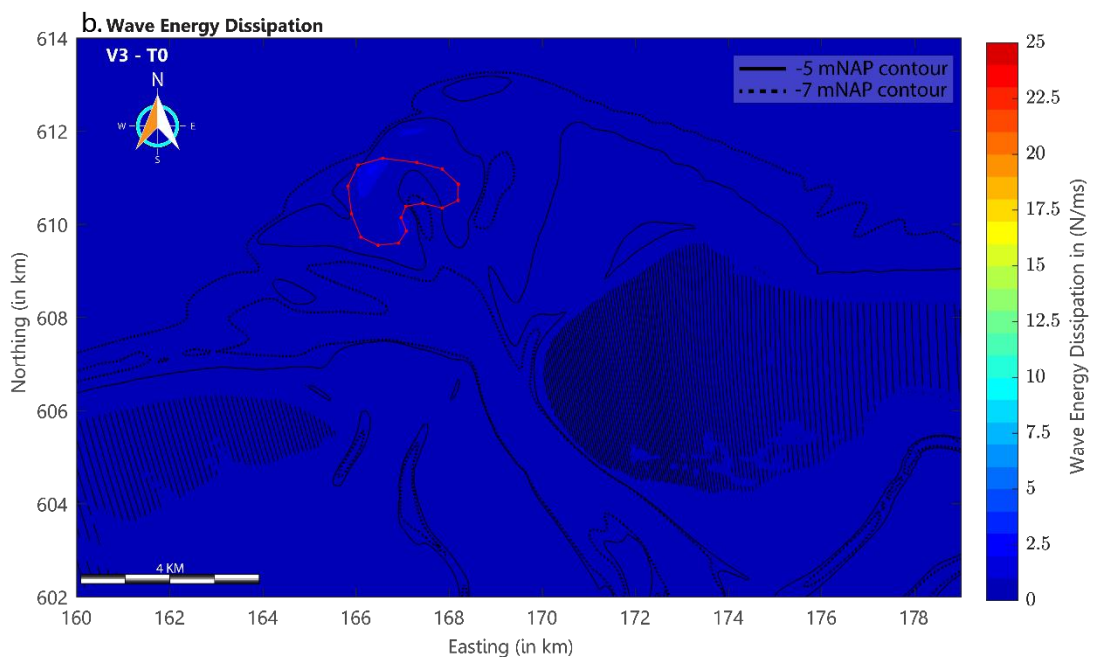


Figure 6-19: Yearly-averaged wave energy dissipation over the ebb-tidal delta for the V3 nourishment with respect to the T0 case. The red polygon indicates the nourishment construction polygon.

6.6.2 Impact on sediment transport

6.6.2.1 V1 Nourishment

The local increase of wave energy dissipation has some implications on the relative magnitude of the sediment transport. Figure 6-20 illustrates the relative impact of the V1 nourishment on the residual sediment transport. Due to the increased wave energy dissipation along the seaward margin of the ebb-shield (Figure 6-20^①), larger transport vectors can be observed in the V1 nourishment case. This can be seen by the transport vectors at the offshore margin of the third ebb-shield (Figure 6-20^①) and by the pronounced transport vectors in the third ebb-chute (Figure 6-20^②). Also larger transport vectors can be observed close to the main-inlet Borndiep (Figure 6-20^③). This may be attributed to the local increase in velocity and subsequently an increase in the local transport vectors. Moreover, the increase in local wave breaking also enables a small increase in the transport vectors east of the third ebb-shield, at the local shoals (Figure 6-20^④).

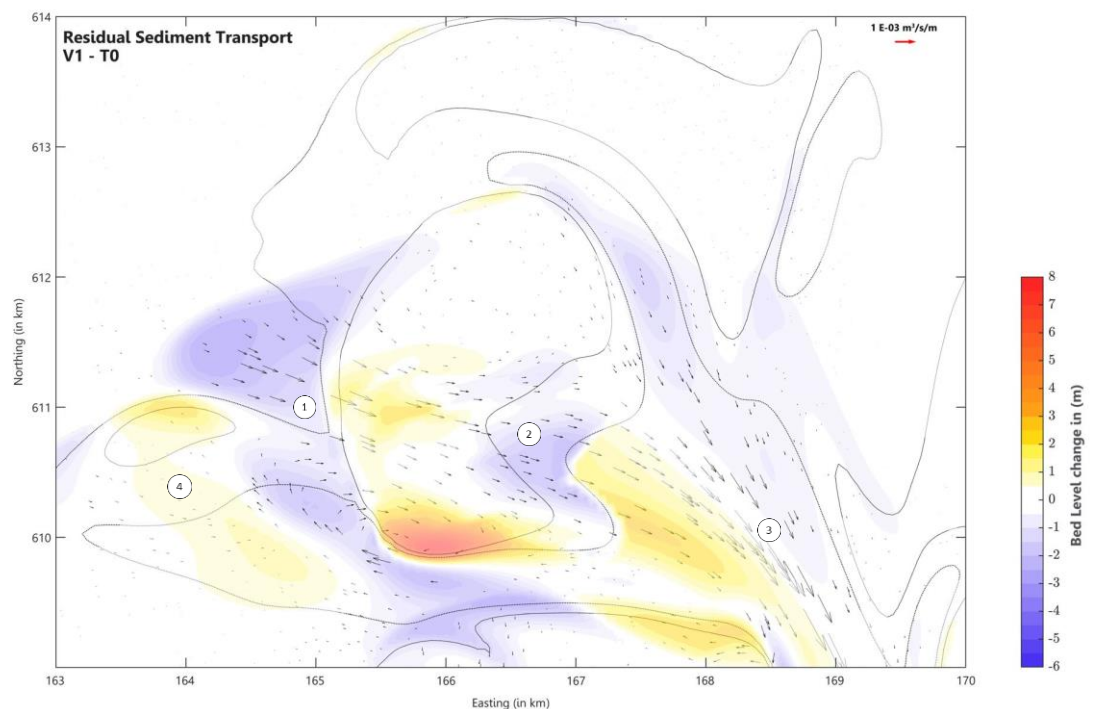


Figure 6-20: Overview plot of the V1 nourishment implication on the transport vectors superposed on the accumulative bed level changes and zoomed in on the area of influence.

6.6.2.2 V2 Nourishment

In the case of the V2 nourishment, the construction of a nourishment on the Zeehondenplaat has several effects on the local transport vectors. Based on an assessment on the water motion and sediment transport patterns in the T0 case, it is apparent that the flood-dominated flow and associated transport patterns are concentrated along the margins of the Zeehondenplaat and in the Borndiep. The ebb-dominant flow and sediment transport patterns prevails prominently in the ebb-chutes, the Akkepollegat and along the elongated channel margin linear bar north of the Westgat. Due to the increased effect of wave-induced processes, the flood-dominated transport close to the Zeehondenplaat shows a relative increase compared to the T0 response. Conversely, an increase in the ebb-dominated transport can be observed over the channel margin linear bar in the direction of the Westgat, and in the Oosterom east of the coast of Terschelling.

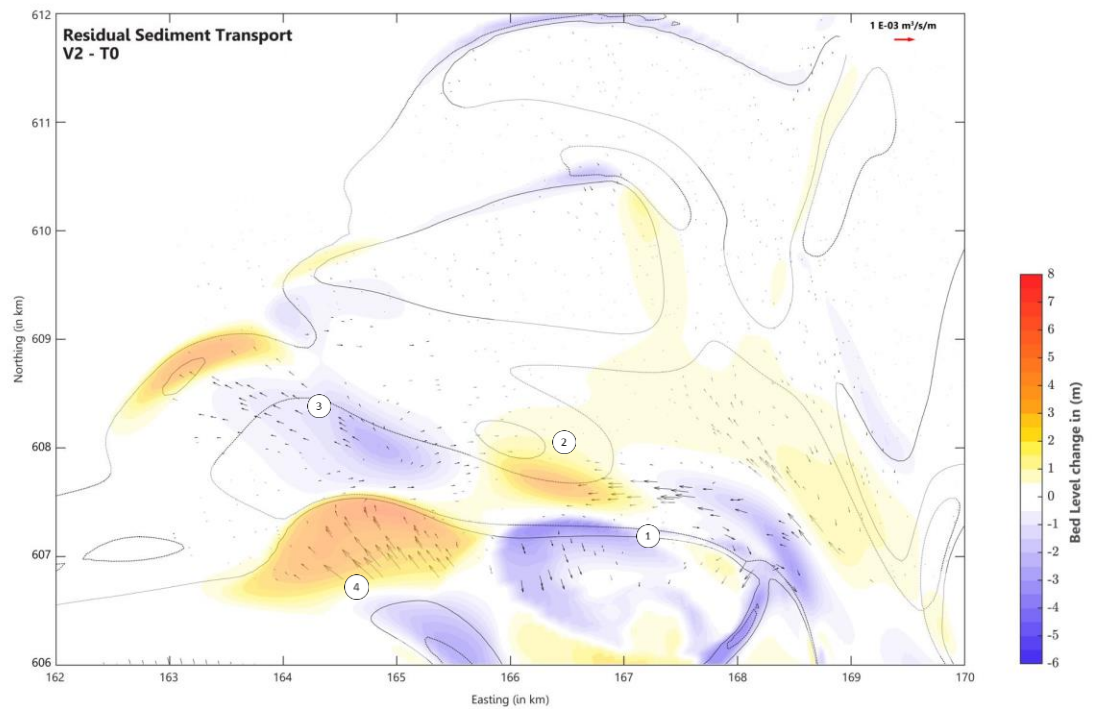


Figure 6-21: Overview plot of the V2 nourishment implication on the transport vectors superposed on the accumulative bed level changes and zoomed in on the area of influence.

6.6.2.3 V3 Nourishment

The case of the V3 nourishment on the second ebb-chute shows a resemblance in the implications of the sediment transport patterns for the height variations runs (nourishment H1 and H2) and the 2019 pilot nourishment. In the height variation runs and the pilot nourishment case, the construction of the pilot nourishment enhanced local wave attenuation. This has also been seen on the basis of the local wave energy dissipation. This resulted in an enhanced sediment transport over the second ebb-shield and over the pilot nourishment polygon. In the V3 nourishment case, a similar phenomenon can be observed.

The placement of the V3 nourishment on the second ebb-shield generates relatively larger transport vectors over the seaward margin of the ebb-shield (Figure 6-22^①). This may be attributed to the local increase in the elevation of the ebb-shield. The effect of this increased transport magnitude can also be observed in the second ebb-chute where larger landward-directed sediment transport vectors are apparent (Figure 6-22^②). Close to the Borndiep the effect of the flow enhancement is significantly reduced. Moreover, the increase in the flow velocity over the third ebb-chute and -shield (Figure 6-22^③) generated a seaward-directed flow over the third ebb-shield (Figure 6-22^④) and over the second ebb-shield (Figure 6-22^⑤). This results in an associated seawards-directed increase in residual transport patterns over the ebb-shields.

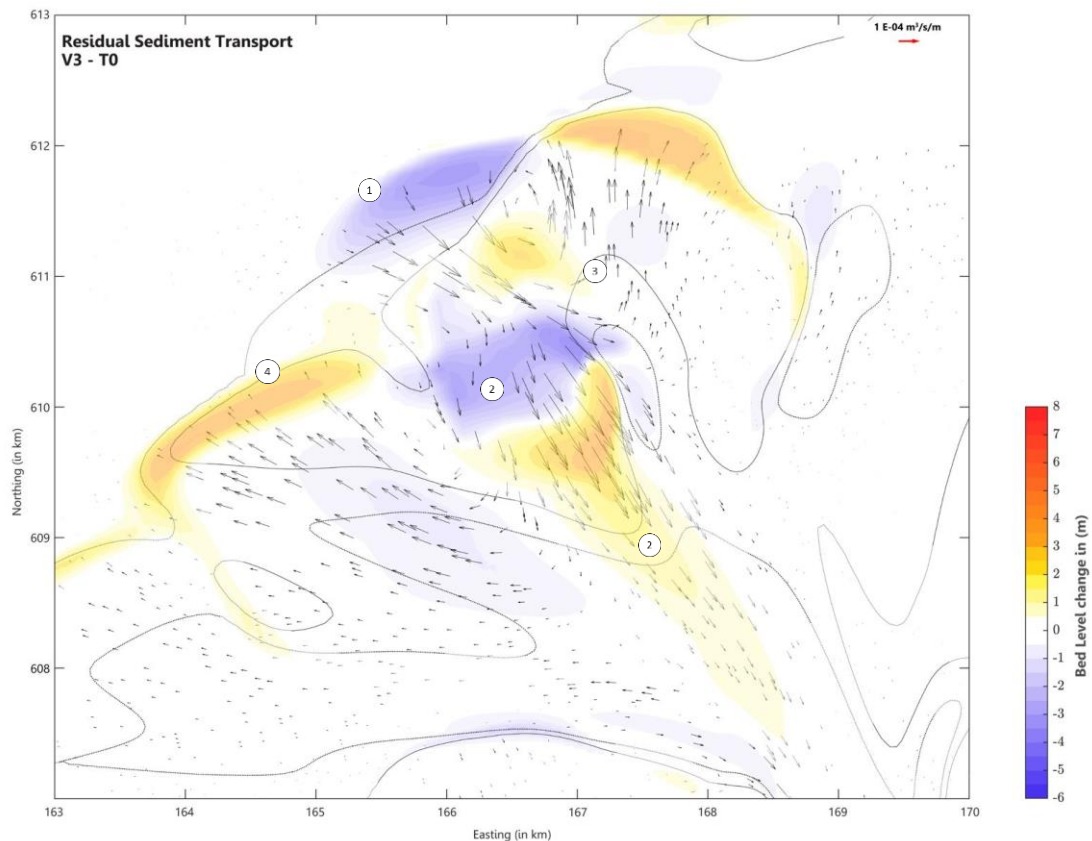


Figure 6-22: Overview plot of the V3 nourishment implication on the transport vectors superposed on the accumulative bed level changes and zoomed in on the area of influence.

6.6.3 Influence on bed level changes

6.6.3.1 V1 Nourishment

The observed variation of residual transport magnitudes over the third ebb-shield has also an impact on the local erosion and deposition patterns. Figure 6-20 shows the relative impact of the V1 nourishment to the accumulative sedimentation and erosion patterns. The largest bed level changes can be observed in the close vicinity of the third ebb-shield. The increase of the transport magnitude along the seaward margin of the third ebb-shield generates a local erosion (Figure 6-20^①). A similar pattern can be observed for the increased transport vectors in the ebb-chute that induces a large erosion in the inner margin of the third ebb-shield (Figure 6-20^②). This sediment is deposited along the converging transport vectors close to the Borndiep where the transport magnitudes gradually decrease (Figure 6-20^③).

6.6.3.2 V2 Nourishment

For the V2 nourishment, the increase of the flood-dominated transport that is concentrated towards the Zeehondenplaat generates a relatively larger erosion on the local shoal than in the T0 response (Figure 6-21^①). Conversely, the transport vector difference over the elongated channel margin linear bar resulted in a local erosion and deposition pattern (Figure 6-21^②). Moreover, the increase in the ebb-dominated flow in the Oosterom induces a larger ebb-dominated transport in the V2 nourishment case (Figure 6-21^④). This has a subsequent influence on the transport through the Westgat which is slightly northward adjusted.

Consequently, relatively larger transport magnitudes can be observed in the Westgat along the channel margin linear bar (Figure 6-21³). This readjustment enables the formation of a sedimentation zone at the local bars west of the third ebb-shield and promotes the sedimentation of the channel margin linear bar close to the Zeehondenplaat.

6.6.3.3 V3 Nourishment

The variation of the transport vectors over the second ebb-shield after construction of the V3 nourishment induces a relative variation in the local sedimentation and erosion patterns Figure 6-22. The increase in transport magnitude offshore of the second ebb-shield induces an increase in local erosion over the ebb-shield (Figure 6-22¹ & ²). This is compensated by a local deposition towards the Borndiep in the direction of the converging transport vectors (Figure 6-22²). Lastly, the large return flows over the ebb-shields generate associate large seaward-directed transports vectors (Figure 6-22³ & ⁴). These transport vectors promote the growth of the second and third ebb-shield as can be seen from the increased depositions along the margins of the ebb-shields (Figure 6-22³ & ⁴).

7 Discussion

This chapter aims to provide a discussion on the obtained results following from the modelling endeavours in this research. Sec.7.1 provides a discussion of the model capability to reproduce the morphological evolution of the ebb-chutes and -shields on the Ameland ebb-tidal delta. Furthermore, Sec. 7.2. provides a discussion on the development of the pilot nourishment on the ebb-tidal delta.

7.1 Modelling meso-scale evolution of the Ameland ebb-tidal delta

7.1.1 Implementation of nonlinear wave orbital velocity formulation

The foundation of this research encompasses a model improvement to increase the wave-related morphological response in present state-of-the-art morphodynamic models for the Ameland ebb-tidal delta. Previous modelling assessments of de Fockert (2008) and Jiao, (2014) had shown that the application of the van Rijn, (2007) transport formulation (VR04) in combination with the near-shore orbital velocity description by Isobe & Horikawa, (1982) promoted a tendency in the model to overpredict the onshore-directed sediment transport. In this research the near-bed wave orbital velocity description has been substituted with a velocity description that incorporates the full nonlinearity in the wave shape and orbital velocity profile (Boechat Albernaz et al., 2019; Ruessink et al., 2012).

Recent insights of van Soest, (2021) demonstrated that the application of this parameterisation can promote larger velocities in the shoaling regions of the ebb-tidal delta, therewith haltering the overprediction of the onshore-directed sediment transport. However, the outcomes of this research have shown that this model improvement had a limited effect on the incorporation of wave-induced processes in the modelled morphological response. Focussing on the hindcast simulations between 2005 and 2010, it becomes apparent that the strong seaward advancement of the terminal lobe is still a persistent feature in recent model predictions (e.g. see for instance de Fockert (2008) and Jiao, (2014)). Also, for hindcast runs after 2010 which emphasise the recent development of ebb-shields and -chutes it becomes clear that the model captures to a limited degree the wave-related morphological development of the latter features.

Therefore, it is anticipated in this research that the implication of the nonlinear wave orbital velocity formulation is particularly relevant for the representation of the near-bed wave orbital velocity magnitude in model simulations and to the morphological calibration of the underlying sediment transport formulation. It is argued that the application of recent sediment transport formulations which allow for nonlinear wave parameter tuning can improve the representation of wave-driven processes in morphodynamic models.

7.1.2 Ebb-chute and -shield development

Simulations of the Ameland ebb tidal delta for a timespan shorter than 4 years has shown that the occurrence of ebb-chutes and -shields is contingent on the appearance of the latter features in the initial bathymetry. This can especially be seen in a comparison between the 2017 and the 2006 model prediction. In the 2005 survey – the initial bathymetry for the 2006 model prediction – (see Figure 5-1) clearly the absence of an ebb-chute and -shield formation can be observed. As a consequence, the 2006 model prediction shows the formation of a shoal instead of the first ebb-chute and -shield development (see Figure 5-2 and Appendix A.1: Figure A 1).

Conversely, the onset of the second and third ebb-chute is apparent in the 2017 model prediction (Figure 5-10). In the 2016 survey – initial bathymetry of the 2017 model prediction – the formation of these chutes was already registered (Figure 5-9 and Appendix A.3).

Hence, an underlying relationship prevails between the models' capability to predict the formation of chutes and the actual presence of these morphological features in the initial bathymetry. Otherwise stated, the model is to a lesser degree capable of capturing the stochastic nature of the ebb-chute and -shield development while being in absence of any sources of initial disturbances. This can be attributed to the choice of model input reduction and efficient morphological updating that allows for yearly-averaged morphological development wherein the effect of episodic wave events is not accounted for.

7.1.3 Modelled response in tide- and wave-dominated areas

Based on the set of validation runs for the Ameland ebb-tidal delta (see Appendix A3, it can be inferred that the model predicts the formation of tide-dominated current-induced morphological development sufficiently better than the morphological development as a consequence to wave-induced processes (compare for instance Figure A 25 **Error! Reference source not found.** and Figure A 27).

In light of the aforementioned and as example, the 2006 bathymetry (Figure A 1) is taken into consideration. Due to the horizontal extend of the downdrift swash platform and the formation of a marginal shoal, the outer channel (i.e. Akkepollegat) is sheltered from wave action by obliquely incident waves coming from the northeast to northwest direction. Consequently, considering the morphological development of the Akkepollegat, the measured bed level changes show a channel linear accretion from the divergence point of the main ebb-channel (i.e. Borndiep) on to the periphery of the first ebb-chute formation. The underlying process attributing towards this accretion is the strong ebb-tidal flow through the inlet gorge that pushes sediment offshore. Moreover, it can also be seen from the measured bed level changes that the appearance of this strong tidal outflow drives the growth of the first ebb-chute in the direction almost parallel to the Akkepollegat.

An accretion at the tip of the terminal lobe is observed in measured bed level changes from 2006 – 2010 (see Figure A 24). Comparison between the modelled and measured bed level changes show that the model produces a local accretion at the outer margin of the ebb-tidal delta. Conversely, the wave-dominated erosion along the outer margin is to a lesser degree reproduced by the model. This is consistent with the notion that the model is producing better results for tide-dominated morphological development.

Furthermore, the 2018 bathymetry (Figure A 19) can also be considered as example of a bathymetry where the combined effects of waves and tides dictate the present morphology. The swash platform is located more east of the Akkepollegat which extends on this time instant towards the periphery of the ebb-tidal delta. Hence, the formation of the shoals and chutes depends highly on the interaction between the wave-induced processes along the ebb-tidal delta periphery and the shore-parallel tidal currents.

Thereby, the ebb-dominated flow through the inlet gorge favours the outer bend erosion of the second ebb chute, whereas the strong flood-dominated shore-parallel currents bring sediment to the east side of the second ebb-shield (see also Figure 6-3). The same can also be observed for the third ebb-chute and -shield where both processes reshapes and migrate this morphological feature.

The 2018 model prediction (Figure A 26) shows a consistency in the location of erosion and deposition at the ebb- shoal and chute formations. However, at the downdrift swash platform the morphodynamic development is to a lesser degree captured by the model. This can be attributed to the fact that the morphodynamic development of the downdrift swash platform is governed by the wave-induced sediment bypassing. These wave-induced processes are not fully captured in the modelled response.

The dissimilarity in morphological development appears to be largest for the validation runs prior to 2010 and seems to decrease over the years, up to the more recent model predictions. Over the timespan of 2016 – 2020, the deviations are reduced to an order of magnitude smaller than the measured bed level changes.

7.2 Impact of pilot nourishment on the Ameland ebb-tidal delta

This research also investigated the impact of the pilot nourishment on the Ameland ebb-tidal delta. In Sec.6.3, the morphodynamic impact of the pilot nourishment had been further reviewed. Based on various ebb-tidal delta nourishment model predictions (see Sec.6.4 – 6.6), a further discussion can be provided on the implication of ebb-tidal delta nourishments on the natural behaviour of the outer delta.

7.2.1 Morphological behaviour of the pilot nourishment

In Ch. 6, the morphodynamic behaviour of the Ameland ebb-tidal delta in the presence of the pilot nourishment has been studied. Based on a comparison between modelled and measured bed level changes, the impact of the pilot nourishment has been deduced from differences in the pre- and post-nourishment behaviour respectively. A volumetric analysis gave also further insights on the decay of the pilot nourishment volume in the construction polygon over time. More precisely, the volumetric analysis showed that the initial response of the ebb-tidal delta to the pilot nourishment is an initial erosion (see Sec.3.4.3 and Figure 3-7).

A morphodynamic model assessment on the impact of the pilot nourishment on the ebb-tidal delta (see Sec. 6.3.4 and Figure 6-12) showed that these eroded volumes are largely to be found in the vicinity of the nourishment construction polygon. This can be inferred from the significant sediment accumulations and erosion zones in and along the second ebb-shield.

Hence, it follows from Figure 6-12 that the pilot nourishment mostly exchange sediment with the Kofmansplaat on which the second ebb-shield is founded and to a lesser degree with the third ebb-shield. The question remains however how the nourishment interacts with the local morphological features and what processes drive these morphological changes.

To get a further understanding on the sediment interaction with the outer delta features, the integration of information on the morphological development of the ebb-tidal delta based on morphodynamic modelling work and an assessment on the sediment transport patterns can give further insights into the underlying dynamics that govern the development of the pilot nourishment.

In Sec.6.3, it is therewith argued that given the position of the pilot nourishment its morphological behaviour is governed by the interplay between the shore-parallel tidal current and wave action. Figure 6-8 and Figure 6-10 sustain the significant role of wave-induced processes in the morphological development of the pilot nourishment, whereas Figure 6-3 and Figure 6-7 identified the role of the tidal motion in the morphological behaviour of the pilot nourishment.

A sediment transport analysis highlighted the prominent patterns over which sediment is exchanged over the updrift swash platform. The residual transport patterns identified that sediment depositions at the edge of the second ebb-shield is exchanged with the third ebb-shield via seaward directed transport paths and subsequently interacts with the outer delta margin (Figure 6-8).

The gross sediment transport patterns show that persistent east-west directed transport is interchanged with periods of northwest and southeast directed sediment transport (Figure 7-1). These transport patterns enable the horizontal displacement of nourished sediment towards and along the ebb-shields.

The combination of the residual transport and the gross transport patterns enable the exchange of nourished sediment with the margin of the outer delta and the downdrift swash platform.

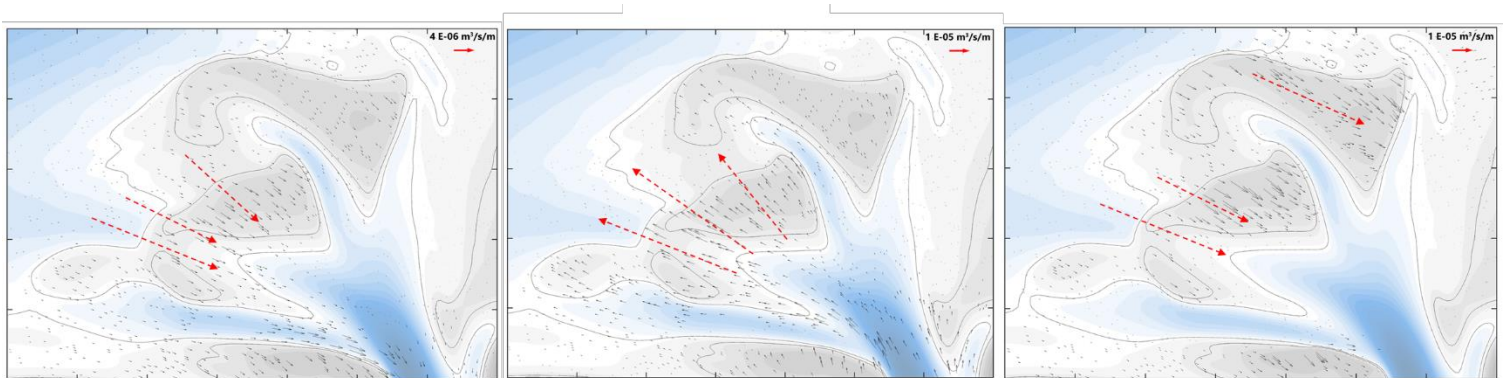


Figure 7-1: Generalisation of gross sediment transport patterns over the tidal cycle. The red arrows solely indicate the apparent transport direction.

Previous studies from van Rhijn (2019) (i.e. numerical tracer study as part of a sediment transport analysis on the pilot nourishment during construction) and Lambregts (2021) (i.e. investigation into the dominant sediment bypassing pathways on the Ameland ebb-tidal delta after the geomorphic transition in natural behaviour) identified probable trajectories on which sediment issued from the nourishment site is interacting with the ebb-tidal delta. Recent studies from Lambregts (2021) showed that under tidal effect the pilot nourishment is most likely to exchange sediment with the third ebb-shield via local deposits from the second ebb-shield.

Under combined tide- and wave-driven processes, these sediment pathways are more pronounced and highlight a much larger sediment exchange with the downdrift Bornrif swash platform.

Morphological computations of the impact of the pilot nourishment has identified the interaction with the second and third ebb-shield. Previous study of Lambregts (2021) establishes thereby a comprehensive foundation on the sediment pathways over the ebb-tidal delta and the impact of the pilot nourishment to the natural ebb-tidal dynamics. This solidifies our notion of sediment exchange along the Ameland ebb-tidal delta and the role of the ebb-shields and -chutes in the morphological processes that are identified in this research.

Moreover, what becomes clear from the transport analysis in this thesis in conjunction with the work of Lambregts (2021) and van Rhijn (2019) is that the behaviour of the pilot nourishment is mainly governed by the interaction between the shore-parallel tidal currents and the wave-induced sediment bypassing. The tidal currents move sediment over the periphery of the second and third ebb-shield. Thereby, wave-induced processes enable the redistribution of sediment into the second ebb-chute and on the outer delta (Figure 6-12). The

influence of waves is also observed in the enhancement of the tide-induced sediment transport as shown in Sec. 6.2. (Figure 6-8). This aligns well with the observations on the sediment pathways under combined processes as shown in the research of Lambregts (2021).

Lastly, Lambregts (2021) and van Rhijn (2019) both show that the nourishment is transported landwards along the ebb-shields in the form of sand bars. It may be argued based on the previous findings that the combined effect of waves and tidal currents drives these bars along the second ebb-shield into the inner margin of the ebb-shield (vanRhijn,2019).

It is therefore hypothesised in this research that the formation of these local bars partially hinders the flow over the periphery of the third ebb-shield which increases and steers the flow more closely to the ebb-shields' margin. Consequently, the seaward advancement of the third ebb-shield is partially compensated by an intensification of the local erosion patterns (see also Figure 6-12a).

Finally, focusing further on the relative difference in bed level changes between the pre- (T0) and post-nourishment (T1) bathymetry, the model shows that the pilot nourishment contributes to three underlying processes (Figure 6-12):

- (1). The deposition of sediment along the periphery of the second ebb-shield due to a local increase of the offshore tidal currents.
- (2). The migration of sediment in the form of sand bars in to the second ebb-chute under the combined effect of the tidal currents and wave action.
- (3). An intensification of the local erosion along the third ebb-shield due to a flow adjustment of the local currents over the third ebb-shield.

7.2.2 Implication of nourishment height

In Sec.6.4. an assessment of ebb-tidal delta nourishment alternatives has been performed. Based on the results as depicted in Figure 6-16 it can be argued that the impact of height variations is solely reflected in the magnitude of the morphological response. The modelled sedimentation and erosion patterns which follows from an assessment on the 2019 pilot nourishment are therewith sustained under the variation of the construction height.

Moreover, given that the sediment transport patterns remain unaltered under the effect of height variations of the ebb-tidal delta nourishment, it can be seen that the increase in elevation of the ebb-tidal delta nourishment only influence the magnitude of the sediment exchange over the ebb-tidal delta. More sediment will most likely be exchanged with the morphological features at the outer delta via the known transport pathways and therefore provides a steady source of sediment for the future time horizon of the ebb-tidal delta.

7.2.3 Implication of nourishment location

The location of the pilot nourishment has been seen to be important for its interaction with the local morphology on the ebb-tidal delta. The placement of ebb-tidal nourishments in the vicinity of ebb-chutes and shields creates a sediment redistribution along these morphological features. Based on the morphological assessment of the ebb-tidal delta nourishment alternatives, it can be deduced that the construction of ebb-tidal delta nourishments to the south of the Westgat invokes a primary sediment exchange between the coast of Terschelling and its surrounding morphological features. A secondary effect of the morphological development of the coast of Terschelling and the Zeehondenplaat is the readjustment of the Westgat which thereby influences the development of the ebb-shields and -chutes on the longer temporal scales (Figure 6-21). The construction of an ebb-tidal

delta nourishment north of the Westgat results in a sediment exchange between the local ebb-shields and the downdrift coast of Ameland (see also Figure 6-20 and Figure 6-22).

8 Conclusions

The objective of this research is to obtain a better understanding on the development of ebb-chutes and shields on the Ameland ebb-tidal delta and the impact of a pilot nourishment on the latter's natural behaviour. In light of the aforementioned, this chapter aims to answer the proposed research questions as stated in Sec. 1.4.

8.1 Morphological capabilities of present-state-of-the-art Ameland models

Can present state-of-the-art Ameland models reproduce ebb-tidal delta development?

A comparison between modelled and measured bathymetric changes of the ebb-tidal delta demonstrated that the model is capable of reproducing the natural ebb-tidal delta behaviour reasonably well over short- to medium- simulation timespans. A further distinction can be made between the model performance of wave-dominated and tide-dominated morphological changes. Based on the outcomes of this modelling assessment it follows that the tide-dominated morphological development of the ebb-shields and -chutes is more accurately reproduced than wave-dominated morphological changes.

How well are present state-of-the-art morphodynamic models for the Ameland ebb-tidal delta capable of producing ebb-chutes and -shields on a short-, medium-, and long-term scale?

In this research, it is shown that the present state-of-the-art model is able to reproduce the evolution of the ebb-chutes and -shields on the Ameland ebb-tidal delta. The predictability of these morphological features remains closely dependent on its pre-existence in the initial bathymetry.

Moreover, the model performance of the ebb-chutes and -shields changed depending on the simulation time span. Over short- to medium-temporal scales (1-4 years), the model produces increasingly better results for longer simulation timespans. For 4-year simulation time spans, the morphological development closely represents the observed morphological changes around the ebb-chutes and -shields. The largest deviations between modelled and measured morphological response can be observed in model simulations over longer temporal scales (i.e. 12 years). This can be attributed to the fact that the dissimilarity in model performance between tide-dominated and wave-dominated morphological changes becomes more important on longer temporal scales.

8.2 Morphodynamic Impact of the pilot nourishment

Is the model suitable as a forecasting tool for the prediction of ebb-tidal delta nourishment evolution on the Ameland ebb-tidal delta?

The present-state-of-the-art morphodynamic model for the Ameland ebb-tidal delta has been shown to accurately reproduce the morphological changes along the second and third ebb shield on the outer delta in model simulations with a simulation timespan up to 4 years. These findings have built confidence that the model can be applied to investigate the morphological development of ebb-tidal delta nourishments over short- to medium-temporal scales. Provided the limited simulation timespan wherein the model can accurately reproduce the measured morphological response, this model cannot be applied as forecasting tool for the longer-term evolution of ebb-tidal delta nourishments.

What is the initial response of the Ameland ebb-tidal delta to the ebb-tidal delta nourishment?¹⁰

The initial response of the Ameland ebb-tidal delta to the pilot nourishment is a redistribution of sediment along the second and third ebb-shield. Based on an assessment of the known transport patterns before and after construction of the pilot nourishment, it can be concluded that the pilot nourishment primarily influences the local behaviour of the ebb-tidal delta. Conversely, it is observed that the averaged morphological response of the pilot nourishment within its initial footprint is an erosion.

What is the long-term trend of the morphodynamic adjustment of the Ameland ebb-tidal delta to the ebb-tidal delta nourishment?¹¹

On long-temporal scales the response of the Ameland ebb-tidal delta has the tendency to restore its initial equilibrium condition. The placement of an ebb-tidal delta nourishment disturbs the natural depth of the ebb-tidal delta. As a consequence, the presence of the ebb-tidal delta nourishment is compensated by an erosion within its initial footprint. As the ebb-shields exchange sediment with the downdrift coast via sediment bypassing processes, it can be argued that nourished sediment will accumulate on the coast of Ameland on longer temporal scales.

Volumetric analysis of the nourishment volumes in the construction polygon concurs with the modelled response as they reflect a persistent linear erosive trend in the years following construction of the nourishment. It is however not certain if the rate of linear decay will be consistent on decadal future time horizons, since the appearance of episodic wave events enables morphological resets in the initial topography of the ebb-tidal delta. This can have a significant impact on the long-term erosive behaviour of the ebb-tidal delta to the pilot nourishment.

How sensitive is the Ameland Ebb-tidal delta to changes in the pilot nourishment location and volume?

In this research, several alternative ebb-tidal delta nourishments have been addressed to assess and identify changes in the impact on the behaviour of the Ameland ebb-tidal delta. The synthesis of these model outcomes has shown that the natural behaviour of the Ameland ebb-tidal delta is highly dependent on the initial location of the ebb-tidal delta nourishment.

In general, the natural response of the Ameland ebb-tidal delta to ebb-tidal delta nourishments is a redistribution of sediment along the morphological features that it borders. The placement of ebb-tidal delta nourishments to the south of the Westgat invokes a primary sediment exchange between the coast of Terschelling and its surrounding morphological features. A secondary effect of the morphological development of the coast of Terschelling and the Zeehondenplaat is the readjustment of the Westgat which thereby influences the development of the ebb-shields and -chutes on the longer temporal scales. The construction of an ebb-tidal delta nourishment north of the Westgat results in a sediment exchange between the local ebb-shields and the downdrift coast of Ameland.

¹⁰ the initial response is here defined as the morphological adjustments that may be observed over a time span of 1 – 4 years post construction of the ebb-tidal delta nourishment.

¹¹ long-term trends are here defined as the persistency of prior observed morphological adjustments over a time span of 10 – 12 years post construction of the ebb-tidal delta nourishment.

9 Recommendations for future research

In this research, the *development* of ebb-chutes and -shields on the central part of the Ameland ebb-tidal delta is largely dependent on whether or not they are present in the underlying initial conditions. Therefore, the present state-of-the-art Ameland models tend to solely reproduce the *evolution* of the ebb-chute and -shield on the outer delta instead of its *development*. This enabled in this thesis a principle assessment on the deterministic process of ebb-chutes and shields which follows from a description of the underlying physical processes based on average conditions.

For the development of ebb-chutes and -shields in future modelling assessments, the model must be able to recognise and reproduce the temporal and spatial varying conditions for the initiation of small-scale instabilities from which ebb-chute and -shield systems arise. This may not be so trivial as these instabilities are highly stochastic in nature and depend on subtle nuances in the ebb-tidal delta morphology.

In order to simulate the development of ebb-chutes and -shields, a process-based morphodynamic model is needed that is able to capture small-scale hydrodynamic and morphodynamic interactions on shorter-temporal scales. This requires a different model schematisation to achieve the latter goal. In light of the aforementioned, it is advised that further possibilities are investigated to develop a new Ameland Delft3D model that incorporates the following features:

Boundary Conditions

- The hydrodynamic boundary conditions used in this research are derived based on a morphological tidal approach as proposed by Latteux, (1995) and with some modifications after Jiao, (2014).
- The wave boundary conditions are derived based on a manual selection of wave classes (see Sec. 4.4) and describe the yearly averaged wave climate for the Ameland ebb-tidal delta.

These boundary conditions can reasonably describe the average morphological development of the Ameland outer delta which has also been observed in this study. However, using these boundaries the implication of individual wave events (i.e. storm waves) on the outer delta morphology may not be investigated in a modelling assessment based on the previously described modelling configuration. This was also one of the underlying pitfalls of the model in this study as the storm erosion on the pilot nourishment has not been captured in the modelling results. To overcome this, the following boundary conditions should be considered:

- **Brute Forcing MorMerge Approach** (Luijendijk, 2019)

The wave boundary conditions are schematised as a quasi-realtime excitation over the simulation. This means that for each month or season over the computational period a characteristic wave condition is prescribed to incorporate the seasonal variations in wave height, period, direction possibly including also the variations in wind speed and direction. For computational efficiency, wave conditions with more or less the same characteristics can be clustered to reduce the amount of conditions used in the model. The MorMerge approach caters the application of parallelisation of the forcing conditions such that the relative contributions of the respective wave classes the weight-averaged bed level changes is simultaneously derived (Harlequin, 2020).

- **Nesting of Ameland model in Waddensea model**

In order to reproduce the morphological development of the Ameland ebb-tidal delta, the overarching complexity of the Ameland inlet system must be successfully implemented in the Ameland model. This means that the time varying flow conditions and sediment concentration conditions over the tidal divides are correctly encompassed in the model. Thereby, the prevailing offshore water level variations must be adequately derived which is only possible from a nesting procedure in the larger Waddensea model which is often used to derive the (non-)tidal residual water levels variations in the Waddensea. These water levels could be quasi-realtime imported in the Ameland model to prescribe the hydrodynamic conditions at the offshore boundary.

Grid resolution

The grid resolution in the modelling assessment of this research was large enough to allow for efficient computations and small enough to reasonably produce the morphological development of the Ameland ebb-tidal delta. In the new Ameland model the grid resolution along the Ameland coast and coast of Terschelling must be as large as the resolution in the vicinity of the main inlet to allow for better computations of the cross- and longshore variations. The high-resolution grid should at least encompass the surf zone after which subsequent coarsening may be advised to the offshore boundary.

Sediment transport formulation

The next step to update the representation of wave-induced processes in sediment transport formulations is to couple present nonlinear wave orbital velocity descriptions (e.g. see Boechat Albernaz et al., 2019; Ruessink et al., 2012) with the latest sediment transport formulations that include additional nonlinear wave tuning parameters. This will allow to incorporate more complexity of cross-shore sediment transport processes such as the effect of asymmetry on the entrainment and deposition of sediment particles, but also the incorporation of phase-lag effects on the displacement of sediment particles. The SANTOSS formulation provides hereby a good step forwards to incorporate such complexity. The SANTOSS sediment transport code incorporates the results from wave flume experiments on non-breaking (SANTOSS database) to calibrate the model's ability in computing sediment transport (Veen, 2014). Veen, (2014) showed that for the 77% of the predictions based on the SANTOSS Database fall within the factor 2 of the measurements. It should be noted that SANTOSS depends also on detailed information on the nonlinearity in the wave shape. This can be provided by the use of the near-orbital velocity formulation as provided by Boechat Albernaz et al., (2019) and the parameterisation of nonlinearity in the wave shape as proposed by Ruessink et al., (2012).

Bibliography

- Blew, J., Günther, K., Hälterlein, B., Kleefstra, R., Laursen, K., Ludwig, J., & Scheiffarth, G. (2017). Wadden Sea Quality Status Report 2017. *Netherlands Journal of Sea Research*, 22 Issue 1. <https://doi.org/https://qsr.waddensea-worldheritage.org/species>
- Boechat Albernaz, M., Ruessink, G., Jagers, H. R. A. (Bert), & Kleinhans, M. G. (2019). Effects of Wave Orbital Velocity Parameterization on Nearshore Sediment Transport and Decadal Morphodynamics. *Journal of Marine Science and Engineering*, 7(6). <https://doi.org/10.3390/jmse7060188>
- Bosboom, J., & Stive, M. J. F. (2021). *Coastal Dynamics*. <https://doi.org/10.5074/T.2021.001>
- Bruun, P., & Gerritsen, F. (1959). Natural By-Passing of Sand at Coastal Inlets. *Journal of the Waterways and Harbors Division*, 85(4), 75–107. <https://doi.org/10.1061/JWHEAU.0000152>
- Carter, R. W. G. (1988). Coastal Environments An Introduction to the Physical, Ecological, and Cultural Systems of Coastlines. In R. W. G. CARTER (Ed.), *Coastal Environments An Introduction to the Physical, Ecological, and Cultural Systems of Coastlines*. Academic Press. <https://doi.org/https://doi.org/10.1016/C2009-0-21648-5>
- Davis, R. A., & Hayes, M. O. (1984). What is a Wave-Dominated Coast? *Developments in Sedimentology*, 39(C), 313–329. [https://doi.org/10.1016/S0070-4571\(08\)70152-3](https://doi.org/10.1016/S0070-4571(08)70152-3)
- de Fockert, A. (2008). Impact of Relative Sea Level Rise on the Ameland Inlet Morphology. In *Delft University of Technology, Repository*. Delft University of Technology.
- De Swart, H. E., & Zimmerman, J. T. F. (2009). Morphodynamics of tidal inlet systems. *Annual Review of Fluid Mechanics*, 41(January 2009), 203–229. <https://doi.org/10.1146/annurev.fluid.010908.165159>
- Deltares. (2020). *Delft3D-FLOW: Simulation of multi-dimensional hydrodynamic flows and transport phenomena, including sediments*. Deltares. https://content.oss.deltares.nl/delft3d/manuals/Delft3D-FLOW_User_Manual.pdf
- Elias, E. P. L. (2017). *Understanding the present-day morphodynamics of Ameland*.
- Elias, E. P. L. (2018). Bench-mark morphodynamic model Ameland Inlet - Kustgenese 2.0 (ZG-C2). *Deltares - Kustgenese 2.0 (ZG-C2)*, 1(1). http://publications.deltares.nl/1220339_008a.pdf
- Elias, E. P. L., der Spek, A. J. F., Pearson, S. G., & Jelmer, C. (2019). Understanding sediment bypassing processes through analysis of high-frequency observations of Ameland Inlet, the Netherlands. *Marine Geology*, 415, 1–19. <https://doi.org/https://doi.org/10.1016/j.margeo.2019.06.001>
- Elias, E. P. L., Pearson, S., & van der Spek, A. J. F. (2020). *Understanding the morphological processes at Ameland Inlet*.
- Elias, E. P. L., Teske, R., van der Spek, A. J. F., & Lazar, M. (2015, July). MODELLING TIDAL-INLET MORPHODYNAMICS ON MEDIUM TIME SCALES. *The Proceedings of the Coastal Sediments 2015*. https://doi.org/10.1142/9789814689977_0230
- Elias, E. P. L., & Tonnon, P. K. (2016). Beschrijving kennisbasis modellering van zeegaten t.b.v. Kustgenese2. *Deltares - Kustgenese 2.0*, 1(1). https://www.helpdeskwater.nl/publish/pages/156535/beschrijving_kennisbasis_modelle ring_van_zeegaten_tbv_kustgenese2.pdf
- Escoffier, F. F. (1940). The stability of tidal inlets. *Shore and Beach*, 8(4), 114–115.
- FitzGerald, D. M. (1988). Shoreline Erosional-Depositional Processes Associated with Tidal Inlets. In *Hydrodynamics and Sediment Dynamics of Tidal Inlets* (pp. 186–225). American Geophysical Union (AGU). <https://doi.org/https://doi.org/10.1029/LN029p0186>
- Harlequin, D. V. (2020). A Heuristic Investigation into Methods to Model Medium-term Mesoscale Morphological features in Tidal and Estuarine Environments. In *Delft University of Technology, Repository*.
- Hayes, M. O. (1980). General morphology and sediment patterns in tidal inlets. *Sedimentary Geology*, 26(1–3), 139–156. [https://doi.org/10.1016/0037-0738\(80\)90009-3](https://doi.org/10.1016/0037-0738(80)90009-3)
- Herrling, G., & Winter, C. (2018). Tidal inlet sediment bypassing at mixed-energy barrier

- islands. *Coastal Engineering*, 140(October 2017), 342–354.
<https://doi.org/10.1016/j.coastaleng.2018.08.008>
- Isobe, M., & Horikawa, K. (1982). STUDY ON WATER PARTICLE VELOCITIES OF SHOALING AND BREAKING WAVES. *Coastal Engineering in Japan*, 25, 109–123.
<https://doi.org/10.1080/05785634.1982.11924340>
- Israel, C. G., & Dunsbergen, D. W. (1999). Cyclic morphological development of the Ameland Inlet, the Netherlands. *Proceedings of Symposium on River, Coastal and Estuarine Morphodynamics (Genova, Italy)*, 2, 705–714.
- Jiao, J. (2014). *Morphodynamics of Ameland Inlet: Medium-term Delft3D Modelling*. Delft University of Technology.
- Lambregts, P. (2021). *Understanding Sediment Bypassing at Ameland Inlet*. Delft University of Technology.
- Latteux, B. (1995). Techniques for long-term morphological simulation under tidal action. *Marine Geology*, 126(1), 129–141. [https://doi.org/https://doi.org/10.1016/0025-3227\(95\)00069-B](https://doi.org/https://doi.org/10.1016/0025-3227(95)00069-B)
- Luijendijk, A. P. (2019). Crossing borders in coastal morphodynamic modelling. *Delft University of Technology, Repository*, 13–15.
<https://doi.org/https://doi.org/10.4233/uuid:75ac8d9e-293f-4bff-90b3-467010352032>
- Ministerie van Landbouw Natuur en Voedselkwaliteit. (2017). *Natura 2000 gebied 1 - Waddenzee: PAS Gebiedsanalyse* (Vol. 1).
https://doi.org/https://www.natura2000.nl/sites/default/files/PAS/Gebiedsanalyses_vigerend/001_Waddenzee_gebiedsanalyse_15-12-17_IW.pdf
- Mulhern, J. S., Johnson, C. L., & Martin, J. M. (2017). Is barrier island morphology a function of tidal and wave regime? *Marine Geology*, 387, 74–84.
<https://doi.org/10.1016/j.margeo.2017.02.016>
- Nolte, A., van Oeveren-Theeuwes, C., van der Werk, J., Tonnon, P. K., Grasmeyer, B., van der Spek, A., Elias, E. P. L., & Wang, Z. B. (2020). *Technisch Advies Sedimentbehoefte Kustfundament*.
- Oertel, G. F. (1972). Sediment Transport of Estuary Entrance Shoals and the Formation of Swash Platforms. *J. Sediment. Petrol.*, 42(4 (DECEMBER, 1972)), 858–863.
<https://doi.org/10.1306/74d72658-2b21-11d7-8648000102c1865d>
- Pawlowicz, R., Beardsley, B., & Lentz, S. (2002). Classical tidal harmonic analysis including error estimates in MATLAB using T_TIDE. *Computers & Geosciences*, 28(8), 929–937.
[https://doi.org/10.1016/S0098-3004\(02\)00013-4](https://doi.org/10.1016/S0098-3004(02)00013-4)
- Rijkswaterstaat. (2021). *Kustgenese 2.0: kennis voor een veilige kust*.
- Ruessink, B. G., Ramaekers, G., & van Rijn, L. C. (2012). On the parameterization of the free-stream non-linear wave orbital motion in nearshore morphodynamic models. *Coastal Engineering*, 65, 56–63.
<https://doi.org/https://doi.org/10.1016/j.coastaleng.2012.03.006>
- Sha, L. P. (1989). Variation in ebb-delta morphologies along the West and East Frisian Islands, The Netherlands and Germany. *Marine Geology*, 89(1–2), 11–28.
[https://doi.org/10.1016/0025-3227\(89\)90025-X](https://doi.org/10.1016/0025-3227(89)90025-X)
- Steijn, R. C., & Roelvink, J. A. (1999). *Morfodynamische berekeningen van het Zeegat van Ameland* (p. 179).
- Tanczos, I. C., Aarninkhof, S. G., & van der Weck, A. W. (2001). *Ruimte voor de zandrivier*.
- Teske, R. (2013). *Tidal Inlet Channel Stability in Long Term Process Based Modelling*. University of Utrecht.
- Van Der Spek, A. J. F. (1995). Reconstruction of tidal inlet and channel dimensions in the Frisian Middelzee, a former tidal basin in the Dutch Wadden Sea. *Special Publication Of The International Association Of Sedimentologists*, 24(January 1995), 239–258.
<https://doi.org/10.1002/9781444304138.ch16>
- van Rhijn, M. W. (2019). *Sediment transport during the execution of the pilot nourishment Ameland Inlet*. Delft University of Technology.
- van Rijn, L. C. (2007). Unified View of Sediment Transport by Currents and Waves. I: Initiation of Motion, Bed Roughness, and Bed-Load Transport. *Journal of Hydraulic Engineering*, 133(6), 649–667. [https://doi.org/10.1061/\(ASCE\)0733-9429\(2007\)133:6\(649\)](https://doi.org/10.1061/(ASCE)0733-9429(2007)133:6(649))

- van Soest, M. (2021). *Wave nonlinearity parametrization for modelling the Ameland inlet*. University of Utrecht.
- Veen, R. (2014). The implementation and testing of the SANTOSS sand transport model in Delft3D. *MSc Thesis, University of Twente*, 68.
- Wang, Z. B., Hoekstra, P., Burchard, H., Ridderinkhof, H., De Swart, H. E., & Stive, M. J. F. (2012). Morphodynamics of the Wadden Sea and its barrier island system. *Ocean and Coastal Management*, 68, 39–57. <https://doi.org/10.1016/j.ocecoaman.2011.12.022>
- Wong, P. P., Losada, I. J., Gattuso, J. P., Hinkel, J., Khattabi, A., McInne, K. L., Saito, Y., & Sallenger, A. (2014). Coastal systems and low-lying areas. *Climate Change 2014: Impacts, Adaptation, and Vulnerability. Part A: Global and Sectoral Aspects. Contribution of Working Group II to the Fifth Assessment Report of the Intergovernmental Panel on Climate Change*, 361–409. https://doi.org/https://www.ipcc.ch/site/assets/uploads/2018/02/WGIIAR5-Chap5_FINAL.pdf

Appendices

A Natural Behaviour of the Ameland Ebb-Tidal Delta – Production Runs

A.1 Figures of Annual Production Runs

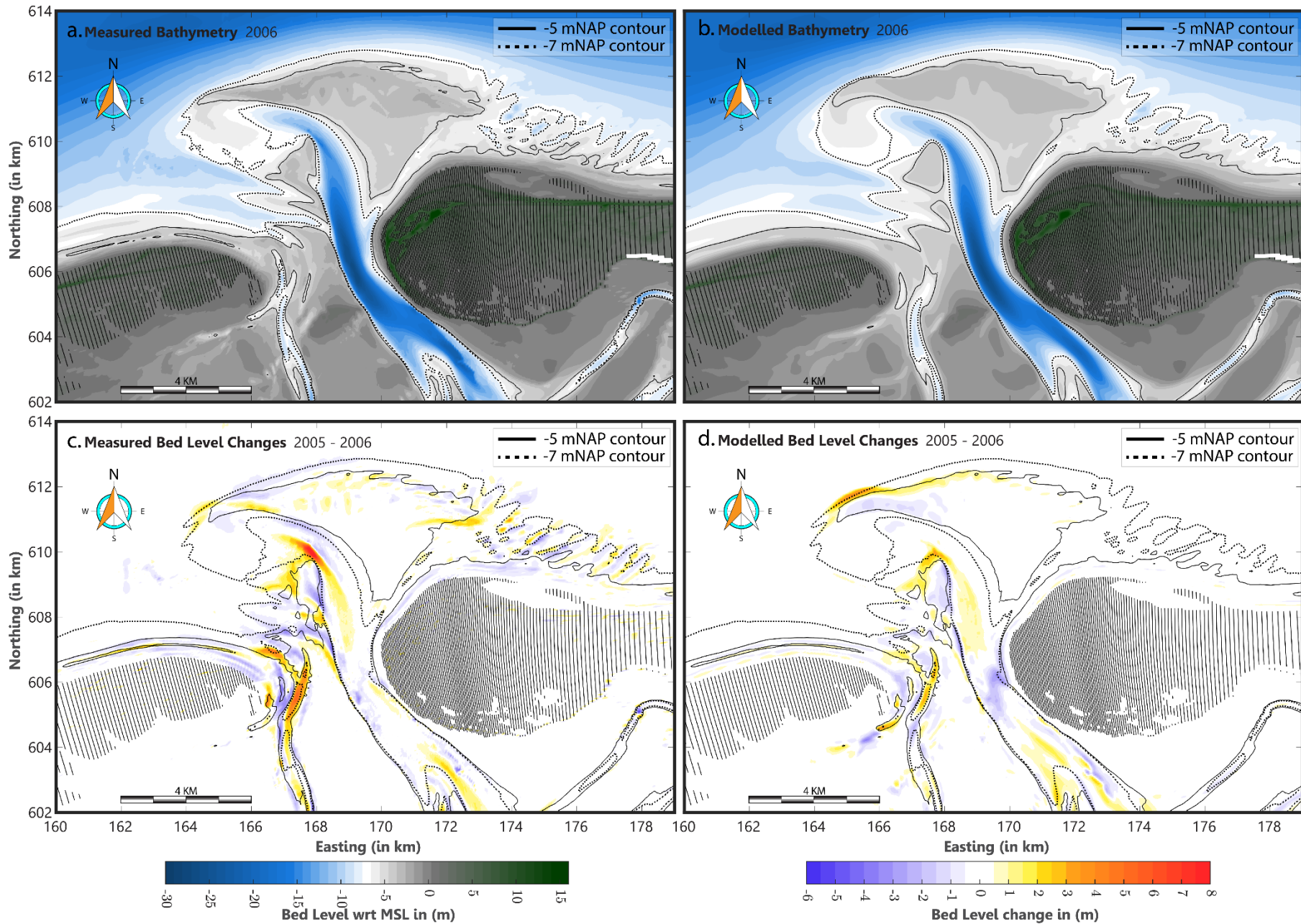


Figure A 1: Model prediction of the Ameland Ebb-Tidal Delta after one year of morphological climate (6 wave conditions and morphological tide – see Ch. 4 for more details on the boundary conditions). The initial bathymetry is consistent with the measured bathymetric observations in 2005. In order of occurrence, a) Measured and b) Modelled bathymetry in 2006, c) Measured and d) Modelled deposition and erosion patterns in 2006.

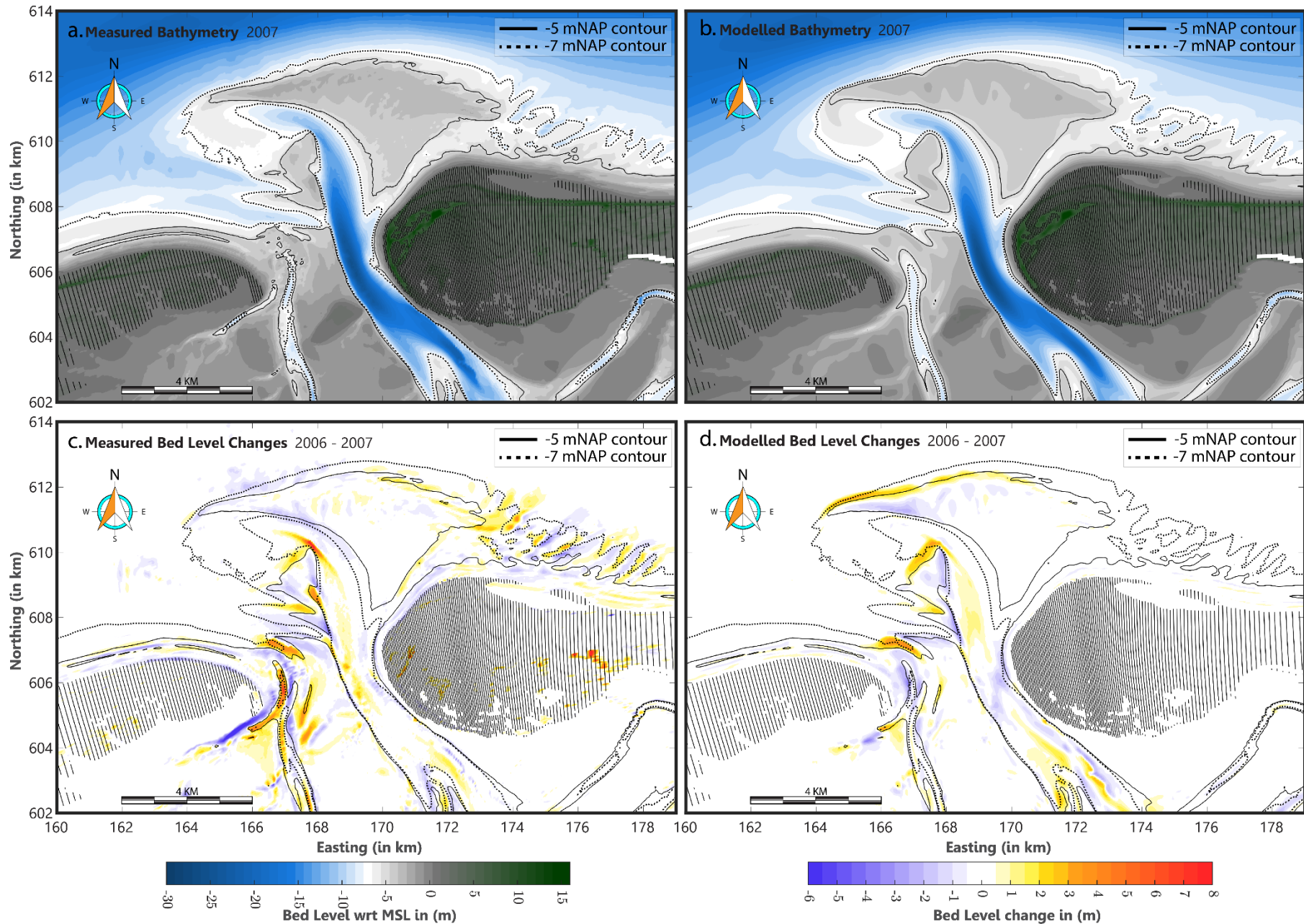


Figure A 2: Model prediction of the Ameland Ebb-Tidal Delta after one year of morphological climate (6 wave conditions and morphological tide – see Ch.4 for more details on the boundary conditions). The initial bathymetry is consistent with the measured bathymetric observations in 2006. In order of occurrence, a) Measured and b) Modelled bathymetry in 2007, c) Measured and d) Modelled deposition and erosion patterns in 2007.

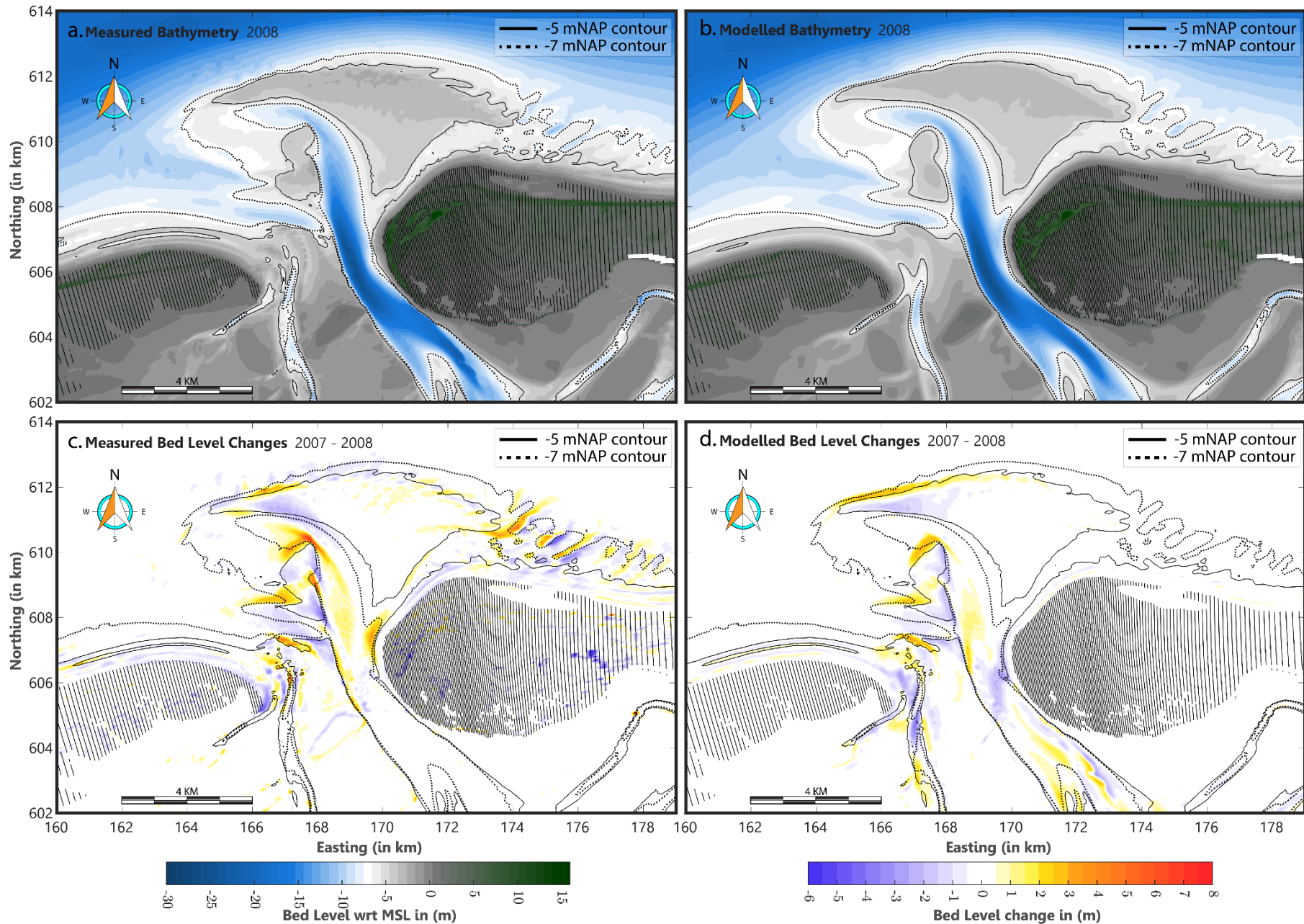


Figure A 3: Model prediction of the Ameland Ebb-Tidal Delta after one year of morphological climate (6 wave conditions and morphological tide – see Ch.4 for more details on the boundary conditions). The initial bathymetry is consistent with the measured bathymetric observations in 2007. In order of occurrence, a) Measured and b) Modelled bathymetry in 2008, c) Measured and d) Modelled deposition and erosion patterns in 2008.

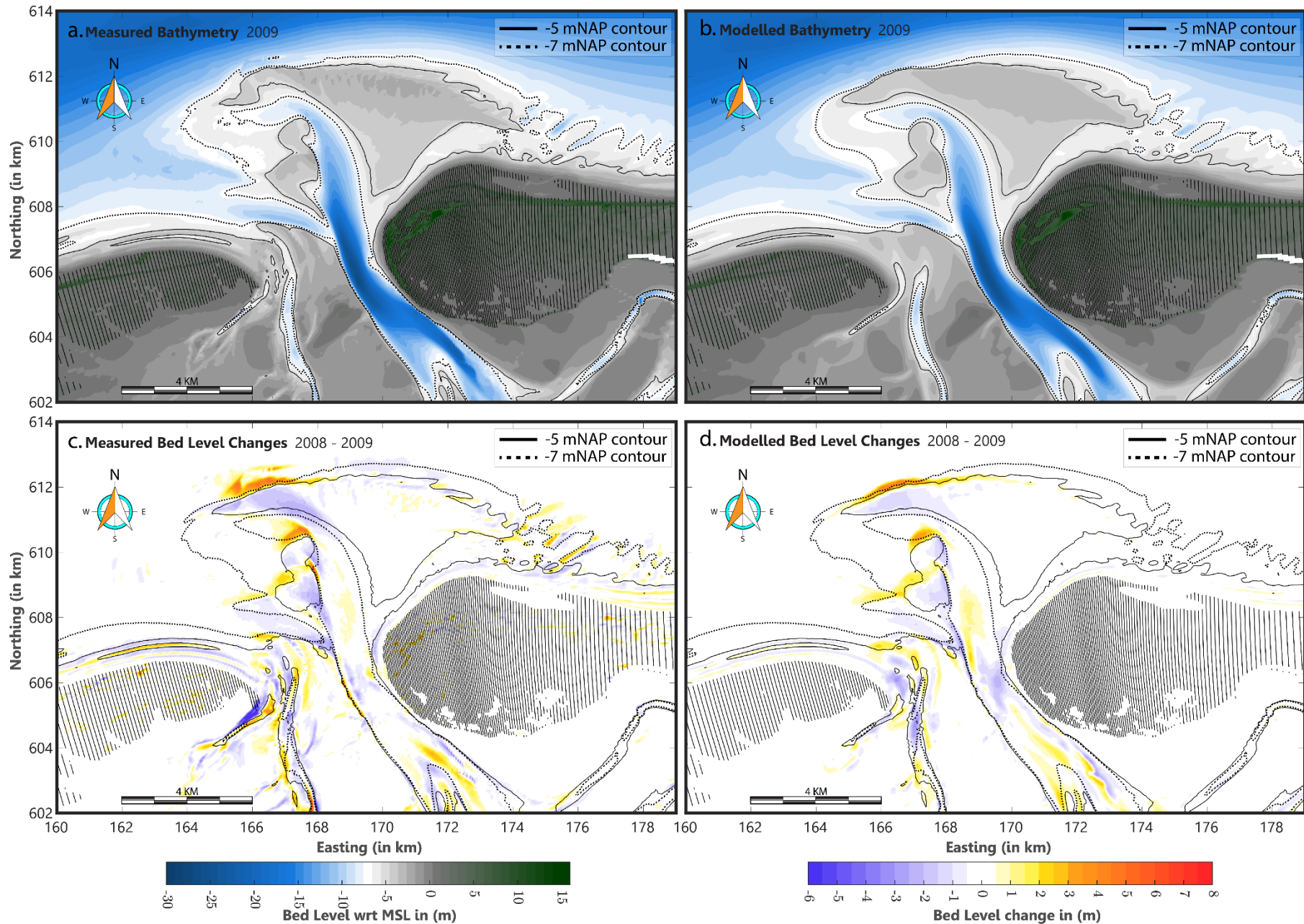


Figure A 4: Model prediction of the Ameland Ebb-Tidal Delta after one year of morphological climate (6 wave conditions and morphological tide – see Ch.4 for more details on the boundary conditions). The initial bathymetry is consistent with the measured bathymetric observations in 2008. In order of occurrence, a) Measured and b) Modelled bathymetry in 2009, c) Measured and d) Modelled deposition and erosion patterns in 2009.

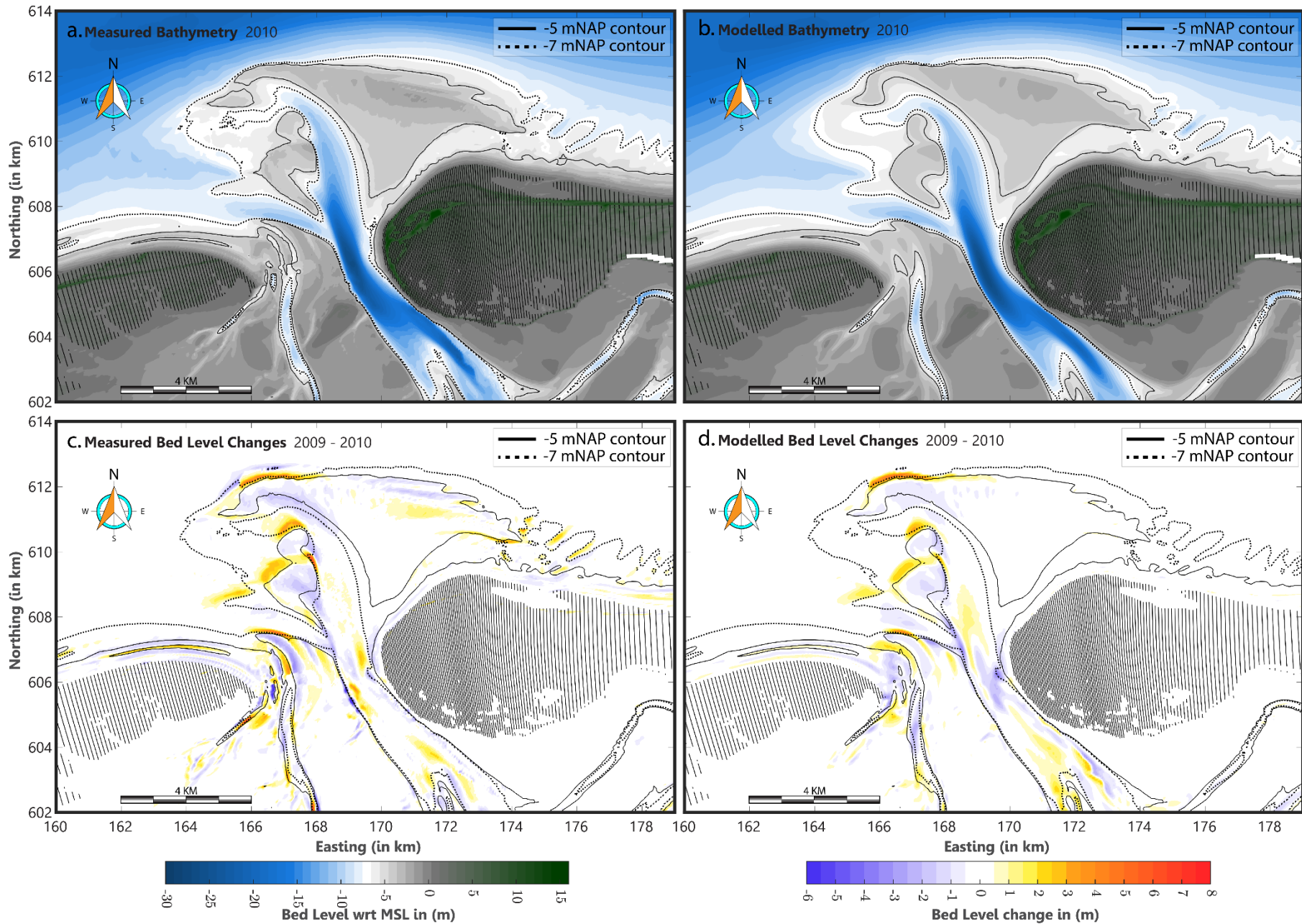


Figure A 5: Model prediction of the Ameland Ebb-Tidal Delta after one year of morphological climate (6 wave conditions and morphological tide – see Ch.4 for more details on the boundary conditions). The initial bathymetry is consistent with the measured bathymetric observations in 2009. In order of occurrence, a) Measured and b) Modelled bathymetry in 2010, c) Measured and d) Modelled deposition and erosion patterns in 2010.

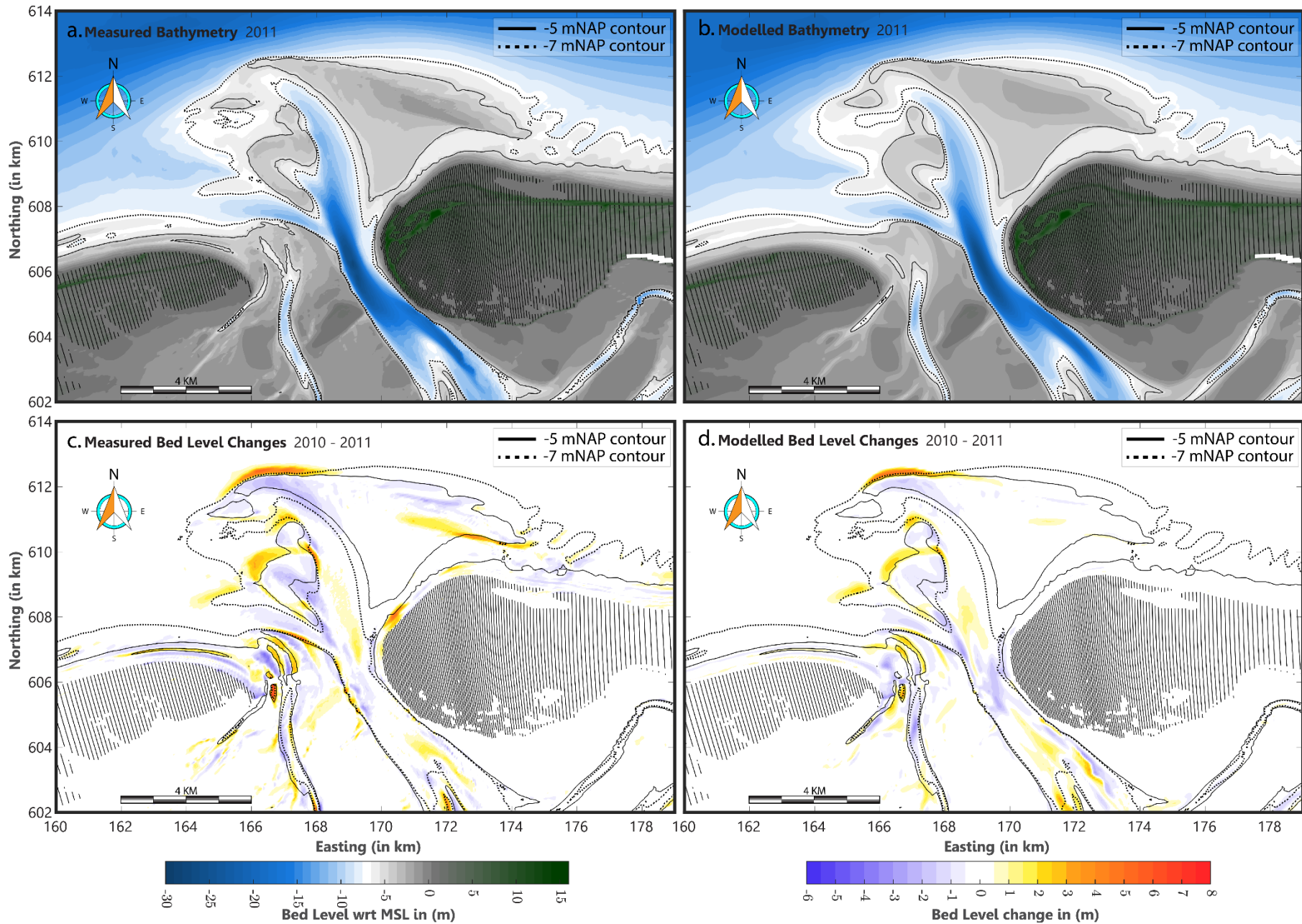


Figure A 6: Model prediction of the Ameland Ebb-Tidal Delta after one year of morphological climate (6 wave conditions and morphological tide – see Ch.4 for more details on the boundary conditions). The initial bathymetry is consistent with the measured bathymetric observations in 2010. In order of occurrence, a) Measured and b) Modelled bathymetry in 2011, c) Measured and d) Modelled deposition and erosion patterns in 2011.

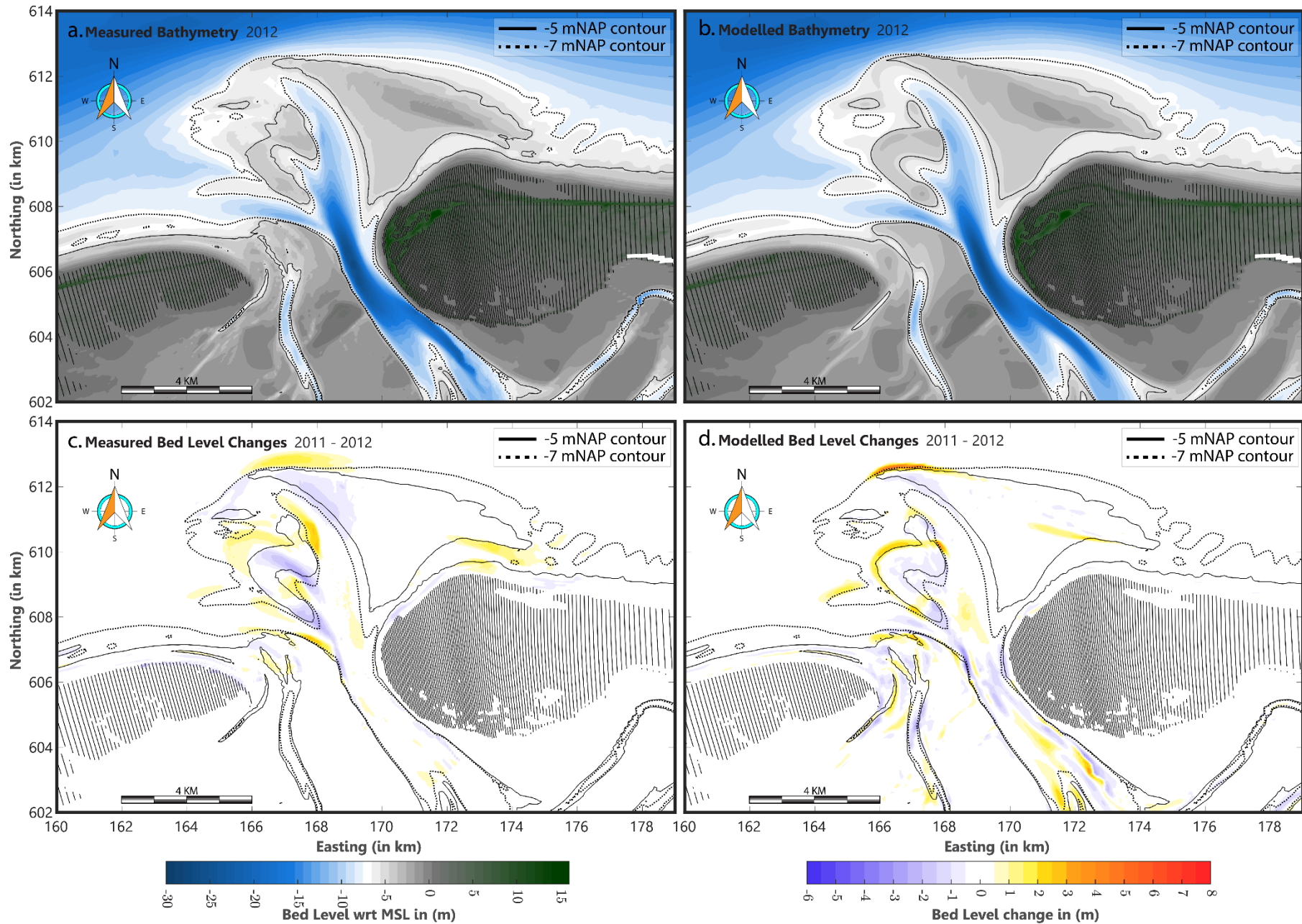


Figure A 7: Model prediction of the Ameland Ebb-Tidal Delta after one year of morphological climate (6 wave conditions and morphological tide – see Ch.4 for more details on the boundary conditions). The initial bathymetry is consistent with the measured bathymetric observations in 2011. In order of occurrence, a) Measured and b) Modelled bathymetry in 2012, c) Measured and d) Modelled deposition and erosion patterns in 2012.

* The measured bathymetry and bed level changes are derived based on linear interpolation between the bathymetric data of 2011 and 2014.

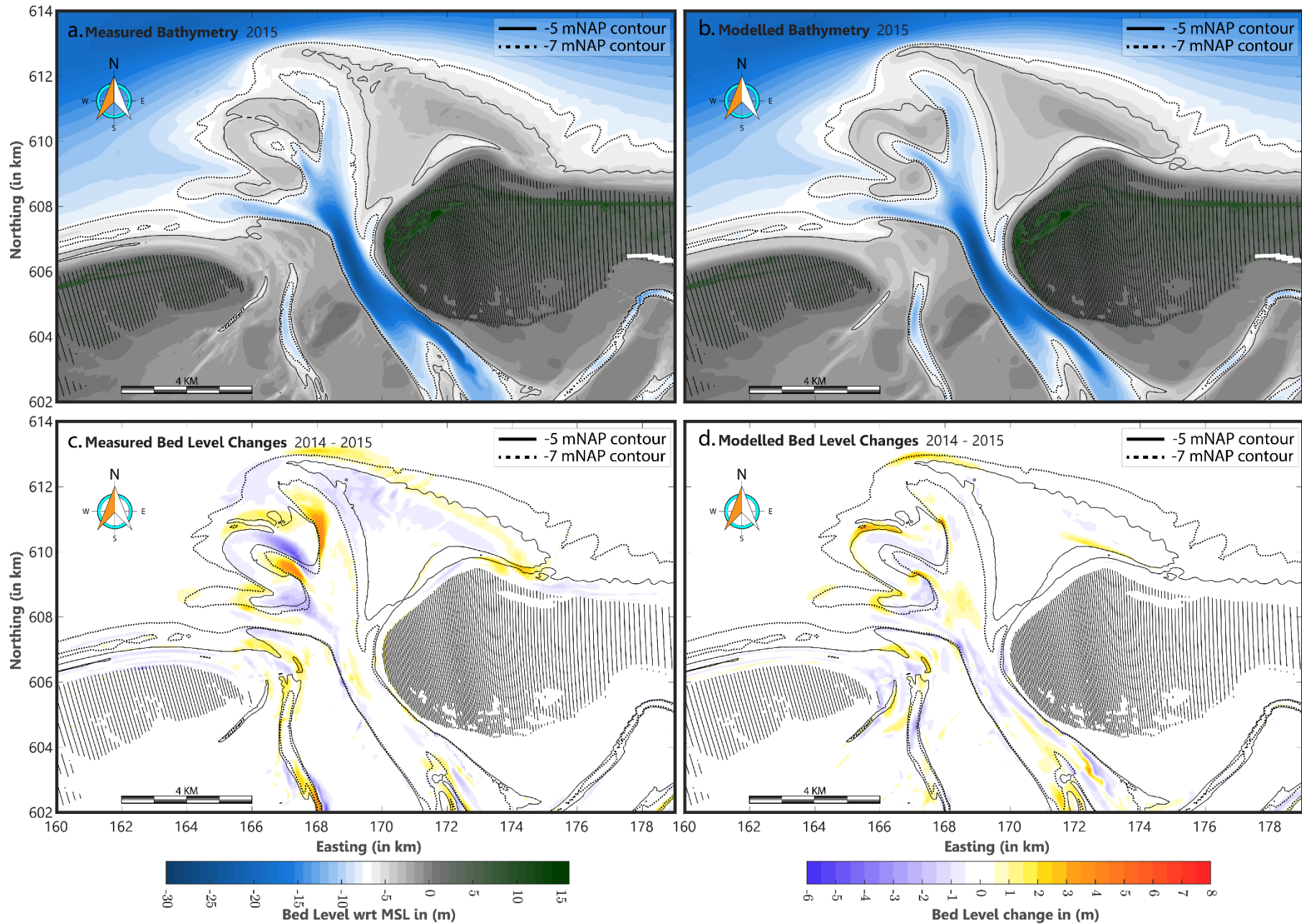


Figure A 8: Model prediction of the Ameland Ebb-Tidal Delta after one year of morphological climate (6 wave conditions and morphological tide – see Ch.4 for more details on the boundary conditions). The initial bathymetry is consistent with the measured bathymetric observations in 2014. In order of occurrence, a) Measured and b) Modelled bathymetry in 2014, c) Measured and d) Modelled deposition and erosion patterns in 2015.

* The measured bathymetry and bed level changes are derived based on linear interpolation between the bathymetric data of 2014 and 2016.

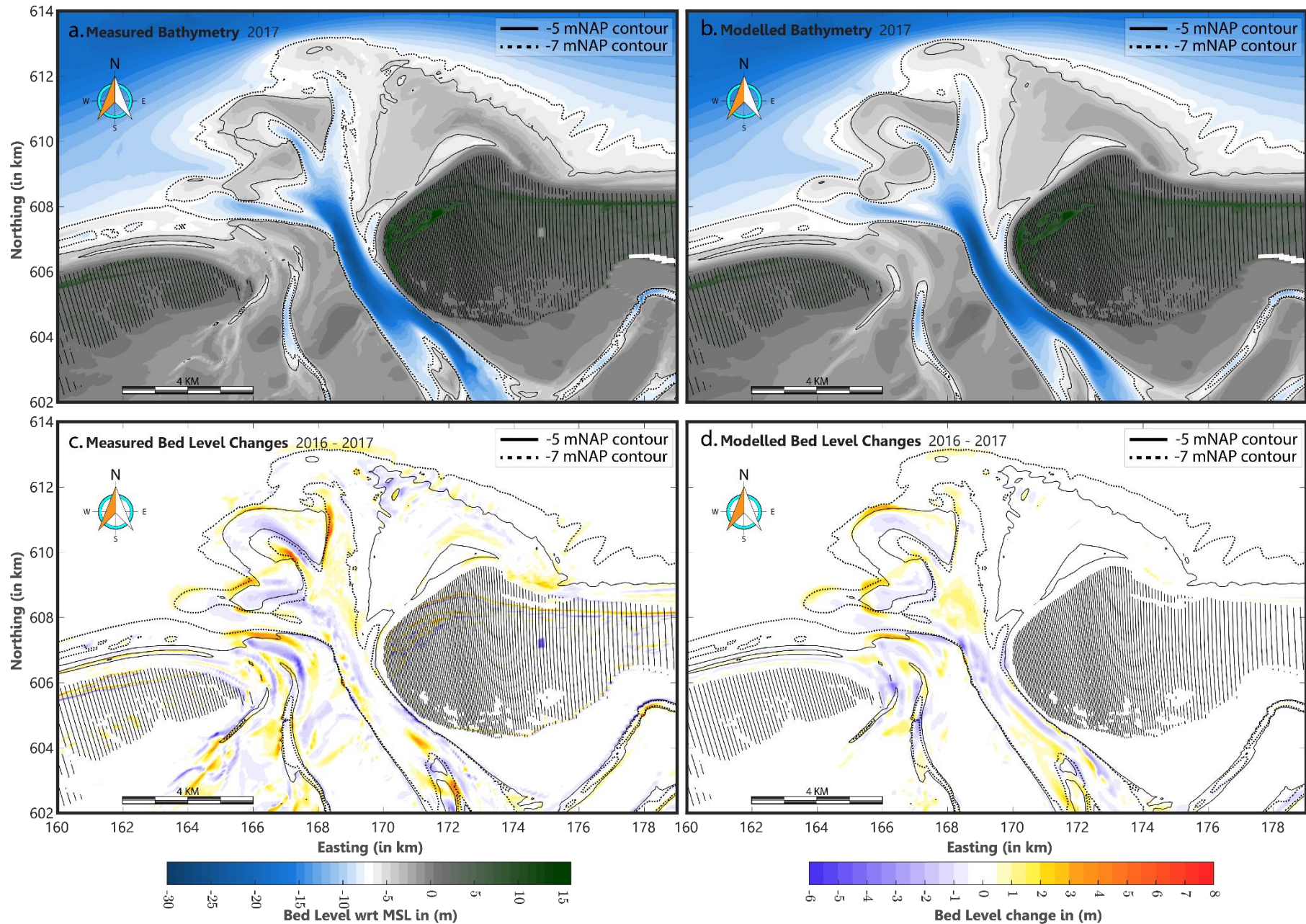


Figure A 9: Model prediction of the Ameland Ebb-Tidal Delta after one year of morphological climate (6 wave conditions and morphological tide – see Ch.4 for more details on the boundary conditions). The initial bathymetry is consistent with the measured bathymetric observations in 2016. In order of occurrence, a) Measured and b) Modelled bathymetry in 2017, c) Measured and d) Modelled deposition and erosion patterns in 2017.

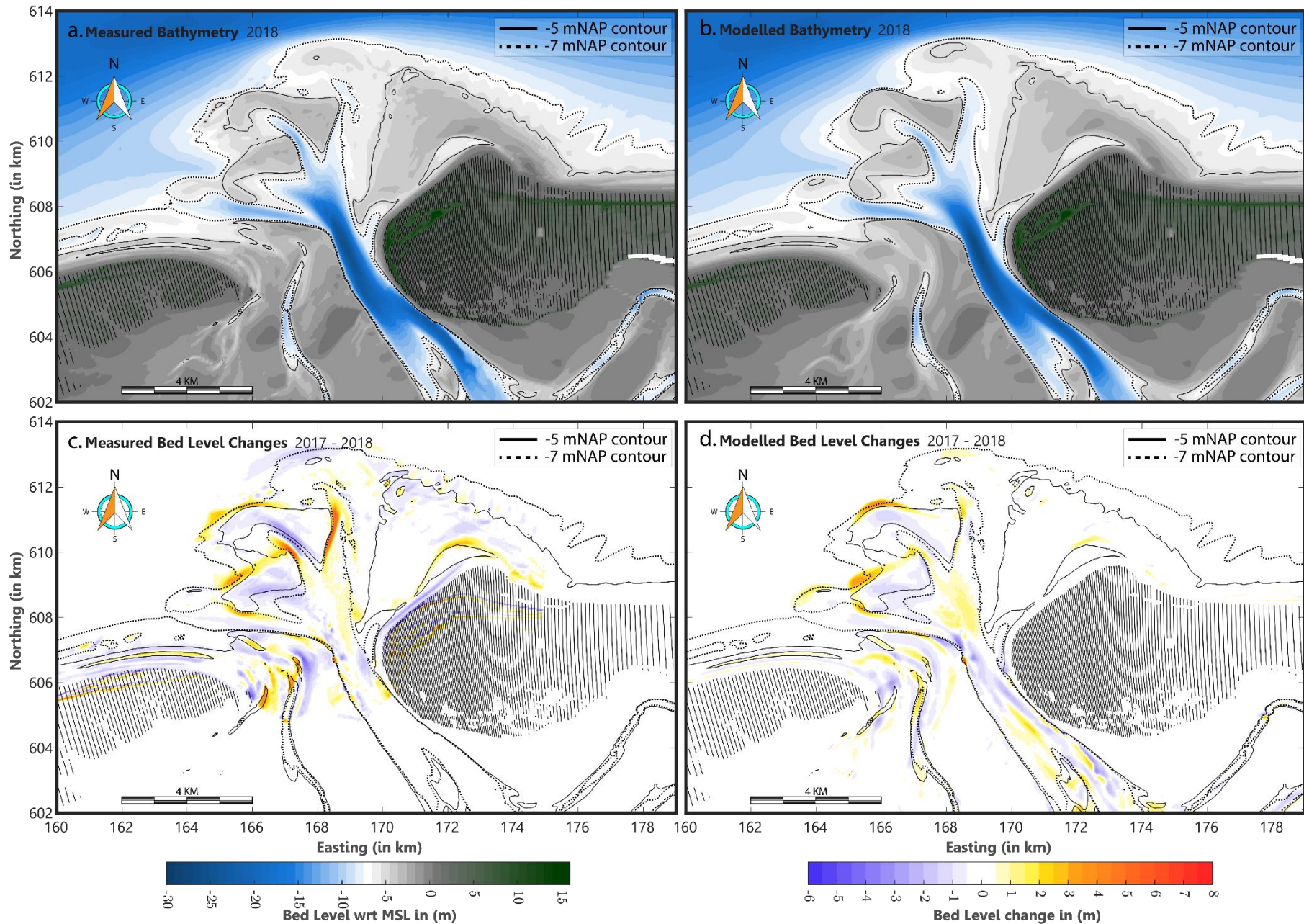


Figure A 10: Model prediction of the Ameland Ebb-Tidal Delta after one year of morphological climate (6 wave conditions and morphological tide – see Ch.4 for more details on the boundary conditions). The initial bathymetry is consistent with the measured bathymetric observations in 2017. In order of occurrence, a) Measured and b) Modelled bathymetry in 2017, c) Measured and d) Modelled deposition and erosion patterns in 2018.

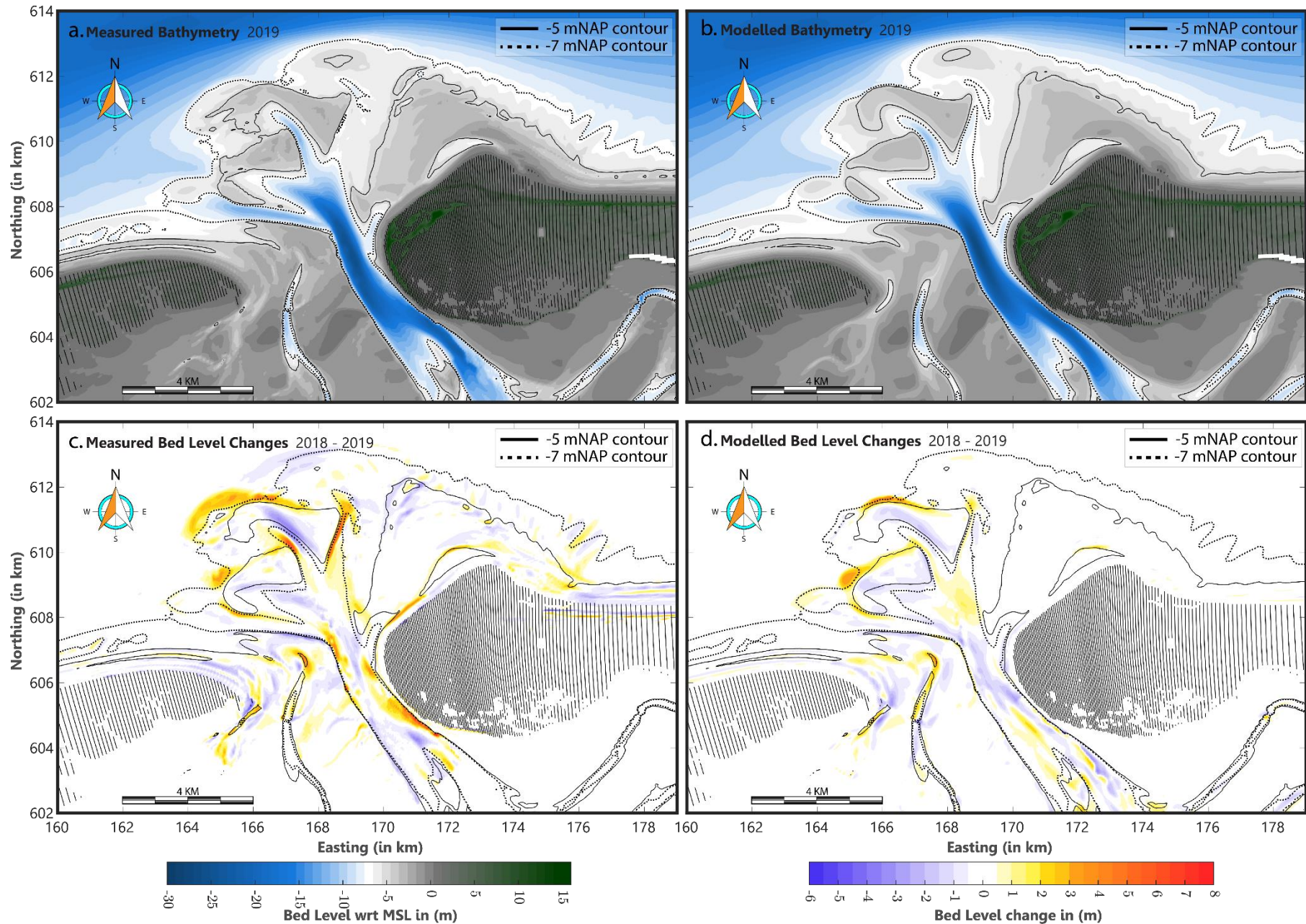


Figure A 11: Model prediction of the Ameland Ebb-Tidal Delta after one year of morphological climate (6 wave conditions and morphological tide – see Ch.4 for more details on the boundary conditions). The initial bathymetry is consistent with the measured bathymetric observations in 2018. In order of occurrence, a) Measured and b) Modelled bathymetry in 2019, c) Measured and d) Modelled deposition and erosion patterns in 2019.

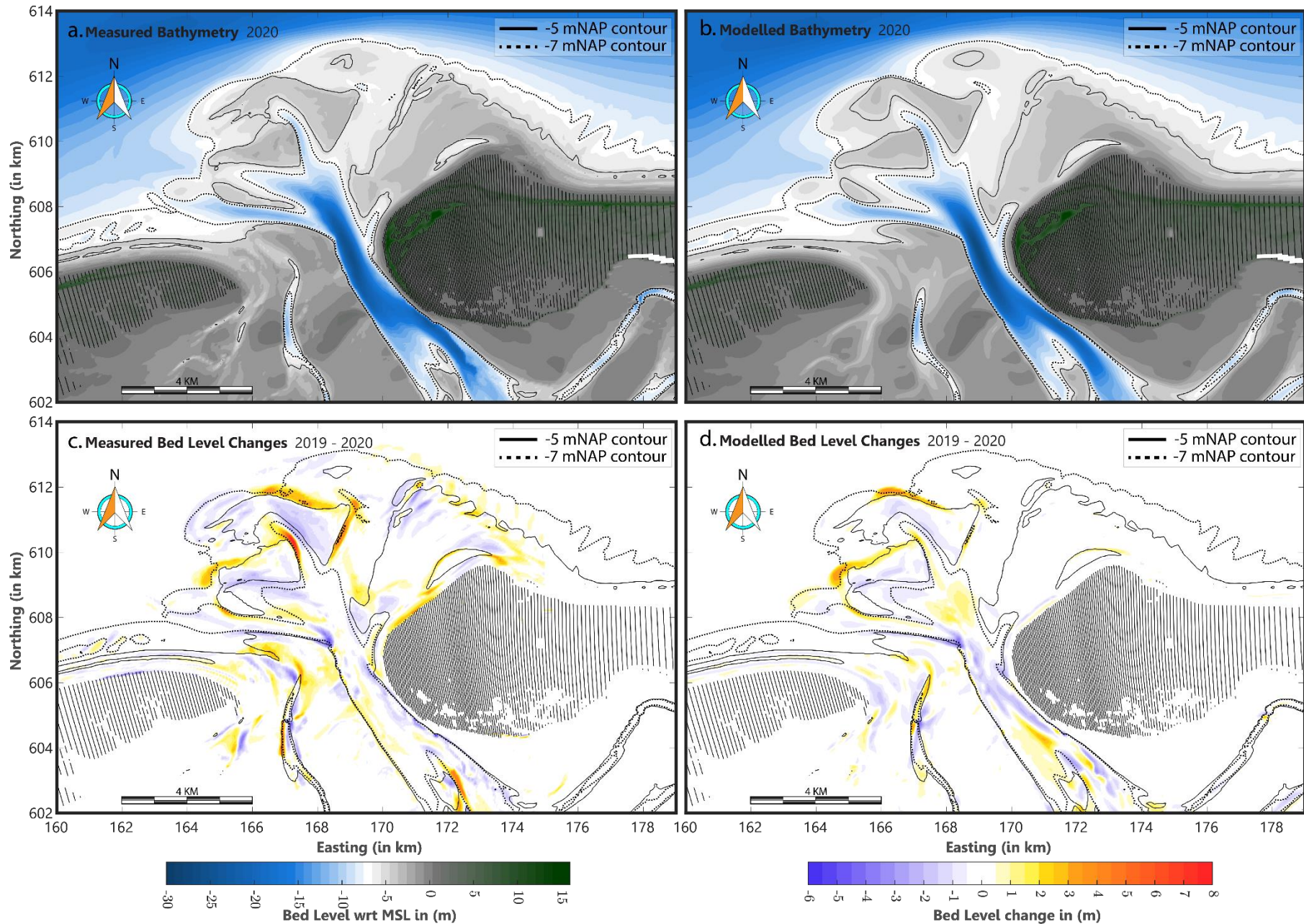


Figure A 12: Model prediction of the Ameland Ebb-Tidal Delta after one year of morphological climate (6 wave conditions and morphological tide – see Ch.4 for more details on the boundary conditions). The initial bathymetry is consistent with the measured bathymetric observations in 2019. In order of occurrence, a) Measured and b) Modelled bathymetry in 2020, c) Measured and d) Modelled deposition and erosion patterns in 2020.

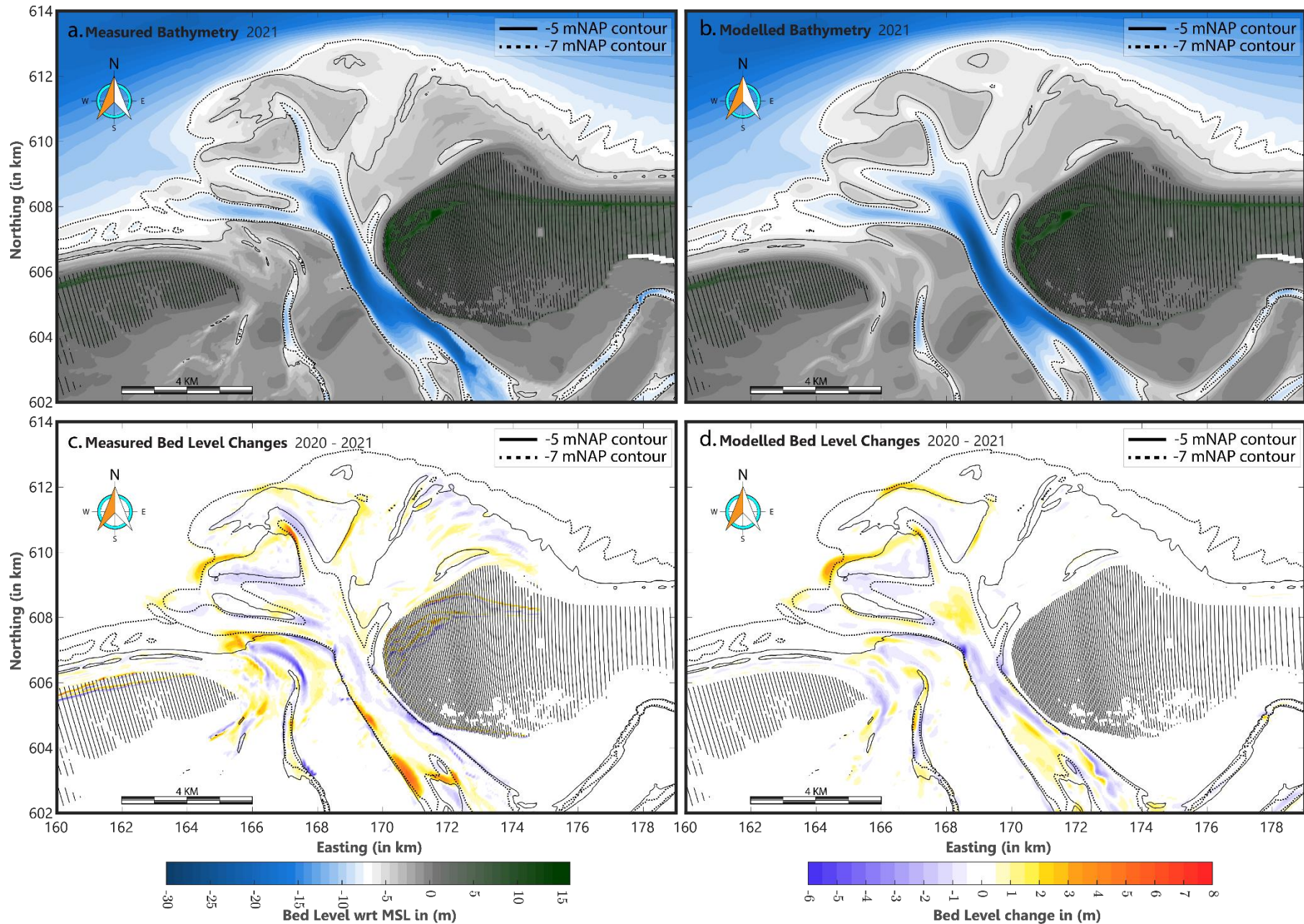


Figure A 13: Model prediction of the Ameland Ebb-Tidal Delta after one year of morphological climate (6 wave conditions and morphological tide – Ch.4 for more details on the boundary conditions). The initial bathymetry is consistent with the measured bathymetric observations in 2020. In order of occurrence, a) Measured and b) Modelled bathymetry in 2021, c) Measured and d) Modelled deposition and erosion patterns in 2021.

A.2 Figures of Two-Year Production Runs

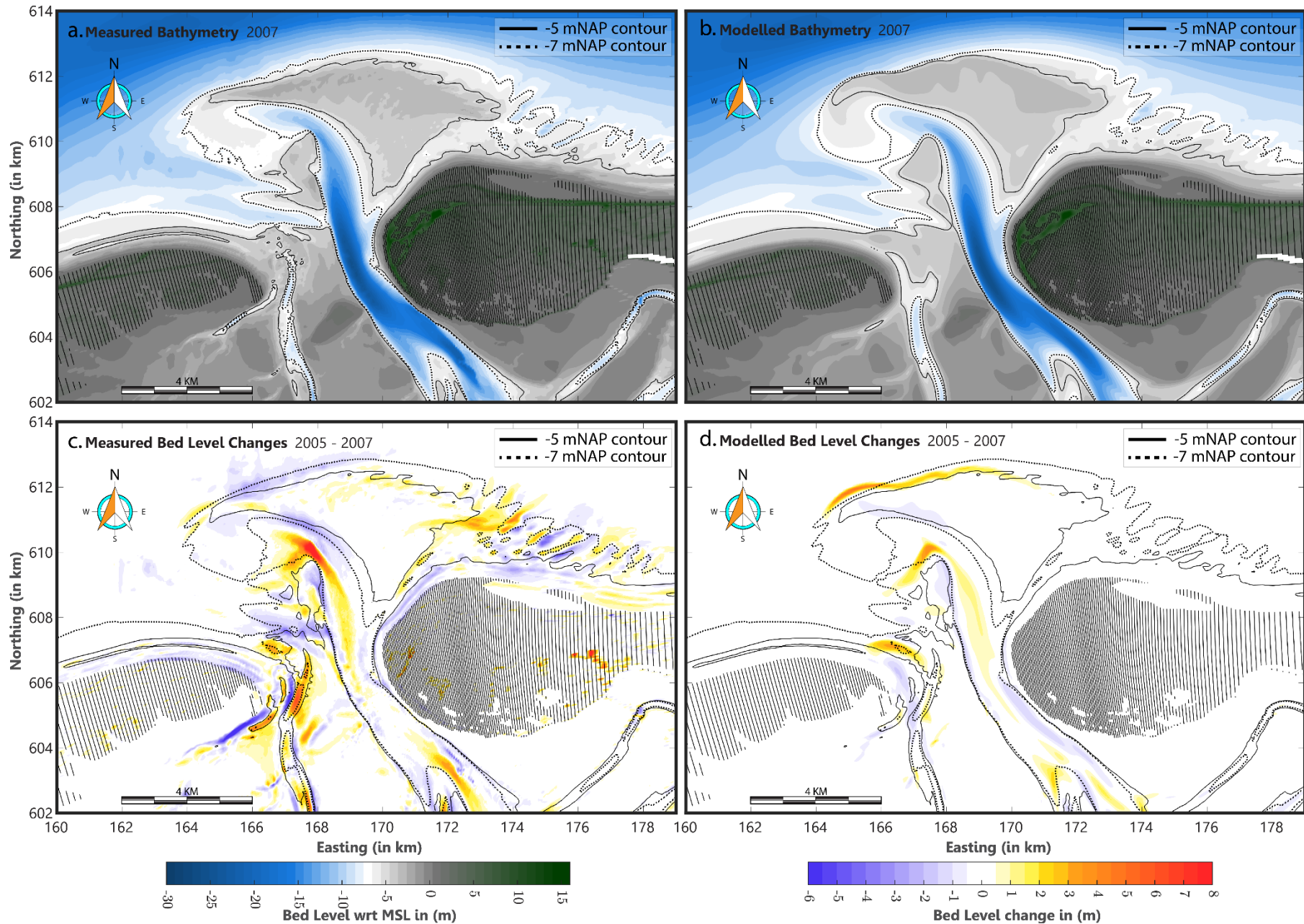


Figure A 14: Model prediction of the Ameland Ebb-Tidal Delta after two years of morphological climate (6 wave conditions and morphological tide – see Ch.4 for more details on the boundary conditions). The initial bathymetry is consistent with the measured bathymetric observations in 2005. In order of occurrence, a) Measured and b) Modelled bathymetry in 2007, c) Measured and d) Modelled deposition and erosion patterns in 2007.

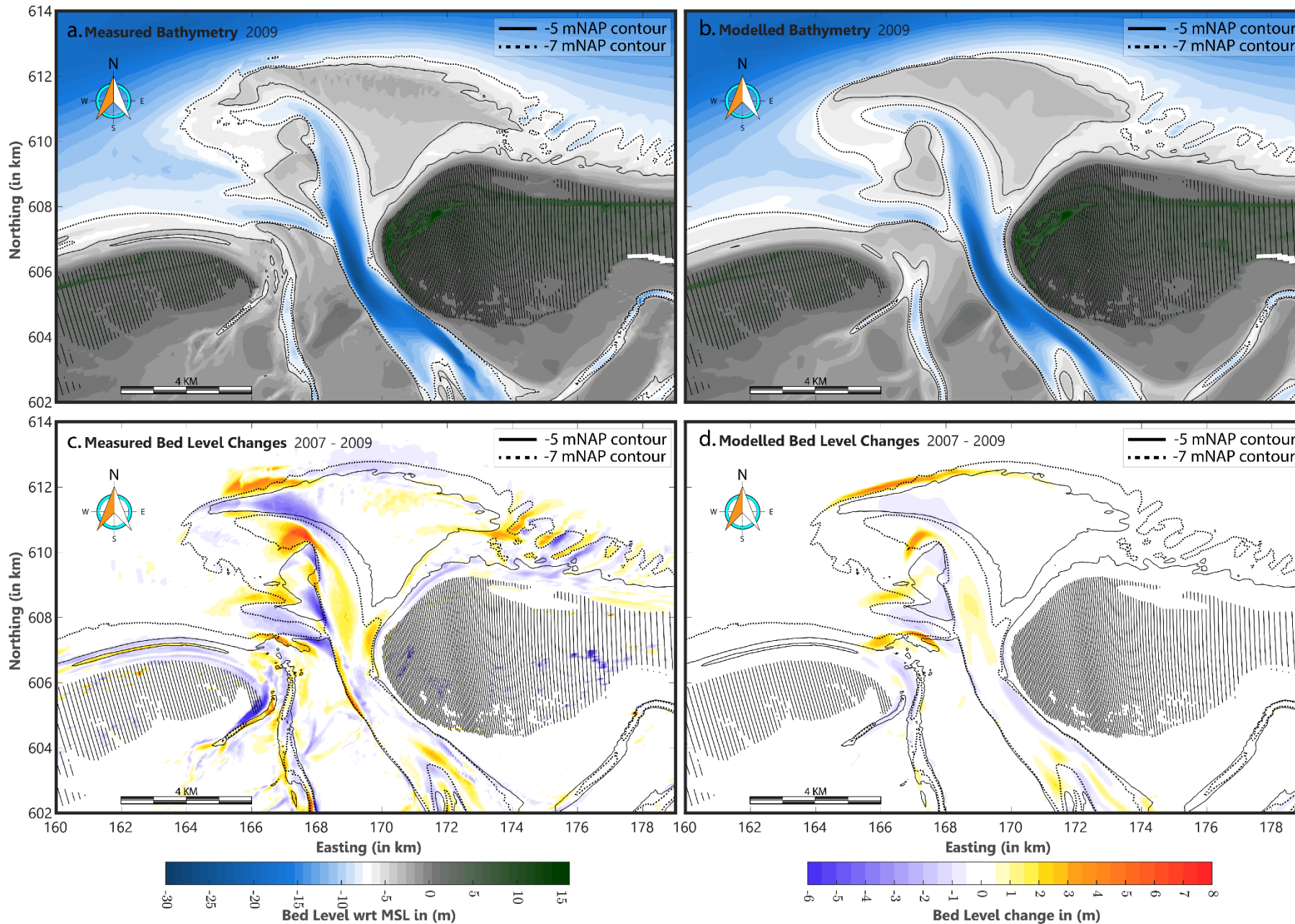


Figure A 15: Model prediction of the Ameland Ebb-Tidal Delta after two years of morphological climate (6 wave conditions and morphological tide – see Ch.4 for more details on the boundary conditions). The initial bathymetry is consistent with the measured bathymetric observations in 2007. In order of occurrence, a) Measured and b) Modelled bathymetry in 2009, c) Measured and d) Modelled deposition and erosion patterns in 2009.

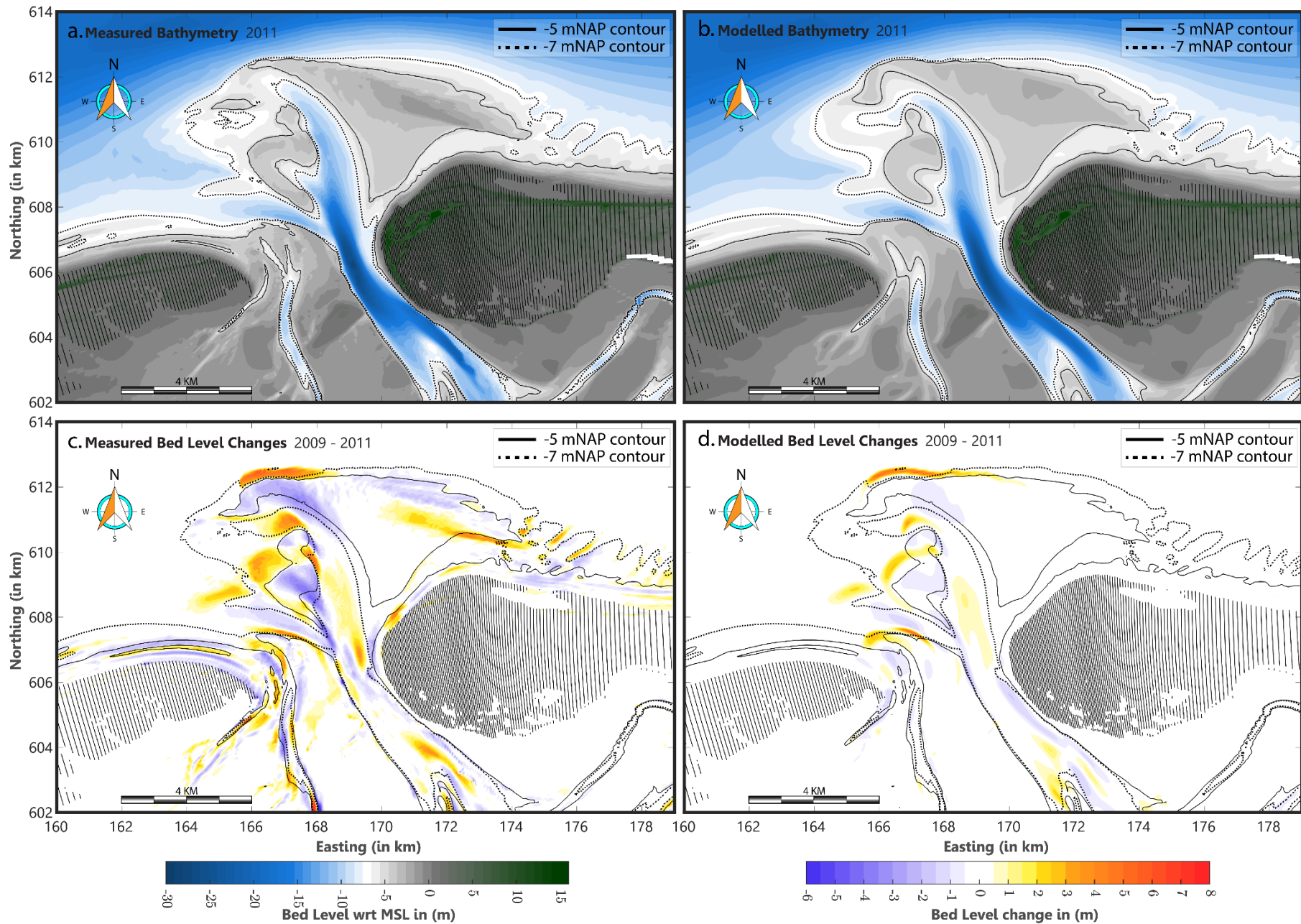


Figure A 16: Model prediction of the Ameland Ebb-Tidal Delta after two years of morphological climate (6 wave conditions and morphological tide – see Ch.4 for more details on the boundary conditions). The initial bathymetry is consistent with the measured bathymetric observations in 2009. In order of occurrence, a) Measured and b) Modelled bathymetry in 2009, c) Measured and d) Modelled deposition and erosion patterns in 2011.

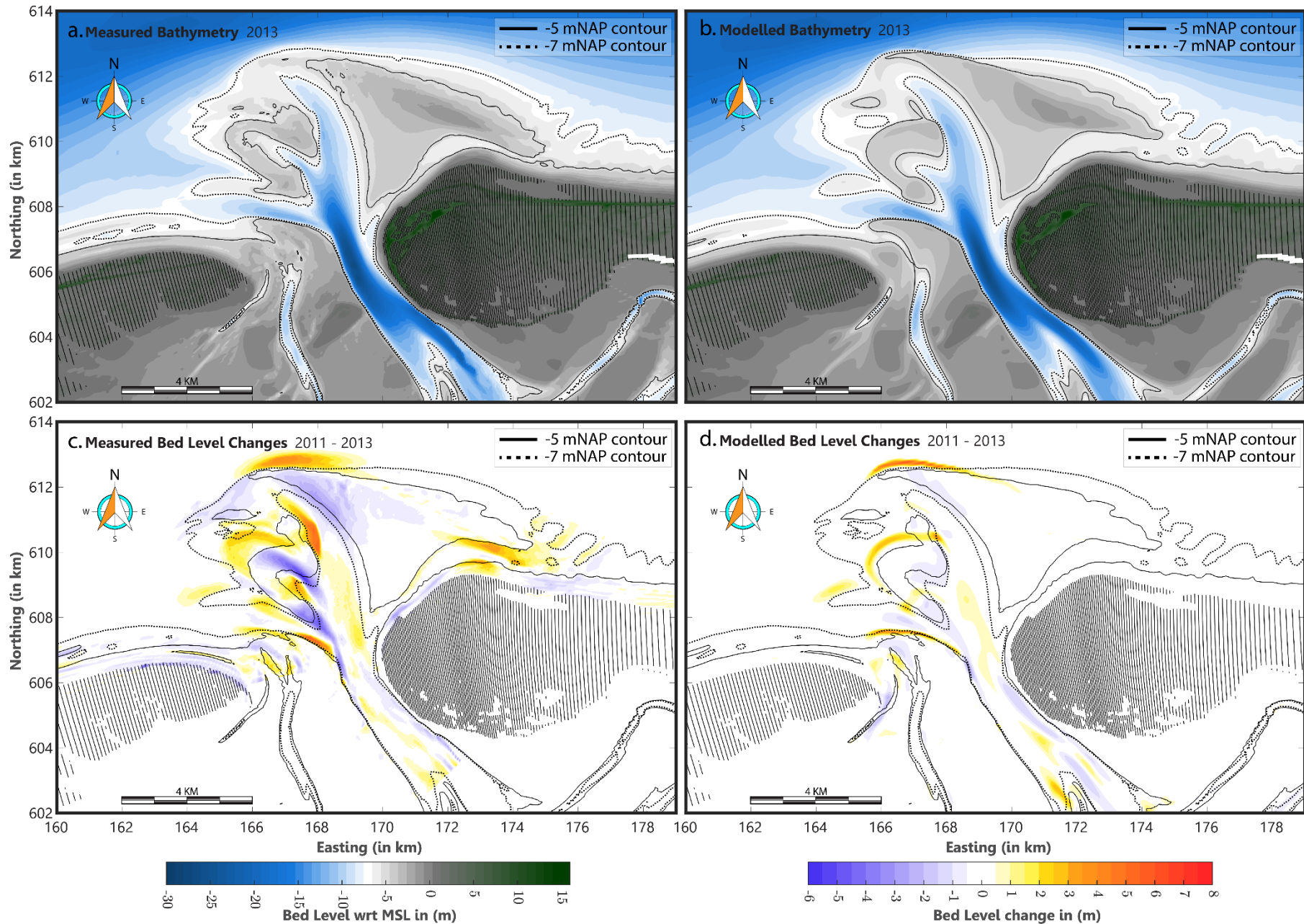


Figure A 17: Model prediction of the Ameland Ebb-Tidal Delta after two years of morphological climate (6 wave conditions and morphological tide – see Ch.4 for more details on the boundary conditions). The initial bathymetry is consistent with the measured bathymetric observations in 2011. In order of occurrence, a) Measured and b) Modelled bathymetry in 2013, c) Measured and d) Modelled deposition and erosion patterns in 2013.

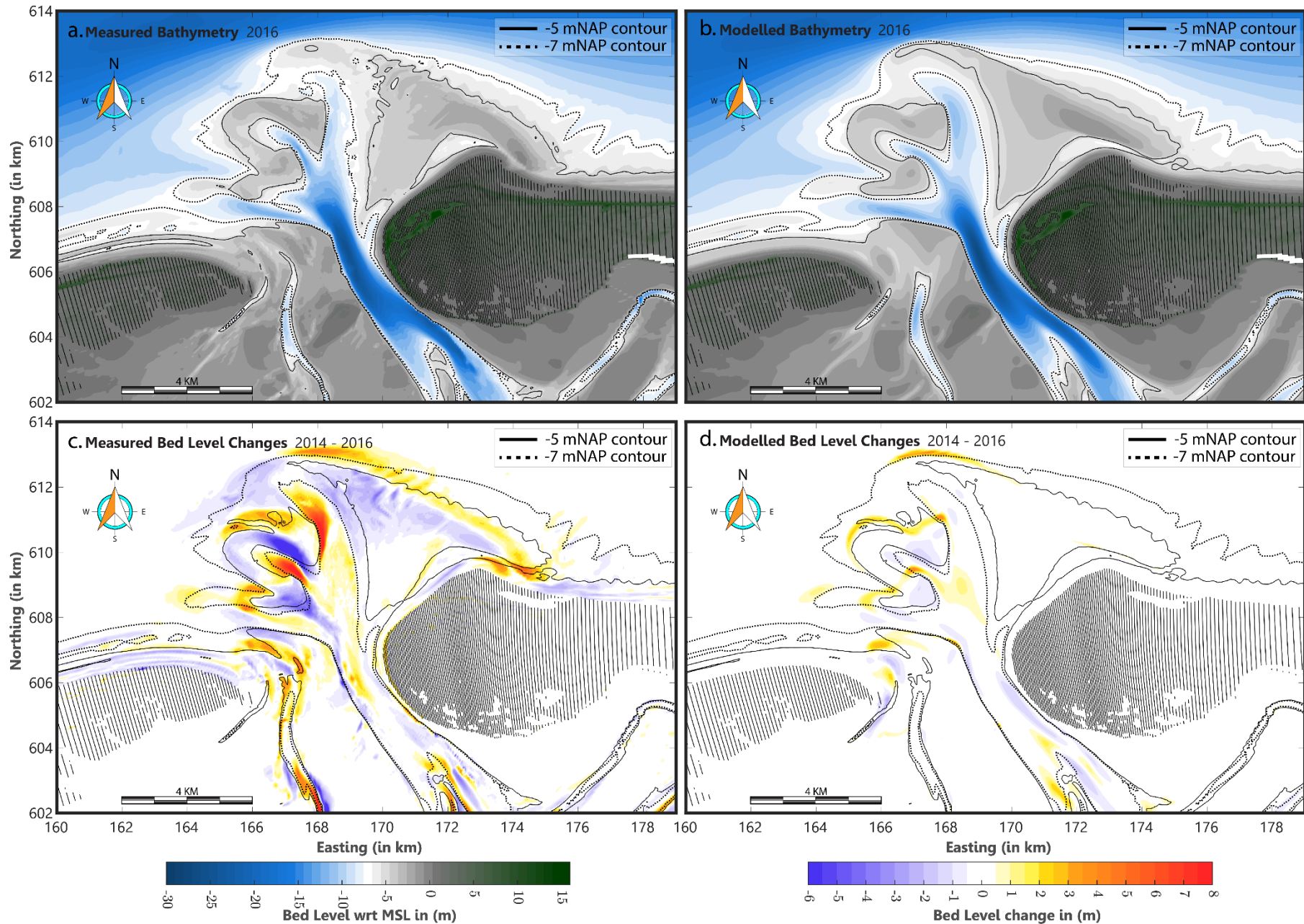


Figure A 18: Model prediction of the Ameland Ebb-Tidal Delta after two years of morphological climate (6 wave conditions and morphological tide – see Ch.4 for more details on the boundary conditions). The initial bathymetry is consistent with the measured bathymetric observations in 2014. In order of occurrence, a) Measured and b) Modelled bathymetry in 2016, c) Measured and d) Modelled deposition and erosion patterns in 2016.

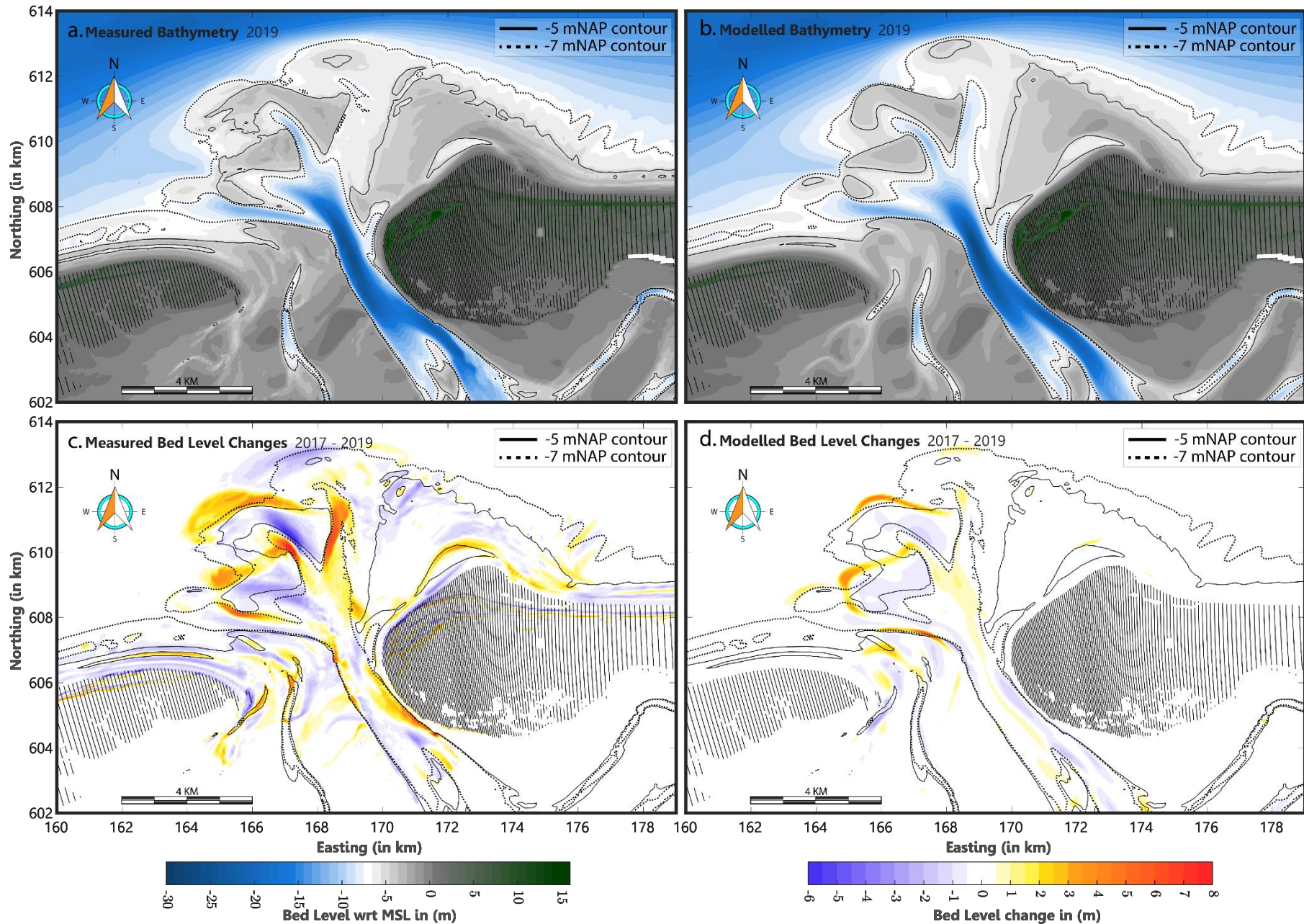


Figure A 20: Model prediction of the Ameland Ebb-Tidal Delta after two years of morphological climate (6 wave conditions and morphological tide – see Ch.4 for more details on the boundary conditions). The initial bathymetry is consistent with the measured bathymetric observations in 2017. In order of occurrence, a) Measured and b) Modelled bathymetry in 2019, c) Measured and d) Modelled deposition and erosion patterns in 2019.

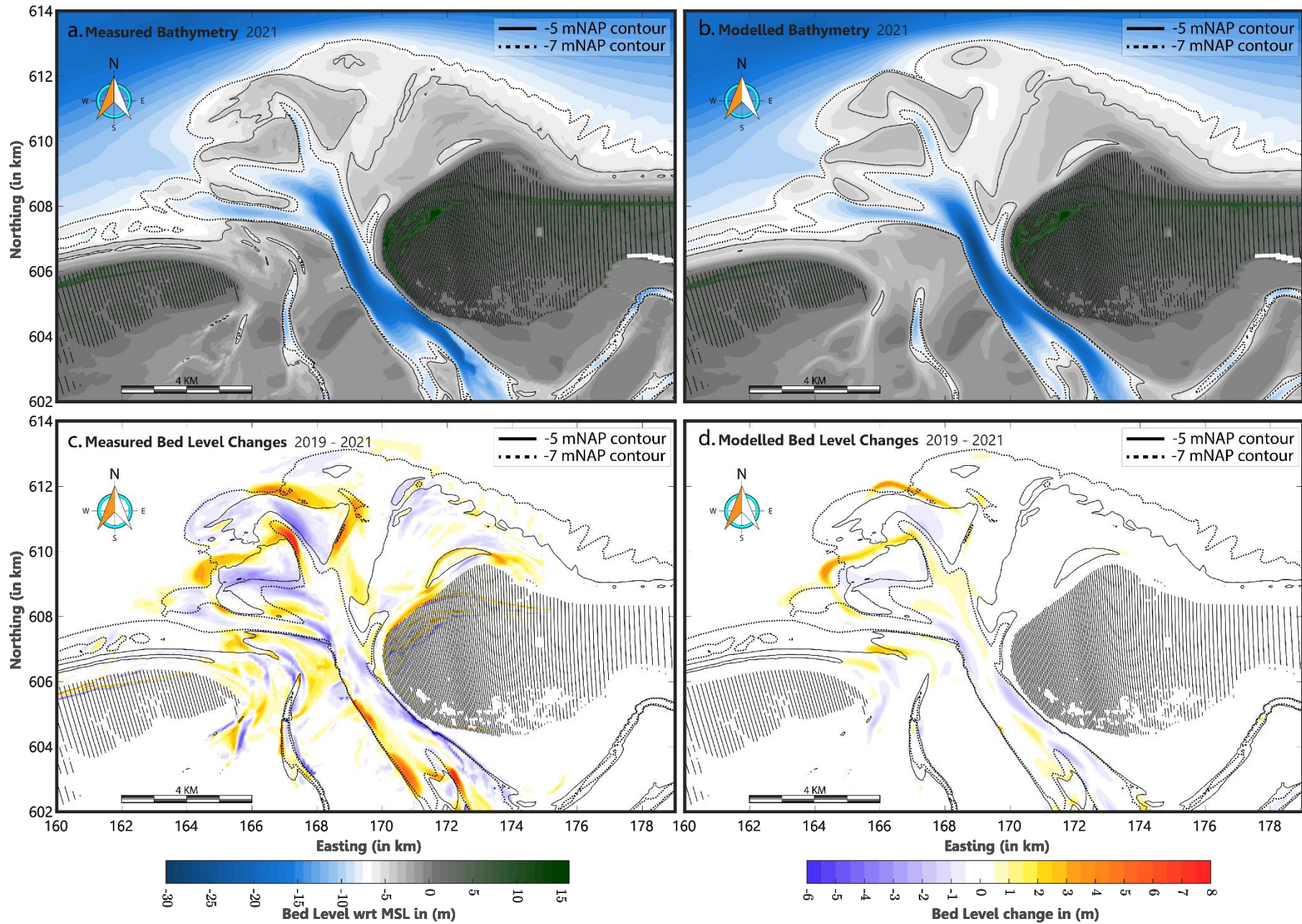


Figure A 22: Model prediction of the Ameland Ebb-Tidal Delta after two years of morphological climate (6 wave conditions and morphological tide – see Ch.4 for more details on the boundary conditions). The initial bathymetry is consistent with the measured bathymetric observations in 2020. In order of occurrence, a) Measured and b) Modelled bathymetry in 2021, c) Measured and d) Modelled deposition and erosion patterns in 2021.

A.3 Figures of Four-Year Production Runs

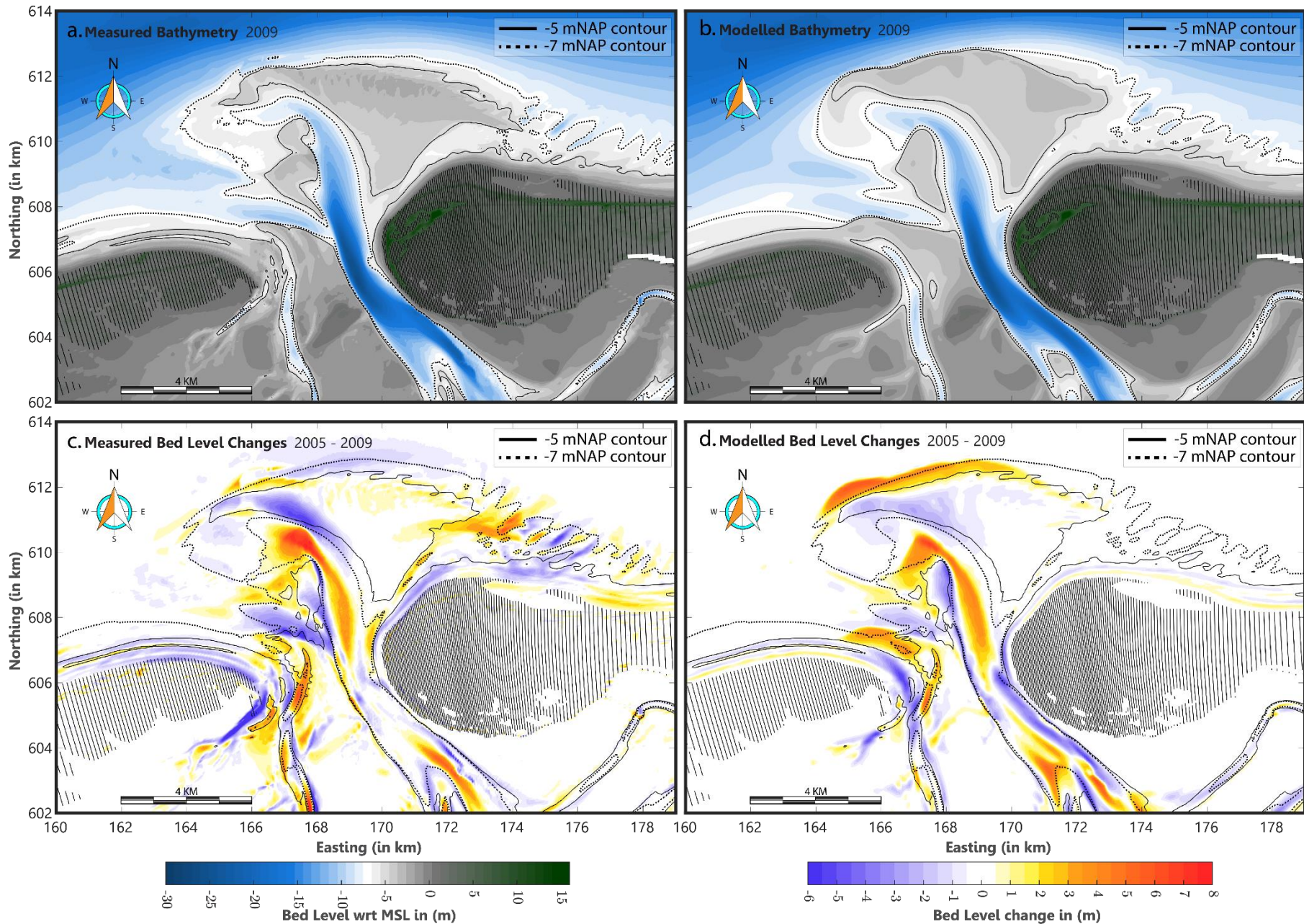


Figure A 23: Model prediction of the Ameland Ebb-Tidal Delta after four years of morphological climate (6 wave conditions and morphological tide – see Ch.4 for more details on the boundary conditions). The initial bathymetry is consistent with the measured bathymetric observations in 2005. In order of occurrence, a) Measured and b) Modelled bathymetry in 2007, c) Measured and d) Modelled deposition and erosion patterns in 2009.

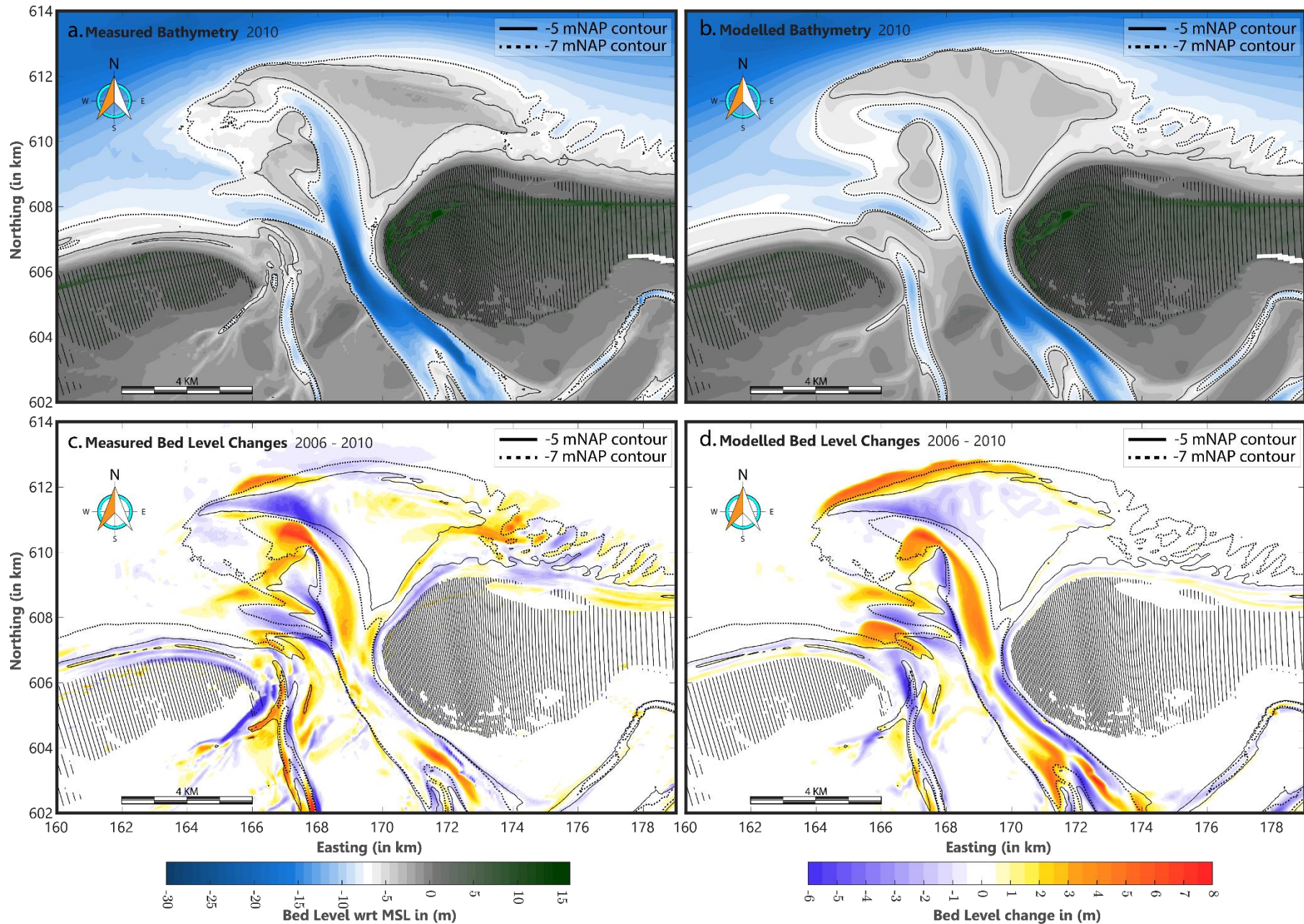


Figure A 24: Model prediction of the Ameland Ebb-Tidal Delta after four years of morphological climate (6 wave conditions and morphological tide – see Ch.4 for more details on the boundary conditions). The initial bathymetry is consistent with the measured bathymetric observations in 2006. In order of occurrence, a) Measured and b) Modelled bathymetry in 2010, c) Measured and d) Modelled deposition and erosion patterns in 2010.

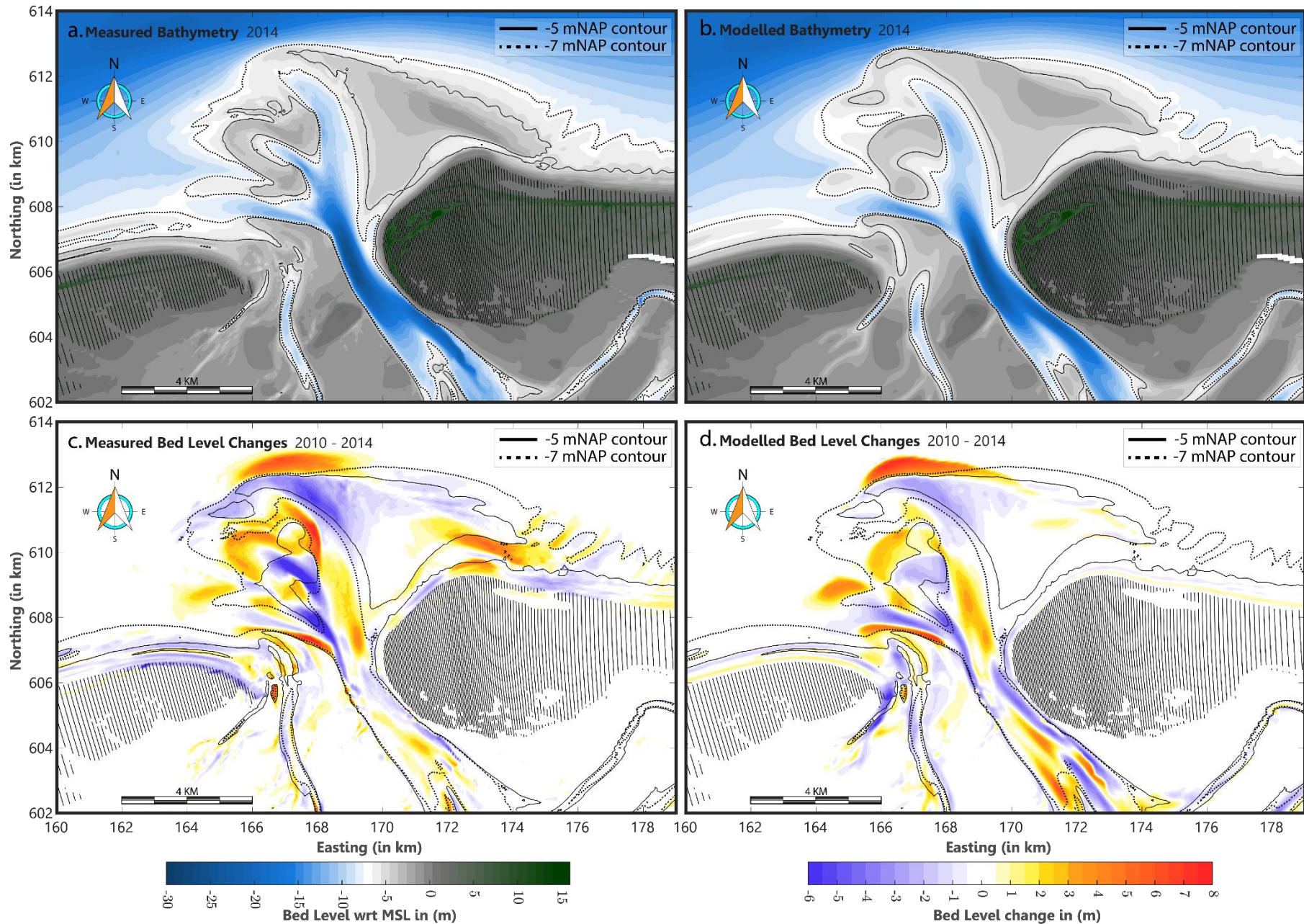


Figure A 25: Model prediction of the Ameland Ebb-Tidal Delta after four years of morphological climate (6 wave conditions and morphological tide – see Ch.4 more details on the boundary conditions). The initial bathymetry is consistent with the measured bathymetric observations in 2010. In order of occurrence, a) Measured and b) Modelled bathymetry in 2014, c) Measured and d) Modelled deposition and erosion patterns in 2014.

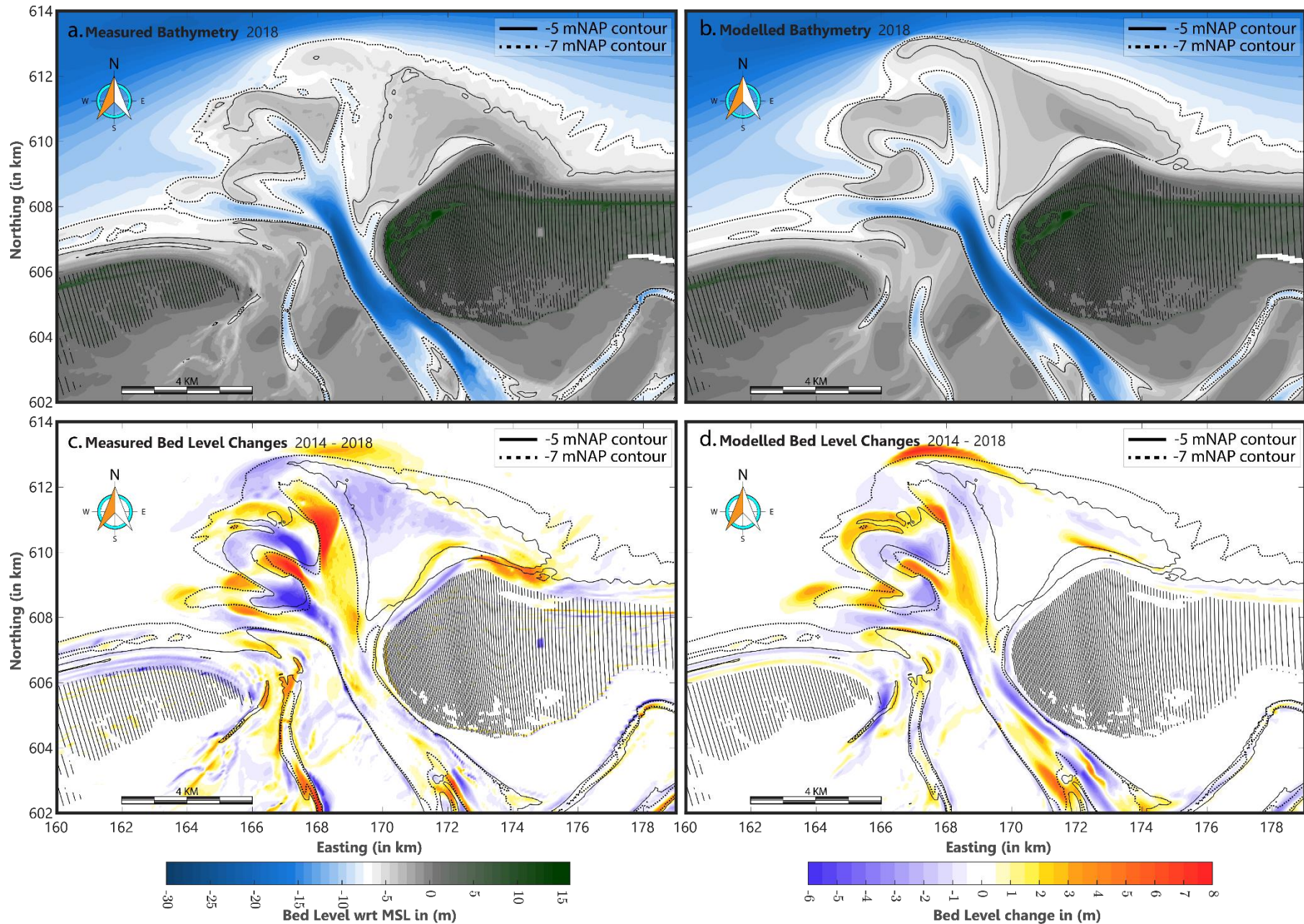


Figure A 26: Model prediction of the Ameland Ebb-Tidal Delta after four years of morphological climate (6 wave conditions and morphological tide – see Ch.4 for more details on the boundary conditions). The initial bathymetry is consistent with the measured bathymetric observations in 2014. In order of occurrence, a) Measured and b) Modelled bathymetry in 2018, c) Measured and d) Modelled deposition and erosion patterns in 2018.

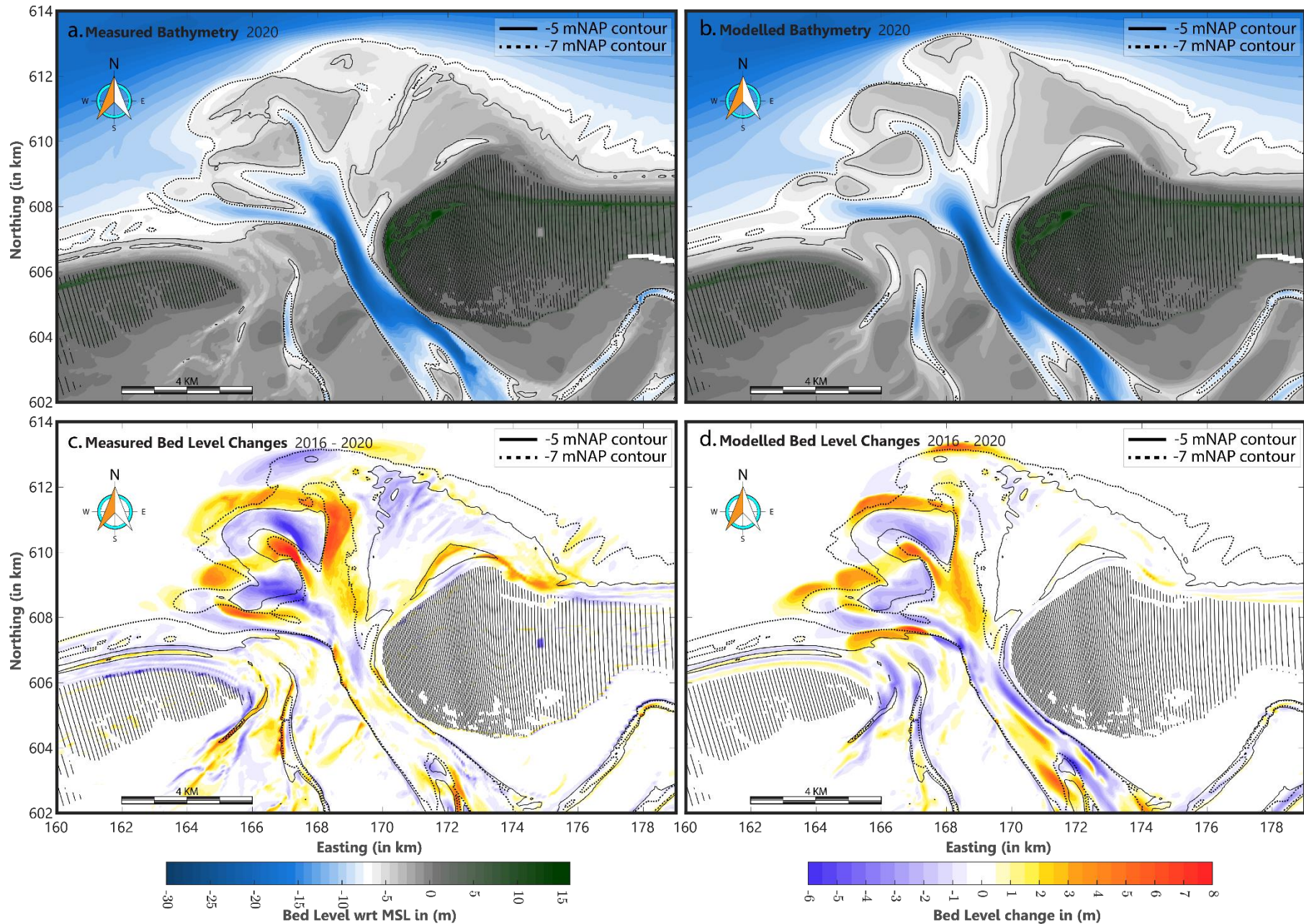


Figure A 27: Model prediction of the Ameland Ebb-Tidal Delta after four years of morphological climate (6 wave conditions and morphological tide – see Ch.4 more details on the boundary conditions). The initial bathymetry is consistent with the measured bathymetric observations in 2016. In order of occurrence, a) Measured and b) Modelled bathymetry in 2020, c) Measured and d) Modelled deposition and erosion patterns in 2020.

B Morphodynamic Impact of Pilot Nourishment 2018 – 2022 – Production Runs

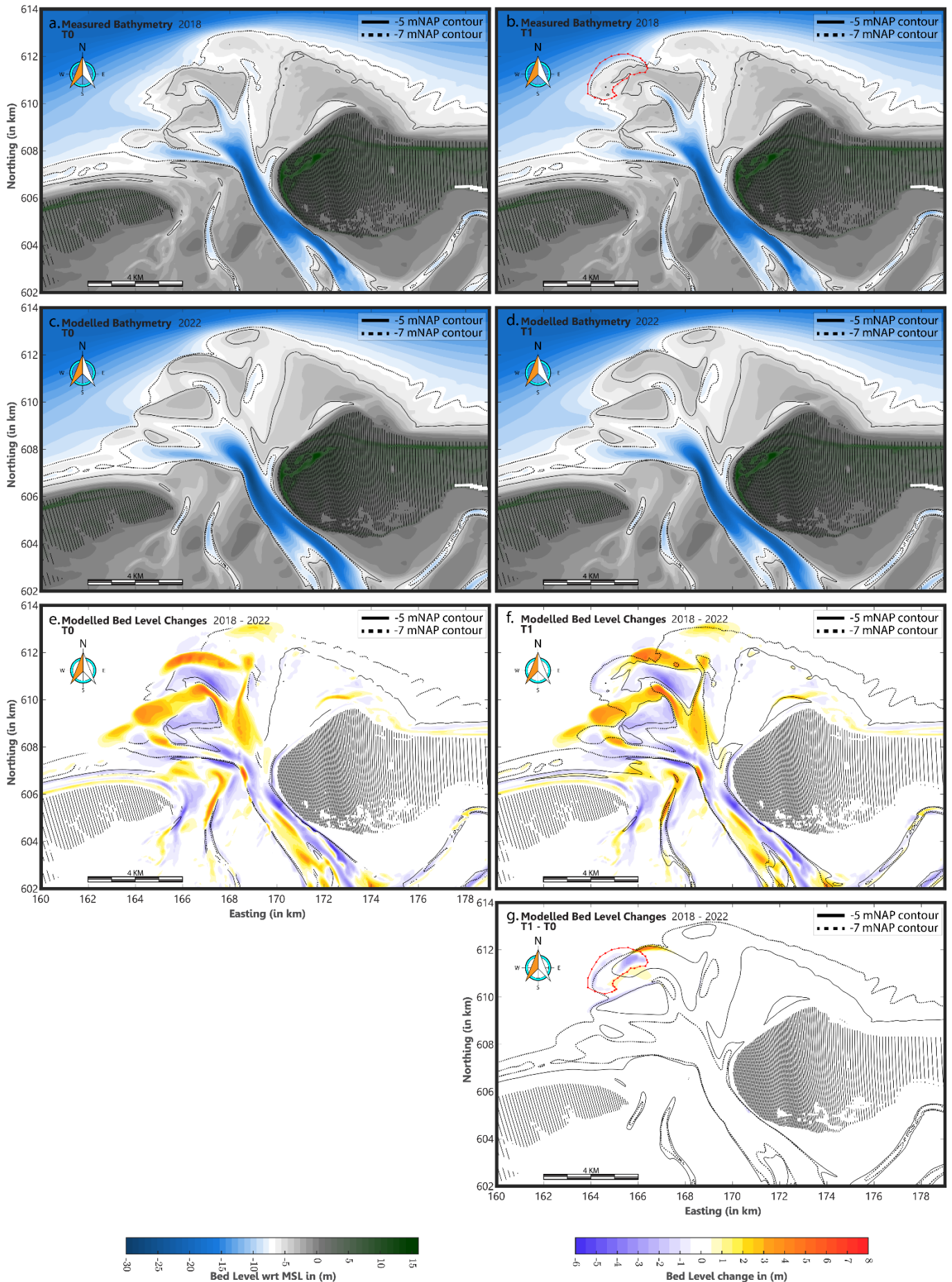


Figure B 1: Morphodynamic computation of the 2022 Ameland Ebb-Tidal Delta after four years of morphological climate (16 wave conditions and morphological tide – see Ch.4 for more details on the boundary conditions). The figure illustrates the effect the pilot nourishment on the natural behaviour of the Ameland ETD. The left panel (c,e) highlights the pre-nourishment response (T0) of the Ameland ETD over the respective period. The right panel (d,f) shows the morphodynamic development of the Ameland ETD after construction of the pilot nourishment (T1). g) emphasizes the morphodynamic impact of the pilot nourishment to the Ameland ETD. It may be seen that the impact is limited to the periphery of the second and third ebb-shield.

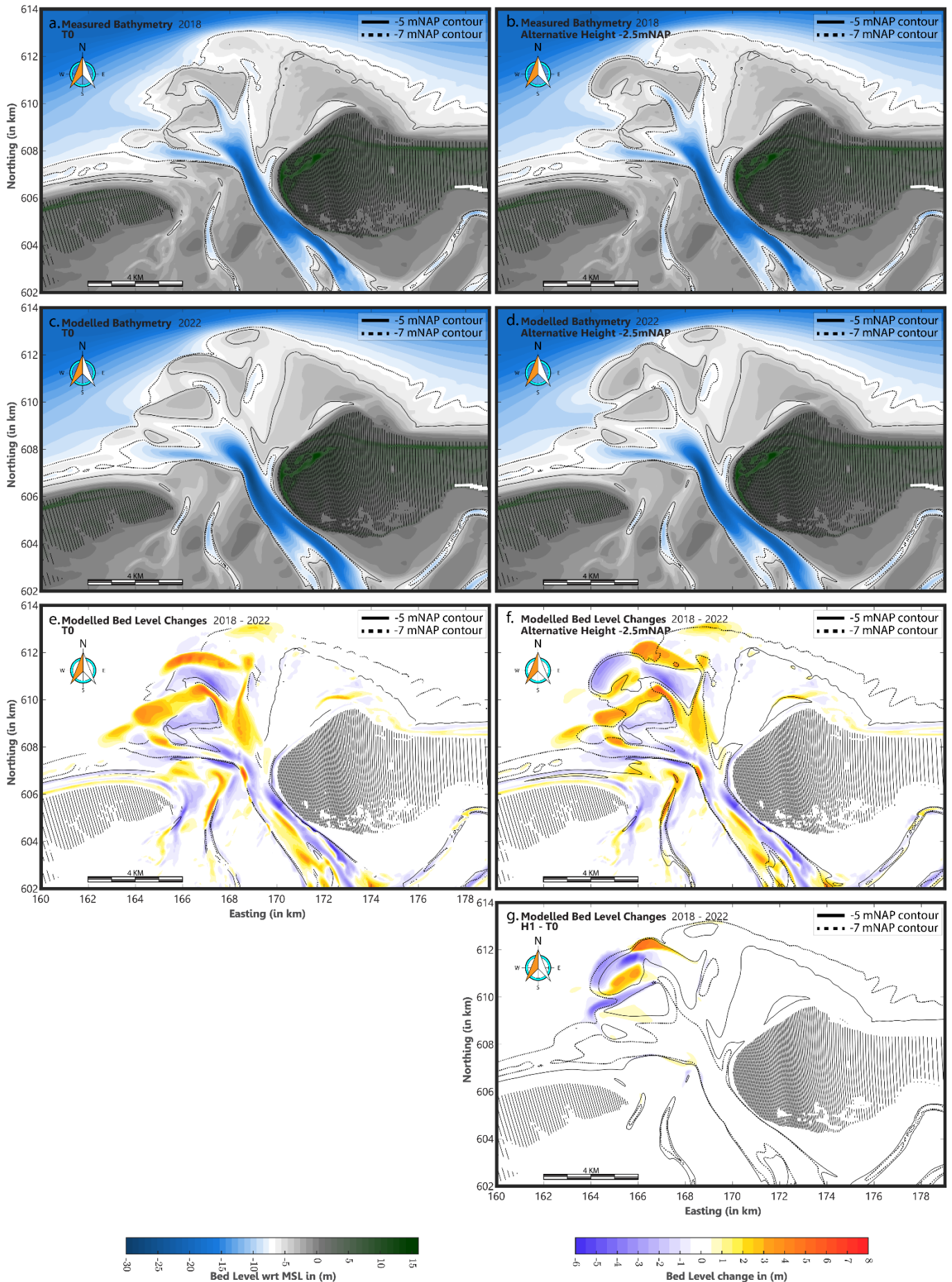


Figure B 2: Morphodynamic computation of the 2022 Ameland Ebb-Tidal Delta after four years of morphological climate (16 wave conditions and morphological tide – see Ch.4 for more details on the boundary conditions). The figure illustrates the impact of variations in construction height of the pilot nourishment on the natural behaviour of the Ameland ETD. The left panel (c,e) highlights the pre-nourishment response (T0) of the Ameland ETD over the period of 2018 – 2022. The right panel (d,f) shows the morphodynamic development of the Ameland ETD after construction of a pilot nourishment (H1) with a sill height of -2.5mNAP. g) emphasizes the morphodynamic impact of the pilot nourishment to the Ameland ETD.

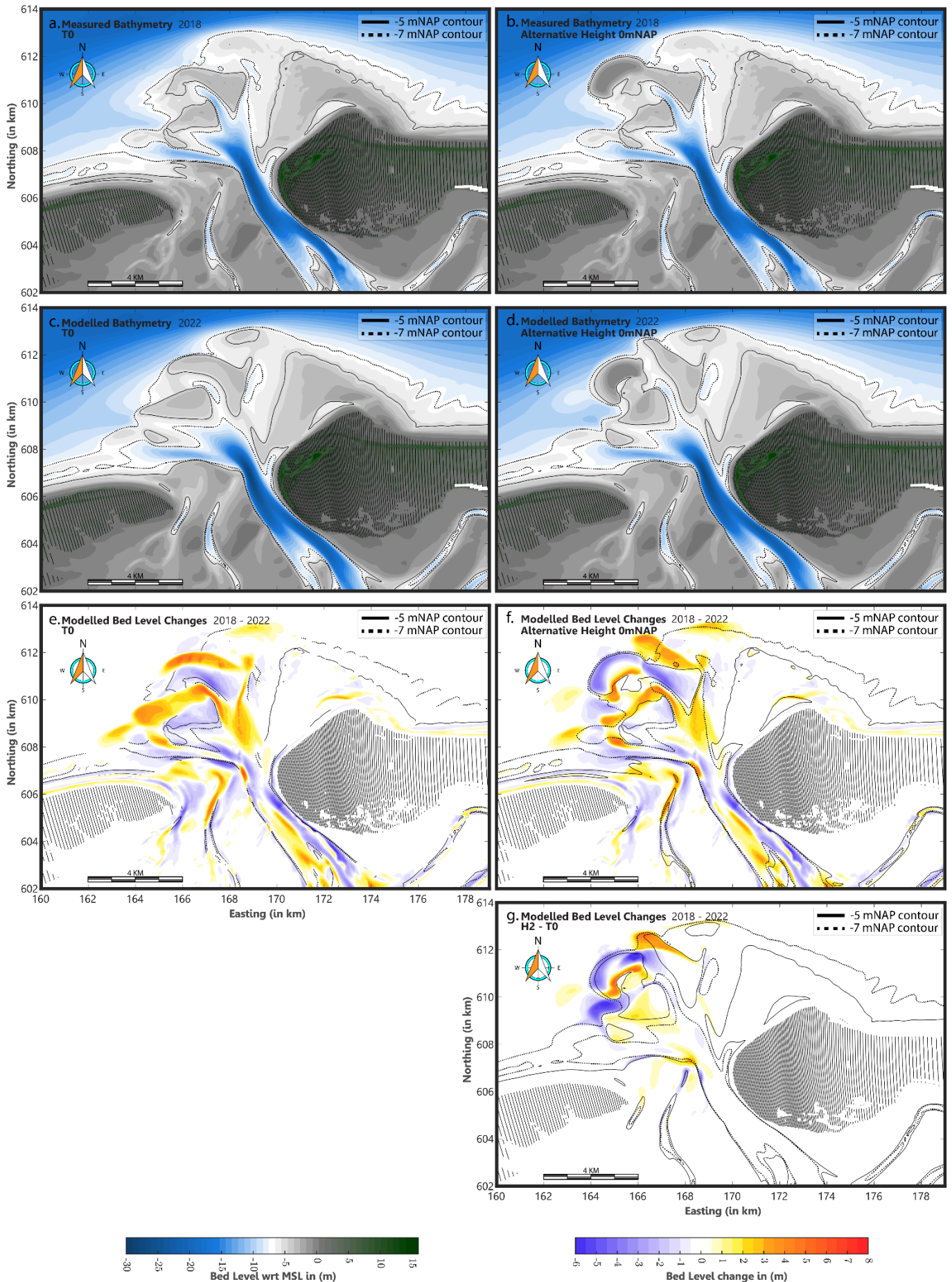


Figure B 3: Morphodynamic computation of the 2022 Ameland Ebb-Tidal Delta after four years of morphological climate (16 wave conditions and morphological tide – see Ch.4 for more details on the boundary conditions). The figure illustrates the impact of variations in construction height of the pilot nourishment on the natural behaviour of the Ameland ETD. The left panel (c,e) highlights the pre-nourishment response (T0) of the Ameland ETD over the period of 2018 – 2022. The right panel (d,f) shows the morphodynamic development of the Ameland ETD after construction of a pilot nourishment (H2) with a sill height of 0mNAP. g) emphasizes the morphodynamic impact of the pilot nourishment to the Ameland ETD.

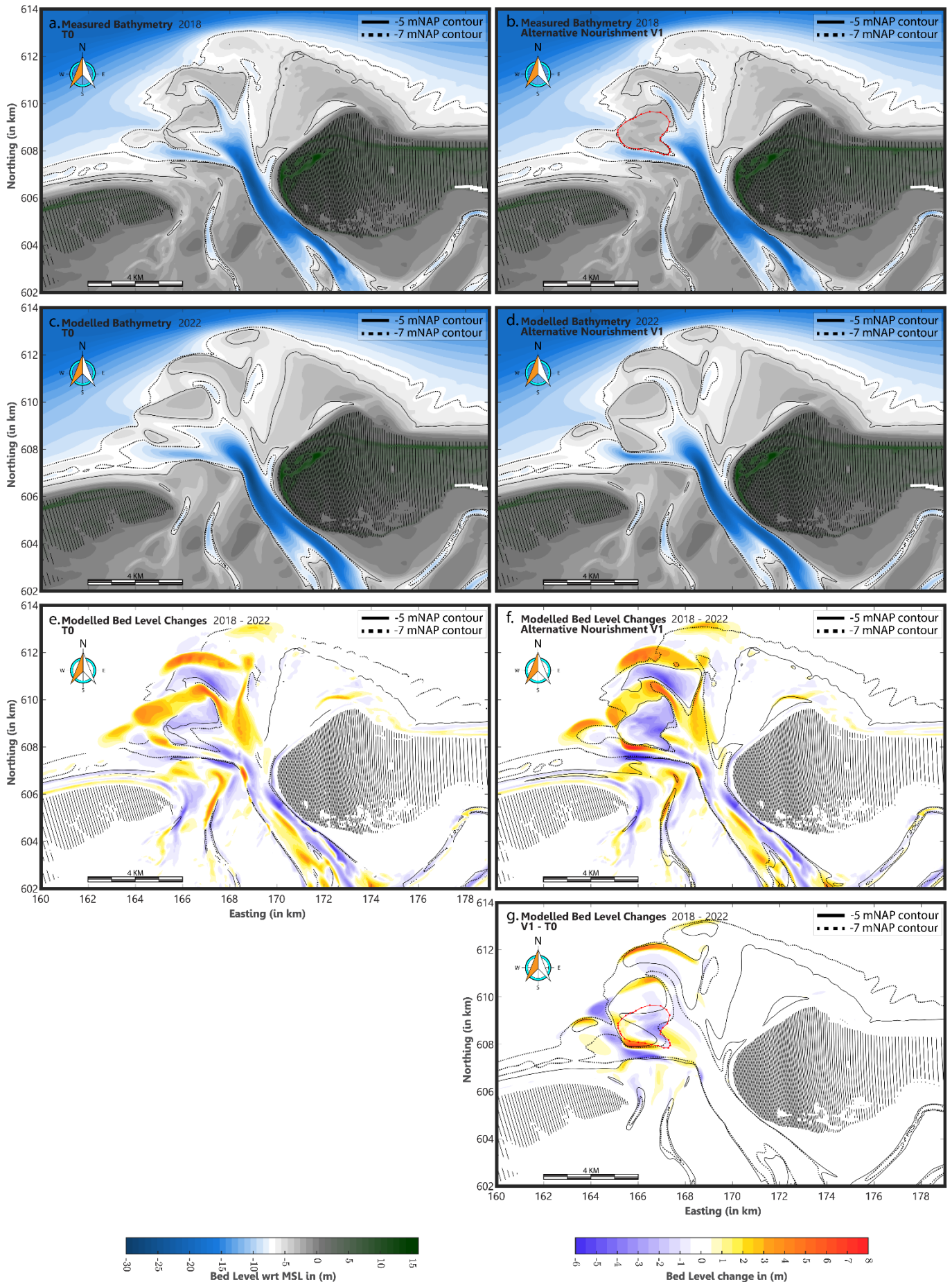


Figure B 4: Morphodynamic computation of the 2022 Ameland Ebb-Tidal Delta after four years of morphological climate (16 wave conditions and morphological tide – see Ch.4 for more details on the boundary conditions). The figure illustrates the impact of variations in the construction location of the pilot nourishment on the natural behaviour of the Ameland ETD. The left panel (c,e) highlights the pre-nourishment response (T0) of the Ameland ETD over the period of 2018 – 2022. The right panel (d,f) shows the morphodynamic development of the Ameland ETD after construction of the nourishment V1 located in the third ebb-chute. g) emphasizes the morphodynamic impact of nourishment V1 to the Ameland ETD.

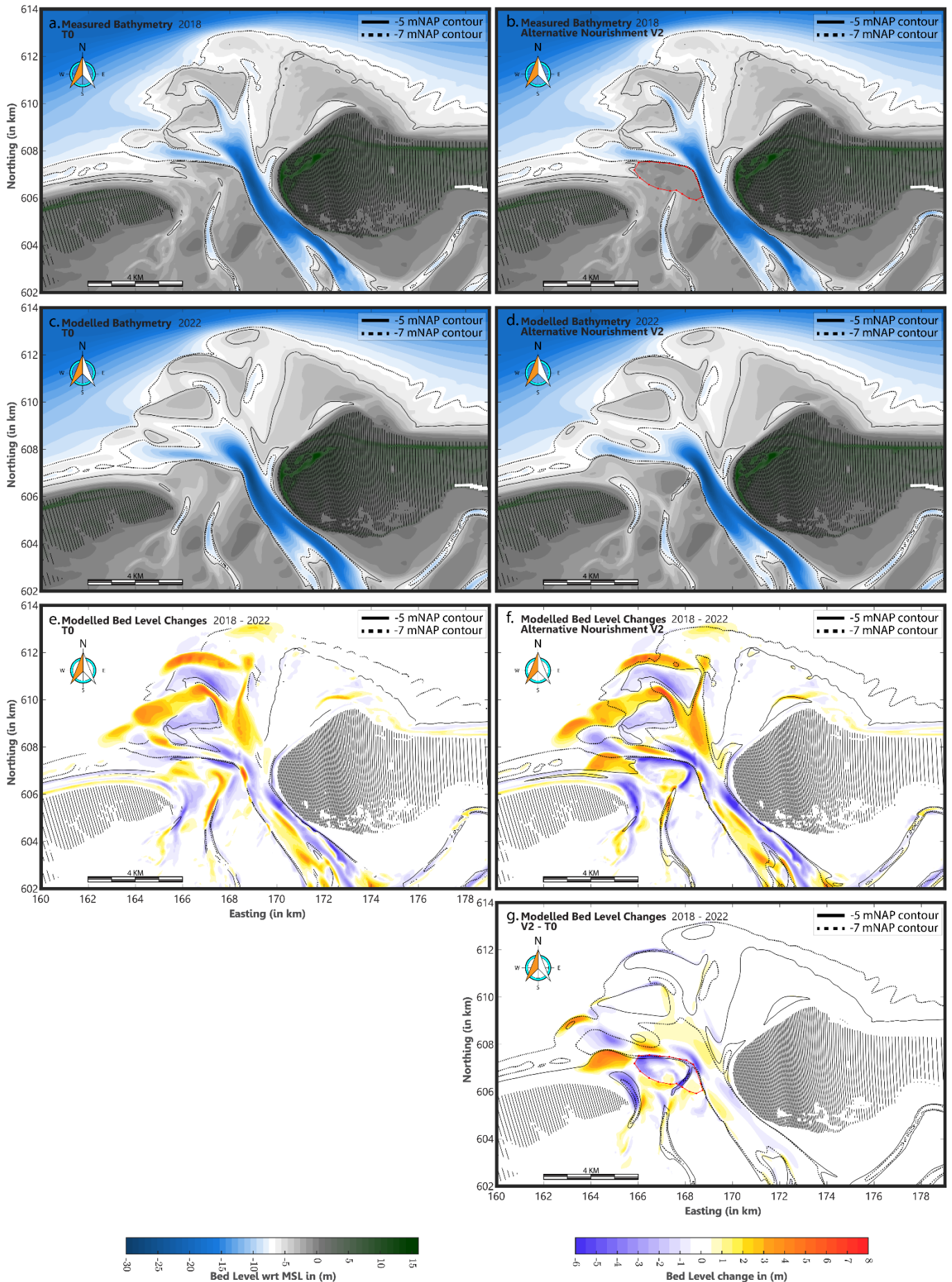


Figure B 5: Morphodynamic computation of the 2022 Ameland Ebb-Tidal Delta after four years of morphological climate (16 wave conditions and morphological tide – see Ch.4 for more details on the boundary conditions). The figure illustrates the impact of variations in the construction location of the pilot nourishment on the natural behaviour of the Ameland ETD. The left panel (c,e) highlights the pre-nourishment response (T0) of the Ameland ETD over the period of 2018 – 2022. The right panel (d,f) shows the morphodynamic development of the Ameland ETD after construction of the nourishment V2 located on the Zeehondenplaat. g) emphasizes the morphodynamic impact of nourishment V2 to the Ameland ETD.

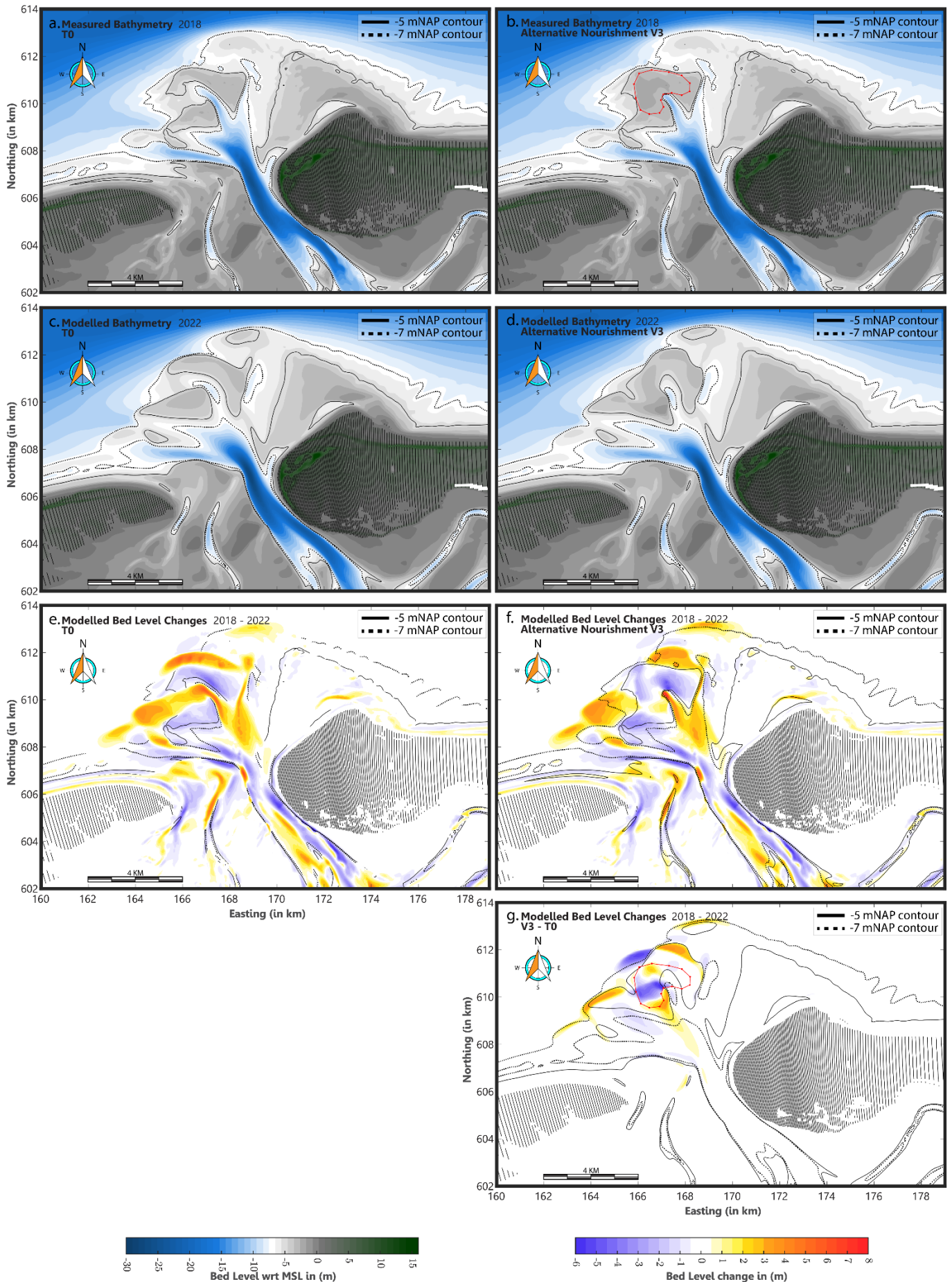


Figure B 6: Morphodynamic computation of the 2022 Ameland Ebb-Tidal Delta after four years of morphological climate (16 wave conditions and morphological tide – see Ch.4 for more details on the boundary conditions). The figure illustrates the impact of variations in the construction location of the pilot nourishment on the natural behaviour of the Ameland ETD. The left panel (c,e) highlights the pre-nourishment response (T0) of the Ameland ETD over the period of 2018 – 2022. The right panel (d,f) shows the morphodynamic development of the Ameland ETD after construction of the nourishment V3 located in the second ebb-chute. g) emphasizes the morphodynamic impact of nourishment V3 to the Ameland ETD.

C Long-Term Behaviour of Ameland Ebb-Tidal Delta – Production Runs

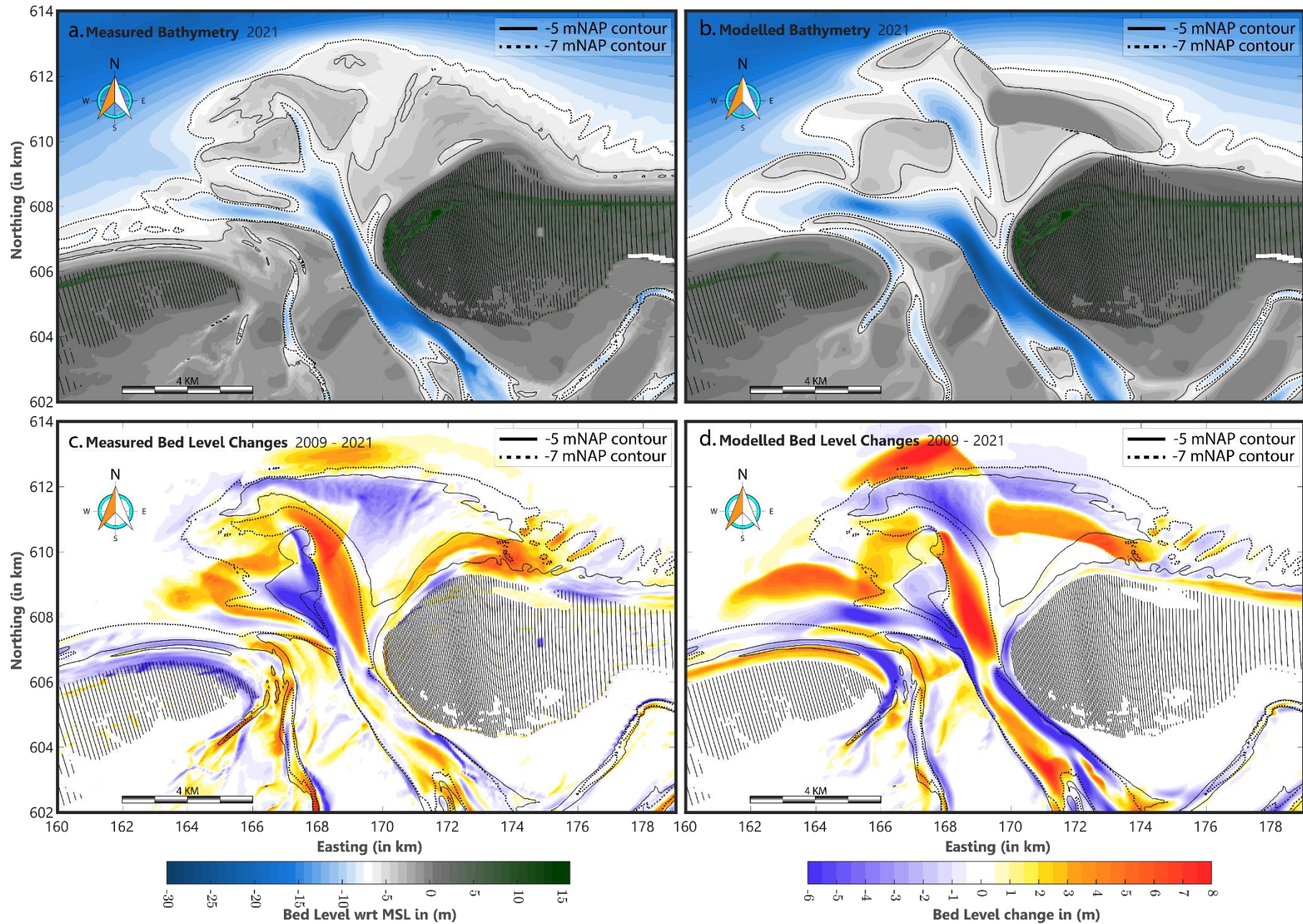


Figure C 1: Model prediction of the Ameland Ebb-Tidal Delta after 12 years of morphological climate (16 wave conditions and morphological tide – see Ch.4 for more details on the boundary conditions). The initial bathymetry is consistent with the measured bathymetric observations in 2009. In order of occurrence, a) Measured and b) Modelled bathymetry in 2021, c) Measured and d) Modelled deposition and erosion patterns in 2021.

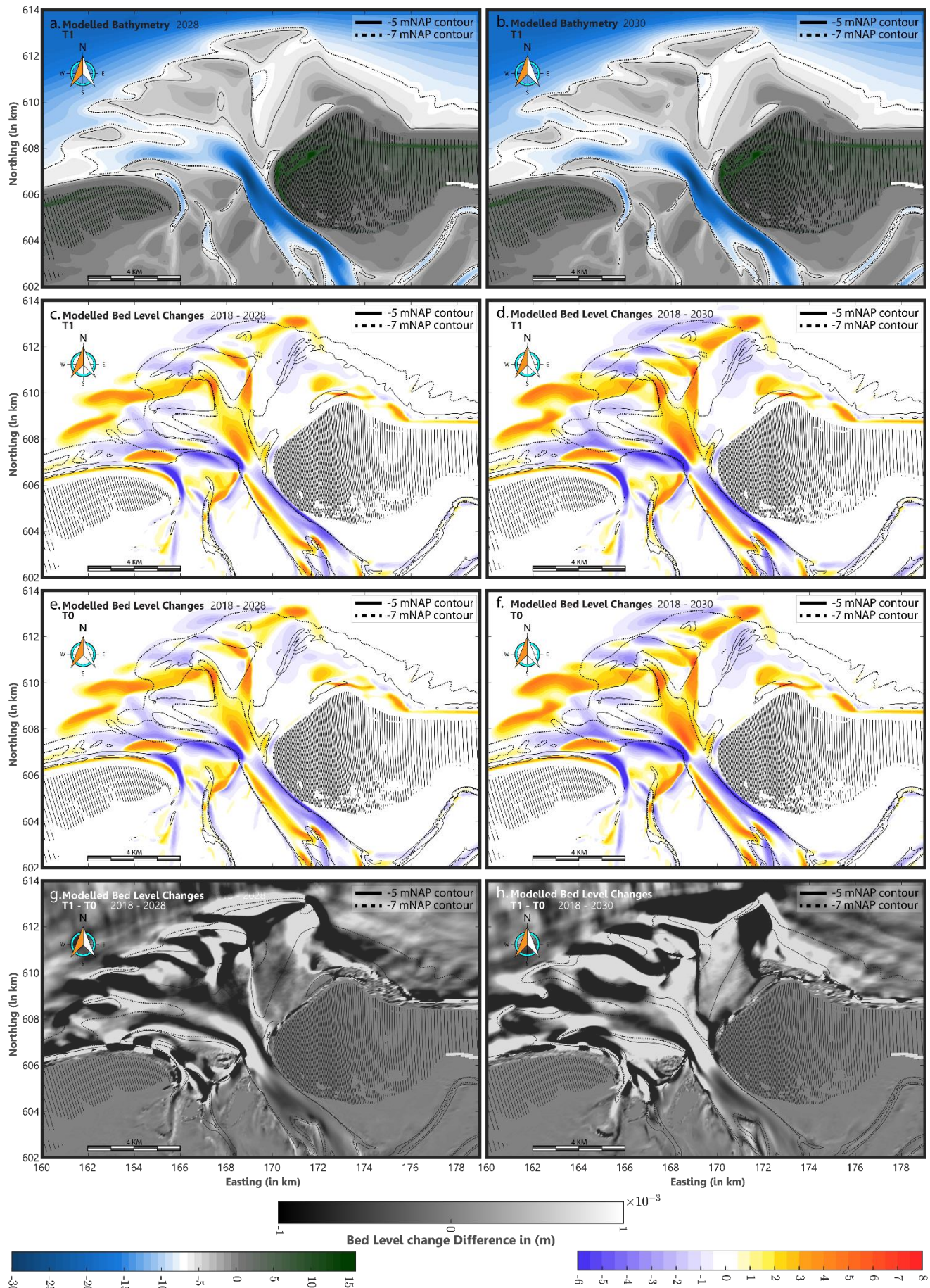


Figure C 2: Long-term morphodynamic computation of the Ameland Ebb-Tidal Delta after 10 and 12 years of morphological climate respectively. The figure illustrates the predicted morphodynamic development of the Ameland ETD after construction of the pilot nourishment. The left panel (c,e) highlights the pre-nourishment response (T0) of the Ameland ETD over the period of 2018 – 2028/2030. The right panel (d,f) shows the morphodynamic development of the Ameland ETD after construction of the pilot nourishment (T1). g) and h) emphasizes the wide redistribution of the pilot nourishment over the entire premises of the Ameland ebb-tidal delta in this model simulation.

Deltares is an independent institute for applied research in the field of water and subsurface. Throughout the world, we work on smart solutions for people, environment and society.

Deltares

www.deltares.nl